

**NASA TECHNICAL
MEMORANDUM**

NASA TM X-62,397

NASA TM X-62,397

(NASA-TM-X-62397) TELESCOPE SYSTEMS FOR
BALLCOON-BORNE RESEARCH (NASA)

N75-12735
THRU
N75-12763
Unclas
G3/74 03575

TELESCOPE SYSTEMS FOR BALLOON-BORNE RESEARCH

Proceedings of a Symposium
held at

Ames Research Center
Moffett Field, Calif. 94035

February 21-22, 1974

Edited by

Charles Swift, Fred C. Witteborn
Ames Research Center

and

Alfred Shipley
National Scientific Balloon Base

Co-Sponsors

National Aeronautics and Space Administration
National Center for Atmospheric Research

REPRODUCED BY
U.S. DEPARTMENT OF COMMERCE
NATIONAL TECHNICAL
INFORMATION SERVICE
SPRINGFIELD, VA 22161

November 1974

CONTENTS

Paper	Page
ABSTRACT	vii
ACKNOWLEDGMENTS	viii
WELCOME: Dr. Hans Mark, Director, Ames Research Center	ix

SESSION I INVITED AND CONTRIBUTED PAPERS ON BALLOON-BORNE RESEARCH

1.1	Balloon-Borne Infrared Coronagraph John Strong, University of Massachusetts	1	✓
1.2	100 Micron Surveys in the Northern and Southern Hemispheres William Hoffmann, Per A. Aannestad, University of Arizona	7	✓
1.3	Astronomical Observations With The University College London Balloon Borne Telescope R. E. Jennings, University College, London	17	✓
1.4	The Liège-Balloon Program R. J. Zander, University of Liège	26	✓
1.5	A Balloon-Borne 1-Meter Telescope for Far-Infrared Astronomy G. G. Fazio, D. E. Kleinmann, R. W. Noyes, and E. L. Wright, Harvard and Smithsonian Observatories F. J. Low, University of Arizona	38	✓
1.6	Multicolour Far Infrared Photometry of Galactic HII Regions Henk Olthof, University of Groningen	51	✓

SESSION II INVITED AND CONTRIBUTED PAPERS ON TELESCOPE AND INSTRUMENT SUBSYSTEMS

2.1	Design and Performance of a 39 cm Balloon-Borne Telescope H. S. Tomlinson, W. A. Towlson, T. E. Venis, University College London	58	✓
2.2	An Orientable, Stabilized Balloon-Borne Gondola for Around-the- World Flights George R. Ricker, Walter H. G. Lewin, Massachusetts Institute of Technology	71	✓
2.3	A Cooled Telescope for Infrared Balloon Astronomy Carl Frederick, Michael R. Jacobson, Martin Harwit, Cornell University	81	✓

pages i & ii blank

Paper	Page
2.4 A Balloon-Borne Cryogenically Cooled Filter Radiometer Arthur G. DeBell, Rockwell International	91 ✓
2.5 Not Presented	
2.6 Ultraviolet Stellar Spectrophotometry from a Balloon Platform . . . Yoji Kondo, Johnson Space Center Curtis Wells, Lockheed Electrical Co.	107 ✓
2.7 AIROscope: Ames Infrared Balloon-Borne Telescope O. L. Koontz, S. G. Scott, Ames Research Center	120 ✓
2.8 Balloon Platform for Extended-Life Astronomy Research L. T. Ostwald, Ball Brothers Research Corp.	136 ✓
2.9 Low-Background Far-Infrared Telescope for Balloon-borne Infrared Astronomy Frank J. Low, Wade Poteet, Robert Kurtz, University of Arizona	145 ✓
2.10 Sky Survey at Far Infrared Wavelengths using a Balloon-borne Telescope M. W. Friedlander, J. Goebel, R. D. Joseph, Washington University	151 ✓

SESSION III
MODERN BALLOONING CAPABILITIES AND FLIGHT OPERATIONS

3.1 The National Scientific Balloon Facility in Palestine, Texas . . . Robert S. Kubara, National Scientific Balloon Facility	156 ✓
3.2 Air Force Cambridge Research Laboratories Balloon Operations . . . Thomas J. Danaher, Air Force Cambridge Research Laboratories	160 ✓
3.3 Special Panel Discussion on Long Duration Ballooning Panelists: Dr. Ricker, Dr. Lewin, M.I.T. Mr. Pavey, Mr. Snider, Mr. Shipley, NCAR	165 ✓

SESSION IV
INVITED AND CONTRIBUTED PAPERS ON STABILIZATION AND TRACKING SUBSYSTEMS

4.1 The Stellar and Solar Tracking System of the Geneva Observatory Gondola Daniel Huguenin, Geneva Observatory	167 ✓
4.2 A High Sensitivity Balloon-Borne X-Ray Telescope System M. R. Pelling, University of California at San Diego	176 ✓

Paper		Page	
4.3	Balloon-Borne Ultraviolet Stellar Spectrometer: Acquisition, Tracking and Command Systems	190	✓
	W. C. Gibson, Lockheed Electronics Co.		
4.4	Stabilization, Pointing and Command Control of a Balloon-Borne 1-Meter Telescope	202	✓
	N. L. Hazen, L. M. Coyle, S. M. Diamond, Harvard College Observatory		
4.5	AIROscope Stellar Acquisition	225	✓
	Gordon J. Deboo, Gilbert T. Parra, Roger C. Hedlund, Ames Research Center		
4.6	The AIROscope Pointing and Stabilization System	239	✓
	James P. Murphy, Kenneth R. Lorell, Ames Research Center		
4.7	Balloon Infrared Astronomy Platform (BIRAP).	268	✓
	M. E. Greeb, G. A. True, Ball Brothers Research Corp.		
4.8	A General Purpose Stabilized Balloon Platform	284	✓
	J. How, Marconi Space & Defense Systems		

SESSION V

INVITED AND CONTRIBUTED PAPERS ON TELEMETRY AND COMMAND SUBSYSTEMS

5.1	NCAR Telemetry and Command System	294	✓
	W. Jack Snider, National Center for Atmospheric Research		
5.2	AIROscope Telemetry System	299	✓
	Kenneth J. Pitts, Ames Research Center		
5.3	AIROscope Command System	309	✓
	W. Barrows, Ames Research Center		

APPENDIX: LIST OF ATTENDEES	319
---------------------------------------	-----

ABSTRACT

This publication contains the papers presented at a symposium on Telescope Systems for Balloon-borne Research held at Ames Research Center in February 1974.

The papers covered both the description of several balloon-borne telescopes and the research conducted using these instruments.

Discussions following each presentation have been summarized by the editors.

ACKNOWLEDGMENTS

Considerable effort went into the planning, organization, and conduct of this symposium. The editors are especially grateful to Mrs. Norma Formy Duval for serving so well as arrangements secretary.

WELCOME

Dr. Hans Mark, Director
Ames Research Center

It is a great pleasure for me to welcome this group to the Ames Research Center. Balloons have been an important tool for scientific research for many decades. It is interesting to note that the first discovery in astrophysics that led to a Nobel prize was made with a high altitude balloon in 1912. This was, of course, the discovery of cosmic rays by Victor Hess. At the present time balloons are still one of the most effective and least expensive ways of getting to high altitudes and doing significant scientific research in that environment.

The last Skylab flight, as you know, was concluded last week. For the next few years we are going to be relying exclusively on unmanned space vehicles to perform space exploration missions until the Space Shuttle becomes operational early in the 1980's. I very strongly believe that balloons are going to be very important in this interim period for a number of reasons:

1. Balloons have the capability to carry large payloads to interesting altitudes.
2. Balloons are relatively inexpensive and so is the payload instrumentation associated with them. This point is something that we are going to have to pay much more attention to in the coming years.
3. I believe that there are interesting technical developments on the horizon that will make balloons very much more useful than they have been in the past. I am referring here to things such as high pressure balloons, tethered balloons and possibly ways of controlling balloon trajectories that have yet to be tried. I hope very much that some of these things will be discussed in more detail at this conference.
4. Finally, I believe that balloons are test platforms that can be used to iron out some of the engineering problems that may be encountered in the construction of Space Shuttle payloads before they actually will be flown in space.

I believe that, for these reasons, your conference here is particularly important and significant. I am going to try to attend as many sessions as I can and perhaps to participate in some of the discussions which I hope will ensue.

Let me now stop and introduce the co-chairmen, Mr. Charlie Swift, from the Ames Research Center and Mr. Al Shipley from the National Center for Atmospheric Research. I would appreciate it if you gentlemen come up for introduction. With this let me now declare the conference launched.

Thank you.

BALLOON-BORNE INFRARED CORONAGRAPH

John Strong
Astronomy Research Facility
University of Massachusetts
Amherst, Massachusetts 01002

ABSTRACT

The use of balloon vehicles to observe the solar corona with an infrared coronagraph is reviewed: both the scientific results and the instruments employed. A parallel is drawn between the required functions of a coronagraph and of a far-infrared cold telescope.

Scientific ballooning has been attractive for providing observation stations for astronomical observations by virtue of two features: 1) the altitude lies above substantially all infrared absorption by the polyatomic atmospheric constituents (H_2O and CO_2); and 2) above substantially all of the sky scattering of the infrared solar radiation.

A third feature of observations at balloon altitudes, perfect "seeing," we have never required.

The reliability of the scientific balloons themselves, and the management of their flights, have both improved substantially over the 20 years that we have been involved. During the past 10 years our experience has been excellent. Now that the art has matured I am gratified to be here to see how scientific programs have developed, and to see if our attempts to adapt to the changed climate of funding may be typical.

I shall describe our program and its projections: the scientific results and the instruments involved. Finally, I shall point out similarities of function between a coronagraph and a far-infrared helium-cooled telescope.

My remarks on the scientific side will be largely restricted to an infrared ($\lambda \sim 2.2\mu$) emission feature in the corona at $4R_\odot$ elongation (first observed at the 1966 Bolivian eclipse) and to an aura of infrared emission around the sun of substantially constant strength out to $6R_\odot$ (observed on our October 1971 balloon coronagraph flight).

MacQueen used, for his dissertation, the eclipse results and a subsequent 1967 balloon coronagraph flight that confirmed the $4R_\odot$ feature and added other subsidiary emission features (MacQueen, 1968). The 1967 balloon observations showed, significantly, that the $4R_\odot$ feature was strongest at the azimuth angle corresponding to the solar system's invariable plane (approximately the plane of Jupiter's orbit).

Our observations have been equivocal regarding the $4R_\odot$ feature: On our March 1971 flight, the increment of insolation on the servo-sensors, due to altitude, was less than we were led to expect, so that the solar tracking was sluggish. As a result, we had frequent sunlight leaks which made the data uncertain. However, correcting for this, on our two subsequent flights the

servo-mechanism has tracked our equipment on the center of the sun to within ± 10 arc sec angle--and that uninterrupted throughout both of the two data-taking periods.

Five hours of data on the October 1971 flight showed the $4R_{\odot}$ feature weak and more diffuse than formerly. It was at $\sim 4.3R_{\odot}$ (rather than $4.1R_{\odot}$, after MacQueen); and it varied uniformly with azimuth across the invariable plane.

Also, the aura or shelf out to $6R_{\odot}$, first observed on this flight, was more than an order of magnitude "too strong." I say "too strong" because it disagreed with MacQueen. Since we did not participate in the reduction of the 1967 data, we, perhaps, gave his data more respect than justified. Nevertheless, we suspected that we may have been measuring the coronagraph, rather than the corona with it. I shall confront this possibility later. For now, let it suffice to say that we "believe" these 1971 results.

Last summer we observed the infrared corona in Africa at the eclipse. These measurements with S-1 photomultipliers were filtered at $\lambda \lambda 1\mu$ (as contrasted, $\lambda \lambda 2$ to 3.5μ with the balloons). The eclipse results (Smartt *et al*, 1974) must be believed implicitly. They show neither a $4R_{\odot}$ feature nor a shelf.

Since the African^o eclipse, another balloon flight in October 1973 shows, in preliminary data reductions, no shelf; but, perhaps, a weak feature near $5R_{\odot}$ elongation.

In the context of^o these variable results, we plan one more flight with the present coronagraph, adding polarization analysis to the instrumental functions. If the infrared corona continues to behave transiently, as is now indicated, then regular studies will be indicated. But since regular studies with our present heavy equipment would be very expensive, we have been planning, in anticipation, a program with an order of magnitude lighter package. With such, several flights a year would be supportable--leading eventually, perhaps, to continuous monitoring observations from a space lab.

Since 1971 we have used a mirror coronagraph; the tracking has been described (Li, 1973). Below we describe the optical system:

Our program depends primarily on the twilight-bright sky, in the visible, at altitude--a sky that is midnight-dark in the infrared. But one must cope with the sun--even brighter at altitude than at the earth. The conventional means of coping is to create an artificial eclipse by means of an exterior occulting disk--a moon surrogate.

I broke convention by substituting exterior occulting paddles. This new procedure was invented primarily to cope with a tracking error we had at the time--annoying vertical nodding. Characteristics of the new system are: (1) the paddle obscuration effectiveness is immune to nodding; (2) since one is scanning horizontally, over-occultation at other azimuths was inconsequential; (3) Fresnel diffraction of the paddle edge is much weaker than the Lummel diffraction of a disk.

The use of primary mirrors, rather than a fused silica lens, constituted another innovation (since 1971). With mirrors we

obtained an order of magnitude improvement in the signal-to-noise quality of the recorded read-out. The use of mirrors was cued by Zirin and Newkirk (1963). They showed that mirrors supplied by the Liberty Mirror Division of Libbey-Owens-Ford Glass Company scattered incident light close to coronagraph quality. Accordingly, primary mirrors that had been super-polished were procured from Frank Cooke Inc. Smartt and Dalton (1971) coated them with gold by thermal evaporation, and investigated their scattering. Smartt has recoated these mirrors by thermal evaporation several times, and re-measured relative scattering. Each time the mirrors exhibited the same hierarchy of quality, showing that it is the polished glass surface which is limiting. This is not to imply that of these mirrors those that scatter most do not have a superb finish. It only means the testing method is very sensitive. I do not think Frank Cooke regards his procedures as proprietary; but I do think that the people who accomplish such extraordinarily excellent work in his shop may often neglect to tell all the nuances of technique that they practice.

There are a pair of occulting paddles in tandem. The front occulting paddle shades the rear one, while the rear paddle obscures the front paddle edge so that its diffracted radiation cannot irradiate its primary mirror. The rear of this pair of paddles lies 215 inches in front of its primary mirror. Thus, it must extend out, laterally, by at least one inch farther than the outer edge of its primary mirror, if all of that mirror is to be in full shade. As a result, the paddles begin to occult their mirror's view of the corona at $<5R$ --and fully occult it at the inner-limit of the scan. This arrangement avoids excessive dynamic range; but it requires that corrections be applied to the data (based on laboratory calibrations).

There are two primary mirrors. They are scanned by swinging their common mounting arm--one scans out on the right side of the sun as the other scans in on the left, and *vice versa*. There are two identical optical trains which bring the corona views to a single aspheric silicon lens which closes the opening in an LN-2 cooled chamber containing six detectors (5 PbS and 1 InAs). The optical trains are each comprised of two off-axis ellipsoidal mirrors; a 400 cps Bulova chopper (reflecting a view of the N-sky to detectors in the off-phase of each chop cycle); an image dissector that divides a $1R_\odot$ by $1R_\odot$ corona image into three samples, and separates them so they are focused by the silicon lens on three filtered detectors ($\lambda\lambda$ 2.2 μ , 2.5 μ , and 3.4 μ).

We tested the efficiency of the light baffling of the coronagraph--to restrict the detector irradiation to its corona view--as follows: A black box with a 2.8 x 6 inch "mouth" in one end, enclosing in it two black pitch polished mirrors (6 x 16 inch rectangles) to form a wedge of 10° included angle, was prepared. With the coronagraph just outside our laboratory, in Amherst, and tracking the sun, we separately mounted this box parallel to the boom that supports the paddles, and in their shade. Then we scanned the primary mirrors so that the detector view fell entirely within the mouth of the rectangular black hole that the box provided. Thus, we found that the detector response was less

than the smallest in-flight responses, at the greatest elongation angles ($\sim 12R$). Even so, the primary mirrors used in this instance were not subject to in-flight scrupulosity: they had been used for the calibration above mentioned. And certainly the Amherst ambient light was at a higher level than in-flight.

Let us return now to the October 1971 flight data. Adney (1973) has made an ardent analysis for us, motivated to impugn the October 1971 data. He tried out every possibility we could imagine of instrumental artifacts--especially emitted or reflected paddle radiation.

Our confidence that the shelf was coronal, not instrumental, is based on the following (with no contrarywise evidence):

- 1) The three views of the corona are separated $3/10R$ in elongation. We asked if the features as seen by the three detectors on one side collated as to coronal position, or with time. They were found to collate in coronal position--both the $4.3R$ feature and the $6R$ fall-off of the shelf.

- 2) The shelf is established by the detector view fields lying outside of the point where the field of view first intrudes on the paddle.

- 3) On the October 1973 flight the in-flight paddle temperature was $\sim 0^\circ\text{C}$. This confirms a conclusion that Adney had come to: that thermal emission of the paddles is negligible, particularly for the two $\lambda \lambda 2.2\mu$ detectors.

- 4) Reflected telluric light is estimated as negligible.

Scientifically, we can draw a very tentative conclusion and indulge a fantasy:

It is currently supposed that the $4R$ feature is comprised of interplanetary particles coming into the sun by loss of angular momentum through the Poynting-Robertson effect. As they get close to the sun, they get hot enough to evaporate--near the sun, at $4R$, irradiation is like that at the focus of an $f/2$ solar furnace. This evaporation reduces particle diameters until radiation pressure turns their inward drift outward, to provide the $4R$ maximum. If this process were correct, then the infrared corona should have a very long characteristic time; a much longer period than we have observed--seven years.

If, contrarywise, the features are of solar origin, how are they to be explained? Here we have indulged the fantasy that they are clouds constituted of the "metallic" elements of the sun--particles grown and concentrated by fractional distillation, the residue as the solar wind is evaporated away. We suppose that clouds of such particles may be dispersed from time to time.

We have also fantasized that the individual particles may be whiskers. Whiskers are a strange form of matter, too little known to be modeled into the harsh environment of the corona, but particles that could have a larger infrared than visual "antenna cross section."

Now, finally, we shall consider applications of coronagraph procedures to helium-cooled far-infrared astronomical telescopes. A requirement for them is protection of the detector from saturation by emitted or scattered infrared radiation. In my design, a large helium-cooled primary mirror is fed by a

tessellated system of parallel optical trains. In each optical train there is a pair of confocal infrared achromatic lenses (Strong, 1971 and 1972). The forward lens of the pair focuses the far field on a plate that is perforated by a small sampling hole. The rear achromat collimates the radiation passed by this hole. A single chopper next to this plate, with slots for each optical train, modulates the radiation transmitted by the plate. All parallel beams are brought to the detector with a single mirror system.

Each optical train is comprised of two parts: one lies before, and the other aft of the lens pair. The forward parts are enclosed in LN-2 cooled tubes; the latter in helium-cooled tubes.

The prime advantage of this system is that diffraction at the forward opening and LN-2 wall radiations are occulted. The prime disadvantage is that the angular resolution of the system is limited to that of the diameter of the achromatic lenses.

Rather than apologize for this complicated gadget, I shall quote Goethe:

"Ein Mann, der recht zu wirken denkt,
Muss auf das beste Werkzeug halten.
Bedenkt, Ihr habet weiches Holz zu spalten."

REFERENCES

- Adney, K.J., "Reduction of Data, Balloon-Borne Infrared Coronagraph Flight of October 24, 1971," NASA Report, October 1973; UMSS-ARF-73-284.
- Li, T.C., Appl. Opt. 12, 2828 (1973).
- MacQueen, R.M., Astrophys. J. 154, 1059 (1968).
- Smartt, R.N. and W.S. Dalton, J. Opt. Soc. Am. 61, 665 (1971).
- Smartt, R.N., J. Strong, W.S. Dalton, and T.C. Li, "1973 Africa Eclipse Observations," NASA Report, January 1974.
- Strong, J., Appl. Opt. 10, 1439 (1971).
- Strong, J., Appl. Opt. 11, 2331 (1972).
- Zirin, H. and G. Newkirk, Appl. Opt. 2, 977 (1963).

DISCUSSION SUMMARY — PAPER 1.1

Paper 1.1 submitted but not presented.

PAPER 1.2

100 MICRON SURVEYS IN THE NORTHERN AND SOUTHERN HEMISPHERES*

William F. Hoffmann
Per A. Aannestad**
Steward Observatory
University of Arizona

ABSTRACT

Partial surveys in the far infrared in the Northern and Southern Hemispheres have covered 40% of the galactic equator and assorted regions away from the galactic plane. Approximately 120 100-micron objects are known. These are distributed extensively in galactic longitude and concentrated within \pm two degrees in galactic latitude. From this information, some general conclusions can be drawn about the sensitivity and coverage required for a general sky survey in the far infrared.

INTRODUCTION

As new techniques of detection open up new parts of the spectrum to astronomical observation, a survey of the sky at the new wavelength is appropriate and valuable. Sometimes, although not always, this is a means for making unexpected new discoveries. In general, such surveys are of value for providing a general picture of the sky at the new wave length, making possible classification and statistical analysis, and providing a guide to detailed studies.

In the infrared and submillimeter part of the spectrum, there are the 2.2 micron Cal Tech sky survey (Neugebauer and Leighton 1969) and the 10 micron Air Force Cambridge Research Laboratory rocket survey (Walker and Price 1974). The shortest wavelength continuum radio survey of the galactic plane are the surveys at 6 cm of Altenhoff et al (1970) and Goss and Shaver (1970). The shortest wavelength radio survey of substantial portion of the entire sky is at 21 cm. Thus, there is a substantial gap in our systematic knowledge of the sky between the wavelengths of ten microns and 6 cm (60,000 microns).

The phenomena which dominate the emission processes over this large spectral range vary sufficiently so that knowledge gained in the infrared at 10 microns or in the radio region at 6 cm does not provide much of a clue as to the objects to be found at the intermediate wave length of 100 microns. The stellar photospheres and circumstellar dust envelopes which dominate the 10 micron sky provide little contribution at 100 microns. Similarly, the hot ionized gas which accounts for the thermal radio-continuum emission in HII regions provides very little flux in the far infrared. On the other hand, interstellar dust clouds, dust in HII regions, and dust in galactic nuclei, because of its low temperatures, emits thermally primarily in the far infrared.

For this reason, a balloon-borne far infrared astronomy program was initiated at Goddard Institute for Space Studies and is now being continued

*Much of this work was carried out at the Goddard Institute for Space Studies. It is currently partially supported by NASA grant NGR 03-002-371 at Steward Observatory.

**P.A.A. gratefully acknowledges support from the Smithsonian Astrophysical Observatory.

100 μ SURVEY

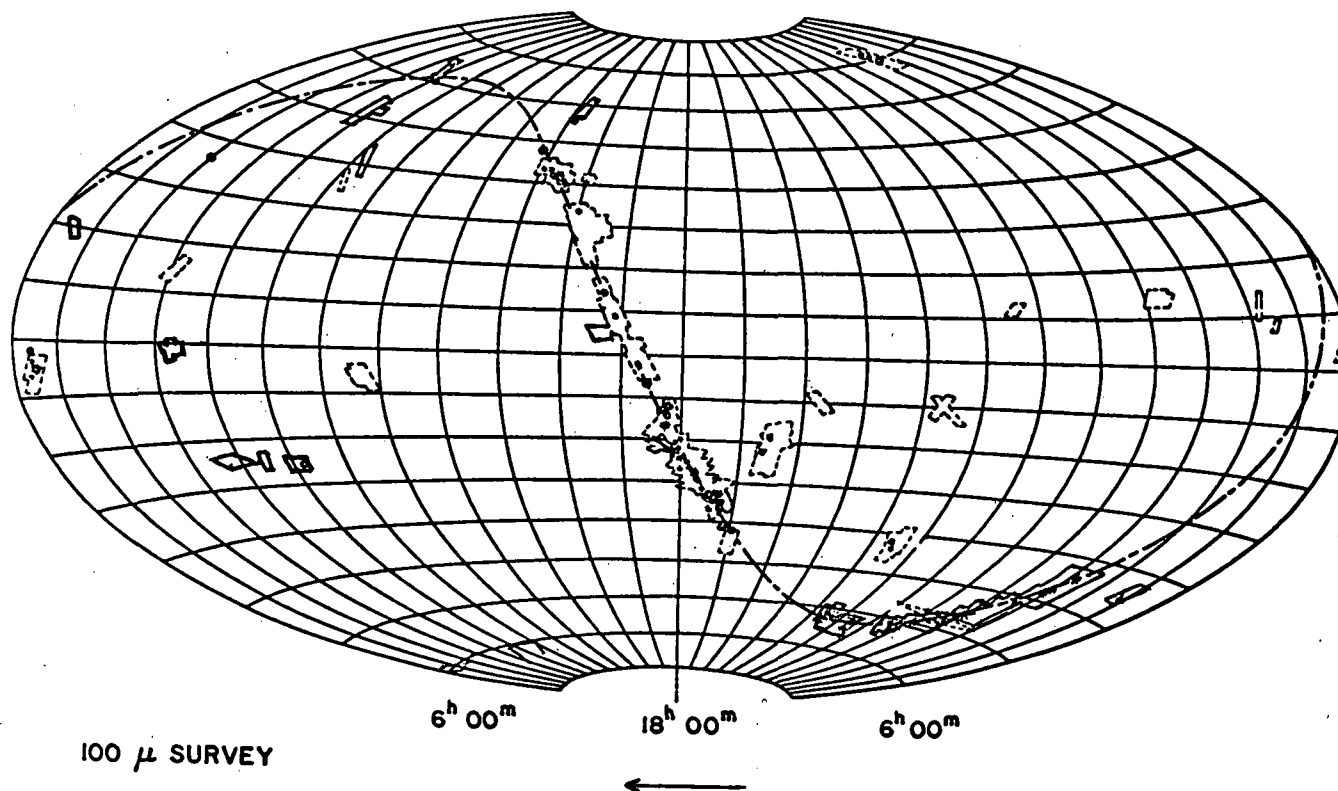


Figure 1 - The regions of the sky that have been surveyed in the balloon experiment when plotted on an equal areas projection of the entire celestial sphere. The *'s show the positions of 100 micron sources observed in the balloon survey. The open circles show the positions for additional sources observed in other experiments.

at the Steward Observatory in order to survey the sky at 100 microns. This survey is not complete. In this paper we would like to discuss what has been observed, what can be said statistically about the spatial and brightness distribution of known sources, and what level of performance is required for a more detailed and more complete survey. While the largest number of sources analyzed has come from the Goddard/Arizona balloon surveys, we have attempted to include a number of other objects not observed in that program but reported by other groups. The sources for the data analyzed are: Harper and Low (1971), Hoffmann, Frederick, and Emery (1971), Soifer, Pipher, and Houck (1972), Emerson, Jennings, and Moorewood (1973a), Emerson, Jennings, and Moorewood (1973b), Harper and Low (1973), Olthof (1974), and Hoffmann, Frederick, Emery, and Aannestad (1974).

OBSERVATIONS

Figure 1 shows the regions of the sky that have been surveyed in the balloon experiment. The *'s give the positions of 100 micron sources observed in the balloon survey. The open circles give additional sources observed in other experiments. 140° or 40% of the galactic plane has been covered in a band varying from 4° to 8° wide. 700 sq. degrees of sky along the plane and 250 sq. degrees elsewhere have been surveyed. This represents about 2.4% of the entire celestial sphere. Some of the interesting areas are: to the extreme left, the Orion infrared nebula; at RA 45 min DEC- 26° , the galaxy NGC 253; at 20 hrs. 40 min., $+42^\circ$ the Cygnus region; a stretch centered on 19 hours including W51, W49, and M17; another stretch centered on the galactic center at 18 hours including M8 and the galactic center complex; in the region of 16 hrs. 30 min., -20° , dark clouds in the Ophiuchus region; centered on 13 hrs., -63° the Coal Sac Nebula; near 13 hrs. 20 min., -43° the Centaurus A region; at 11 hours, -59° the Carina Nebula; and at 10 hrs., $+70^\circ$, the galaxy M82. As can be seen from Figure 1, this is a patchy and highly selected sample of the sky.

With some caution to avoid extracting more than is present from this limited sample, we have attempted to learn something about the distribution of the known 100 micron objects in galactic coordinates. Figure 2 shows a histogram of the sources in galactic longitude. The lower part gives the number of sources in 10° blocks of longitude. Since this distribution can be heavily biased by the spottiness of the sample of the galactic plane, we have shown in the upper part a histogram indicating the regions of the galactic longitude which have been scanned. The full value indicates that the scans cover 4° or more across the galactic plane. The half value indicates a narrower region less than 4° wide. The lower part of Figure 2 shows a slight concentration of sources toward the galactic center, although this concentration is not nearly as much as might have been expected. In addition, since the region between 320 and 345 degrees galactic longitude has not been covered in the Goddard surveys, this apparent peaking may be a selection effect. The results of Ricker, Lewen, and Low (1974), when available, should partially cover this region. The relatively small number of bright sources between M17 and the Cygnus region, however, does appear to be a real effect rather than an observational selection effect. Although there remains a substantial gap in the data along the galactic equator in the northern hemisphere, it does appear that the preponderance of sources are in the southern hemisphere. From left to right, the main peaks occur in the areas of the Carina Nebula, the Coal Sac Nebula, the Galactic Center, and the Cygnus Region.

NUMBER OF OBJECTS: 105

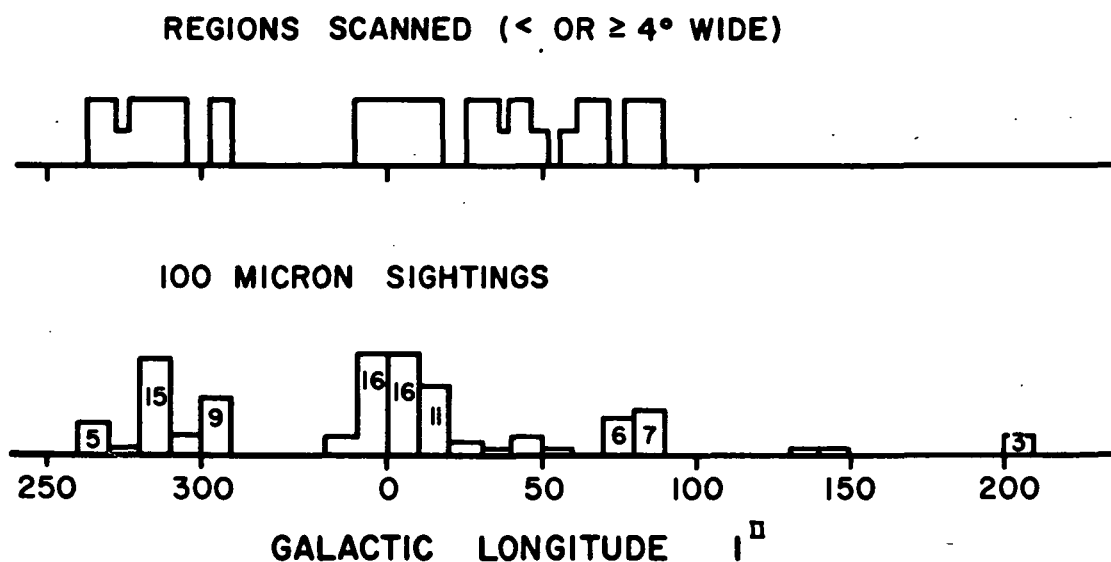


Figure 2 - Lower portion: A histogram of 100μ objects as a function of galactic longitude. Upper portion: A diagram indicating the regions in galactic longitude which have been scanned. The full value indicates that the scans covered 4° or more in the direction normal to the galactic plane, the half value corresponds to scans less than 4° wide.

Figure 3 gives a histogram in galactic latitude with intervals of 1° from the galactic equator. As in figure 2, the upper part indicates the distribution of scans in galactic latitude. The three levels represent the portion of scans at various widths. Approximately half were 6° wide or wider. Of the remaining, most were at least 4° wide and a small number were as small as 3° in width. The histogram in the lower half is substantially more concentrated toward zero galactic latitude than the distribution of scan widths. We, therefore, conclude that the distribution of 100 micron sources is very much concentrated within $\pm 2^\circ$ or less of the galactic equator. For the sample over a 6° wide band, 62% are within $\pm 1^\circ$ galactic latitude and 93% are within $\pm 2^\circ$. While the fall-off at the edge of this histogram is biased by the finite width sample, we conclude from this that the far infrared sources within 3° of the galactic equator are substantially concentrated toward the equator with over half within $\pm 1^\circ$ of it. From the present survey information, it is not possible to tell what the wings of the distribution look like with increasing galactic latitude.

SCAN WIDTH

NUMBER OF OBJECTS: 97

100 MICRON OBJECTS

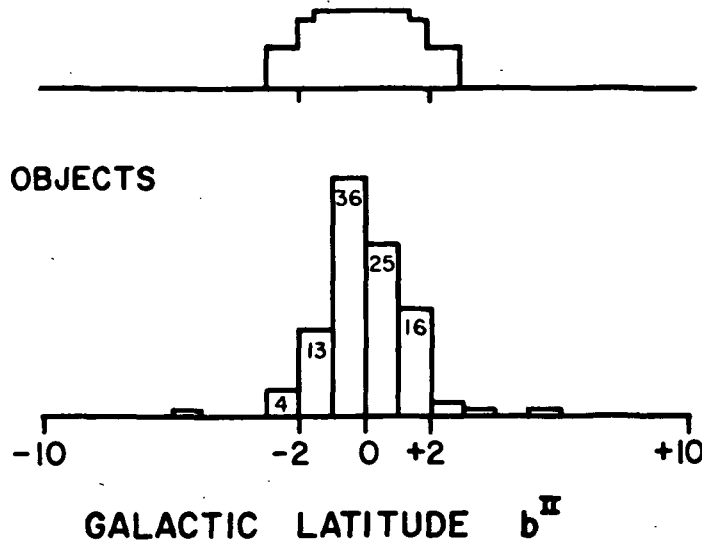


Figure 3 - Lower portion: A histogram of 100 μ objects as a function of galactic latitude. Upper portion: A diagram indicating the portion of scans of various widths across the galactic plane. See text for details.

It is also interesting to analyze the known sources in terms of their brightness (flux density), as a guide to the sensitivity that should be achieved in a more extensive survey. Figure 4 shows a histogram of the sources as a function of 100 micron flux density in units of 10^{-22} W/m²Hz. The intervals are logarithmic. The rapid falloff for the faint sources is representative of the sensitivity limit of the apparatus near 1×10^{-22} W/m²Hz. The steepness of the rise in numbers from the brightest sources toward weaker ones is much slower than one would expect from a group of sources of identical intrinsic brightness uniformly distributed in volume. This is consistent with the picture that the bulk of the sources are neither solar neighborhood sources nor extragalactic sources but are primarily confined to the Milky Way and hence, constrained to a limited range of distance. It appears from Figure 4, that as the sensitivity of a survey is increased from 10,000 flux units (1 flux unit = 10^{-26} W/m²Hz) to 1,000 flux units, the number of sources along the plane should increase substantially. As the sensitivity is further increased to 100 flux units, one would expect a continuous mapping of 100 micron emission along the galactic plane similar to the radio maps where the "sources" are peaks in a continuous distribution flux.

NUMBER OF SOURCES: III

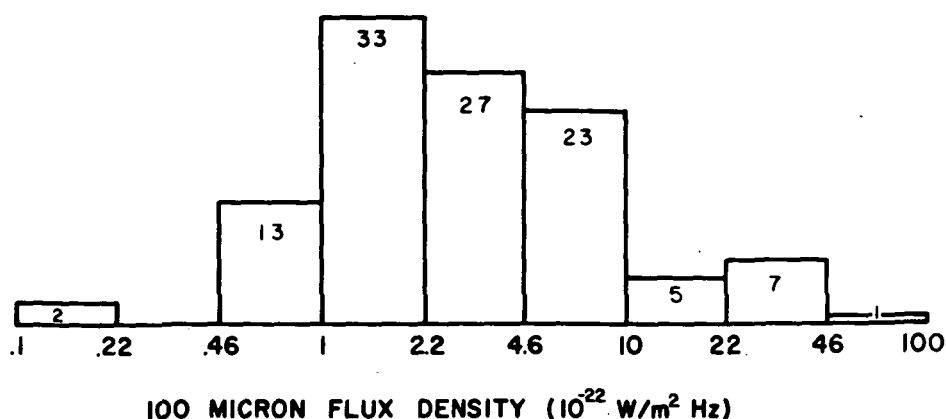


Figure 4 - A histogram of 100 μ objects as a function of their 100 μ flux density.

FUTURE SURVEYS

Two balloon programs now being carried out to substantially improve the sensitivity of survey type instruments are the 8-inch low emissivity off-axis Hershellian telescope of Frank Low, at the University of Arizona, and the Cornell/Arizona 16-inch cryogenically cooled telescope. Both of these instruments are aimed at high throughput (product of solid angle in sky and telescope aperture) with the thermal emission of the instrument reduced to, or below, the atmospheric emissivity in order to make possible the use of more sensitive detectors optimized for very low background flux. These two instruments are described elsewhere in these proceedings. In order to provide a set of numbers from which to start, we have considered two possible survey objectives, (a) a survey of the galactic plane, and (b) a survey of most of the celestial sphere. The first goal is compatible with a number of short duration balloon flights. The entire celestial sphere survey is ideally suited to a long duration super pressure balloon flight. Table 1 gives a set of parameters for the short duration balloon flights. Some of these are taken from our experience with the current Goddard Institute for Space Studies/Arizona balloon gondola. It would appear that with reasonable scan rates and overlapping coverage, the galactic plane can be covered redundantly in five flights. The resolution given is 3 arc minutes. The location of all but the faintest sources should be obtained to approximately 1 arc minute. While this can be achieved with a rather larger beam by careful determination of the center point of the scan signal, large beams (greater than 12 min. of arc) will probably suffer substantially from source confusion at these high sensitivity levels along the galactic plane. The integration time of 0.12 seconds is derived from the 3 min. resolution and the 48 hours of flight. While this resolution is required for adequately

determining the center of sources to 1 arc minute, very faint sources can be analyzed at lower resolution to take advantage of a larger beam size. For this reason, we have shown sensitivity figures for both 3 arc minute resolution and 12 minute resolution. The latter is $1 \times 10^{-24} \text{ W/m}^2\text{Hz}$. The detector NEP assumed, $10^{-14} \text{ W}/\sqrt{\text{Hz}}$ appears to be the best that is currently available.

TABLE 1

SHORT DURATION BALLOON FLIGHTS

Coverage:	Galactic Plane 3600 deg^2
Rate:	$75 \text{ deg}^2/\text{hr}$ (48 hours)
Number Flights:	5
Resolution:	3'
Integration Time:	.12 sec
Telescope Area:	$.13\text{m}^2$ (16")
Wavelength:	100μ
Detector NEP:	$10^{-14} \text{ Watt}/\sqrt{\text{Hz}}$
Overall Efficiency:	10%
Sensitivity (3σ) in 3':	$4 \times 10^{-24} \text{ W/m}^2\text{Hz}$
Sensitivity in 12':	$1 \times 10^{-24} \text{ W/m}^2\text{Hz}$

A survey of the entire celestial sphere would be aimed at discovering extragalactic sources of far infrared radiation. As such, to be of use, it would have to be even more sensitive than a survey of the galactic plane and, at the same time, cover a substantially larger area. Assuming the same detector sensitivity, this objective can be realized by only more observing hours, hence a long duration balloon flight. In table 2, we have assumed a two-week flight with an ambient temperature low-emissivity telescope of 25 centimeter diameter (and a liquid helium-cooled detector). This system offers a sensitivity of only $1 \times 10^{-23} \text{ W/m}^2\text{Hz}$ (1,000 flux units) at the 3 arc minute resolution. At 12 minutes, the sensitivity is 250 flux units. If the throughput is increased sufficiently to provide a $50'$ (1°) beam, the sensitivity could be as good as 50 flux units. Since the density of infrared objects at high galactic altitudes is expected to be substantially less than that along the galactic plane, the problem of source confusion should be much less than along the galactic plane. For this reason, a compromise favoring greater throughput and sensitivity at the expense of resolution and position accuracy would probably be desirable.

TABLE 2

LONG DURATION BALLOON FLIGHT

Coverage	Declination $+30^{\circ}$ to -90°
Area:	31000 deg^2
Resolution:	$3'$
Data Points:	12×10^6
Time:	2 weeks $\approx 1.2 \times 10^6$ seconds
Integration Time:	0.1 second
Telescope Area:	$.05 \text{ m}^2$ (25 cm diameter)
Wavelength:	100μ (80μ - 120μ)
Detector NEP:	$10^{-14} \text{ Watts}/\sqrt{\text{Hz}}$
Overall Efficiency:	10%
Sensitivity in $3'$ (3σ):	$1 \times 10^{-23} \text{ W/m}^2 \text{ Hz}$
Sensitivity in $12'$:	$2.5 \times 10^{-24} \text{ W/m}^2 \text{ Hz}$
Sensitivity in $60'$:	$5 \times 10^{-25} \text{ W/m}^2 \text{ Hz}$

CONCLUSION

With a little over one hundred objects known from far infrared sky surveys to date, some characteristics of these objects in the Galaxy are beginning to become known. Two extragalactic objects have been measured in directed (non-survey) efforts (Harper and Low 1973). It is now possible to define with reasonable confidence the surveys required for detailed mapping of the galactic plane and for an all-sky survey for galactic and extragalactic objects.

REFERENCES

- Altenhoff, W. J., Downes, D., Goad, L., Maxwell, A., and Rinehart, R., 1970. *Astr. and Ap. Suppl.*, 1: 319.
- Emerson, J. P., Jennings, R. E. and Moorwood, A. F. M., 1973a. *Nature (Phys. Sci.)* 241: 108.
- Emerson, J. P., Jennings, R. E., and Moorwood, A. F. M., 1973b. *Ap. J.* 184: 401.
- Goss, W. M., and Shaver, P. A., 1970. *Au. J. Phys., Ap. Suppl.*, 14: 1.
- Harper, D. A., and Low, F. J., 1971. *Ap. J. (Letters)*, 165: L9.
- Harper, D. A., and Low, F. J., 1973. *Ap. J. (Letters)*, 182: L89.
- Hoffmann, W. F., Frederick, C. L., and Emery, R. J., 1971. *Ap. J. (Letters)*, 170: L89.
- Hoffmann, W. F., Frederick, C. L., Emery, R. J., and Aannestad, P. A., 1974. To be published.

Neugebauer, G., and Leighton, R. B., 1969. NASA SP-3047
Olthof, H. 1974. To be published.
Ricker, G., Lewen, W., and Low, F. J., 1974. To be published.
Soifer, B. T., Pipher, J. L., and Houck, J. R., 1972. Ap. J., 177: 315.
Walker, R. G., and Price, S. D., 1974. To be published.

DISCUSSION SUMMARY — PAPER 1.2

It was pointed out from the floor that a collaborative investigation involving scientists from the University of Arizona and from MIT had produced a partial survey of the Milky Way. This investigation used a system with a field-of-view of $3/4$ of a degree and a sensitivity threshold of 700 to 1000 flux units at 100 microns. With this system the Milky Way appears as a bright band several degrees wide. Observations were made from south of the galactic center northward to W3. It is not known if this is radiation from a continuous emitting volume such as the interstellar dust, or if it is from unresolved discrete sources.

This was observed as well by Dr. Hoffmann when surveying the galactic plane in the vicinity of the galactic center.

The discussion continued with consideration given to the relative merits of low resolution and medium resolution surveys. Higher resolution surveys of the galactic plane are in order since the initial low resolution surveys have been performed. A survey of the entire sky can be done adequately with a field-of-view of 12 to 15 arcminutes if the number of sources expected can be resolved on the average with this field-of-view.

It was asked if any evidence had been detected of water vapor associated with the balloon. None had.

PAPER 1.3

ASTRONOMICAL OBSERVATIONS WITH THE UNIVERSITY COLLEGE
LONDON BALLOON BORNE TELESCOPER. E. Jennings
University College London

ABSTRACT

Since 1970 the U.C.L. balloon borne telescope had made fourteen flights in different parts of the world. Some of the features of the detection system used are described together with examples of the different types of astronomical observations that have been made.

INTRODUCTION

The telescope system was designed and built by the engineering group in the physics department at University College. The timing was most opportune, coming as it did just when the early observations by F.J. Low from aircraft and W.F. Hoffmann from balloons were showing the importance of making observations in the far infrared ($\sim 100\mu\text{m}$) where many objects, principally HII regions, were radiating most of their power, amounting to as much as 10^5 to 10^8 times the energy from the sun. The great advantage of the system was its ability to point, by means of a star tracker, to better than a minute of arc enabling the identifications of sources to be made with little chance of ambiguity.

All our photometric observations have used the same broad band of wavelengths, from 40 to $350\mu\text{m}$. The short wavelength 'cut on' is determined by the quartz Fabry lens and black polythene filter mounted on the base of the cryostat together with the rigidex entrance window (see Fig.2). The long wavelength limit is determined by diffraction effects. The detector used is a 1mm square gallium doped germanium bolometer (Infra-red Laboratories Inc.). The system's relative response is known from laboratory measurements in a vacuum tank using a Michelson interferometer and this is put on an absolute basis by observing a suitable planet during flight. The aperture stop most frequently used is 5 arc min.

FEATURES OF THE DETECTION SYSTEM

It is hoped that a brief mention of one or two particular features will be of interest to other experimenters.

(i) Chopping System

Two types of chop have been employed, both oscillating the secondary mirror. The mirror is supported by a phosphor bronze disc with a rod some 20 cm in length firmly attached to the back of the secondary mirror mounting. The type of chop is determined by the movement given to the further end of this rod.

A 'circular chop' has been used for a number of flights and the phase sensitive detection (P.S.D.) performed parallel to and perpendicular to the direction of scan. The resulting infra-red signals - INFRARED A and INFRARED B respectively - are shown in Fig.1, which shows the signals recorded while calibrating on Saturn.

88751 27W

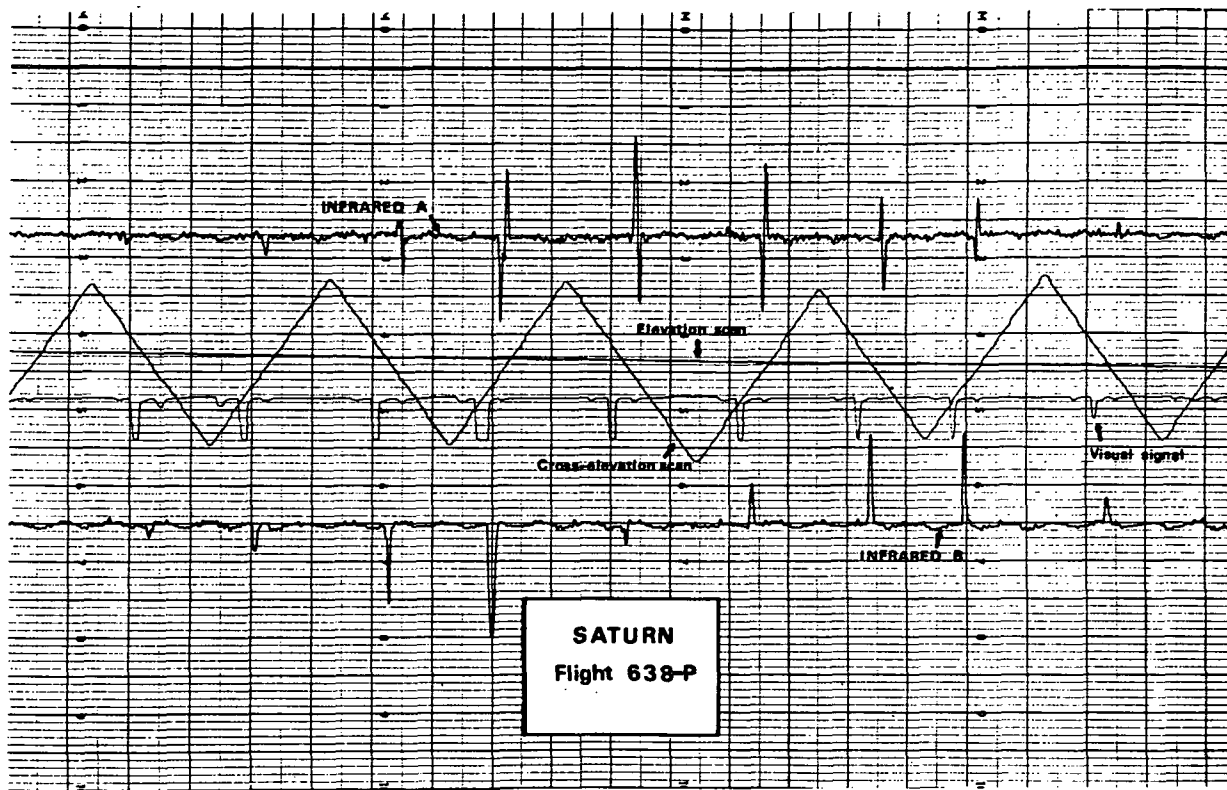


Figure 1. Signals Recorded while Calibrating System.

The star tracker is locked on to Saturn and the main telescope is being commanded to make a small raster scan about the planet. Whilst a chart record is sufficient during the flight, data on tape is used for the final analysis.

For detailed mapping of regions we prefer to use a linear chop in which the secondary is rocked from side to side (by solenoids operating on the top end of the bar). The resulting movement, as determined by a laser shining onto a mirror attached to the back of the secondary mirror, is a fair approximation to a square wave.

(ii) Importance of Phasing in Flight

We phase sensitively detect at the balloon end and find that it is important to be able to adjust the phase of the reference signal to the P.S.D. system during flight, by repeated observations of a bright object (planet). This applies particularly to the linear chop, where the optimum phase has been found to be as much as 30° different to what was thought to be the optimum on the ground - an awkward adjustment to make without special equipment.

(iii) "Red Button"

To offset residual mismatch of telescope radiations between the two parts of the chop, we make use of a simple sample and hold circuit immediately prior to the D.C. amplifiers. By command, it samples the D.C. signal immediately after the P.S.D. and applies it to the other side of the operational amplifier in the first D.C. stage.

It is called a 'Red Button' because we heard that a ground based observatory made use of such a device of that name - only to find later that they had never heard of it !

(iv) Visual Maps

The beam out of the telescope is separated into its infra-red and visual components by means of a dichroic mirror as shown in Fig.2.

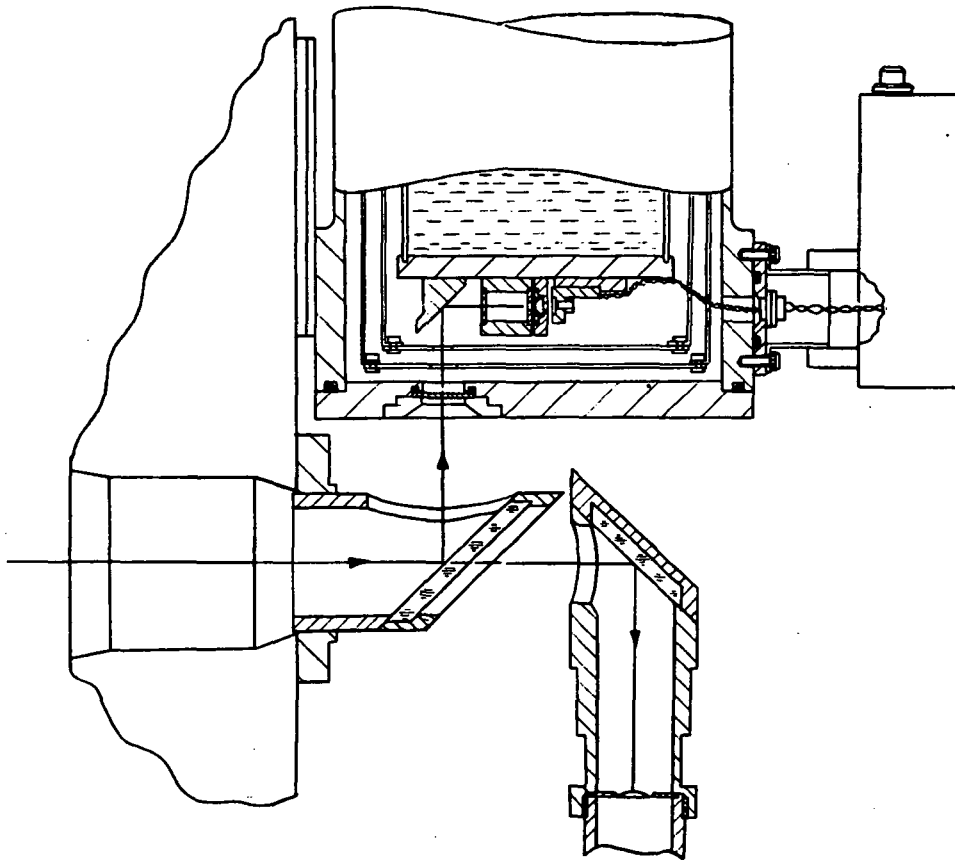


Figure 2. Dichroic mirror reflecting the infra-red beam up into the cryostat and passing the visual beam, which is then reflected into the photomultiplier.

Thus in effect an infra-red map is recorded over which can be laid the corresponding visual map. By superimposing the visual signal on the X-Y plotter, which is used to indicate the telescope position relative to the guide star, a visual map as shown in Fig.3 can be produced. In practice it is far more accurate

to use the digitised coordinates off tape when use is being made of the visual signals in the analysis. In practice better use can be made of the observing time by only scanning limited regions.

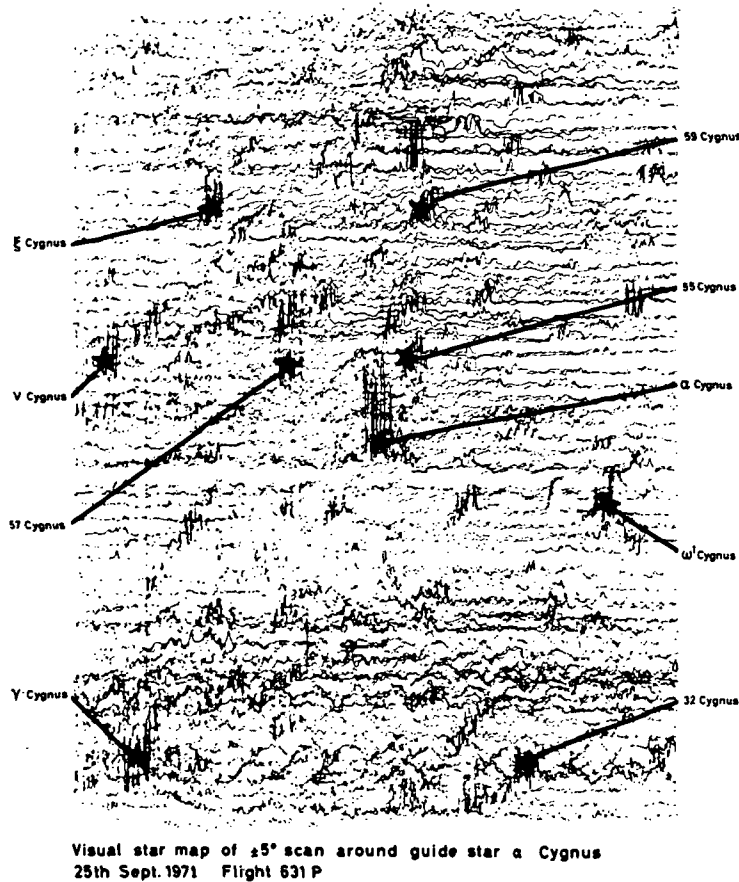


Figure 3. Visual record of stars around guide star.

OBSERVATIONS

Rather than attempting to present a comprehensive account of our observations to date, examples of the different types of measurement which have been made with the U.C.L. system will be given.

Much of our observing time has been spent in determining the far infra-red flux of HII regions known or expected to be bright in this wavelength region. Data from considerably more than fifty objects has now been obtained many of which have not previously been measured in the far infra-red. A sample of the results is shown in Fig.4. (overleaf).

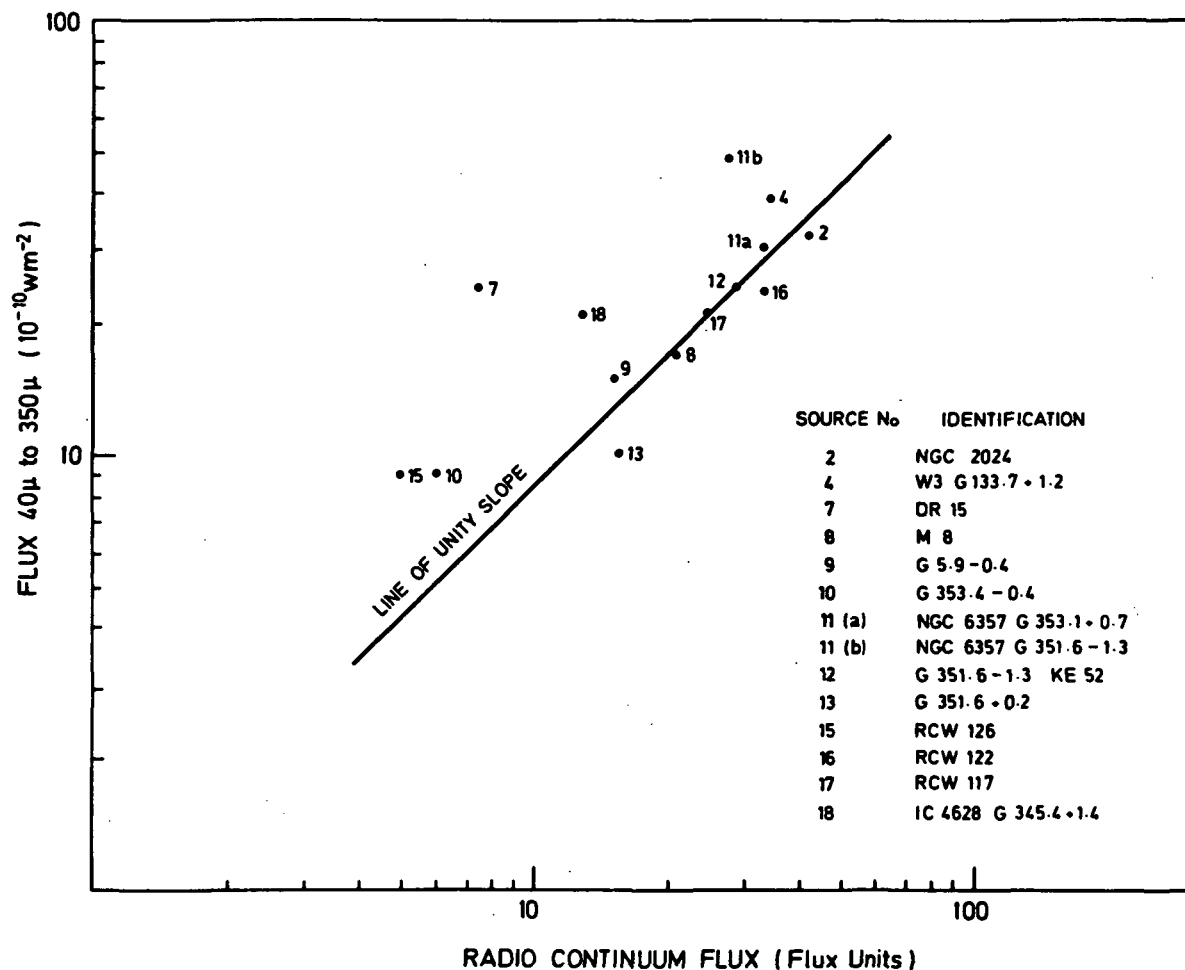


Figure 4. Plot of far infra-red flux against radio-continuum flux.

In general there is a close correlation between the infra-red flux and the radio continuum flux but there are a number of exceptions. At the present time there is considerable interest in explaining exactly what is happening in these complex regions. The far infra-red flux gives a good measure of the energy output of the exciting star(s) but the mechanism by which the radiating dust is heated is not fully understood and is the subject of a number of theoretical studies.

The half power beam width of 3.5 arc min unfortunately means that sizes can only be determined to \sim arc minutes and better angular resolution is required to decide whether or not a significant fraction of the radiation is being emitted from outside the HII region. Whilst agreement with the radio position was in all cases within 3 arc minutes it is not yet possible to say whether there is any real displacement between the centres of the infra-red and radio sources.

A second type of measurement which gives far more information is to closely scan a region so that a contour map in the infra-red can be constructed and compared with the corresponding radio map. A number of such maps have now been completed, in particular of NGC 6357 and NGC 6334, the latter being shown in Fig.5.

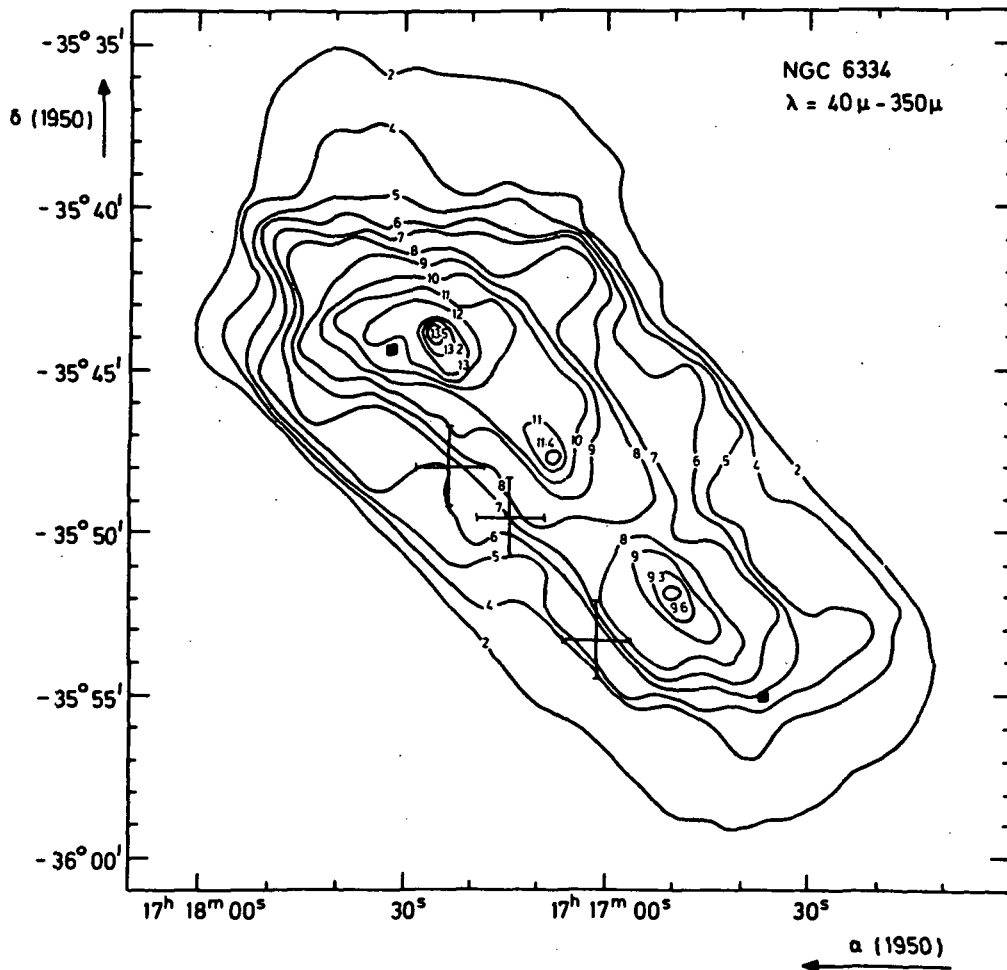


Figure 5. Far infra-red map of NGC 6334. Contour units are $2.3 \times 10^{-10} \text{ W m}^{-2}$

The three crosses marked indicate the position of the three radio peaks and, in view of the positional accuracies of the infra-red peaks and the radio peaks no special significance is attached to their relative displacement. However, no convincing correlation between them all can be obtained by adjusting their position and it appears that the brightest infra-red component corresponds to the OH maser source, whose position is marked with a square, while the other two infra-red peaks correspond to the radio sources, the central infra-red peak being double but unresolved in our beam. Confidence that this is a correct interpretation is strengthened by the immediate correlation of the radio and infra-red peaks in the case of NGC 6357 (not shown). NGC 6334 obviously requires further study but at the present time the observations could be interpreted in terms of a massive protostar to explain the northern infra-red peak.

Further details of both the photometric measurements and the infra-red maps are given in a paper by Emerson, Jennings and Moorwood 1973, which also has the relevant list of references.

Finally, we have made some preliminary spectral measurements, using a Michelson interferometer. For various reasons progress has not been as rapid as hoped but low resolution spectra have been obtained of two objects, Saturn and W51. The spectrum of Saturn is shown in Fig.6.

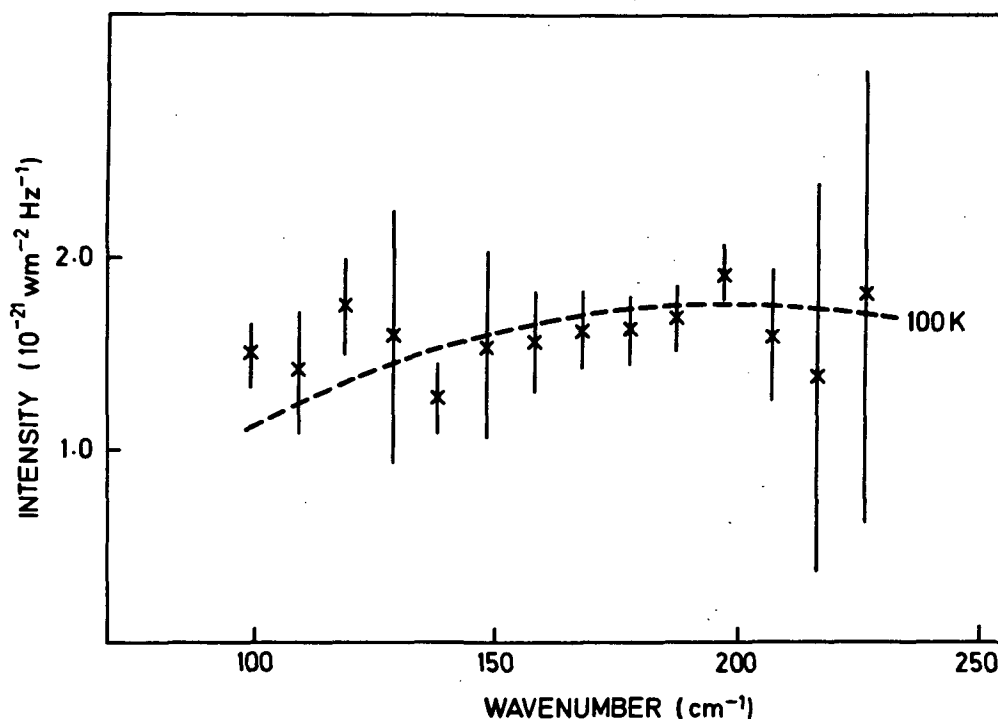


Figure 6. Spectrum of Saturn.

Saturn was not the prime object and the interferograms were obtained in nine minutes. The spectrum was calibrated photometrically with respect to Jupiter. The brightness temperature is 100K at about 100 cm^{-1} and it is of interest to note that the brightness temperature tends to increase with wavelength in this region as found by Armstrong, Harper and Low 1972. The 100K curve shown corresponds to the colour temperature which gives the best fit. The angular resolution was insufficient to separate the contribution from the disc and rings.

It is intended to continue to develop this type of instrument for spectral measurements of continuous sources and also, hopefully, to detect line emission in the far infra-red.

ACKNOWLEDGEMENTS

Professor Sir Harrie Massey initiated this programme of observations and has always taken a keen and active interest in its progress. The stabilised platform and telescope were designed and built by Dr. W.A. Towlson and Mr. T.E. Venis, together with the late Mr. Tomlinson; this group has played a major part in the overall project, keeping the system in working order and assisting on campaigns. The members of the infra-red group who have made the observations and analysed the data include Dr. A.F.M. Moorwood, together with Mr. J.P. Emerson and Dr. I. Furniss. Mr. J.A. Alvarez developed the Michelson system, operated it during flight and reduced the data. Valuable technical assistance before and during the flights was willingly provided by Mr. R.W. Catch, Mr. F. Want and Mr. A.H. Watts.

We wish to thank the N.S.F. and the personnel at the NCAR base for flying the payload for us on many occasions. This program is supported in part by a grant from the Science Research Council.

REFERENCES

- Emerson, J.P., Jennings, R.E. and Moorwood, A.F.M., 1973. Far infra-red observations of HII regions from balloon altitudes. *Ap.J.*, 184:401-414.
- Armstrong, K.R., D.A. Harper, Jr. and Low, F.J., 1972. Far infra-red brightness temperatures of the planets. *Ap.J.*, (Letters), 178:L89-L92.

08731 274

DISCUSSION SUMMARY — PAPER 1.3

The telescope was 15 inches in diameter. A beam size of five arcminutes was used and the detector NEP was 10^{-13} watts/Hz^{1/2} with a one-second integration time. Observations of Saturn using this system and an interferometer yielded a signal-to-noise ratio of about two.

PAPER 1.4

THE LIEGE-BALLOON PROGRAM

R. ZANDER

Institut d'Astrophysique - University of Liège, Belgium.

ABSTRACT

The Liège-balloon program is intended to make high-spectral resolution observations of the sun in the near- and intermediate infrared regions not accessible from the ground. A description of the equipment, followed by a summary of the data obtained till now is presented.

INTRODUCTION

Since over 20 years, Professor M. Migeotte's group of the Institute of Astrophysics of the University of Liège, has been involved in spectroscopic observations of the sun with a spectral resolution as high as possible. Most of these observations have been done at the International Scientific Station of the Jungfrauoch, located in the Swiss Alps, at 3580 m altitude.

Despite high-mountain advantages, the solar spectrum above 1.0 micron, is only partially accessible to ground observations. This situation is mainly due to the absorption of radiation by minor atmospheric constituents such as water vapor, carbon dioxide, methane, ozone, . . . , which only allow extraterrestrial infrared radiation to reach the ground in the well known atmospheric windows (1.65 ; 2.30 ; 4.6 ; 10.5 microns). Except for ozone whose maximum of concentration lies near 25 Km altitude, the residual mass distribution of the other mentioned molecules decreases with altitude. This is a self-explanatory argument for carrying out spectroscopic observations from platforms transcending the densest layers of the earth's atmosphere.

The Liège balloon equipment is primarily intended for very high-resolution solar observations from about 27-30 Km altitude, in all spectral regions between 1.5 and 15.0 microns, not accessible from the ground.

THE EQUIPMENT

Figure 1 represents the optical layout of the system.

The gimbaled plane mirror M1 directs the solar radiation within the 38.5 cm-aperture telescope of the Ritchey-Chrétien type, having an effective focal length of 6 meters ; a solar image of 56 mm diameter is produced in the focal plane S of the telescope. The central part of that image is then transferred and focussed onto the entrance slit E of the spectrometer by the mirrors M5 and M6.

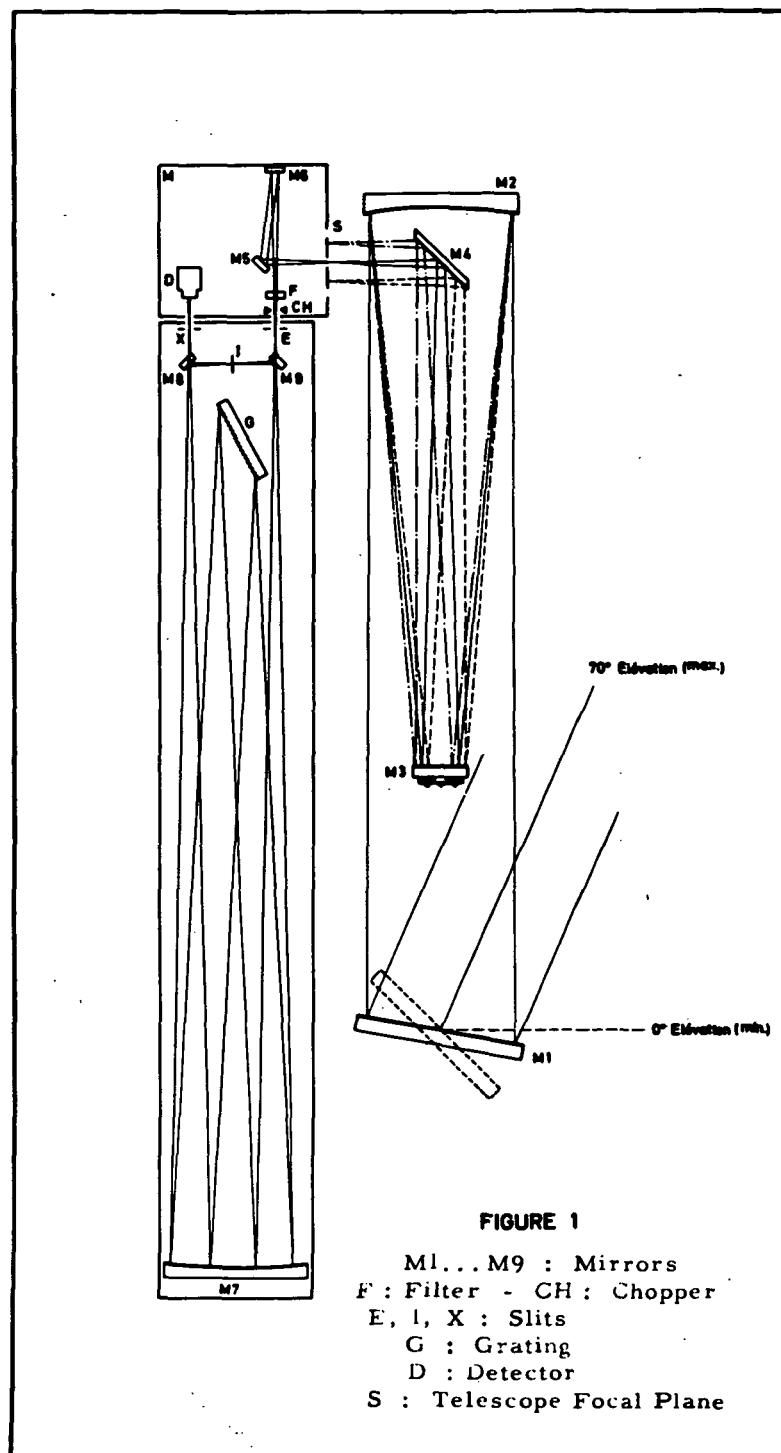


Figure 1. Optical layout of the balloon equipment.

The grating spectrometer is of the Ebert-Fastie type; the main mirror M7 is spherically shaped to a radius of curvature of 5 meters. Two different gratings G are actually available for covering the 1.5 to 15 microns region; they are Bausch and Lomb "echelle" replicas with a ruled area of 102 mm x 208 mm; their principal other characteristics are given in the following table.

	Grating No. 1 for 1.5 to 3.2 microns region	Grating No. 2 for 3.0 to 15 microns region
Rulings/mm	79.0	31.6
Blaze angle	63°26'	63°26'
Working Orders	14 to 7	18 to 4

The working order selection is obtained with a set of interference filters mounted on a filter-wheel.

All mirrors and mounts are made from light aluminium alloy, kani-gen-coated to a depth of about 0.12 mm; the optical surfaces worked in this last layer are aluminized.

In the classical single-pass configuration of a grating spectrometer, the spectrum corresponding to the radiation admitted through the entrance slit E, is formed in the focal plane of M7, after only one dispersion by the grating. The adopted double-pass configuration only requires the addition of two plane mirrors M8 and M9 and of an intermediate slit I; the real and fictitious entrance and exit slits of both passes, all lie on a circle of Fastie (Fastie and Sinton, 1954) of 11.0 cm radius. The advantages of the double-pass configuration with a narrow intermediate slit have been given elsewhere (Zander, 1970). For the 1.5 to 3.0 microns region, the double passed radiation traversing the exit slit X is focussed onto a lead sulfide cell, cooled down to -70°C by thermoelectrical effect; a second PbS detector located near and parallel to the intermediate slit I, allows to record simultaneously the spectrum in single pass. For the 3-15 microns region, a gallium doped germanium detector cooled with liquid helium, is being integrated now to our equipment.

During the scanning of a spectrum through continuous rotation of the grating, the signals detected by the cells are synchronously amplified and recorded on an on-board magnetic tape recorder; they are also transmitted to the ground by telemetry for real-time monitoring and subsequent optimisation of the equipment by telecommand.

A tungsten lamp, which can be placed temporarily in the optical path at S, is used for in-flight realignment of the spectrometer; it also allows to determine spectroscopically, the amount of water vapor inside of the equipment.

Figure 2 represents the 4.75 m-high balloon gondola which contains the optics shown in Figure 1 and all components, necessary to render the equipment automatic.

The gondola, as well as the telescope and spectrometer frames are made out of aluminium honeycomb; a crash-pad (not shown) fixed under the instrument, dissipates the energy of the vertical impact shock, when the equipment returns to the ground by parachute.

The acquisition of and guidance on the sun are reached in two steps. The first one consists to direct the aperture seen on Figure 2, towards the sun, in order for solar radiation to fall onto M1. This coarse azimuth orientation is realized to + or - 2 degrees of arc by using coarse silicon solar sensors, installed on the top of the gondola and which control the rotation of the 24 Kgs inertial wheel located in the upper part of the equipment. The second step which follows the first one with a lag time of 10 seconds, is accomplished by the mirror M1, mounted in a two-axis gimbaled system, positioned by torque motors servo-controlled by two pairs of fine solar sensors located under M3. The fine guidance accuracy is better than + or - 3 minutes of arc in azimuth and in elevation.

The total weight of the balloon equipment is approximately 1100 Kgs.

RESULTS

a. - New solar lines identifications.

Up to now, the spectral regions from 1.81 to 1.89 and from 2.46 to 2.83 microns have been recorded with a resolving power better than 0.04 cm^{-1} . H_2O in the first interval, H_2O and CO_2 in the second one, are the molecules responsible for almost all the telluric absorption observed in these regions.

Figure 3 shows a sample of the original unfiltered data, as recorded between 1.841 (5431 cm^{-1}) and 1.847 microns (5413 cm^{-1}), in single pass (trace A, resolving power $\sim 30,000$) and in double pass (trace B, resolving power $\sim 150,000$).

The distinction between telluric and Fraunhofer lines is only possible on trace B, the atmospheric lines being, in our case, narrower than the solar ones. This first discrimination is very important in the regions of telluric absorption where, until recently, only very scarce informations were available for the identification of new observed solar features.

Biémont and Grevesse (1973) have undertaken systematic theoretical calculations of the wavelengths and transition probabilities of atomic lines, between 1 and 25 microns; their already published results concern the following elements : LiI, BeI and BeII, BI, CI, NI, OI, NaI, MgI and MgII, AlI and AlII, SiI and SiII, PI and PII, SI, KI, CaI and CaII ; more than 100 new solar lines have already been identified.

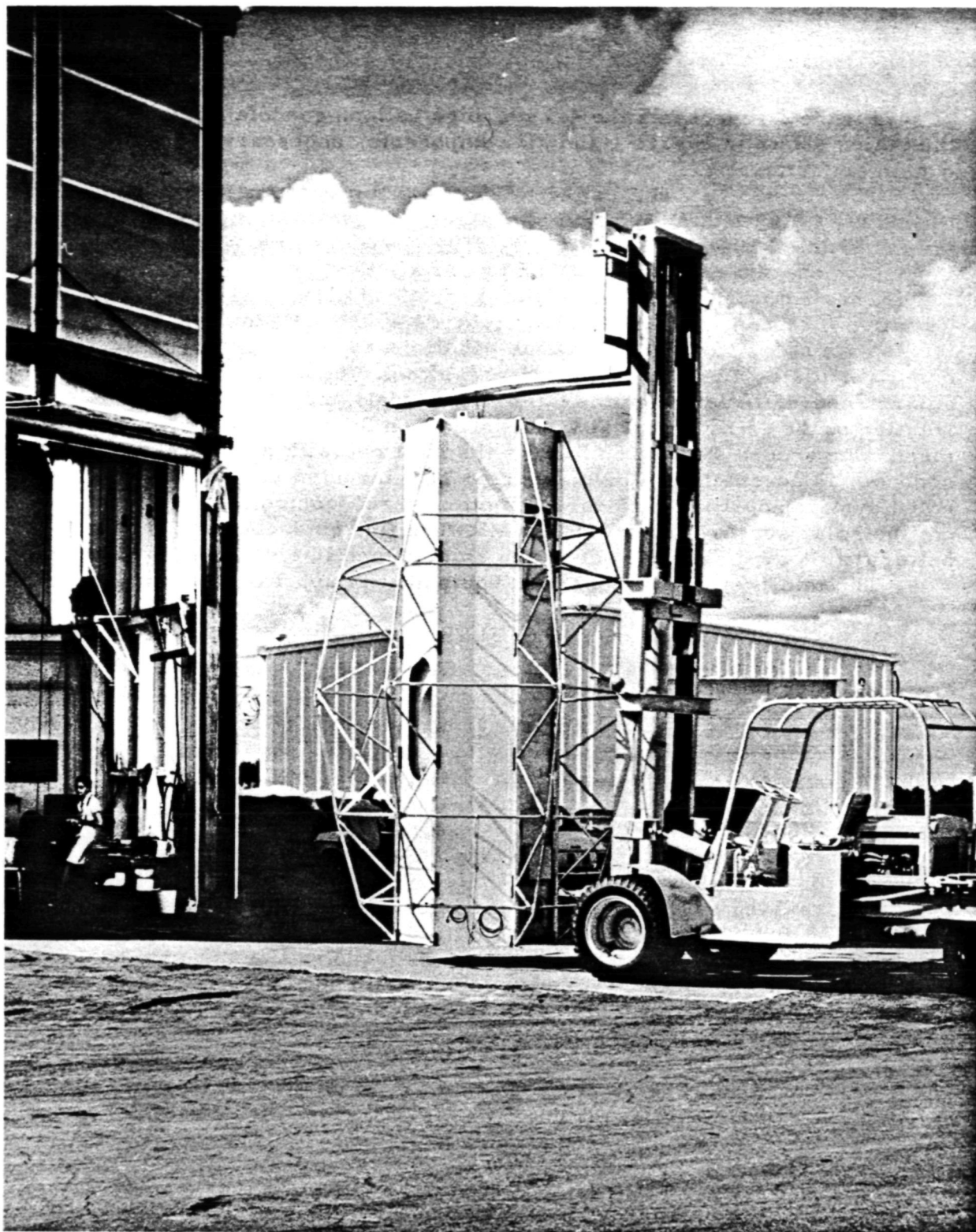


Figure 2. Balloon gondola with protective frames

REPRODUCIBILITY OF THE
ORIGINAL PAGE IS POOR

1.4-5
30

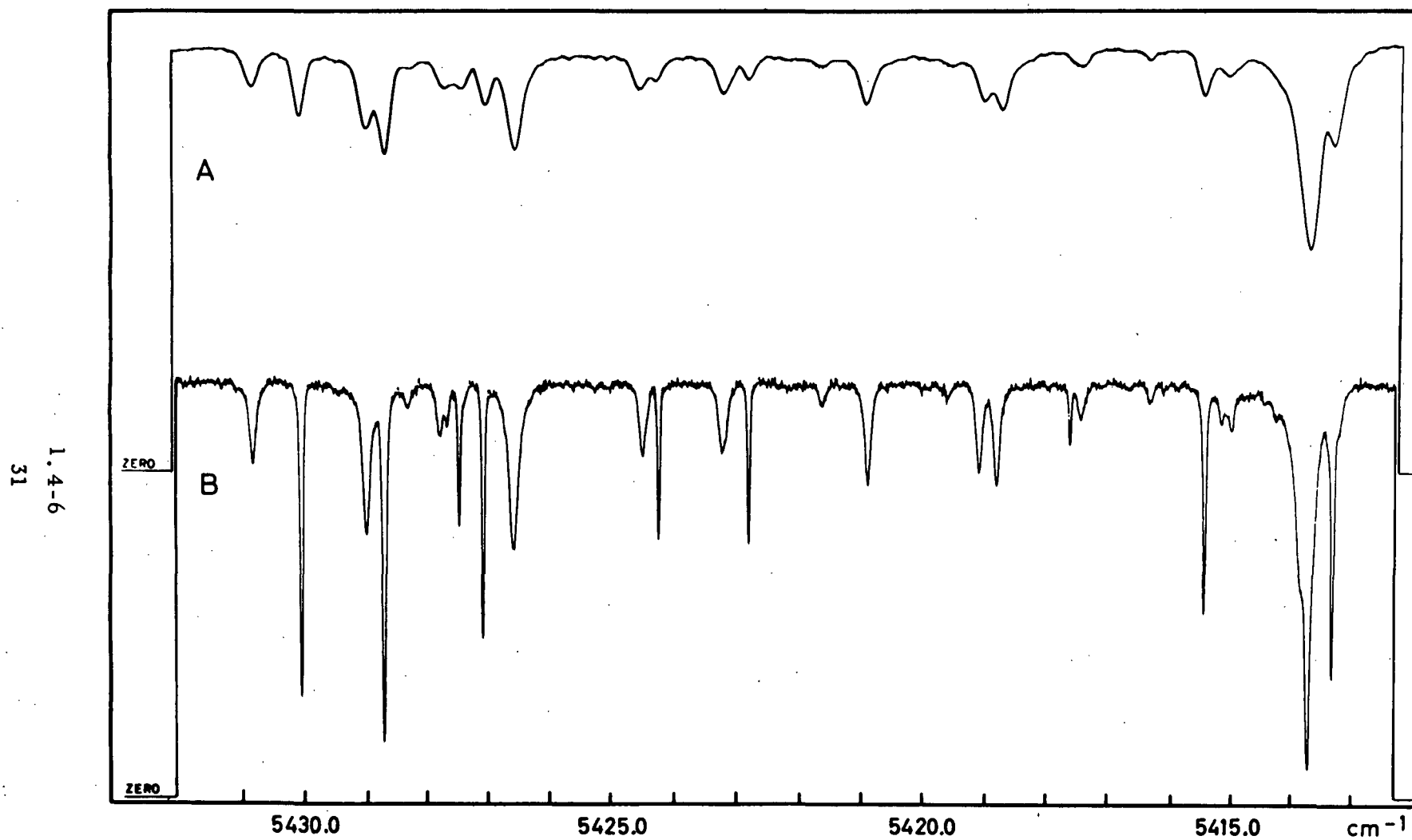


Figure 3. Sample data recorded in single pass (trace A) and in double pass (trace B).

Extensive molecular lines studies have been undertaken by A. Sauval (1972) and predictions are available for the intermediate infrared domain. The interest of infrared solar observations towards longer wavelengths λ arises from the fact that the opacity increases roughly as λ^2 , which means that the continuum will originate from higher and higher layers in the solar atmosphere.

We expect to have soon good quality solar spectra in the 5 - 15 microns region (and later on up to 25 microns) in order to determine, whether or not, weak absorption lines are still present at such wavelengths. If they could be detected, these lines would allow to determine physical conditions in the upper layers of the solar photosphere.

b. - H_2O and CO_2 in the upper stratosphere.

The telluric absorption features present on the solar tracings are useful by-products of our observations.

There remains, indeed, a need for qualitative informations about the chemical composition of the upper stratosphere; concentrations and distributions, above 25 Km, of minor constituents such as H_2O , CO_2 , CH_4 , NO_2 , N_2O , HNO_3 , ..., remain one exploratory aspect of our balloon program.

The major difficulty encountered when studying the telluric H_2O concentration in the stratosphere is a consequence of the desorption at altitude, of the humidity adsorbed by the equipment during the launch preparation (Mastenbrook, 1964 ; Zander, 1966).

At the occasion of our last flights, using the on-board tungsten lamp as a source of radiation, sample spectra have been recorded regularly and H_2O amounts present in the equipment were then deduced. Subtracting these amounts from the quantities of H_2O derived from water vapor absorption lines present on the solar recordings, has allowed us to deduce data concerning telluric H_2O above float level. The results have already been given elsewhere (Zander, 1973); important conclusions are :

1. - the rate of water vapor desorption by the equipment varies approximately as the inverse of the square root of the local pressure.
2. - the H_2O concentration above 25 Km altitude lies in the range $(3.5 \pm 1.5) \times 10^{-6} \text{ gg}^{-1}$. All our data as well as those obtained by other investigators having taken the contamination effect into consideration, can be "bracketed" as shown in Figure 4; they are in favor of a "dry" stratosphere.
3. - the amount of moisture per meter optical path inside of the equipment, is approximately equal to 0.25 microns ppt H_2O at 25 Km altitude.

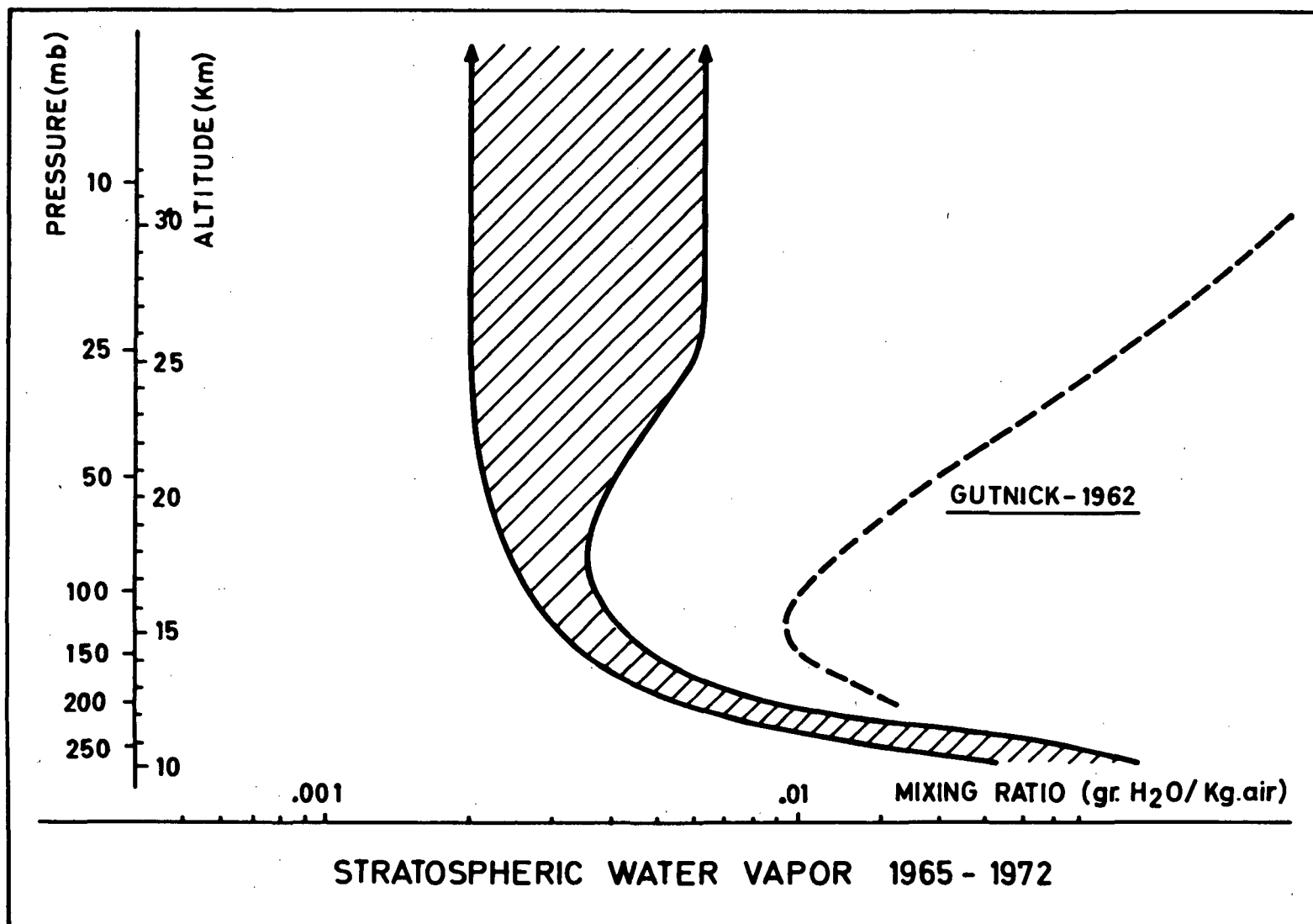


Figure 4. Most realistic range of H₂O-mixing ratio.

The telluric absorption between 2.65 and 2.80 microns is mainly due to CO_2 . A line by line analysis of the P and R branches of the strong $00^{\circ}0 \rightarrow 10^{\circ}1$ band of CO_2 has been carried out for values of the quantum number J between 0 and 60. Using the line intensities given by Gates and Benedict (1966), we have deduced the relative variations of the line half-widths γ_0 versus J, assuming γ_0 to be equal to 0.075 cm^{-1} for $20 < J < 35$; the results are given in Figure 5. If one assumes the telluric CO_2 -mixing ratio to be constant throughout the stratosphere, and equal to 330 ppmv, then the γ_0 -values for $J > 20$ have to be much smaller, of the order of 0.050 cm^{-1} ; such low values have never been reported in earlier CO_2 investigations.

A final conclusion concerning the carbon dioxide concentration in the upper stratosphere has to await further laboratory measurements on CO_2 line half-widths.

Financial supports of the ballon program have been provided by the belgian government and by the Air Force Cambridge Research Laboratory, Bedford, Mass., U.S.A., Contract No. AFOSR-72-2317.

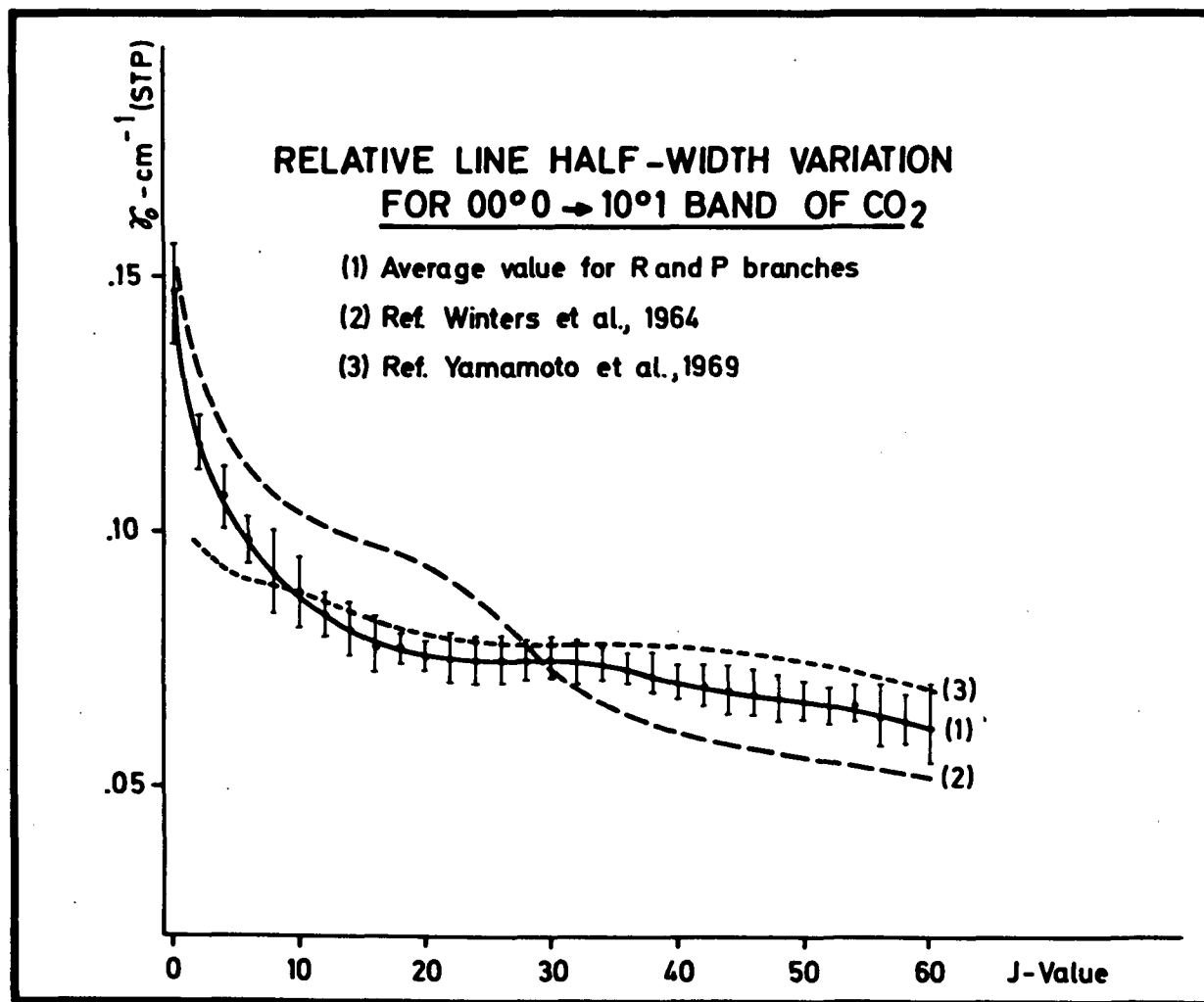


Figure 5. Relative line half-width variation of carbon dioxide.

REFERENCES

- Biémont, E., and N. Grevesse, 1973, Raies atomiques dans l'infrarouge; Soc. Royale Sci. Liège, Nos. 7-8, 307 p.
- Calfee, R. F., and W. S. Benedict, 1966, Carbon dioxide spectral line positions and intensities calculated for the 2.05 and 2.7 micron regions; Technical Note No. 332, National Bureau of Standards.
- Fastie, W. G., and W. M. Sinton, 1954, Multiple diffraction in grating spectroscopy; J. O. S. A., 44, No. 2, 103 p.
- Mastenbrook, H. J., 1964, Frost-point hygrometer measurements in the stratosphere and the problem of moisture contamination; in Humidity and Moisture, Vol. 2, edited by E. J. Amdur, Reinhold Publishing Corp., New-York, p. 480.
- Sauval, A. J., 1972, Contribution à l'étude des molécules dans le soleil; Ph. D. Thesis, University of Liège.
- Winters, B. H., S. Silverman, and W. S. Benedict, 1964, Line shape in the wing beyond the band head of the 4.3μ band of CO_2 ; J. Quant. Spectrosc. Radiat. Transfer, 4, 527 p.
- Yamamoto, G., M. Tanaka, and T. Aoki, 1969, Estimation of rotational line widths of carbon dioxide bands; J. Quant. Spectrosc. Radiat. Transfer, 9, 371 p.
- Zander, R.
- 1966, Moisture contamination at altitude by balloon and associated equipment, J. Geophys. Res., 71, No. 15, 3775 p.
 - 1970, Observations, par ballon stratosphérique, du spectre solaire à 1,85 microns avec un pouvoir de résolution de 135.000; Acad. Royale de Belgique, Cl. Sci., 5e série, 7, 729 p.
 - 1973, Water vapor above 25 Km altitude; PAGEOP, 106-108, 1346 p.

DISCUSSION SUMMARY — PAPER 1.4

This system weighs a thousand kilograms. It is stabilized in azimuth to plus or minus two degrees using signals from silicon solar cells. Reaction is provided by a 24-kilogram fly wheel. Final pointing accuracy of plus or minus two arcminutes is achieved using a heliostat at the entrance to the telescope.

Two gratings are used in this system. Each is 102 mm by 208 mm, and has a blaze angle of $63^{\circ}26'$. There are 72.25 rulings per millimeter on the grating used for the 1.5 to 3 micron range. For the 3 to 15 micron range a grating with 31.6 rulings per millimeter is used. Observations have been made between 1.81 and 1.89 microns and between 2.46 and 2.83 microns.

Observations are planned for the 2.3 to 3.3 micron range and for the 5 to 10 micron range. This will allow solar observations to reach higher levels in the photosphere. In addition observations of HNO_3 , CH_4 , and N_2O in the telluric atmosphere will be possible.

A BALLOON-BORNE 1-METER TELESCOPE FOR FAR-INFRARED ASTRONOMY

G. G. Fazio
D. E. Kleinmann
R. W. Noyes
E. L. Wright

Center for Astrophysics
Harvard College Observatory and Smithsonian Astrophysical Observatory
Cambridge, Massachusetts 02138

and

F. J. Low
Lunar and Planetary Laboratory
University of Arizona, Tucson, Arizona 85721

ABSTRACT

The Harvard College Observatory, the Smithsonian Astrophysical Observatory, and the University of Arizona have been engaged in a cooperative program to develop a balloon-borne 1-m telescope for infrared astronomy in the wavelength interval 40 to 250 μ . The first successful flight of the telescope occurred in February, 1974 from Palestine, Texas. During 5.5 hr at float altitude, the gyro-stabilized telescope mapped the intensity of far-infrared radiation from NGC 7538, Mars, the Orion Nebula, and W3 with a resolution of 1' and from selected regions of these sources with a resolution of 30". Use of an N-slit photometer and a star-field camera will permit absolute positions of the sources to be determined to $\leq 30''$. Numerous weak sources were also observed.

The infrared detection system consisted of an array of four gallium-doped germanium bolometers cooled to 1.8 K. Preliminary results indicate that sources with an intensity of 10^3 f.u. were easily detectable.

This paper is concerned primarily with the description of the 1-m telescope and its instrumentation, orientation system, and modes of observation.

INTRODUCTION

In early 1971, a group of scientists at the Harvard College Observatory (HCO) and the Smithsonian Astrophysical Observatory (SAO) initiated a new research program in the promising field of far-infrared astronomy. The primary observational instrument was to be a balloon-borne telescope that could accomplish unique measurements with at least an order-of-magnitude increase in sensitivity and angular resolution over previous experiments in aircraft and high-altitude balloons. The University of Arizona agreed to collaborate and contributed the primary and secondary mirrors and the infrared detectors. Thus, a 1-m balloon-borne far-infrared telescope was designed and constructed that was capable of high-resolution ($\leq 1'$) mapping in the 40- to 250- μ region and of absolute position determination to $\leq 30''$, with at least a factor-of-10 increase in sensitivity ($\leq 10^3$ f.u.) over previous experiments.

INSTRUMENTATION

Telescope Optics

Figure 1 shows the optical arrangement of the f/13.5 Cassegrain telescope. The 1-m primary mirror is spherical (f/2) and constructed of an aluminum alloy, and the 18-cm secondary mirror, made of pyrex, is figured to match the primary mirror. The Cassegrain focus occurs behind the primary mirror, yielding a scale in the focal plane of 15"/mm. At a wavelength of 100 μ , the diffraction limit of the telescope is 25". Forward of the focal plane, the infrared beam is reflected by a dichroic

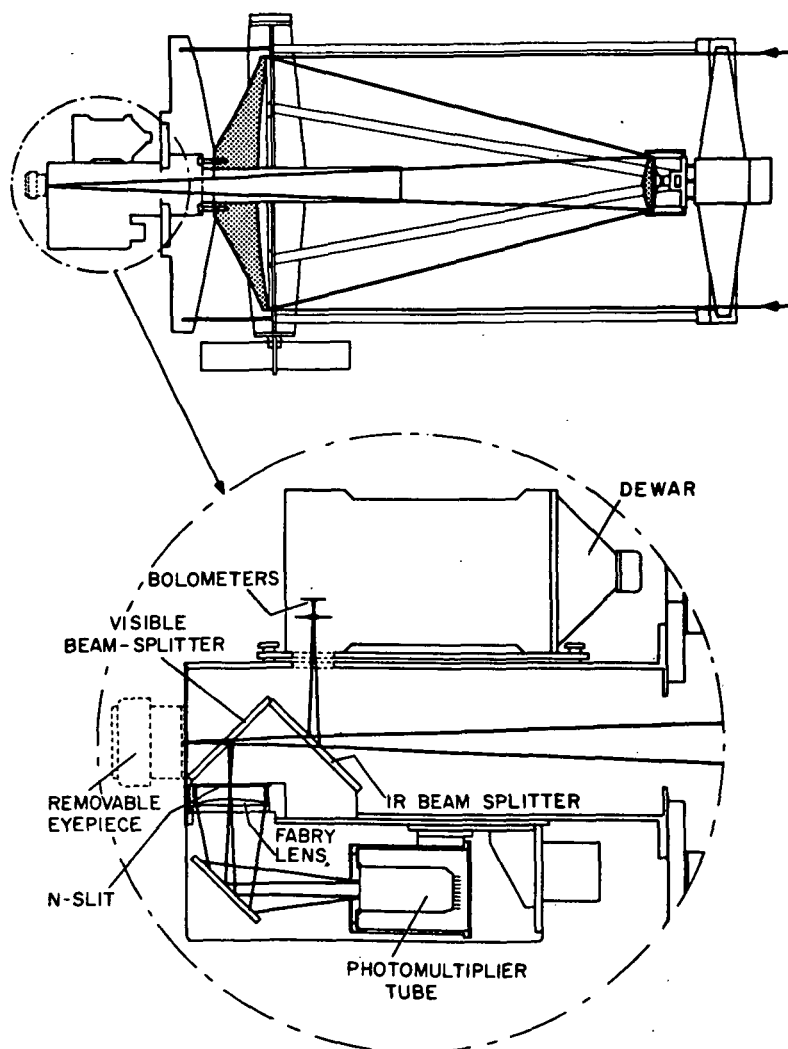


Figure 1. Optical arrangement of the 1-m telescope.

beam splitter that passes visible light. A second beam splitter directs half the optical light onto an N-slit mask at a second focal plane. Light passing through the mask is focused onto a photomultiplier tube. A removable eyepiece, mounted in the focal plane behind the second beam splitter, serves to aid in the optical alignment

and testing of the telescope. The secondary mirror is mounted by means of a central bolt to a solenoid-driven chopper mechanism that causes the mirror to oscillate in the azimuthal direction in a square-wave motion of 20-Hz frequency. This beam-switching technique cancels out the background radiation from the sky and the mirror by subtracting the contribution from two fields of view separated by 5'. The chopper mechanism is further mounted on a commandable-focus drive. The whole secondary system is supported by four sheet-metal spiders to the external support ring and then through conventional tubular trusses to the central telescope ring. The weight of the telescope assembly out to the elevation axis, including optics and instrumentation, is ~400 kg.

Infrared Detectors

The infrared detection system consists of four gallium-doped germanium bolometers, cooled to 1.8 K in a liquid helium dewar vented to ambient atmospheric pressure. The ambient pressure at the flight altitude of 29 km is 10.5 torr. As shown in Figure 2, three of the detectors are arranged in a linear array, with each subtending an angle of 1.5 in elevation by 1' in azimuth; the fourth detector, with a circular field of 0.5, is located immediately adjacent to the central detector in the linear

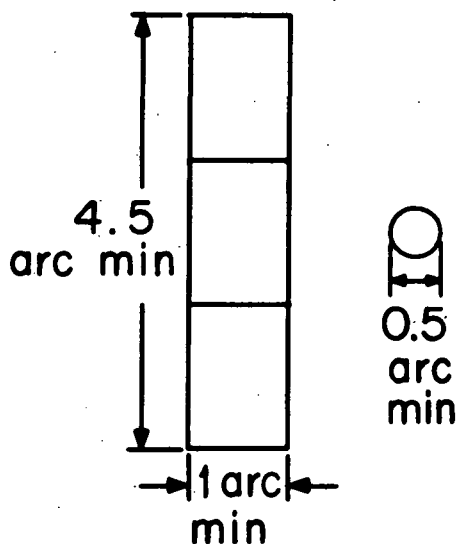


Figure 2. Arrangement of the infrared-detector beams.

array. The cooled optics, all at 1.8 K, consists of a sandwich of 0.86-mm crystalline quartz and 1-mm calcium fluoride with one surface coated with diamond dust plus four silicon field lenses. The field of view in the sky is determined by the aperture of the silicon lenses. All the cooled elements are antireflection-coated for maximum transmission at 65 μ . The dewar vacuum window, of 1-mm high-density polyethylene, is coated on the inner surface with diamond dust to reject radiation less than 5 μ and is at a temperature of ~250 K. The passband of the system has a sharp cuton at 40 μ , a peak transmission at 65 μ , and a long wavelength cutoff defined primarily by diffraction. For the three larger detectors, this cutoff is ~250 μ ; for the small detector, it is ~125 μ .

Each of the four bolometer signals is amplified by an AC-coupled voltage pre-amplifier, with a gain of 10^3 , followed by postamplifiers with gains of 0.5, 10, and

30. The 12 signal lines are then connected directly to the telemetry system through teflon coaxial cables. The signals are digitized at a sampling rate of 128 s^{-1} and transmitted to the ground station by PCM telemetry. Phase-sensitive demodulation and further processing are done at the ground station by using the telemetered chopper-coil current signal as a phase reference. The onboard signal amplifiers are made immune to external electrical noise by individual batteries and by ground isolation from the gondola.

ORIENTATION OF THE TELESCOPE

Stabilization

The telescope is mounted in a rectangular aluminum-frame gondola (Figures 3 and 4) 5.1 m high and 3.4×2.9 m wide. The entire system weighs approximately 1814 kg. Of primary importance are the heavy structural elements used throughout the central portion of the gondola to maintain the integrity of the telescope tube, the elevation and azimuth axes, and the payload electronics. The telescope is stabilized and pointed by means of positional servo controls on the elevation and azimuth axes. The entire gondola moves in azimuth, but the telescope motion in the elevation direction is with respect to the gondola frame. The driving element for each axis is a DC torque motor mounted directly on the axis without gearing. In elevation, the reaction mass is the main frame of the suspended gondola. Reaction forces for the azimuth position control are provided by a large reaction wheel mounted on the gondola center line below the telescope. Complications are introduced, however, by the needs to control the reaction-wheel speed and to isolate the gondola from random and rapid balloon rotations. These needs are met through the use of a "momentum dump" device — a bearing, supporting the shaft passing up to the balloon, whose outer race is driven in sinusoidal excursions of about 2° at a frequency of 5 Hz. Under normal conditions, this motion is symmetrical and yields no net torque, nor momentum transfer, to the balloon, thereby providing some isolation of the payload. If, however, energy accumulates in the reaction wheel so that its angular velocity exceeds 1 rad s^{-1} , the sinusoidal bearing drive is proportionally biased to permit momentum transfer to the balloon. This enables the reaction wheel to slow to a near-zero control speed.

Pointing and Acquisition

Positioning the telescope optical line of sight is accomplished in two modes: first, an acquisition mode, determined with respect to the horizontal component of the earth's magnetic field in azimuth and with respect to the local vertical in elevation, to an accuracy of 0.1° ; and second, an inertial mode, determined by a two-axis gyroscope system mounted on the telescope tube, which gives stability in inertial space to $\sim 1'$. For the acquisition mode, a null magnetometer is mounted on a table and servo-driven in azimuth so as to remain fixed to local magnetic north. The angular position of the magnetometer with respect to the gondola is determined by a 13-bit shaft encoder (smallest bit equals 2.6°). An azimuth position command, in the form of a digital word, is transmitted to the gondola and stored in an onboard register. The encoder output is compared with the stored azimuth position command, and the difference signal drives the azimuth servo system. The azimuth position stability is $\sim 6'$. In the elevation axis, the telescope angle referenced to the gondola is determined by a potentiometer and compared with the analog equivalent of a 12-bit elevation



Figure 3. Payload just before launch.

1.5-5

REPRODUCIBILITY OF THE
ORIGINAL PAGE IS POOR

command stored in another register. As in azimuth, the difference is used to drive the servo motor. The smallest bit in elevation is $1/3$, and the stability is of the order of $1'$.

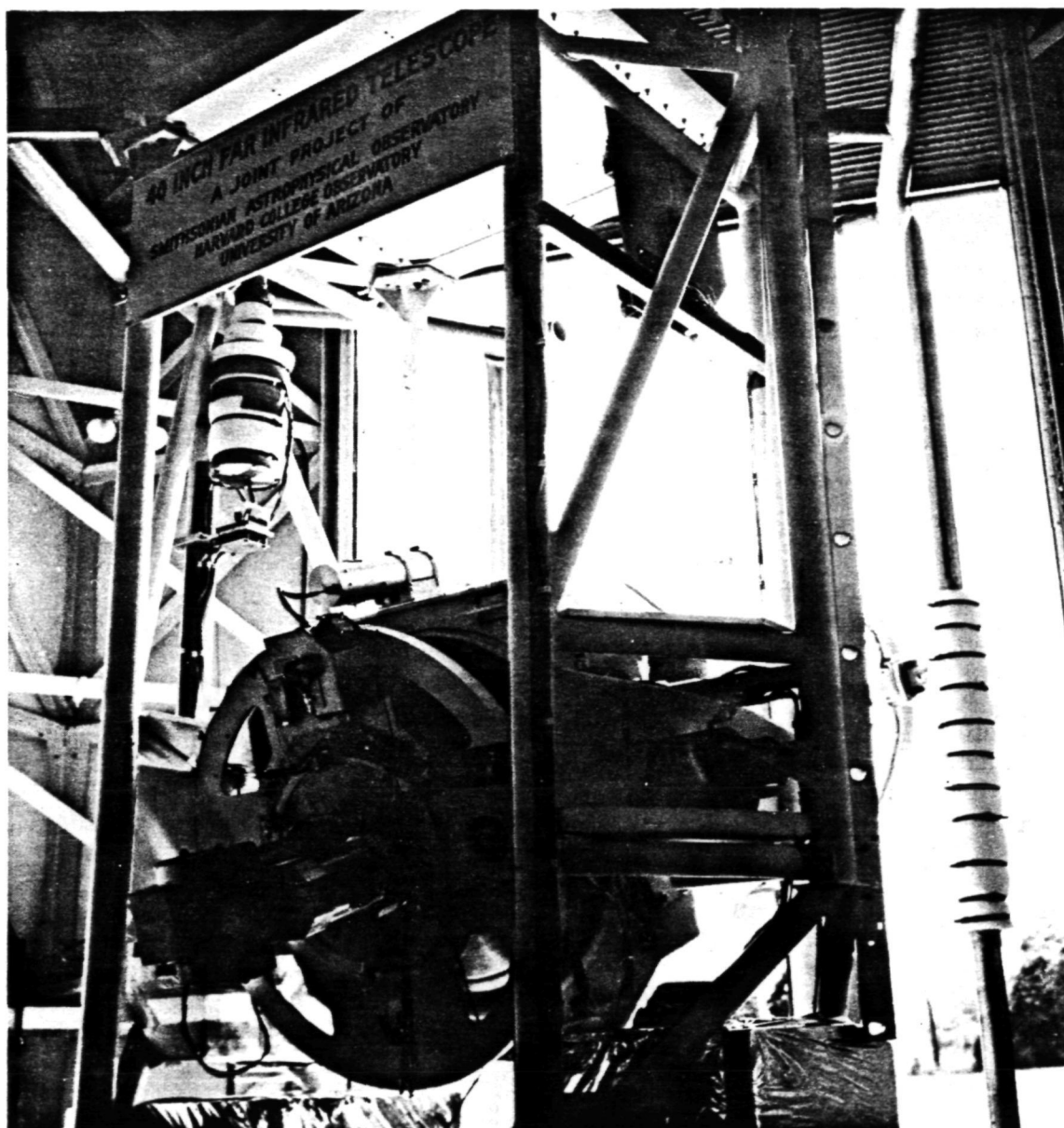


Figure 4. Back assembly of the payload.

To avoid major perturbations in the acquisition pointing mode, the rate of change of position is limited to 0.5 s^{-1} .

In the inertial pointing mode, position information is obtained from two rate-integrating gyros mounted on the telescope base ring. One senses motions about the elevation axis directly, while the other senses motions about an axis perpendicular to both the elevation axis and the telescope line of sight. In combination with a

potentiometer-derived secant function of the elevation angle, this latter output controls the gondola azimuth. At higher elevation angles, the "azimuth" gyro becomes increasingly sensitive to gondola motion about the roll axis, and this places a maximum limit on the useful elevation angle of about 35° . The gyros have random drift rates of the order of $3' \text{ hr}^{-1}$; however, the present electronic circuitry has limited the drift rate to the order of $\sim 0.5 \text{ min}^{-1}$. A much larger drift rate in azimuth was observed during the flight.

By exciting torquing coils on the gyro axes, the gyros can be precessed, and when they are coupled to the pointing control system, controls can, in effect, be imposed on angular rates in azimuth and elevation on the telescope. Provision has been made for "manual" scan rates of $\pm 1' \text{ s}^{-1}$ about both axes; these rates are selected independently from the ground with durations controlled by the operator in real time. Further, and most important, an onboard raster-pattern generator can be commanded to control the gyro torquers so as to produce a raster-like scan of the telescope over a large field of view. Two sizes of raster patterns, each with 32 lines per pattern, are available by command: One set has a line scan rate of $1' \text{ s}^{-1}$ and $2:25$ spacing between lines, yielding a scanned field of about $30'$ in azimuth and 1° in elevation in about 18 min; the second set has the above values multiplied by a factor of 3, yielding a $1:5 \times 3^\circ$ field in the same time. The raster scan can be aborted at any time.

OBSERVATIONAL TECHNIQUES DURING FLIGHT

During the payload flight, the observational method consists of a series of operations performed in turn for each object to be observed. First, the expected azimuth and elevation positions for the object are computed on the ground for an appropriate future time and given payload latitude and longitude. An HP9810A programmable calculator computes the magnetic deviation and applies corrections from the magnetic azimuth and elevation calibrations. The printed output contains the azimuth and elevation commands to be executed, as well as the expected values of the elevation position potentiometer and the output voltages from a crossed pair of magnetometers on the payload. The azimuth and elevation commands are telemetered in advance to the payload, which, on receipt of an "execute" command, moves the telescope slowly to the desired position and maintains it. At the predetermined time, the gyros are uncaged, activating the inertial mode; the telescope then tracks the point in the sky to which it has been positioned. In most cases, the desired object is not in the field of view — primarily owing to uncertainty in magnetic-azimuth position — and a search pattern must be initiated. The type of search pattern employed depends on the celestial object. For an infrared source without an associated bright object, a large raster scan is initiated. When the source is observed with the infrared detectors, the raster is aborted, the telescope is manually scanned to a new position, and a small raster is initiated to remap the object. If no object is found, the raster goes through 10 lines and then is aborted. A new position in the acquisition mode is calculated and the above process repeated. For an infrared object that is also optically bright, the search mode involves the use of the optical N-slit with a field of $20'$; a spiral pattern is generated by manual scans in azimuth and elevation in the inertial mode until the object is found. Typically, an area 3° in azimuth and 1° in elevation can be covered in approximately 4 min. When the object is discovered, the telescope is repositioned and a small raster pattern is initiated. Again, if no object is discovered, the spiral scan is stopped after three azimuth scans and the position reacquired in the acquisition mode.

When an infrared object is being mapped with the telescope in the inertial mode, it is extremely important to know, in real time, the relative position of the telescope axis with respect to the object. Otherwise, valuable time can be lost if it is assumed that the telescope is carrying out a given command when actually the wrong command was sent or the command was not received. To avoid these difficulties, a series of payload-status lights, actuated only by commands received and executed by the payload, are displayed at the ground station. They indicate such functions as inertial mode, azimuth or elevation direction, rastering, and direction of raster line. In addition, the same signals drive an X-Y recorder, which displays the motion of the telescope. Superimposed on the Y axis of the recorder is the output of the N-slit photometer (Figure 5). By observing the X-Y recorder, the telescope can be positioned for mapping by rasters.

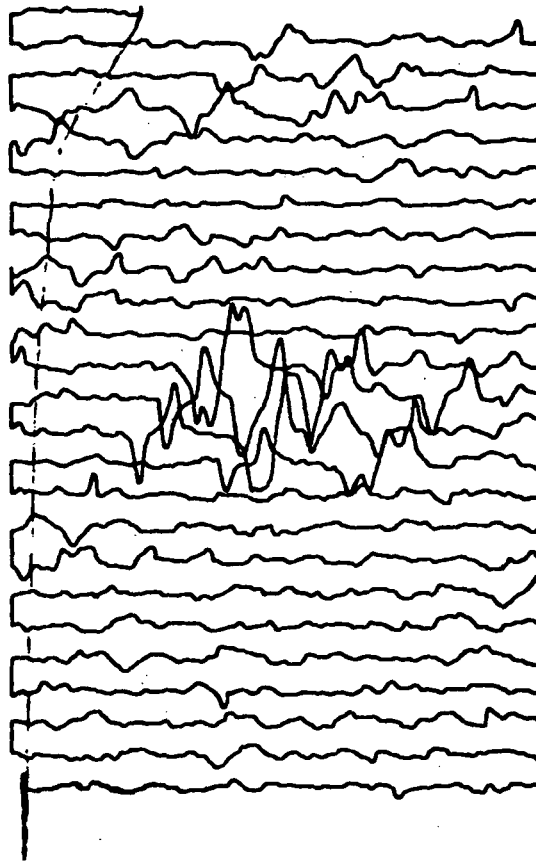


Figure 5. X-Y recorder output during a large raster scan of the telescope. The output of the N-slit optical photometer is added in the Y direction.

A number of other means are also available for calculating the position of the telescope. Some provide data for real-time determination, others, a postflight record.

The pointing control system generates telemetry readouts of the elevation and azimuth positions: In elevation it is an analog voltage, and in azimuth it is an analog voltage indicating the difference between the commanded position and the instantaneous pointed position. Both these readouts provide a sensitivity sufficient to monitor fine-pointing control performance.

An additional determination of magnetic azimuth is provided by a pair of crossed magnetometers mounted on the gondola.

The most useful device for fine-position determination is the N-slit photometer, discussed earlier. Star transits across the three branches of the N mask, telemetered to the ground, indicate with high precision the elevation and azimuth of the optical object with respect to the star field during scanning activities. The photometer output is AC-coupled to reduce its sensitivity to scattered light. The photometer is effective for stars down to 9th magnitude.

An independent device for postflight pointing verification is the star-field camera, a 35-mm-sequence camera mounted on the telescope, which provides an effective field of view of about 15°. The camera photographs star images and records a projected reticle pattern, along with data indicating frame number, time, and status of the payload. In addition to taking pictures on command from the ground, the camera is automatically triggered during the various payload scanning functions.

BACKUP CONTROL SYSTEM

In the event of failure of one or more major systems in the primary operation of the telescope pointing, a simple backup control system can be activated by tone commands. This system serves two functions: automatic stow of the telescope and crude pointing control of the telescope in azimuth and elevation.

The telescope is normally stowed by commanding it to point vertically, placing it in a position such that a commandable motor-driven pin can capture a lug mounted on the telescope for this purpose. Should this primary technique fail owing to loss of battery power or to excessive telemetry range, an independent system, after a preset time and on descent through a particular altitude, will engage the elevation axis and drive the telescope to the vertical position by utilizing its own battery power. In doing so, it also turns off the main payload. Associated with this is a pneumatically actuated capture device that, although locked out during launch, will thereafter retain the telescope in the vertical position on its descent through 9.2-km altitude.

If the primary azimuth or elevation command servo systems should fail, an independent system can be actuated to drive the telescope in elevation by using the same motor as in the emergency stow procedure described above. An independent elevation potentiometer is also provided. The motion in azimuth is achieved by directly driving the motor in the momentum-dump system in either direction. Azimuth position is determined from the cross magnetometers and the N-slit photometer.

POWER, TELEMETRY AND TELECOMMAND

The main power for the payload (except for the telemetry and telecommand systems) is supplied by a silver zinc battery pack with a capacity of 400 amp hr, loaned by NASA Johnson Space Center. The nominal voltage is 28.5 V. With all systems operating, the battery current varies between 17 and 20 amp.

The telemetry system, provided by the National Scientific Balloon Facility (NSBF), consisted of a PCM system with 48 analog inputs and 4 digital words and a bit rate of 40.96 kbits s⁻¹. After decommutation at the ground station, the data were processed by a PDP-11 computer and digitally recorded on tape. Real-time output of the data could also be obtained on a teletypewriter, where all analog and digital words could be printed in sequence or selected words could be printed on command. Thirty digital-to-analog converters were also available. Any 4 of the 12 infrared data lines from the digital-to-analog converters could be switch-selected, processed by the phase-sensitive amplifiers, and displayed on a strip-chart recorder.

Thirteen analog channels of FM/FM telemetry also provide redundancy for the most important data.

The telecommand equipment, supplied by NSBF, comprises a PCM command system, of which 30 momentary commands are used. Because of the number of commands required for this payload, the PCM system is used to address and execute commands within a more elaborate command matrix in the payload. Seven tone commands are also employed.

TESTING AND FLIGHT HISTORY OF THE PAYLOAD

Design of the 1-m telescope began in August 1971, funded from the internal budgets of SAO and HCO, with the hope that the equipment would be ready for flight in a year. Payload construction was completed in August 1972, and the experiment was moved to the NSBF in Palestine, Texas. Operational testing, payload debugging, and other improvements continued into October, at which time the first flight took place. However, it failed shortly after reaching float altitude owing to a short circuit on one of the principal voltage reference lines, probably caused by a spiral metal chip.

A second flight, in April 1973, also failed, this time before reaching float altitude. The failure again occurred in the electronic systems because of a shorted transistor in the elevation motor drive system.

Following the second failure, extensive payload refurbishment was undertaken, particularly in the electronics system, from July through September 1973. Thermal-vacuum tests of the entire payload were then conducted, with assistance from NASA Johnson Space Center. Three simulated flights were performed, by matching temperature and pressure profiles of an actual flight as closely as possible. During the tests, a 3' infrared source was positioned in the chamber, and one wall of the chamber was cooled to 70 K.

The thermal-vacuum tests offered many benefits at relatively low cost. First, the payload design was qualified under conditions it was to experience in flight. Second, valuable data were obtained on the infrared detection system. The sensitivities of the detectors were measured and the noise background evaluated. Third, the differing thermal environments of the three tests provided enough data to allow us to cope with the expected seasonal atmospheric variations for flight at any time of the year. Fourth, the tests gave us the opportunity to build up operational experience with the payload while virtually eliminating any chance of damage that might occur during actual flight and recovery.

A third flight was launched in December 1973, but the balloon burst during ascent. The telescope was stowed while the parachute descended and was recovered with no damage to the payload. For the brief period of ascent, all systems appeared to function properly.

The fourth flight, in February 1974, was a complete success. After an ascent of 2 hr to 28.4 km, the flight lasted 5.5 hr, limited only by telemetry range. The payload was recovered without damage.

PRELIMINARY SCIENTIFIC RESULTS

The data from the February flight are still in an early stage of analysis. However, some preliminary results can be quoted from real-time records.

During the 5.5 hr at float altitude, data were obtained that will permit the generation of infrared maps of NGC 7538, Mars, Orion A, and W3. Angular resolution of 1' was achieved for these maps, and selected scans were accurate to 30" resolution

(Figure 6). The sensitivity was such that sources with an intensity of 10^3 f.u. are easily identifiable. Scans along the galactic plane indicated numerous weak sources. The number of stars detected in the N-slit photometer are sufficient for absolute positions of the infrared sources to be determined.

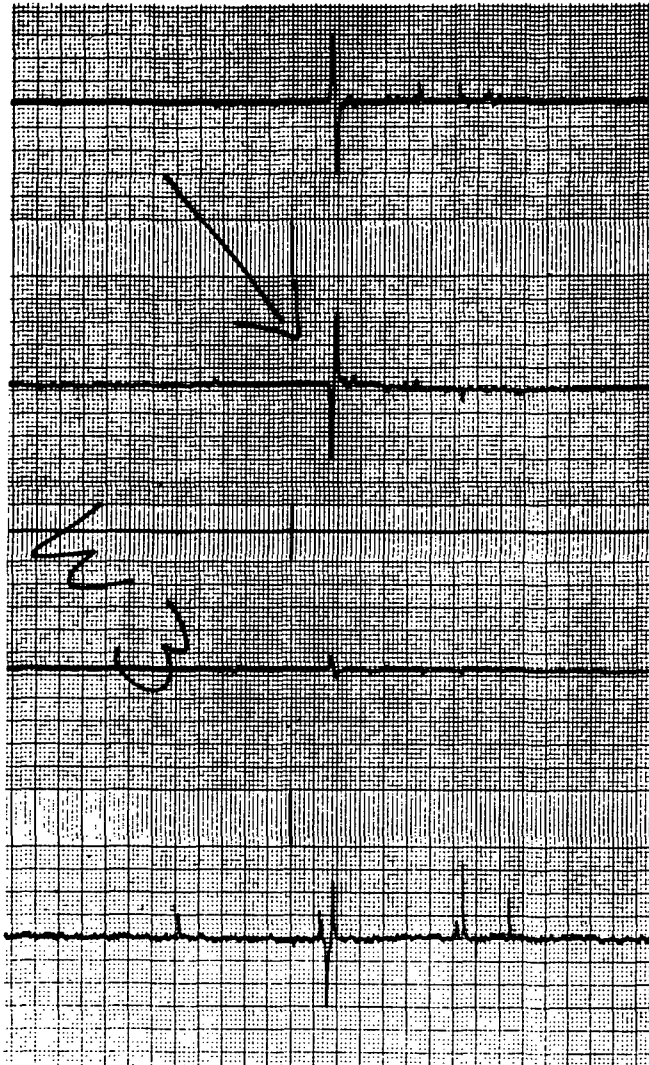


Figure 6. Infrared detector outputs during a raster scan of W3. The top three traces are from the 1' detectors; the bottom trace is from the 30'' detector. The chart speed was 0.5 mm s^{-1} , and the telescope scan rate, $3' \text{ s}^{-1}$ in azimuth.

The pointing stability of the payload was excellent during the flight.

ACKNOWLEDGMENTS

The payload was designed and constructed by the Solar Satellite Engineering Group, Harvard College Observatory. Details of the payload attitude and command control systems are presented in a paper at this symposium by N. Hazen, L. Coyle, and S. Diamond.

M. Zeilik assisted in the flight preparation.

We had several very valuable suggestions on payload design and construction from Dr. W. Hoffman, University of Arizona.

We are most grateful to NASA Johnson Space Center, Space Environment Test Division and, in particular, to Mr. E. E. Peck, for assistance in the thermal-vacuum tests.

The National Scientific Balloon Facility was responsible for the launch, tracking, and recovery of the experiment and contributed all the onboard telemetry, as well as the data-processing equipment at the ground station. Without their assistance, this flight would have been impossible.

This work was supported in part by funds from the National Aeronautics and Space Administration under grant NGR 22-007-270.

DISCUSSION SUMMARY — PAPER 1.5

It is expected that it will be possible to fly this system two to four flights each year. There is very little damage to the system on landing. Most of the impact is taken by aluminum rings around the system. They have not experienced misalignment of the gimbals. In order to avoid fouling of motors and bearings, these parts are disassembled and cleaned after each flight. This is the most time-consuming task between launches.

Telemetry is provided by the NCAR system available at Palestine. It provides 48 analog words and four digital words at a 40 kilobit rate. A 350-mile telemetry range has been realized. In addition, the NCAR PDP-11 computer is used to provide digital tapes of the data.

Telescope suspension is through a universal joint to the momentum dump system which includes ball bearings. Stabilization in two axes instead of three was used as a cost savings approach. No problems are encountered for observations below 40° ; at 40° oscillations in roll set in.

The primary mirror provided by the University of Arizona is aluminum and weighs 250 pounds. It has a one-arcsecond image when warm and a 15-arcsecond image when cold.

MULTICOLOUR FAR INFRARED PHOTOMETRY OF GALACTIC HII REGIONS

Henk Olthof
Kapteyn Astronomical Institute
Department of Space Research
University of Groningen

ABSTRACT

Results are presented of far infrared photometric measurements of HII regions in the galactic plane between longitudes 350 and 40 degrees. The results are combined from balloon flights in 1972 and 1973 carried out in cooperation with CNES in the south of France.

INTRODUCTION

The far infrared survey by Hoffmann et al (1971) has shown that a large fraction of the 100μ sources can be identified with galactic HII regions in which strong visual absorption is present. Presumably the dust component in these regions reradiates the absorbed high energy photons from the exciting sources in the infrared thermal region of the electromagnetic spectrum.

The temperature of the dust grains is determined by the energy density in the radiation field, by the absorption efficiency of visual and ultraviolet photons and by the behaviour of the grain emissivity in the infrared.

After the survey by Hoffmann et al (1971) much work has been done on the observations of galactic HII regions in different infrared wavelength bands. A survey of most of the recent observations can be found in the review paper by Wynn-Williams et al (1973).

Our aim was to observe HII regions in two wavelength bands simultaneously. The ratio of the observed fluxes in both wavelength bands is a function of the temperature and emissivity of the dust grains.

INSTRUMENTATION

The photometers consist of multiple reststrahlen reflection filters at pumped liquid helium temperature followed by gallium doped germanium bolometers (Wijnbergen et al 1972). Two filter-detector combinations are located at the cold plate of a helium dewar. Each photometer is fed by a 20 cm parabolic reflective f/5 telescope observing off-axis. Both telescopes are mounted vertically in a balloon gondola and are looking outward via a rocking flat mirror. A 26 degrees rotation of the flat mirror around a horizontal axis driven by a stepper motor allows to scan the sky in elevation while the gondola is oriented in a southern direction by means of a servo control system that senses the local horizontal earth magnetic vector as positional reference. The stability of the servo system is about 0.5 degree. The sidereal motion gives rise to a series of scans at different hour-angles. The off-set of the magnetic sensor can be changed in both directions on ground command, thus allowing repeated observations of the same celestial area during a single flight. The

The cooled aperture stop restricts the full field of view on the sky to 30 arc.min. Flight altitude is 4.7 mbar.

CALIBRATION

The final experimental result obtained in photometric observations is dependent on the calibration of the instrument. Absolute calibration is usually hard to achieve. In infrared astronomy planets have been used most often as in-flight calibration standards. A comparison of the infrared signal as observed from the planet yields the observed energy provided that the output of the planet in the appropriate wavelength range is known. To check the consistency of the results an attempt has been made to calibrate the photometers in the laboratory. A vacuum collimator and a thermostated black body have been used to determine the output of the photometer in the relevant wavelength bands. A fit of the laboratory calibration with the observations of Jupiter in the two bands gives a brightness temperature of 140 ± 5 K for this planet. This value is in good agreement with the results of Aumann et al (1969) and Armstrong et al (1972) and will be used in the further analysis of the data.

The noise equivalent flux densities as observed during the flights was of the order of $2 \times 10^{-22} \text{ Wm}^{-2}\text{Hz}^{-1}$. This corresponds to a detector noise-equivalent-power of $2 \times 10^{-12} \text{ WHz}^{-1}$ which is considerably higher than might be expected from the detector specifications and the background photon shot noise contributions. We attribute the excess noise to the effects of mechanically driven parts in the gondola.

OBSERVATIONS

The results reported here have been obtained during flights on June 6, 1972, June 7, 16 and July 2, 1973 from the Tallard balloon launch facility operated by French Space Research Organisation C.N.E.S. The performance of the balloon gondola was satisfactory with the exception of the occurrence of oscillatory motions both in azimuth and elevation. The character and amplitude of this motion varied during flight. Reduction of the observed signals to intensity distribution on the sky is complicated by these residual oscillations.

During each flight observations have been made in two wavelength bands simultaneously. The wavelength bands we have flown up to now are shown in table 1.

Table 1.

flight	wavelength bands	
1972	71 - 95 μ	84 - 130 μ
1973 I	71 - 95 μ	30 - 38 μ
1973 II	71 - 95 μ	114 - 196 μ
1973 III	111 - 154 μ	30 - 38 μ

The transmission characteristics of these bands have been published earlier by Wijnbergen et al (1972).

In the data reduction proces each signal that is clearly

distinguishable from the noise is coded according to its amplitude. Using the position information from the scanning mirror, the azimuth error from the servo system, the time recorded simultaneously with the photometer output and the position of the gondola as obtained during flight, each coded signal is transformed to its celestial coordinates. Only those sources that show up on at least 5 successive scans have been analysed. For some sources the number of scans are as high as 100. Due to residual pointing errors the signals attributed to the same source, show variation of amplitude in different scans. The errors quoted in the final results take these uncertainties into account.

Flight 1972. Due to identification problems some numbers given by Olthof and van Duinen (1973) are wrong. A re-analysis of these data has shown that we did not observe M17. It is now clear that this source was outside our scanned area. Also the signals identified with W31 and W33 have been mixed up. As a result the number given for the 84-130 μ band for W31 was too high and the number given for W33 was too low. The results of this flight based on the re-analysis have been included in tables 2 and 3.

Flight 1973 I. Due to problems with the low noise amplifier data for the 30-38 μ band were unreliable for 2/3 of the flight. Only in the last part of the flight this channel has given reliable results for M17 and Jupiter. Fortunately this did not influence the observations in the 71-95 μ band.

Flight 1973 II. A flight without problems. During this flight Jupiter has been observed at elevations 17 and 27 degrees above the horizon to determine residual atmospheric absorption at balloon altitudes. At each elevation several scans through Jupiter have been made. In both cases the mean signal amplitude was the same within the 10% r.m.s. error.

Flight 1973 III. Due to degradation of the system only the strongest sources could be observed.

Results of the above four flights are given in tables 2 and 3. Table 2 gives the observed flux ratio to Jupiter. During all flights Jupiter has been observed for calibration. For the 71-95 μ band an average has been taken for the flights during which this filter was included. The same has been done for the observation of M17 in the 30-38 μ band. Table 3 gives the observations converted to W_m-2 using a black body temperature of 140 K for Jupiter.

DISCUSSION

Hoffmann et al (1971) have observed most of the sources in the wavelength band from 80 to 135 μ with a balloon gondola using a differential beam switching technique, while Soifer et al (1972) have observed NGC 6357 and M8 with a cooled rocket telescope using full field chopping.

In general our results are a factor of 3 higher than the results obtained by Hoffmann et al with a 0.2 degree beam. We are tempted to conclude that the surface brightness distribution is generally peaked with an extended background. This conclusion is supported by the observation of Soifer et al of NGC 6357 which shows this source to be extended while Hoffmann et al classify this object as two point sources.

Table 2

Observed flux ratio with respect to Jupiter

Sources	gal. coord.	30-38 μ	71-95 μ	84-130 μ	111-154 μ	114-196 μ
NGC 6334	351.4 + 0.7		0.44 \pm 0.05	0.65 \pm 0.06	0.59 \pm 0.11	0.56 \pm 0.14
" 6357	353.1 + 0.7		0.28 \pm 0.04	0.40 \pm 0.07	0.38 \pm 0.07	0.38 \pm 0.13
" 6383	355.2 + 0.1		0.07 \pm 0.01			0.19 \pm 0.07
63.2-0.5	3.2 - 0.5		0.05 \pm 0.01			0.13 \pm 0.02
M8	6.0 - 1.2		0.11 \pm 0.02	0.12 \pm 0.02		0.13 \pm 0.02
W30	8.5 - 0.3		0.07 \pm 0.02	0.12 \pm 0.03		0.13 \pm 0.02
W31	10.3 - 0.1		0.12 \pm 0.02	0.15 \pm 0.03		0.19 \pm 0.06
W33	13.2 + 0.0		0.15 \pm 0.02	0.24 \pm 0.04		0.25 \pm 0.07
M17	15.1 - 0.7	0.22 \pm 0.04	0.53 \pm 0.07		0.59 \pm 0.11	0.56 \pm 0.14
M16	17.0 + 0.8		0.12 \pm 0.02			0.19 \pm 0.07
W35	18.5 + 1.9		0.07 \pm 0.01			0.13 \pm 0.06
W39	19.1 - 0.3		0.08 \pm 0.03			0.13 \pm 0.06
W41	22.8 - 0.3		0.08 \pm 0.02			0.19 \pm 0.07
W42	25.4 - 0.2		0.08 \pm 0.03			0.19 \pm 0.07
W43	30.8 + 0.0		0.15 \pm 0.03			0.25 \pm 0.07
W44	34.3 + 0.1		0.06 \pm 0.01			0.19 \pm 0.07
W40	28.8 + 3.5		0.10 \pm 0.02			0.19 \pm 0.07

1.6-4
54

Table 3

Deduced mean fluxes based on $T_{BB}(\text{Jup}) = 140 \text{ K}$ in
units of 10^{-9} W m^{-2}

Source	30 -38 μ	71-95 μ	84-130 μ	111-154 μ	114-196 μ
NGC 6334		4.80 \pm 0.55	6.20 \pm 0.55	2.30 \pm 0.45	2.75 \pm 0.70
" 6357		3.05 \pm 0.45	3.80 \pm 0.65	1.50 \pm 0.30	1.85 \pm 0.60
" 6383		0.75 \pm 0.10			0.95 \pm 0.35
63.2 - 0.5		0.55 \pm 0.10			0.65 \pm 0.10
M8		1.20 \pm 0.20	1.15 \pm 0.20		0.65 \pm 0.10
W30		0.75 \pm 0.20	1.15 \pm 0.30		0.65 \pm 0.15
W31		1.30 \pm 0.20	1.45 \pm 0.30		0.95 \pm 0.30
W33		1.65 \pm 0.20	2.30 \pm 0.40		1.25 \pm 0.35
M17	8.30 \pm 1.50	5.80 \pm 0.75		2.30 \pm 0.45	2.75 \pm 0.70
M16		1.30 \pm 0.20			0.95 \pm 0.35
W35		0.75 \pm 0.10			0.65 \pm 0.30
W39		0.85 \pm 0.30			0.65 \pm 0.30
W41		0.85 \pm 0.20			0.95 \pm 0.35
W42		0.85 \pm 0.30			0.95 \pm 0.35
W43		1.65 \pm 0.30			1.25 \pm 0.35
W44		0.65 \pm 0.10			0.95 \pm 0.35
W40		1.10 \pm 0.20			0.95 \pm 0.35

ACKNOWLEDGEMENTS

These results would not have been obtained without the laborious work, skillfully performed by the technical staff of our department. They actually did the job.

This program is supported by the Dutch commission on Geophysics and Space Research of the Royal Academy of Sciences.

REFERENCES

- Armstrong, K.R., Harper, D.A., Low, F.J. 1972, *Astrophys.J.Letters* 178, L89
Aumann, H.H., Gillespie, C.M., Low, F.J. 1969, *ibid* 157, L67
Hoffmann, W.F., Frederick, C.L., Emery, R.J. 1971, *ibid* 170, L89
Olthof, H., Van Duinen, R.J. 1973, *Astron. and Astrophys.* 29, 315
Soifer, B.T., Pipher, J.L., Houck, J.R. 1972, *Astrophys.J.* 177, 315
Wijnbergen, J.J., Moolenaar, W.H., De Groot, G. 1972, *Proc. 5th ESLAB/ESRIN Symp. on infrared detection techniques for space research*, Ed. V. Manno, J. Ring. Publ. Reidel
Wynn-Williams, C.G., Becklin, E.E. 1973, preprint, to be published in *P.A.S.P.*

SAVSI 27M

DISCUSSION SUMMARY — PAPER 1.6

These flights were made at the French balloon launch facility. In June it is possible to obtain flight durations of approximately eight hours. In the autumn near turn around times, ten-hour flights are possible. It was suggested that longer flights possible from the NCAR facility might justify the added expenses and more complicated logistics.

Observations of Jupiter were used for inflight verification of the instrument filter performance. These measurements indicated that any residual transmission outside the primary bandpass was negligible.

A sensitivity of twenty-thousand-flux units was realized with this instrument.

PAPER 2.1

DESIGN AND PERFORMANCE OF A 39cm BALLOON-BORNE TELESCOPE

H.S. Tomlinson
W.A. Towlson
T.E. Venis

Dept. of Physics & Astronomy, University College London.

ABSTRACT

The U.C.L. MkI gondola incorporates a 39cm telescope of Dall Kirkham configuration. This is stabilized to about 30 arc sec r.m.s. along its line of sight by means of a star sensor driving torque motors on the azimuth and elevation axes. Guide stars from -4 to +4 in magnitude can be used and the star sensor may be offset with respect to the telescope by up to $\pm 5^\circ$ in elevation and cross elevation to enable parts of the sky containing no suitable guide stars to be viewed. Acquisition of the guide star and setting of the offset coordinates is carried out by ground command and both may be easily changed in flight.

The instrument has been used extensively over the past three years for astronomical observations in the far infra-red and has made 13 flights to date.

INTRODUCTION

In 1969 the Physics Engineering Group at U.C.L., headed by the late H.S. Tomlinson, began the construction of a stabilized balloon-borne telescope. This was designed specifically to meet the requirements of the Infra-Red Astronomy Group under Dr. R.E. Jennings. The following is an account of the design and of the operating experience obtained with the original gondola.

DESIGN CONSIDERATIONS

Whilst a large telescope is desirable, both for reasons of sensitivity and resolution, the financial implications in terms of construction and operating costs limited us, at that time, to a telescope of around 40cm dia. At 100 μ m the diffraction limit is then about 1 arc min so that a pointing accuracy of this order has been aimed for. A simple biaxial configuration has been chosen with the telescope mounted on an elevation axis within a gondola controlled in azimuth by a motor driving against a reaction wheel. The sensor for the servo system is a star tracker attached to the telescope. This can be offset with respect to the telescope to view areas adjacent to the guide star. Since this will introduce a variable pointing error proportional to the offset angle and to the amplitude of any pendulum motion of the gondola the offset has to be limited to a maximum of $\pm 5^\circ$ in the elevation and cross elevation directions. A coarse steering mode, controlled by reference to the Earth's magnetic fields and local vertical, is provided to initially direct the star sensor at the chosen guide star.

An optical system of cassegranian form has been chosen since this enables the masses of the optical components to be conveniently distributed about the elevation axis. It has the further advantage that the final convergent beam can be directed, by means of a 45° flat, out through a hollow elevation shaft

to a focus fixed with respect to the gondola frame. This arrangement was originally adopted so that a dewar containing the liquid helium cooled bolometer used for infra-red detection could be mounted in an upright position. It has proved to be a very convenient interface between the telescope and the experimenter's equipment and is free from any major restriction on the size and weight of such equipment.

The main design parameters may be summarized as follows:

Optics:	39cm f/2 f/5.5 Dall Kirkham. 10 arc sec visible on axis image.
Control axes:	Elevation $0^{\circ} - 70^{\circ}$ Azimuth $0^{\circ} - 360^{\circ}$
Gondola:	size 1.7m x 1.4m x 2.3m height. weight 250 kg bare 500 kg flight ready M.O.I. about Azimuth axis 30 kgm^2 bare 100 kgm^2 flight Reaction wheel M.O.I. 1 kgm^2
Guidance:	coarse sensors - flux gate magnetometer + elevation angle pot. fine sensor - star tracker with offset drives.
Pointing accuracy:	coarse $\pm 0.5^{\circ}$ pk-pk. fine $\pm 1'$ pk-pk at zero offset.
Star tracker:	Allowable guide star magnitudes -4 to +4 (S11 mags). noise equivalent angle at null $> 20''$ r.m.s. error signal B.W. 10 Hz. field of view 2° dia. Offset range $\pm 5^{\circ}$ in elevation and cross elevation. Offset drive rate 0.04 to 10 arc min/sec.
Operating equipment:	temperature $+40^{\circ}$ to -60°C . pressure ambient to 2 mb.

CONSTRUCTION

The layout of the gondola is clearly seen in Fig.1. It consists of a rigid rectangular frame in which the telescope is supported by two elevation bearings, one of which houses the elevation drive motor. The main frame is suspended by the azimuth drive unit from the reaction wheel which is, in turn, suspended from the balloon via a trifilar suspension and a swivel coupling. This swivel prevents the suspension winding up and also leaks momentum through from the reaction wheel to the balloon. The main frame is surrounded by an outer protective framework of small aluminium members within which batteries, telemetry, etc. are housed. During flight protective panels, roll bars and crash pads are added as required. (Fig.2).

A section through the main frame, telescope and bearing assembly is shown in Fig.3. For ease of construction and repair, standard aluminium sections are used for the framework and the main frame is of channel sections bolted together with machined brackets. The elevation bearings are mounted in simple pin and bush gimbals so that they are self-aligning and hence not affected by distortions or inaccuracies in the main frame. An Inland T-4036 D.C. torque motor of 2.4 NM rating is used for the elevation drive.

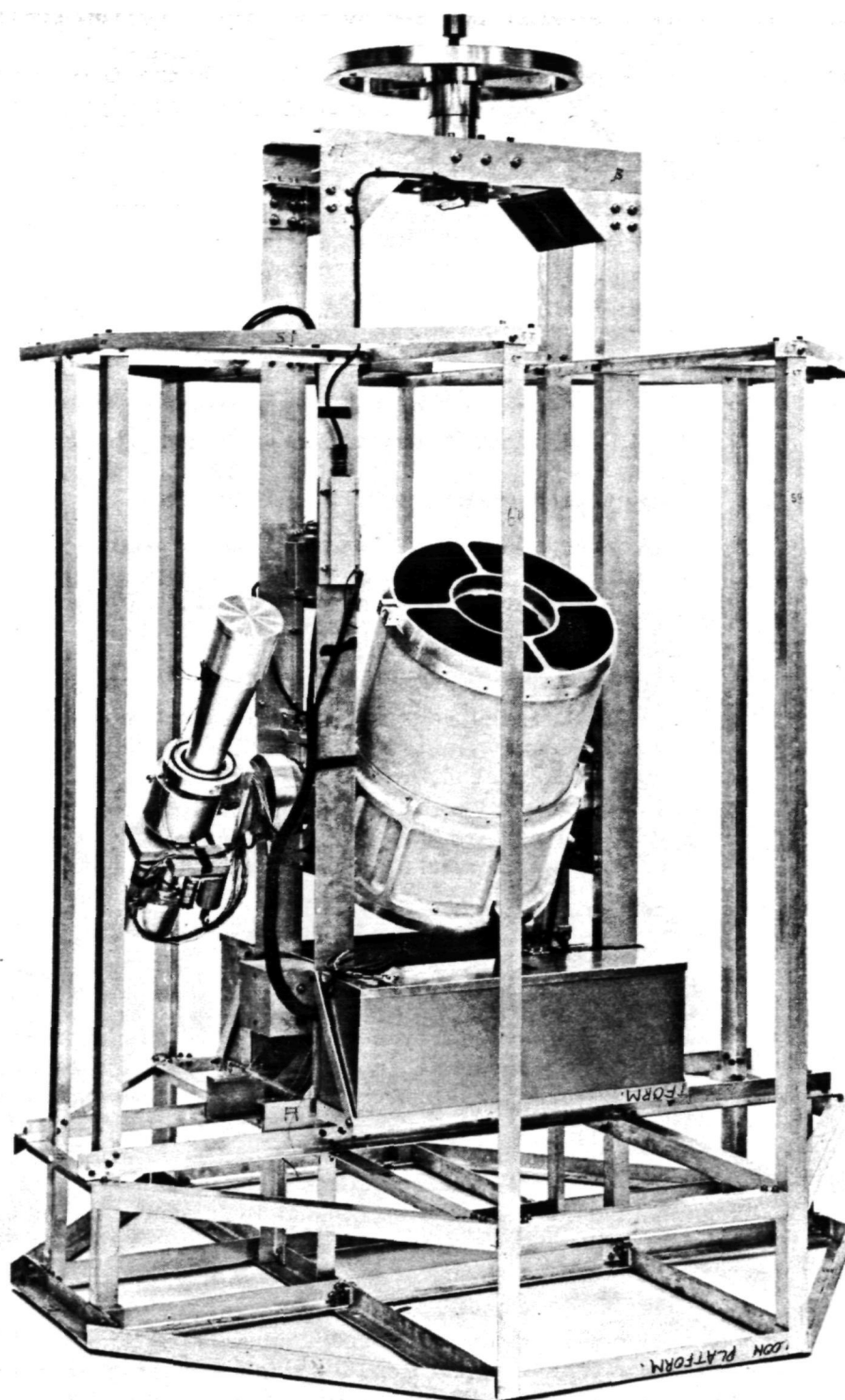


Figure 1. The telescope in the course of construction.

REPRODUCIBILITY OF THE
ORIGINAL PAGE IS POOR

2.1-3

60

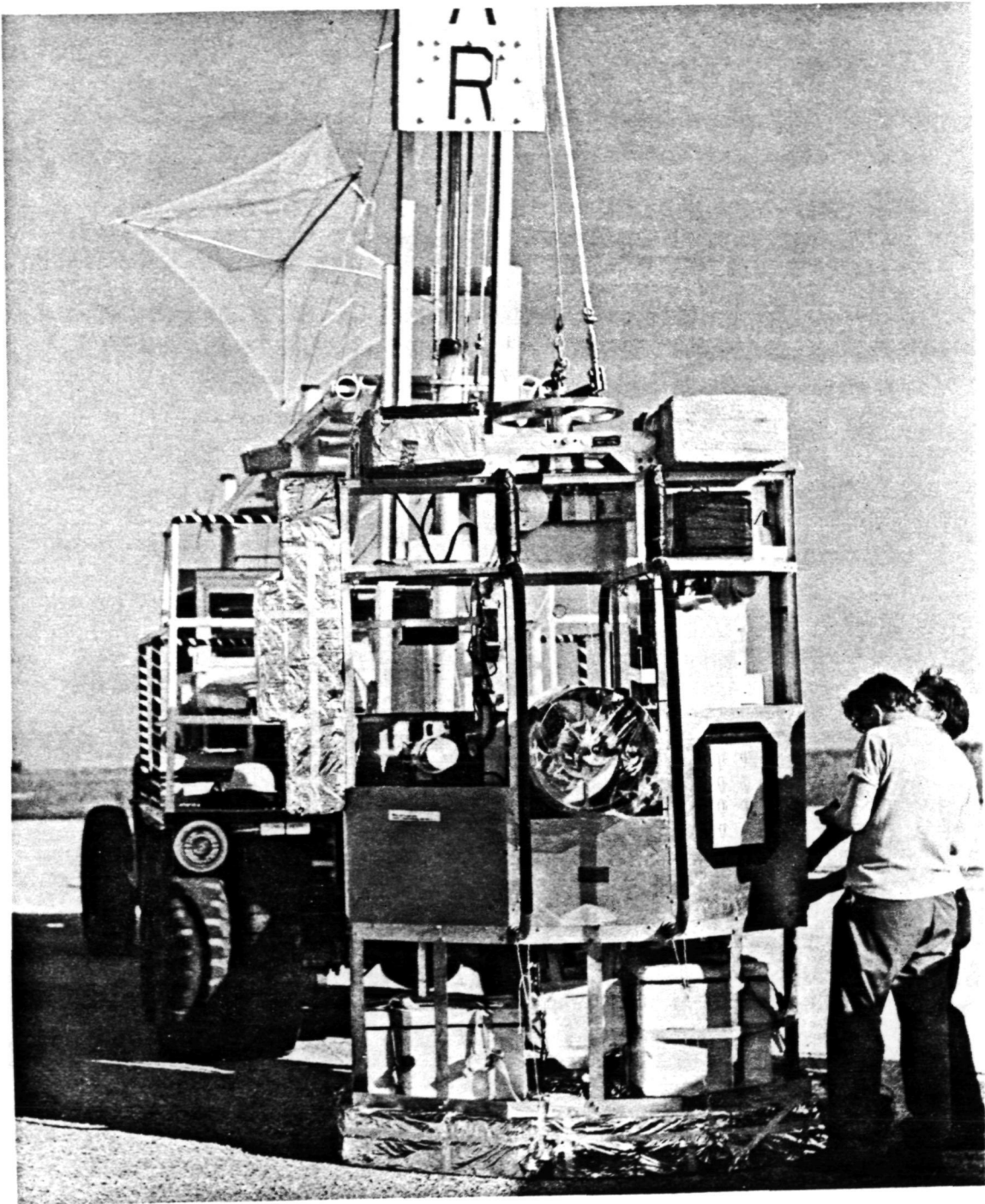


Figure 2. The gondola ready for launch.

2.1-4

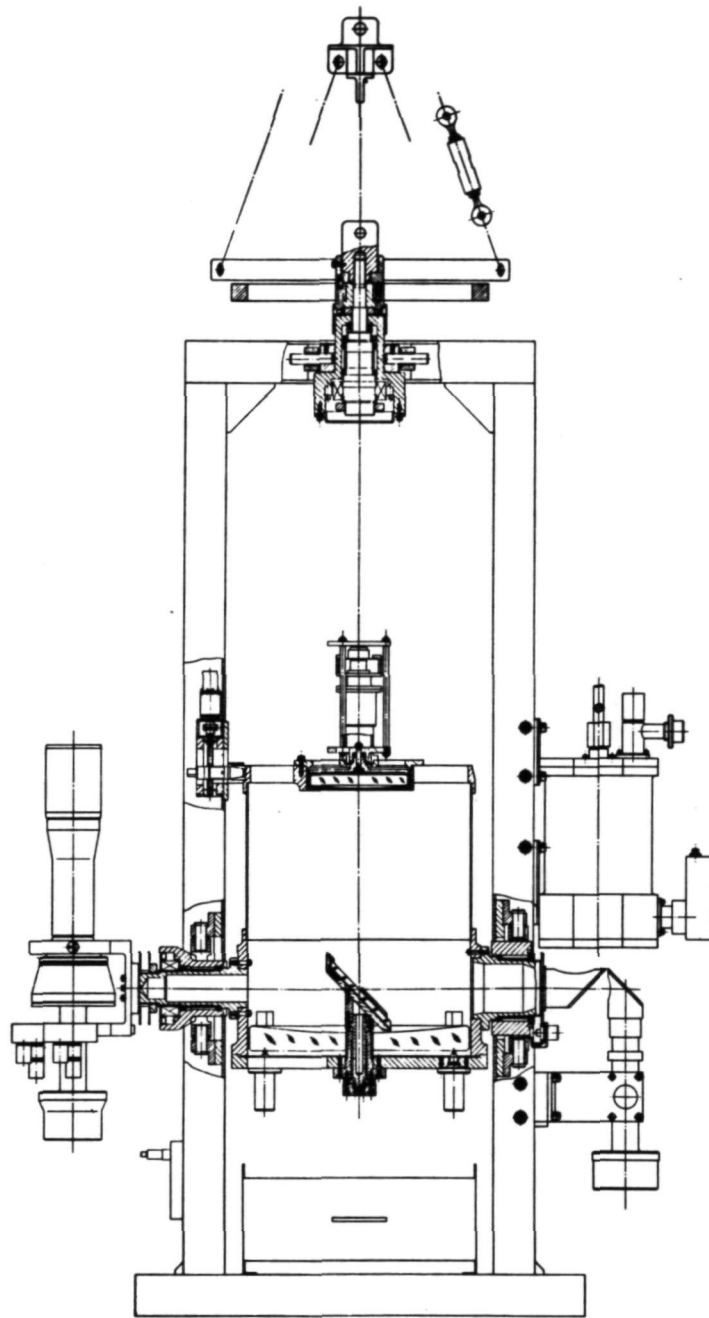


Figure 3. Section through main frame, bearings and telescope.

2.1-5

The azimuth drive unit is also supported in gimbals which take up inaccuracies in the trifilar suspension lengths. The drive motor is an Inland T-5135 of 4 NM rating. When suspended the gondola weight is taken on a low friction thrust race between the bearing housing and the azimuth shaft.

The telescope tube is made from a forged and machined aluminium alloy ring to which the elevation stub axles are bolted. This is connected to the secondary mirror spider by a thin aluminium cylinder. Spigots machined in the strong ring and spider locate and align the primary mirror support plate and the secondary mirror assembly. The primary mirror is centred on the support plate by a stalk which also carries the 45° flat. Three equispaced spring loaded plungers mounted in the support plate push the mirror against teflon stops on the inside of the strong ring with sufficient force to withstand a 4g axial deceleration.

The necessary chopping of radiation to the infra-red detector is achieved by rocking the secondary mirror to shift the effective pointing direction of the telescope. To this end the mirror cell is supported at the spider by a flexible diaphragm and can be moved by a rigid shaft fixed to the back of the cell. Two mirror drive mechanisms have been used. In the original a motor and eccentric bearing were used to move the drive shaft in a circular motion so that the focussed image from the telescope was swept in a circular path of about 8 arc min dia. at 13 Hz. This has now been replaced by a mechanism using two solenoids to impart a square wave motion, of similar amplitude and frequency, to the mirror in the cross elevation direction.

CONTROL SYSTEM AND ELECTRONICS

A simplified block diagram of the electronics is shown in Fig.4. There are two control modes.

(i) Coarse Stabilization using error signals from a flux gate magnetometer for azimuth control and from a potentiometer on the elevation axis for the elevation. Both sensors can be rotated about the appropriate axes by ground commanded stepping motor drives to set the telescope to any desired azimuth and elevation. A read-out of the set angles is provided by 10 bit shaft angle encoders mounted on the sensor drive shafts. The overall accuracy in azimuth and elevation settings relative to the magnetic meridian and local vertical is better than $\pm \frac{1}{2}^\circ$.

(ii) Fine Stabilization uses error signals from the star tracker to control the azimuth and elevation motors. The servo gain useable is limited in elevation by the star tracker bandwidth and in azimuth by the compliance of the main frame. Under steady conditions with a bright guide star and at low elevation angles a pointing accuracy of ± 20 arc sec pk-pk is achieved. This degrades somewhat with elevation angles above 40° and with guide stars dimmer than 3rd mag. A photograph of typical error signals recorded inflight is shown in Fig.5.

The star tracker is mounted in elevation and cross elevation gimbals and can be offset, with respect to the telescope, by up to $\pm 5^\circ$ in either axis by ground commanded stepping motor drives. The resultant effect, with the sensor locked to the guide star, is to offset the telescope pointing direction from that star. An autoscans drive mode is provided to enable raster scans to be made over the $10^\circ \times 10^\circ$ area or smaller scans can be made under manual control. Offset angle readouts are by 10 bit shaft angle encoders geared to the offset drives. These provide offset coordinates to better than 1 arc min but these are subject to alignment errors (about 1') and thermal distortions (about 1'). A check on the telescope pointing direction is provided by a photomultiplier

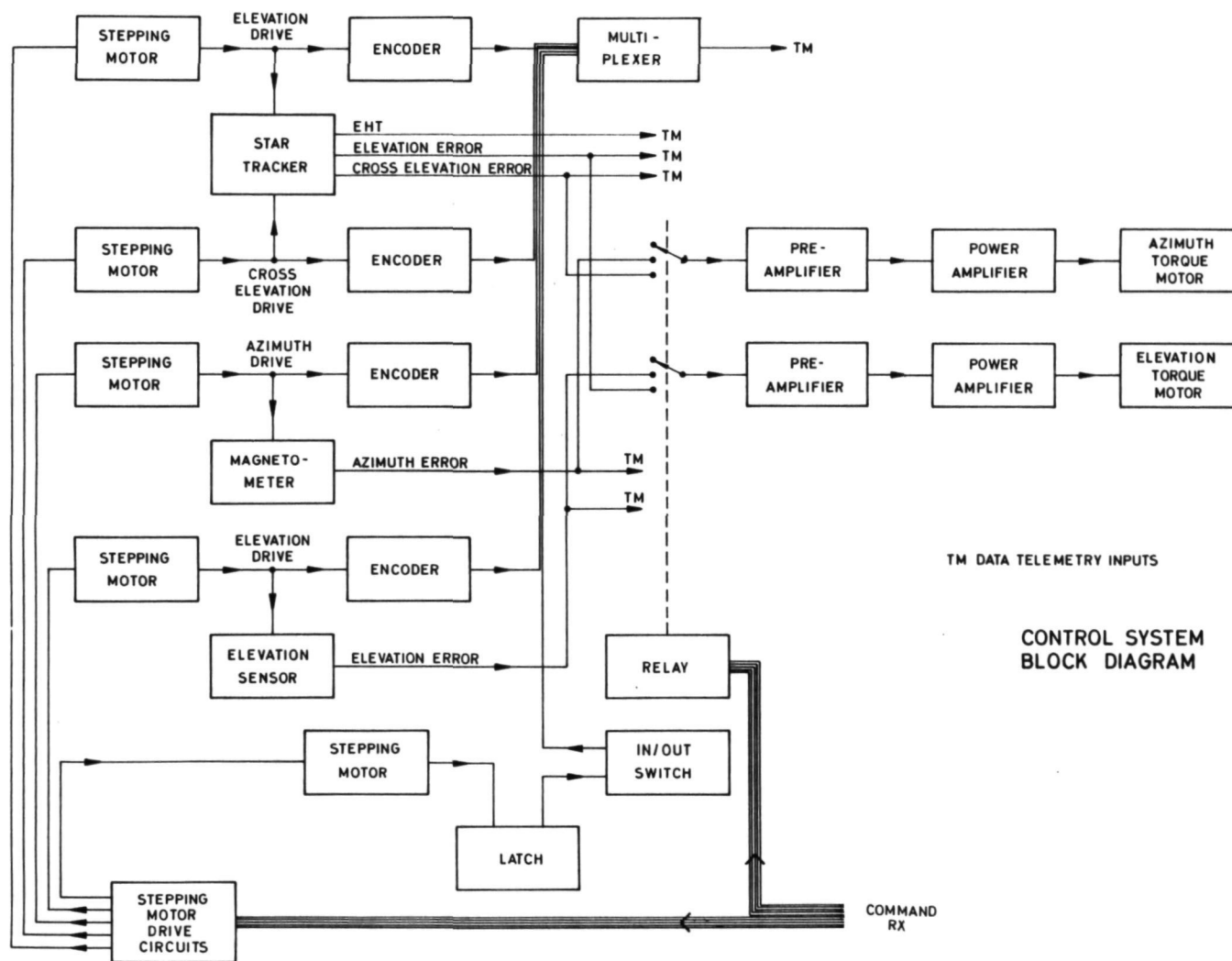


Figure 4. Block diagram of control system.

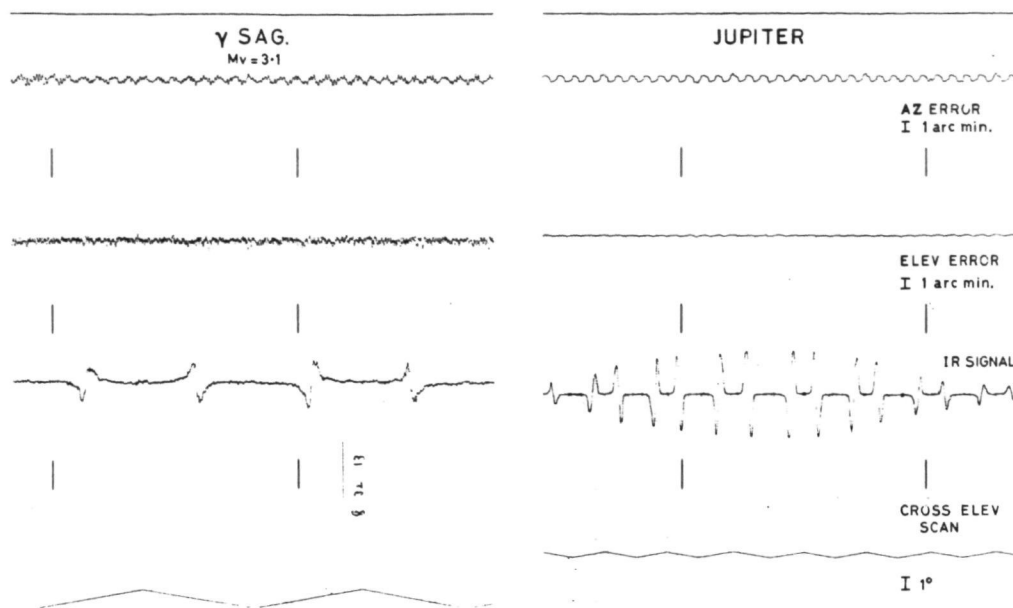


Figure 5. Typical error signal recorded in flight.

monitoring the visible radiation at the telescope focus. This has a 5 arc min dia. field of view and a logarithmic response over the range $M_v = 2$ to $M_v = 8$. During scans this signal can be used to build up a picture of the visible star field in the area for comparison and calibration purposes.

In addition to that described above a small amount of electronics is needed to encode the shaft angle outputs into a suitable form for transmission by the data telemetry, to multiplex housekeeping data and to control the latch used to secure the telescope in a vertical position during ascent and descent. The major part of the electronics is housed in a thermally insulated box sited for protection within the main frame.

The overall power consumption of the gondola is about 50 watts in the coarse stabilized mode rising to about 150-200 watts in the star stabilized mode. This is provided by a 24v 120 A.H. pack of silver zinc cells.

The system requires 10 latched commands and 6 I.R.I.G. F.M. data telemetry channels for its effective control.

STAR TRACKER

To enable all parts of the galactic plane to be accessible within the $\pm 5^\circ$ offset provided, the star tracker must operate on stars down to 4th Magnitude. In addition, the stability of the guidance servos require the star tracker to have a gain stability of 6db and an error signal bandwidth of 10 Hz. For reasonable transient performance at acquisition a linear characteristic near the null at least ± 5 arc min wide is desirable.

The design of the star tracker is fairly conventional and a cross section is shown in Fig.6. A rotating half disc is used to modulate the defocussed image formed by a $f/4$ lens of 30 cm focal length. Analysis of the amplitude and phase

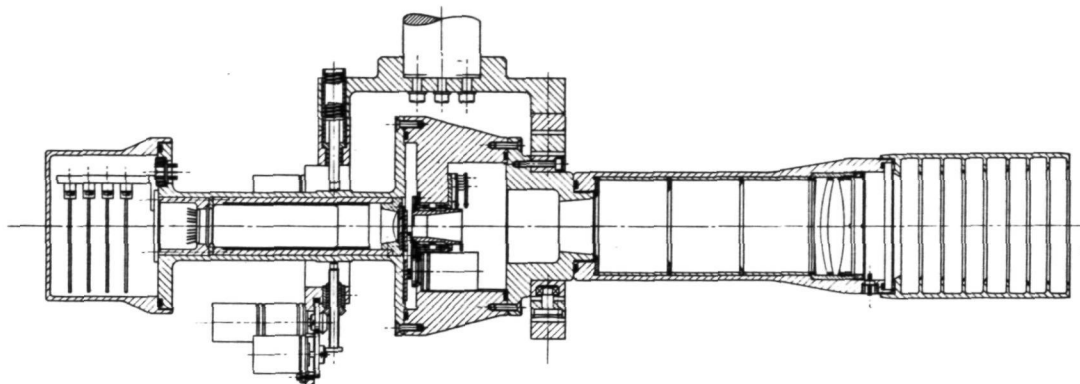


Figure 6. Cross section through Star Tracker.

of the modulated light, as detected by a photomultiplier enables elevation and cross elevation error signals to be derived. This simple arrangement provides no discrimination against sky background radiation which may amount to the equivalent of $1 \text{ Mv} = +4 \text{ star/sq.deg}$. Accordingly a second chopper wheel with closely spaced spokes (3 arc min) has been added to sweep the entire field of view. This modulates only images with dimensions less than the spoke spacing and so enables (by means of an electrical filter tuned to the spoke frequency) star signals to be differentiated from a diffuse background.

A block diagram of the star tracker electronics is shown in Fig.7. A.G.C. is provided by varying the photomultiplier E.H.T. to maintain a constant level in the chopped signal and the star tracker gain varies negligibly over a range of star magnitudes -4 to $+4$. Under A.G.C. conditions the E.H.T. level gives a good indication of star magnitude and is useful for guide star confirmation.

The star tracker is mounted in gimbals from a plate fixed to the elevation shaft. At the rear of this plate two motor driven screws drive the end of the sensor to provide the offset facility. The layout of these offset drives can be seen in Fig.8.

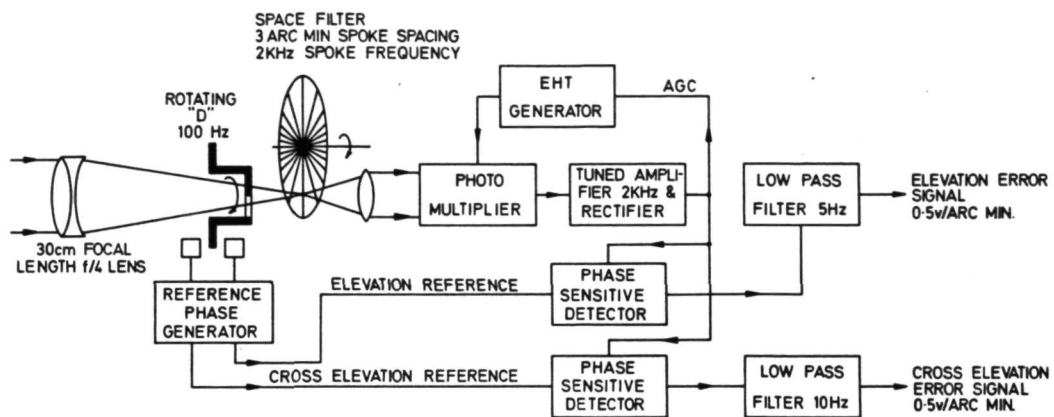


Figure 7. Block diagram of Star Tracker electronics.

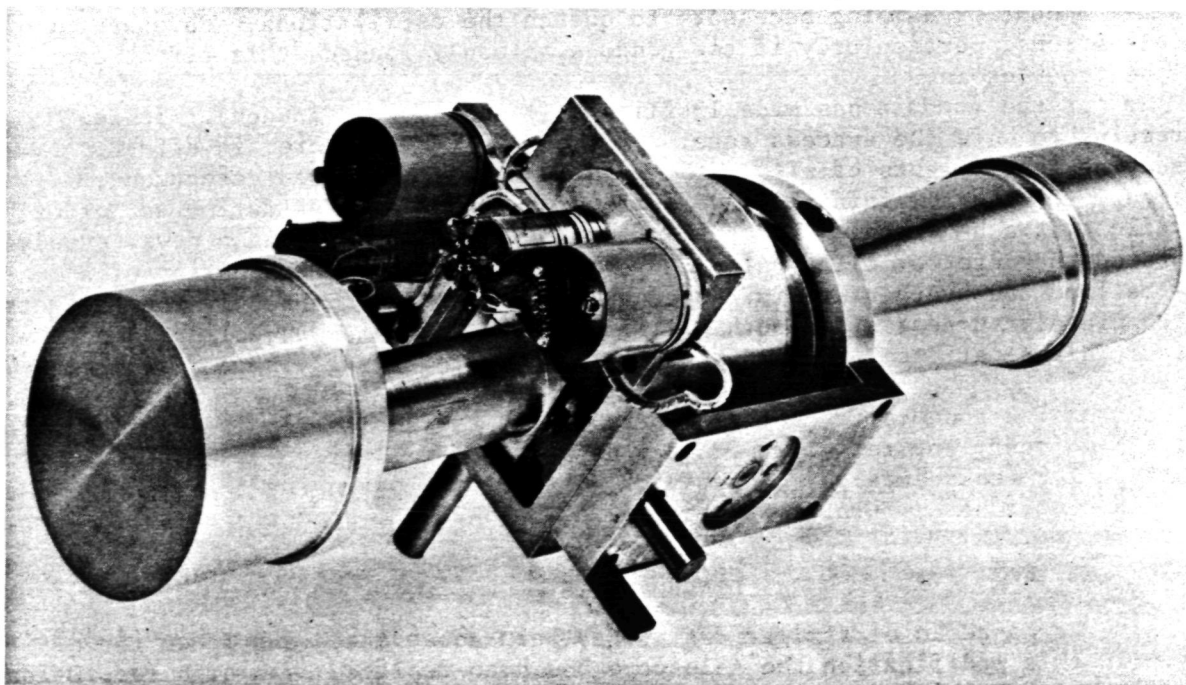


Figure 8. The Star Tracker and offset drives.

REPRODUCIBILITY OF THE
ORIGINAL PAGE IS POOR

OPERATING EXPERIENCE

When the gondola is at altitude a guide star is acquired by following the sequence below.

- (1) Unlatch telescope and switch on coarse stabilization. This action also powers the star tracker.
- (2) Drive telescope to the coordinates computed for the required guide star at this time.
- (3) Check that star tracker is aligned with telescope. If computations and calibrations correct, guide star should appear in star tracker F.O.V. The A.G.C. will then cause the E.H.T. to fall to a level depending on the guide star magnitude.
- (4) When guide star is confirmed, control is switched to the star tracker. Once locked on a star the star tracker offsets may be adjusted or scanning commenced.
- (5) At the completion of the flight the coarse stabilization is used to drive the telescope into the vertical position where it is relatched and made ready for cut down.

At any time during the flight a new guide star can be acquired by switching back to coarse stabilization and repeating the sequence from step 3. The entire procedure usually takes 5-10 mins and up to 14 different guide stars have been used during the course of a 10 hr flight. Originally our guide star coordinates were precomputed and corrections for small changes in balloon position, declination, etc. were added as required. Now we use an H.P.35 calculator to work out the coordinates on the spot.

In the first flights some difficulty was caused by compound pendulum oscillations of the gondola about its centre of mass. This has been largely cured by the use of a nylon trifilar suspension (seen in Fig.2) which provides the small amount of damping necessary to quench the oscillations. However, at high elevations, particularly if the gondola is badly loaded, this effect can still be troublesome.

So far the gondola has made 13 flights (+ one aborted launch). It is interesting to note the success rate. Of the 13 flights 3 were, in effect, engineering test flights of either the gondola or the infra-red detection equipment. Of the remaining 10, two suffered balloon failures during ascent or early float, two had problems with the command telemetry, one had a power supply failure on the detector electronics and one suffered from a combination of a leaky balloon and overheating in the gondola electronics. Thus only four flights were completely successful, though a limited amount of data was collected on the others. This experience seems in line with that of others flying comparable payloads.

So far the gondola has suffered only superficial damage on landings and has usually been ready for reflying within 4 days. We usually fly about 3 or 4 flights in a 6-week campaign. Reports of work carried out using this gondola have been published by Furniss et al. (1972a & b) and Emerson et al. (1973a & b).

DEVELOPMENTS

A second gondola of similar design has been constructed and flown three times. In this modification the telescope has been replaced by a high resolution U.V. spectrograph which incorporates a secondary guidance system to give 2 arc sec r.m.s. in elevation. A brief description of this instrument and reports of observations made with it have been given by Boksenberg et al. (1972, 1974).

ACKNOWLEDGEMENTS

The stabilized telescope project was initiated and has been enthusiastically supported by Prof. H.S.W. Massey of the Dept. of Physics & Astronomy at University College London. Thanks are due to R.W. Catch, R. Przetak, F. Want and to the staff of the Physics workshop at U.C.L. for their excellent technical assistance. Also to the personnel at the NCAR base, Palestine, for their excellent flight operations.

REFERENCES

- Furniss, I., Jennings, R.E. and Moorwood, A.F.M., 1972. Detection of far infra-red astronomical sources. *Nature Phys.Sci.*, 236:6.
- Furniss, I., Jennings, R.E. and Moorwood, A.F.M., 1972. Far infra-red observations of M42, NGC2024 and M1. *Ap.J.(Letters)*, 176:L105.
- Emerson, J.P., Jennings, R.E. and Moorwood, A.F.M., 1973. RCW117 and DR15 observed in the far infra-red. *Nature Phys.Sci.*, 241:108.
- Emerson, J.P., Jennings, R.E. and Moorwood, A.F.M., 1973. Far infra-red observations of HII regions from balloon altitudes. *Ap.J.*, 184:401.
- Boksenberg, A., Kirkham, B., Towlson, W.A., Venis, T.E., Bates, B., Courts, G.R. and Carson, P.P.D., 1972. Interstellar magnesium abundance and electron density in the direction of Orion and Cassiopea. *Nature Phys.Sci.*, 240:127.
- Boksenberg, A., Kirkham, B., Towlson, W.A., Venis, T.E., Bates, B., Courts, G.R. and Carsons, P.P.D. Space Research (in press).

DISCUSSION SUMMARY — PAPER 2.1

Several questions were asked about hardware and operations. One was concerned with whether the telescope system included a reaction wheel. It does. Another question was about a balloon failure experienced during one flight. It was determined that the balloon leaked during ascent and then failed completely at float altitude. Aside from this failure the University College London Group has had four completely successful flights. The other six have been mixed between partial success and failure.

This group has launched from Australia, France, and the United States (among other places). They have found on occasion that it is less expensive to launch in the U.S. than France.

In order to compensate for temperature changes, the telescope is defocused in the appropriate direction before launch. This was compared with the Harvard Smithsonian system which used an aluminum frame, aluminum primary, pyrex secondary and an f/13 beam. Refocussing in flight was found unnecessary.

During a discussion of gondola pendulum motion several points were made. One was that it probably depended on time at float, ranging from perhaps $1/2$ degree peak-to-peak at first to a few minutes of arc later in the flight. In addition, it was reported that the Ames telescope experienced less than $1/10$ degree of pendulum motion during a flight.

The London system has two control axes, azimuth and elevation. The star tracker can be offset in azimuth and cross-elevation. If the gondola balance could be controlled during equipment installation, it would be possible to operate to over 60 degrees with no problems. The main balance problem seems to be associated with properly locating the 300 lbs of ballast on the 800-lb platform.

PAPER 2.2

AN ORIENTABLE, STABILIZED BALLOON-BORNE GONDOLA
FOR AROUND-THE-WORLD FLIGHTS

George R. Ricker

Walter H. G. Lewin

Center for Space Research and Department of Physics
Massachusetts Institute of Technology
Cambridge, Massachusetts 02139

ABSTRACT

A system capable of pointing a balloon-borne telescope at selected celestial objects to an accuracy of ~ 10 arc minutes for an extended period (weeks to months) without reliance on telemetry is described. A unique combination of a sun/star tracker, an on-board computer, and a gyrocompass is utilized for navigation, source acquisition and tracking, and data compression and recording. The possibilities for "intelligent" activities by the computer are also discussed.

DISCUSSION

The success of NCAR's Project Boomerang in demonstrating the possibility of around-the-world balloon flights has ushered in a new era for scientific ballooning. The phrase "low-flying satellite" which has been used to describe this new concept in superpressure ballooning is most apt, even though not strictly accurate, because of the comparable observation times attainable from both around-the-world balloons and true satellites. Unfortunately, the comparison also extends to many of the same experimental difficulties. For an experiment that requires pointing a gondola-mounted telescope with a narrow field of view, among these difficulties are finding answers to three rather fundamental questions:

- Where is the gondola? (Longitude and Latitude)
- In what direction is the telescope pointed?
(Elevation and Azimuth)
- What time is it? (UT)

An ideal system for long duration ballooning should make these determinations without assistance from a ground controller because of the potential difficulty of maintaining a secure (though not necessarily continuous) telemetry link for weeks or even months at a time.

The last question is the easiest to answer: low power, accurate (i.e., stabilities of a few parts in 10^9 - 10^{10}) flights clocks are commercially available. The first part of the second question is also relatively easy, since we can use gravity for a vertical reference. A simple tiltmeter system will suffice, at least for coarse aiming. The remaining questions - determining the gondola geographic location and telescope azimuth - are fundamentally more difficult to answer. During the last year at MIT, we have been working on a system which answers these difficult questions by linking together three components that are not normally present on balloon gondolas: 1) Combination Sun/Star Tracker; 2) Gyrocompass; and 3) Flight Computer. This system that we envision will not require any ground commands once it is in "orbit". It will be capable of an absolute pointing accuracy of a few arc minutes. This level

24731 25W 1

of accuracy is sufficient for the experiments which we are planning in infrared and x-ray astronomy, where we contemplate fields of view ranging upward from 6 arc minutes.

An on-board computer opens up a number of other possibilities for such things as in flight data compression or automatic shutdown over a predetermined recovery area. This point will be discussed in more detail later.

Figure 1 is an overall view of an around-the-world gondola that might use the system which we envision. The torque motor is the driving element for stabilizing the entire gondola in azimuth. The sun/star tracker is the ultimate reference for this azimuth stabilization. It is mounted on a platform that is coupled by rigid bars to the torque motor housing (above) and to the main gondola (below). The tracker will be gimbled only about an elevation axis. During the day, the side of the gondola on which the solar cells are mounted will be continuously pointed in azimuth toward the sun. This arrangement greatly simplifies solar panel pointing, as a straightforward lead screw will suffice to point the panel normal toward the sun. The principal scientific detector, an x-ray or infrared telescope, will be offset-pointed in elevation and azimuth with respect to the gondola frame. A gyrocompass (discussed below in more detail) will provide a continuous readout of platform geographic azimuth, including any oscillatory component.

Figure 2 is a detail of the combination sun/star tracker, shown in a top view relative to Figure 1. Schematically, the situation shown is one that might exist near sunrise with the sun rising in the east and two stars setting in the west.* The elevation axis is pointing north-south. Two independent optical sensors sharing a common focusing mechanism are shown. Both are Fairchild Semiconductor CCD201 charge-coupled device area image sensors. At night, only the star tracker would be active; conversely, during the day, the sun tracker would be active. The relevant operational characteristics of this tracker are given in the following table.

<u>STAR/SUN TRACKER</u>		
(Fairchild CCD201, 10,000 Element Area Image Sensors)		
	<u>Star Mode</u>	<u>Sun Mode</u>
Field of View (FWHM)	1.5°	5.0°
Resolution	1'	4'
Accuracy	1'	2'
Signal/Noise (Per resolution element)	10:1 ($m_V=3,G3$)	> 100:1
Weight	← 8kg →	
Power	← 1 watt →	

*This situation is somewhat hypothetical, as the sky brightness for a solar elevation $>0^\circ$ would probably be too great for the system to simultaneously detect both the sun and stars.

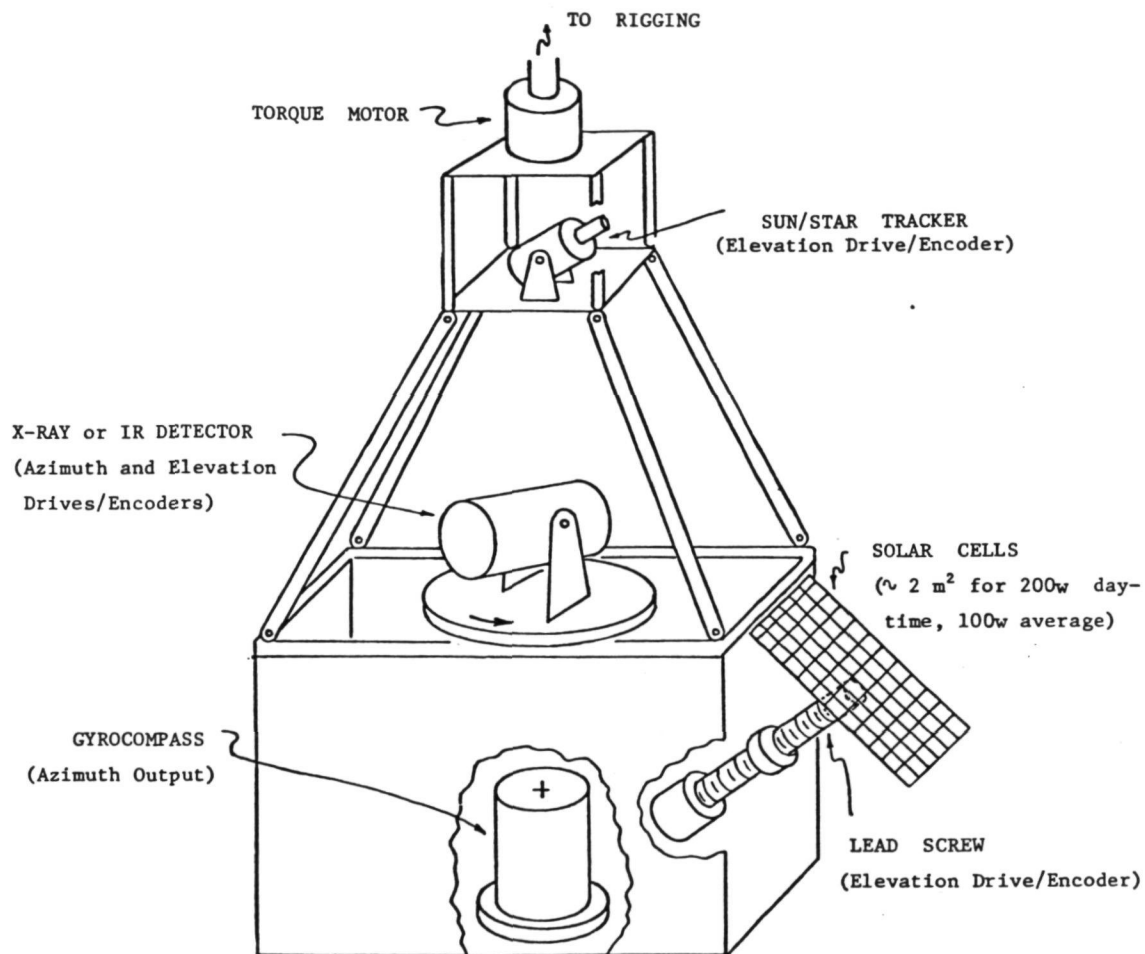


Figure 1. Around-The-World Gondola (Daytime Mode)

REPRODUCIBILITY OF THE
ORIGINAL PAGE IS POOR

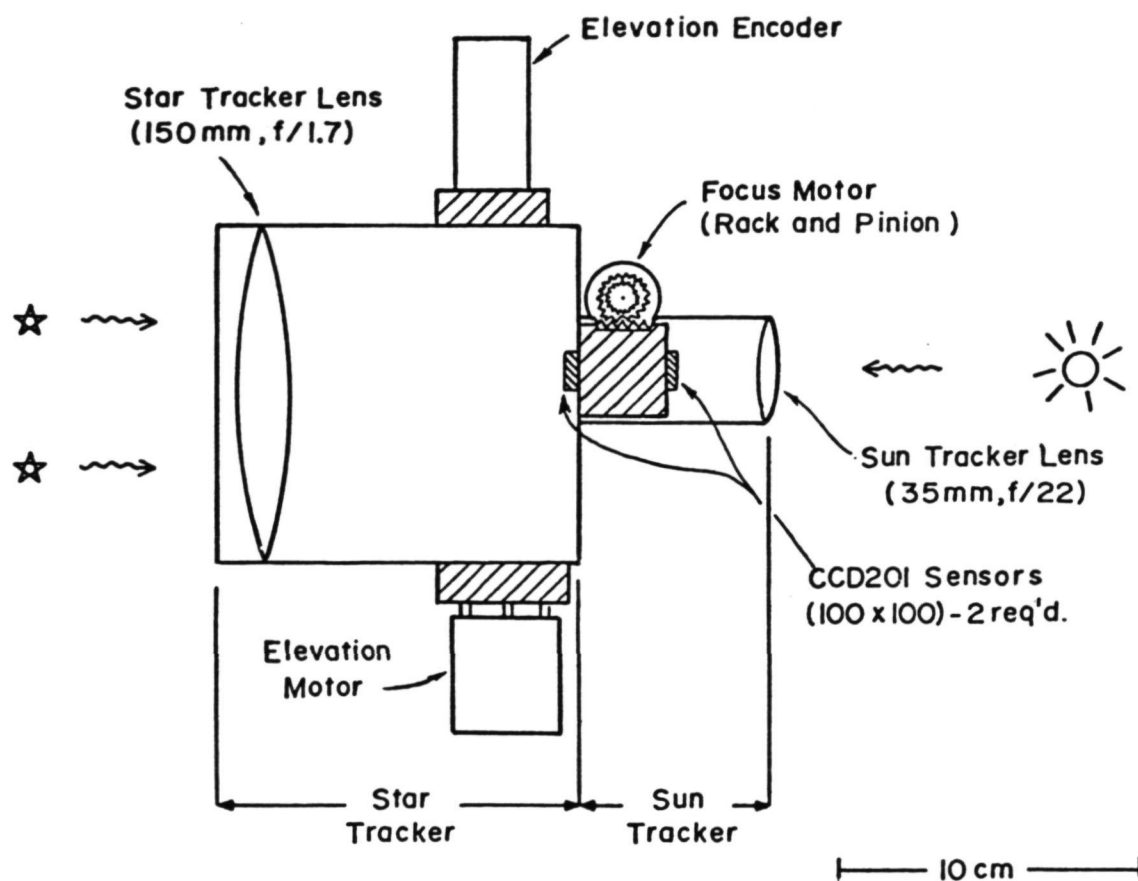


Figure 2. Sun/Star Tracker (Top View)

Next, we consider how the overall system (tracker plus gyrocompass plus computer) would be used to determine the longitude and latitude for the gondola during the night and during the day. Figures 3A and 3B depict the earth during the night and day, respectively. The gondola is over point G on the earth's surface. The vector $\vec{GN'}$ is apparent north determined by the gyrocompass. At night, the star tracker is then used to measure the zenith angle, ϕ , and the azimuth, γ , relative to the gyrocompass azimuth (in the gondola frame) for two stars. The substellar points on the earth for these two stars are SS_1 and SS_2 . The two small circles are the loci of points on the earth's surface at which the stars are observed at the measured zenith angle. From these measurements and the Universal time, we can determine the longitude and latitude of the gondola at night, after the computer has identified the two stars; this will be a rather straightforward operation as we will only use bright stars. We can also determine our gyrocompass error ϵ_{NS} from this same data. Obviously, the on board computer is vital for all these determinations in order to perform the required coordinate transformations.

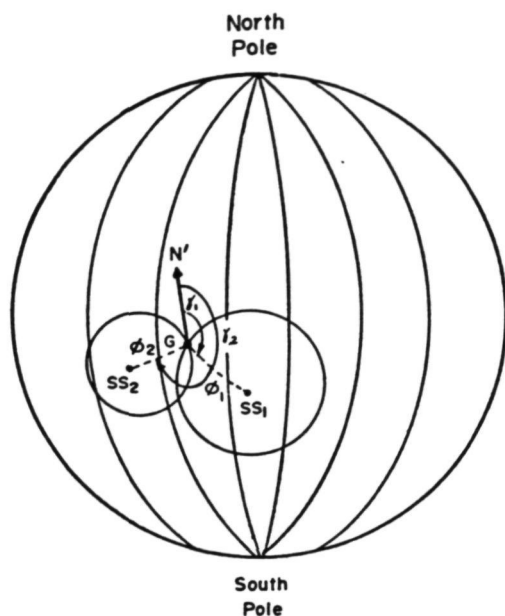
In the daytime, we have only one star to work with - the sun. Therefore, we must rely on our gyrocompass to narrow down the arc along the small circle of constant solar zenith angle where we might be. We are limited in our ability to do this by the gyrocompass error, ϵ_{NS} . This error is composed of several position-, velocity-, and acceleration-dependent components, all of which are systematic (and hence correctable) except for a small random drift. The magnitude of this small random drift is such that it could accumulate to ~ 10 arc minutes between a sunrise and a sunset (~ 12 hours). At night, we do not allow it to accumulate because of repeated star sightings, but during the day we must accept it as an irreducible error; there is only one sun.

Figure 4 is a block diagram for the entire system. The central role of the computer is immediately evident from its origination. The computer that we are planning to use would be based on an Intel 8080 microprocessor with an instruction cycle time of $< 2 \mu\text{sec}$. This is an 8 bit machine, and we would probably require ~ 8 kbytes of memory to run our system.

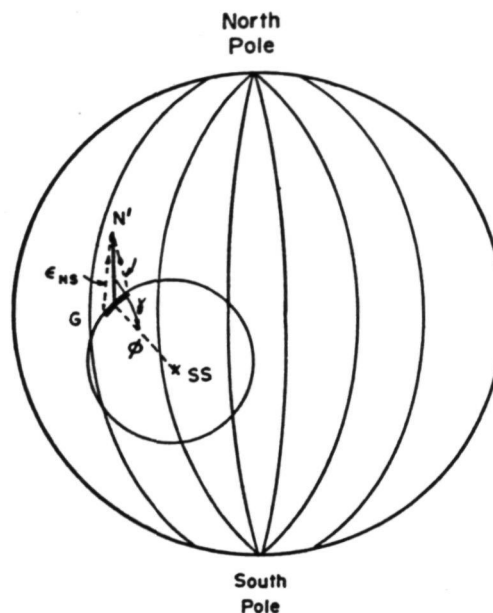
The main telescope (x-ray or IR) would input its data to the computer, and would receive azimuth and elevation commands from the computer. The roll and pitch tiltmeters would tell the computer whether the gondola were out of level (DC-wise). The torque motor servo would have an offsettable azimuth null under computer control. The gyrocompass is a GyroSystems Model 800, which is a 2 axis gimballed system with a full 360° azimuth range. Its basic resolution would be 1.3 arc minutes (14 bits). Its weight is approximately 4 kg, and it requires 20 watts of power. The sun/star tracker has already been discussed. Data from the computer would be recorded on board and a selection from it telemetered to earth continuously on an HF radio link. This data would be of lesser quality than could be obtained from a VHF/UHF line of sight link which would be used when and if the gondola happened to pass over a suitable ground station. A data uplink (through the command receiver) could also be used to modify the observing program or restart the computer system or digital clock in the event of a power loss or other temporary malfunction.

The on board computer can provide a number of functions in addition to those discussed above. These roles can be, somewhat arbitrarily, subdivided into cogitative and incogitative categories. The incogitative roles are the rather straightforward tasks which, regardless of the system, the computer

A. Night (Star Tracker)



B. Day (Sun Tracker)



Define: $\gamma_1 = \angle N' - G - SS_1$
 = Gyrocompass azimuth to Star 1
 $\gamma_2 = \angle N' - G - SS_2$
 = Gyrocompass azimuth to Star 2

Nighttime Calculations:

Gondola Longitude, Latitude --

$$(\lambda, \beta)_G \sim f [(\lambda, \beta)_{SS_1}, \phi_1, (\lambda, \beta)_{SS_2}, \phi_2, \gamma_1, \gamma_2; UT]$$

$$\sim f (\phi_1, \phi_2, \gamma_1 - \gamma_2, UT; \alpha_1, \delta_1, \alpha_2, \delta_2)$$

Gyrocompass Error --

$$\epsilon_{NS} \sim F (\gamma_1 \text{ or } \gamma_2)$$

$$\sim F [(\lambda, \beta)_G, (\lambda, \beta)_{SS_1 \text{ or } SS_2}, \gamma_1 \text{ or } \gamma_2]$$

Daytime Calculations:

$$(\lambda, \beta)_G \sim f' [\phi, \gamma, \epsilon_{NS}, UT; \sigma_\phi(UT), \delta_\phi(UT)]$$

Figure 3. Longitude/Latitude Determination

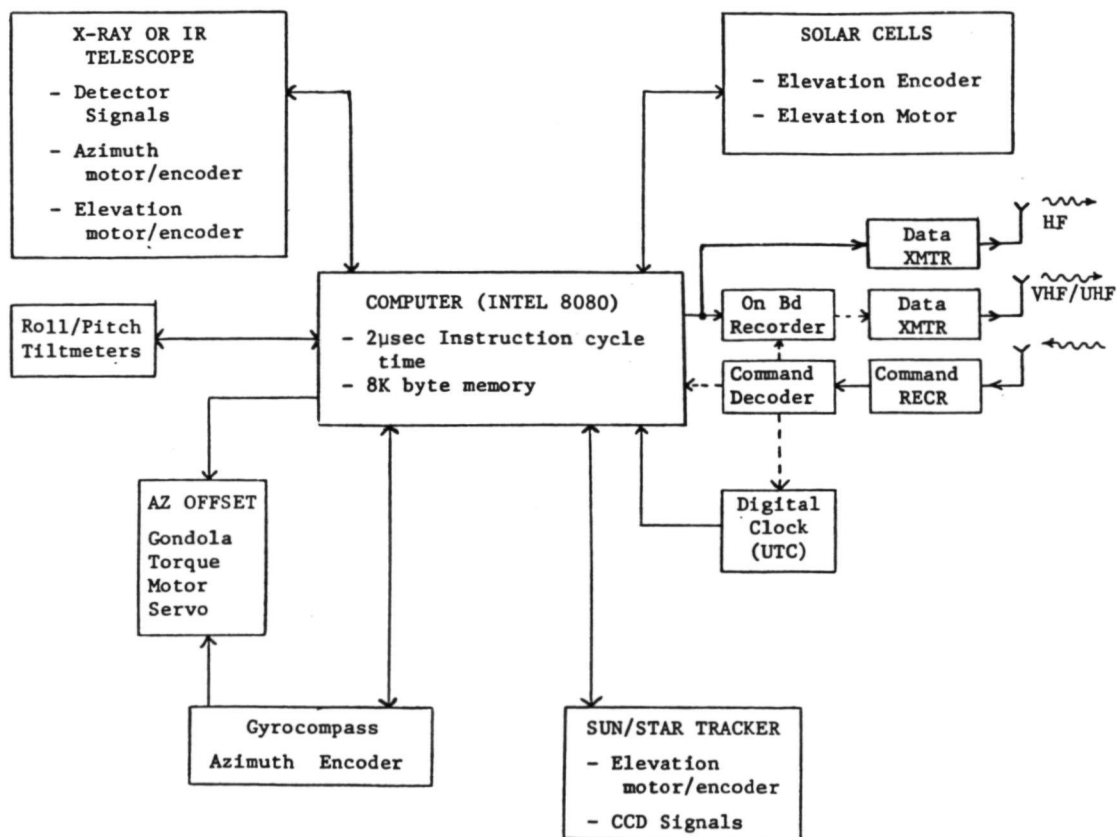


Figure 4. Aspect/Data System

REPRODUCIBILITY OF THE
ORIGINAL PAGE IS POOR

would have to perform. The cogitative roles are more sophisticated ones which would be limited by memory size and computing speed. First, the incogitative:

INCOGITATIVE ROLES FOR FLIGHT COMPUTER

1. Gyrocompass corrections (ϵ_{NS} - Azimuth error; "north steaming error" - velocity, acceleration dependent)
2. Source list look up and coordinate transformation:
[$(\alpha, \delta) \rightarrow (Az, El)$]
 - Sun
 - Coarse: Solar Cell Panel
 - Fine: Sun Tracker
 - Bright Stars
 - X-Ray or IR Sources
3. Data compression (for on-board recorder)
4. "Flywheel" for day/night transition
5. Inflight gondola re-leveling (tiltmeter sensors)
6. Sun/star tracker focusing
7. Star tracker protection (shutter activation)
8. Mode switching (instrument calibration, operational checks, etc.)

For the cogitative roles, one can think of a "computer soliloquy" after the fashion of an experienced human observer using a ground-based telescope. Among the questions such a computer-observer might ask itself are the following (where "I" = The Computer):

COGITATIVE ROLES FOR FLIGHT COMPUTER

1. Observing Program Selection
 - a) What sources are potentially visible now (i.e., sufficiently above the horizon but not behind the balloon)? Of these, which have the highest pre-flight priority?
 - b) What sources have I not looked at recently? Of these, which did I detect the last time I looked at them? Of the candidates not examined recently, which should I look at again?
 - c) If I am observing a given source, am I detecting a positive flux? If not, how much longer should I continue trying to see it? If I am detecting it, is it behaving in such an "interesting" manner (e.g., time or spectral variability) that I should continue taking data on it?
2. Data Dump Decision (VHF or UHF Link)
 - a) Am I within range of a receiving station?
 - b) How long has it been since I last made a dump?

- c) Is the wind velocity such that I will have time for a complete dump?

3. Cutdown Decision

- a) Have I been in "orbit" long enough?
- b) Am I over a suitable recovery area?
- c) Is it daylight?
- d) Have I turned on my tracking beacons and lights?
- e) Have I received an override command from a ground station?

The practical number and effectiveness of the algorithms for these computer decisions will be largely determined by the skill and creativity of the human programmer. Implementing all of the options listed here would likely require a very large computer memory; but with the steady decrease in price/bit and the increase in bits/chip for low power C/MOS memory elements, this is not likely to pose a significant problem.

In summary, the system described here should be able to achieve the high degree of flexibility and pointing accuracy which balloonists have come to expect from ground-controlled gondolas, without requiring a telemetry command "umbilical", a link which could be very tenuous for around-the-world flights.

DISCUSSION SUMMARY — PAPER 2.2

In response to questions about progress on this system, the speaker said that the star tracker and the computer have been started.

It was suggested that the star tracker could be used for the same purpose as the 20-watt two-gimbal gyrocompass and therefore save power. The conclusion of the MIT Group is that at \$5,000 and eight pounds per gyrocompass that they represent a less expensive trade-off. These units are expected to have ten arcminutes of drift per 12-hour period. It is expected that in the future gyrocompasses will be available for \$10,000 to \$20,000 with absolute accuracy of ± 2 arcminutes for indefinite time periods.

The computer planned for this system is inexpensive, lightweight, uses less than a watt of power and uses a CMOS-type memory.

Some of the advantages of the CCD detector planned for the star tracker were mentioned. These are: no mechanical chopping required, location of spatial elements known very well and high quantum efficiency. The cost is about \$500 to \$1000 per unit. This star tracker is expected to have a signal to noise ratio of ten for a third magnitude G star using a 1/30-second integration time.

PAPER 2.3

A COOLED TELESCOPE FOR INFRARED BALLOON ASTRONOMY

Carl Frederick
Michael R. Jacobson
Martin Harwit
Cornell University

ABSTRACT

A 16 in. liquid helium cooled Cassegrain telescope with vibrating secondary mirror is being constructed for far infrared astronomical observations. The system will be capable of housing several different detectors for multicolor photometry. This instrument will be flown jointly with Dr. William F. Hoffmann in a gondola that has been used by him in previous flights.

For several years now, the Goddard Institute for Space Studies gondola has been obtaining data on H II regions in the Galaxy. Some of the more recent results are described elsewhere in these proceedings. The system has been flown 6 to 8 times a year. The Gondola consists of a 12" Newtonian telescope with a vibrating secondary chopper. The beam feeds into a liquid helium dewar containing a bolometer and filter system which transmits in the region around 100μ . The gondola is fully steerable and in addition has a programmable scanning mode.

Mechanically, the gondola was built in three separate sections (Figure 1). The middle unit is the structural support, and houses the orientation machinery. The system is magnetometer stabilized to about $5'$ of arc. An inertial wheel provides the reaction mass against which the gondola stabilizes. In addition, there is an active bearing which transmits excess angular momentum to the balloon. In a sense the middle unit alone should be called "the gondola". The right hand unit, which is simply bolted on to the gondola, is the telescope, detector and preamp section. The left hand unit is a box containing batteries, control electronics, and the telemetry, telecommand system. This unit co-rotates with the telescope. The 2 boxes hanging below the package are N.C.A.R. transmitters, batteries and ballast hopper. These boxes are cut away (onto a long nylon cable) before landing so that the package may land horizontally on the three crash pads shown. A typical flight lasts about 16 hours. The flight configuration of the system has changed in the course of the program as shown in Figure 2.

The success of the 12" balloon borne telescope has prompted us to build a more sensitive instrument. The 12" telescope has discovered approximately 100 objects along about half of the galactic plane. Two thirds of these have been identified clearly with H II regions or infrared stars. The survey was carried out with an uncooled telescope and helium cooled bolometer with a sensitivity of 10^{-23} w/m²Hz at 100μ . The sensitivity of the telescope is fundamentally limited by the thermal flux falling

on the detector due to the telescope and sky emission. The sky emission at 100μ at 100,000 feet is ~ 0.7 percent at the ambient temperature of -65°C . The instrumental emission within the aperture of the telescope is effectively 25 to 50 percent due to mirror emissivity, dewar window emissivity, warm baffles, and diffracted rays reaching the side walls of the telescope tube. At least an order of magnitude improvement in sensitivity can be obtained if the effective telescope emissivity is reduced to a value comparable to or less than the atmospheric emissivity. This can best be obtained by the use of a cryogenically cooled telescope where the emissivity of the mirrors, telescope tube walls, and baffles is reduced by the lower temperature.

One of the principal designers of the gondola (William Hoffmann) is now at the University of Arizona, as is the gondola. The other designer (Carl Frederick) is now at Cornell. The current effort is a collaboration of two groups: William Hoffmann, Murray Campbell and Paul Harvey in Arizona, and Carl Frederick, Martin Harwit, and Mike Jacobson at Cornell. The paper describes principally the Cornell section of the collaboration, i.e. the design and construction of a 16", liquid helium cooled, Cassegrainian telescope for the gondola.

The telescope is outlined in **Figure 3**. It may be described as three distinct units: 1) the dewar, 2) the telescope, 3) the baffle and membrane. In addition, there are two more units not shown in the diagram: 4) the collar and lid, and 5) the external frame and balance mechanism.

We shall briefly describe each unit.

1) The dewar:

The dewar (**Figure 4**) is an 18" aperture, 48" deep, and 52" over all length aluminum and fiberglass double can, made for us by Cryogenic Associates. Within the dewar walls are radiation shields and superinsulation. It is not liquid nitrogen jacketed. There are mounting flanges welded to the inside of the dewar. The only access to the inside of the dewar is through the 18" aperture, i.e. there are no feed throughs or other holes through the dewar. Two aluminum rings are welded to the outside wall of the dewar for mounting to the external frame.

2) The telescope:

The telescope is a 16" diameter Cassegrainian system. The primary is f1.7 and the overall system is f5. The primary and secondary are made of aluminum coated with electroless nickel. The surfaces are polished to within 2 wavelengths (5461\AA) to a spherical configuration, and are overcoated with aluminum and silicon monoxide. The circle of confusion is less than $2.4'$. The on axis spot size is about 1.3mm. The mirrors were fabricated for us by Muffoletto Optical Company.

Behind the primary mirror is the detector block, which accommodates 4 detector units. The units are interchangeable. Each unit contains a detector and its associated post optics and filters. There are two types of detectors useable in our system: photoconductors and bolometers. The post optics for the photoconductors consists of an off axis segment of a parabola which effectively results in a virtual detector diameter of $.34''$.

The bolometer post optics is a spherical cavity at the focus of which the bolometer is suspended. The four units will be filtered so that 4 overlapping regions in the range anywhere from 10 to 300 microns may be observed. The field of view of each detector is about $1/50$.

In the center of the detector array, there is a fiber optics bundle leading out of the detector block, up the inside wall of the dewar and out. An eyepiece is put on the end so that the telescope may be aligned with the gondola. After alignment, the eyepiece is replaced with a detector for the visual region of the spectrum. Signals from this detector will be the principal method of determination of the positions of the infrared sources with respect to the visual stars.

A 4 arm spider connects the mounting disc to the secondary mirror/chopper assembly. The design of the chopper was motivated by the necessity of minimizing vibration and heat loading in the cool telescope environment.

The chopper is a coil-driven resonant system. The chopping is thus sinusoidal rather than square wave. The calculated chopper efficiency is greater than 80 percent of that of a perfect square wave system. However, the high Q of the resonant system allows the system to run with very little power (less than one tenth watt). To minimize vibration, the drive coils are mounted to a movable plate so that when the secondary mirror rotates in one direction, the coil plate moves in the other, so that to first order, the angular momentum of the system is zero. The chopper resonates at about 16Hz. A sensing coil, magnet combination provides the chopper reference for synchronous detection.

Underneath the telescope proper is mounted the helium can. It is shaped roughly like a bunt cake pan. It is so shaped so that it entirely surrounds the detector block. The can is filled with steel wool to keep the 25 liters of liquid helium from sloshing about. The expected hold time aloft is of the order of a day.

All elements of the telescope, i.e. the primary mirror, the Cassegrain baffle, the spider, the detector block, and the helium can are mounted to an aluminum disc which is itself mounted at its periphery to the dewar.

3) The baffle:

Within the dewar is a thin wall stainless steel baffle with a polyethylene membrane accross it some 10 inches from the front end. The baffle O.D. is $1/4$ " less than the dewar I.D. The helium gas which is forced up the sides of the dewar efficiently cools the dewar. Above the level of the membrane, vents in the baffle channel the escaping gas over the front surface of the membrane to prevent water vapour frosting. There is a little hole in the membrane above the chopper in order that some of the gas will escape around the chopper, thus providing additional cooling for it. The baffle also contains knife edge rings to prevent grazing light rays from reaching the primary.

4) The collar and lid:

Above the front of the dewar, a 1 1/2" high collar has been mounted (Figure 4). The collar contains the wiring feed through connectors, and it supports the lid mechanism (Figure 5).

The motor-driven lid is made of foam (presently styrofoam, soon to be replaced with thurane) interspaced with foil reflecting layers. A liquid nitrogen compartment will be added to the lid to increase the hold time on the ground. The nitrogen will be blown off before flight.

5) The frame and balance mechanism:

The dewar is mounted within an aluminum and stainless steel protective frame. The frame is bolted to the gondola. On top of the frame, a balancing mechanism is mounted. It is a way of moving a 10 pound weight up and down the telescope length. It is used to compensate for the weight loss during flight of the liquid helium. This compensation is required because the telescope is a scanning instrument which is very sensitive to weight imbalance.

Figure 5 shows the gondola during preliminary integration of the system at Arizona in January, 1974. The overall system has been modified so that the electronics side no longer co-rotates with the telescope.

The first two flights of the system are currently scheduled for June of 1974.

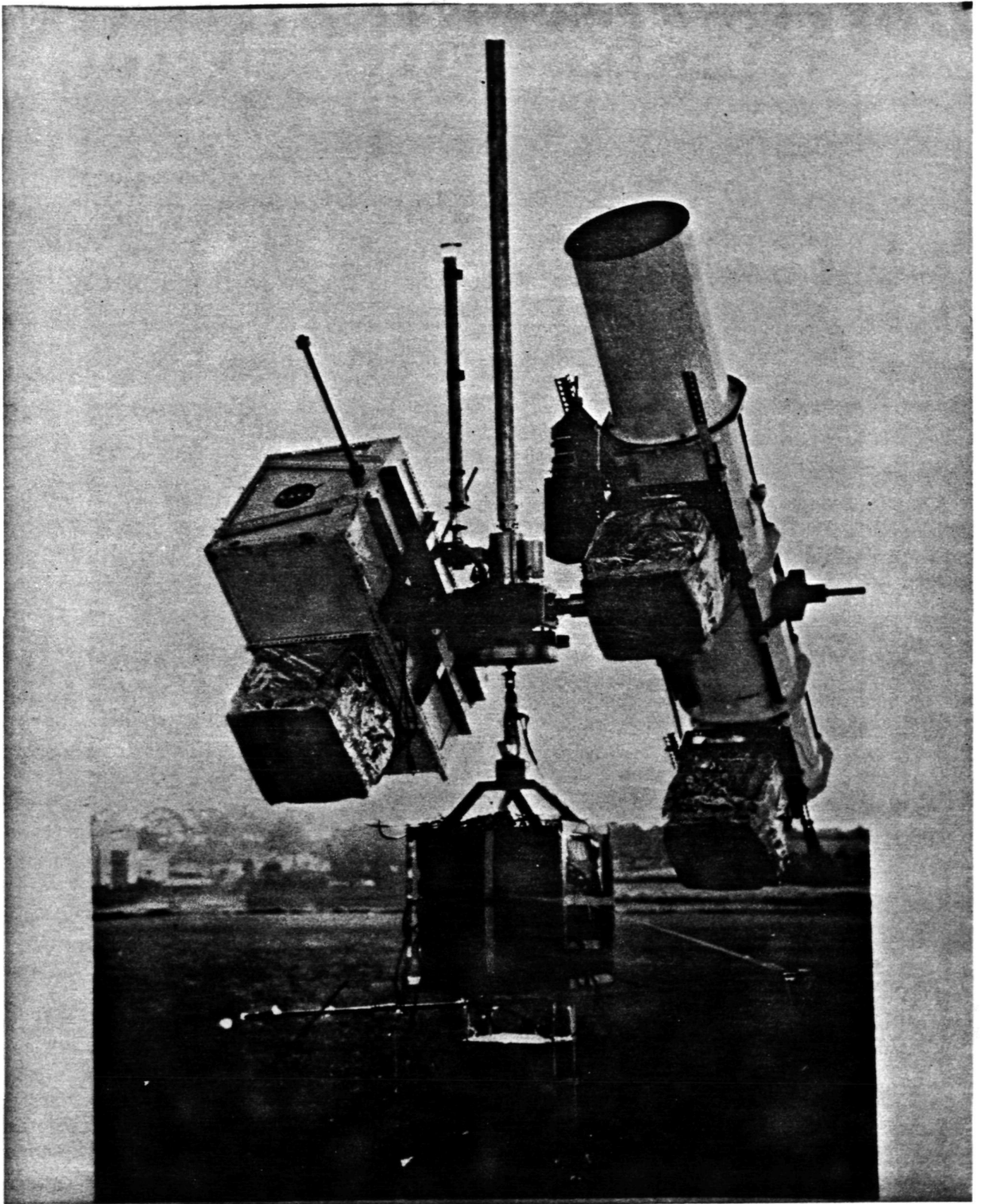


Figure 1.

2.3-5

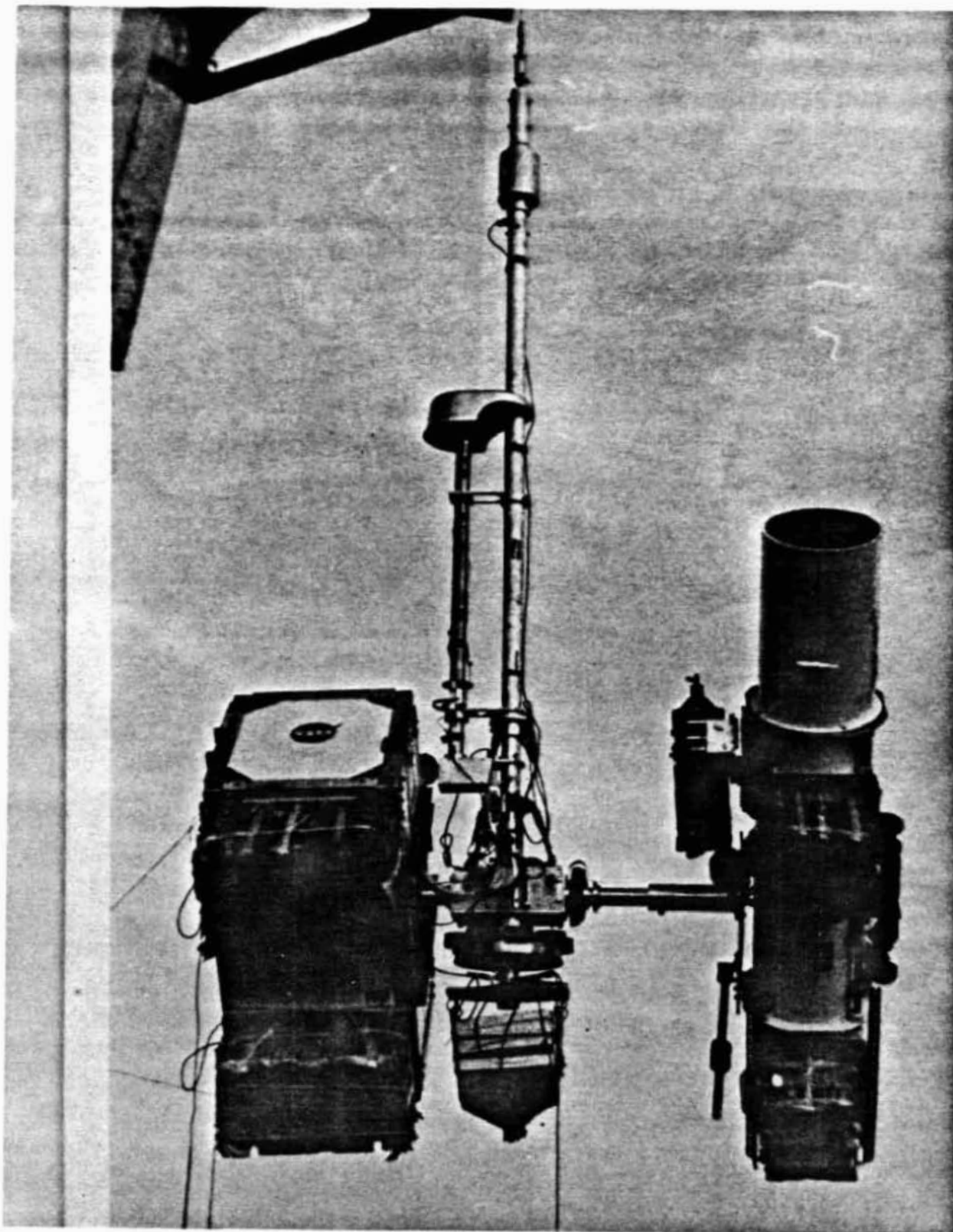


Figure 2.

2.3-6

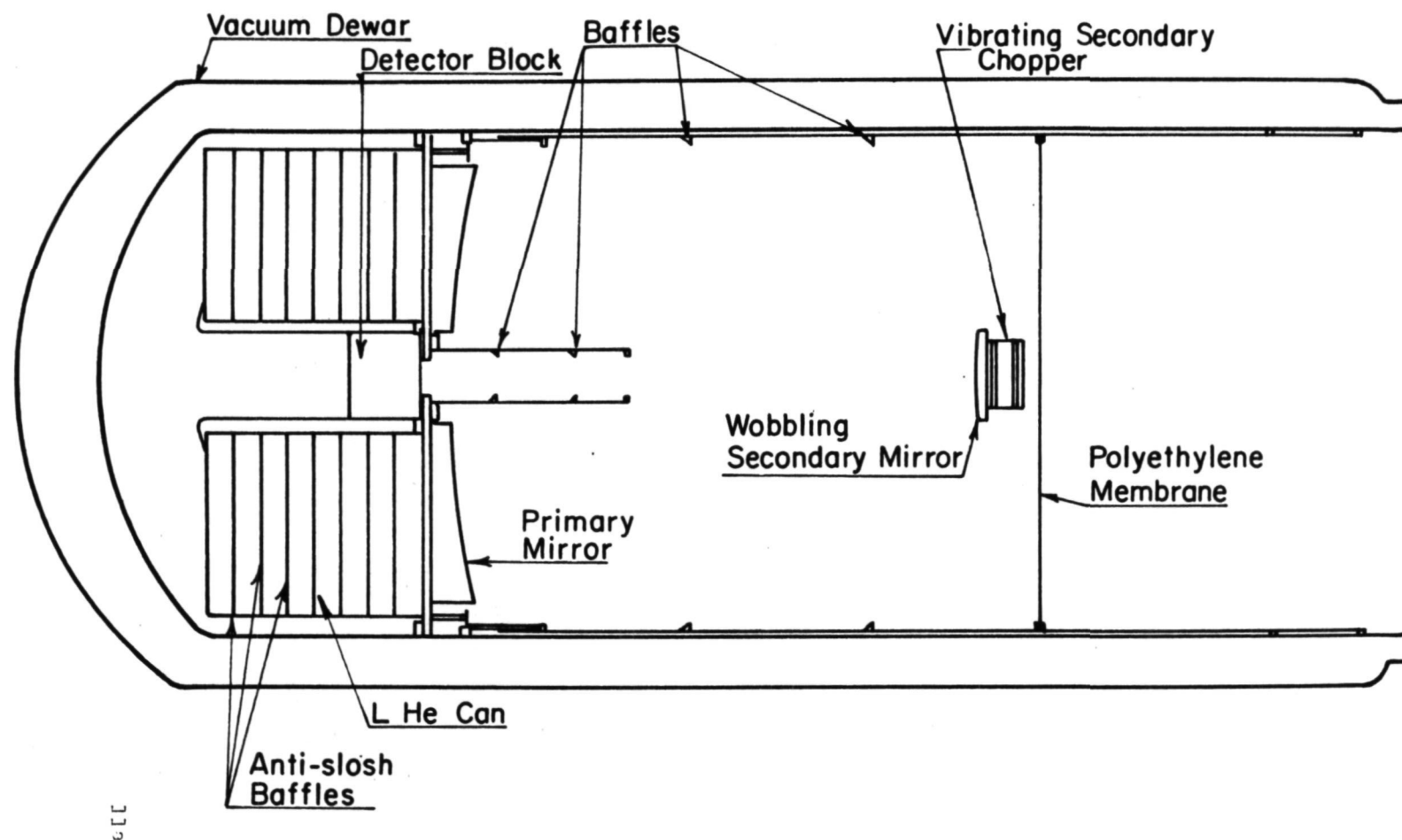


Figure 3.

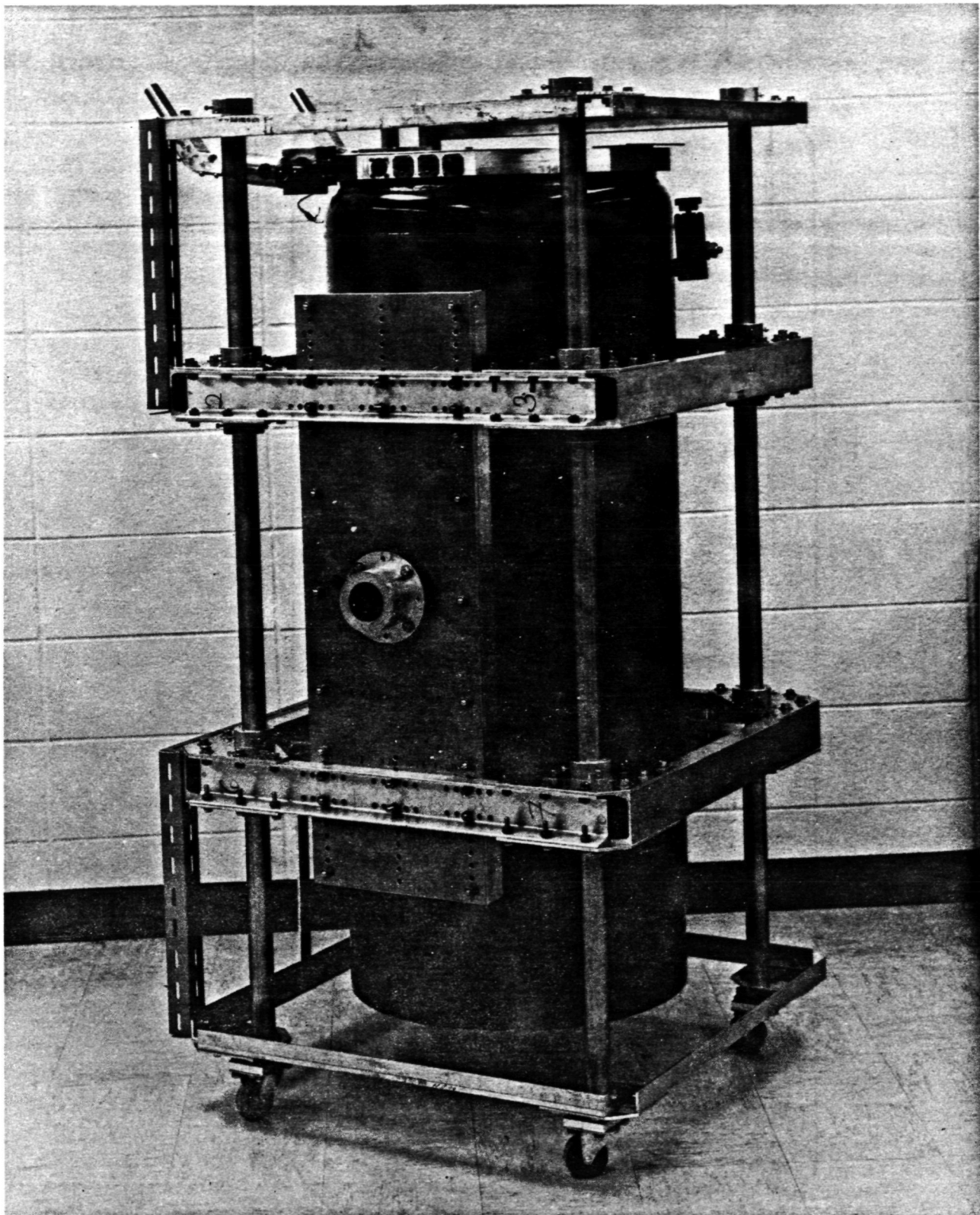


Figure 4.

2.3-8

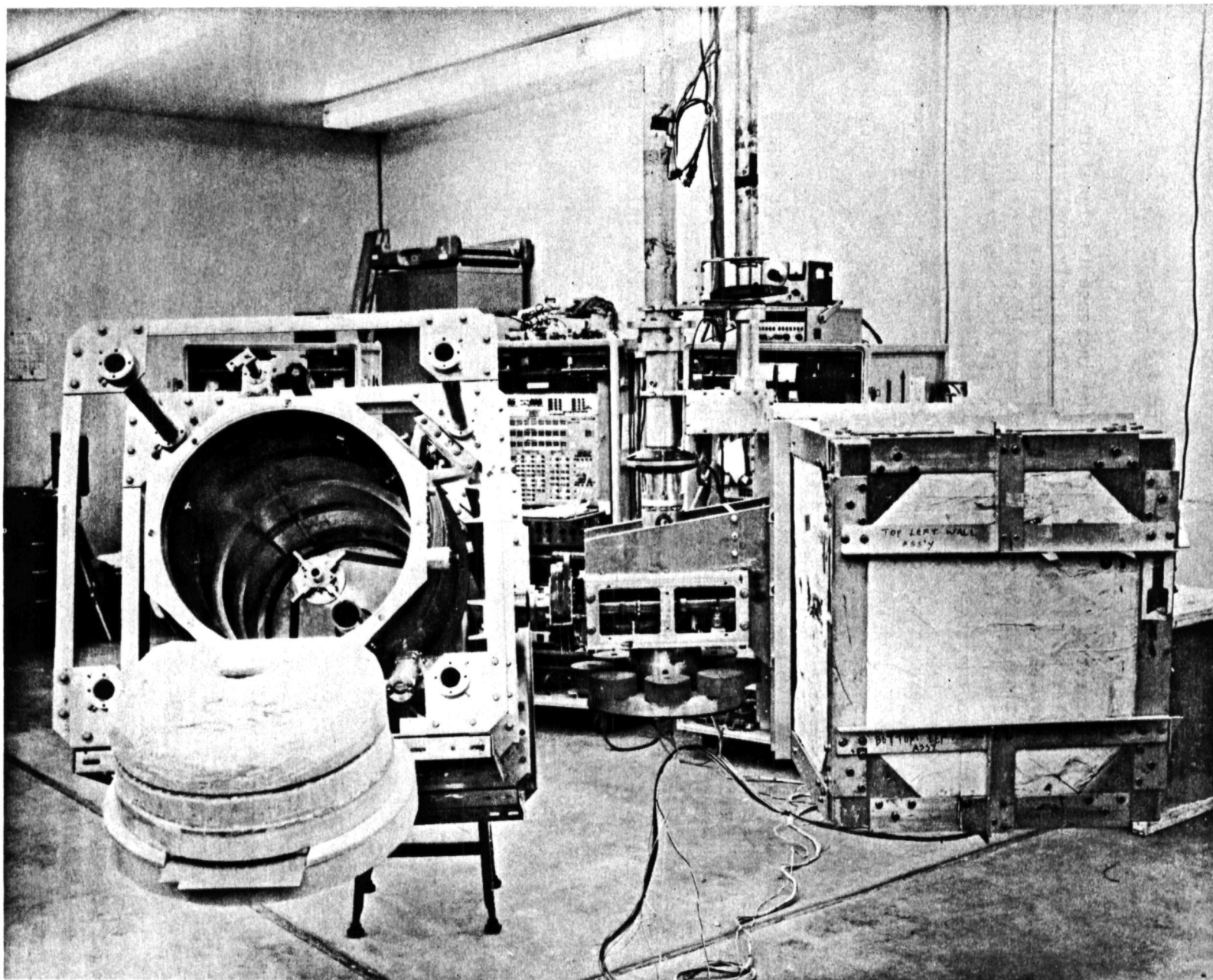


Figure 5.

DISCUSSION SUMMARY — PAPER 2.3

This telescope is expected to have a ten to one increase in signal-to-noise ratio over a similar warm version. There will be a polyethylene diaphragm operated at a temperature below the dew point near the entrance to the telescope. It is expected that frosting of this diaphragm will be no problem because it will have helium boil off gas blown over it and because this has not been a problem in another telescope of 12-inch diameter.

These expectations were contrasted with the experience of the North American Rockwell group.

The Cornell group expects that the ten inches of baffle height outside the membrane will protect the system from frosting.

Experience by F. Low and W. Potete, using a cryogenic telescope aboard a Lear jet were summarized. One outstanding problem was noise introduced by motion of the thin mylar diaphragm used on the airborne telescope. This membrane was three to four microns thick.

It is hoped that the quieter balloon environment in conjunction with the membrane being very cold in the Cornell telescope will minimize this problem.

A BALLOON-BORNE CRYOGENICALLY COOLED FILTER RADIOMETER

Arthur G. DeBell
Rockwell International

ABSTRACT

Under ARPA sponsored contracts with the Air Force Cambridge Research Laboratories, Rockwell International has built and assisted AFCRL in flying a cryogenically cooled filtered infrared radiometer, on a high altitude balloon platform.

This radiometer has several unique features which include the options for the remote operation of two filter wheels each containing six filters at helium temperature, and a cryogenic rotary chopper which may be run at 200 cycles per second or positioned open or closed, and a remotely operable chopped blackbody calibration source. It contains a ten inch diameter liquid nitrogen cooled Cassegranian telescope with nine individually filtered field stops in its focal plane. Each of these field stops is reimaged for stray radiation rejection on a separate detector. The fields of view of the detectors are small and may be varied in size and shape by replacement of the field stop and detector masks. The telescope is mounted on a two-axis alt azimuth/artillery type/servo operated gimbal which is used to make sky scans under the control of an on-board programmer. The cryogenically cooled telescope is fitted with an antifrost device which protects the system from frost at altitudes above 35,000 feet. The system is capable of absolute spectral radiometry in the band from 3 to 25 microns.

OVERVIEW

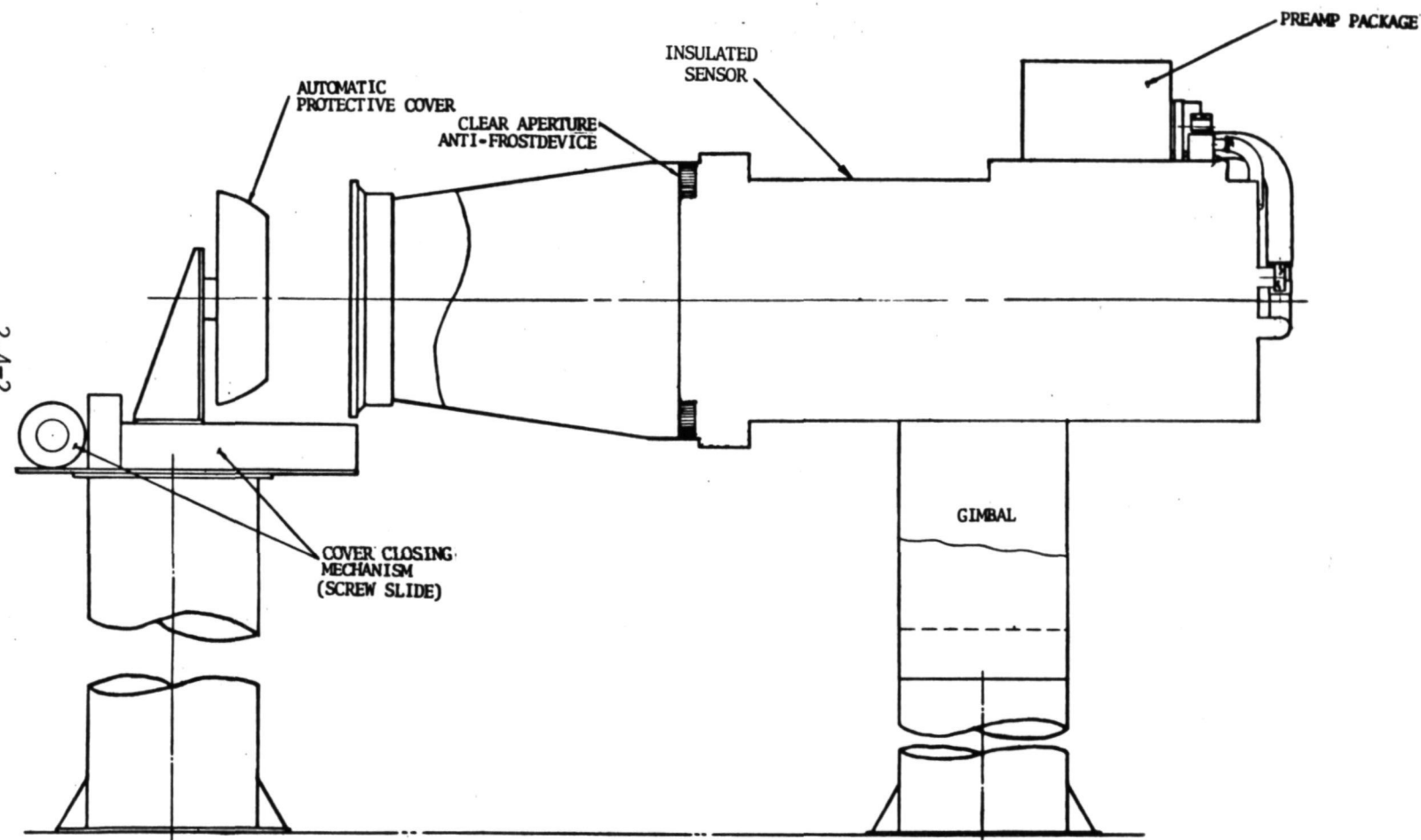
Rockwell International's Contract F19628-72-C-0262 with the Air Force Cambridge Research Laboratories is one in which Rockwell International has furnished technical assistance to the Air Force in calibrating, installing and flying on a high altitude balloon platform, a radiometer which Rockwell International had previously built for AFCRL under Contract F19628-70-C-0126. Three flights were made under Air Force direction from Holloman Air Force Base, New Mexico. Rockwell International refurbished the radiometer between these flights. In the latter contract the contractor's role was largely that of an assistant wherein the contractor endeavored to provide the assistance required by AFCRL on a schedule determined by AFCRL.

During flights radiometric scans were made of the sky from an altitude of approximately 90,000 feet. The telescope was scanned 180 degrees in azimuth while it was systematically elevated at various angles from 0 to 60 degrees. Spectral filters were inserted during the scans to define various bands from 9 to 22.7 microns. Neutral density filters were inserted and gain changes were made at appropriate times. Both "AC" and "DC" signals were recorded. Calibration signals were inserted as the gimbals reversed direction at the end of each scan.

A unique feature of the radiometer is the capability of remotely operating its many controls by means of commands radioed from the ground. Figure 1 is a schematic of the radiometer system. Figure 2 is a photograph of the system mounted on the balloon gondola.

2.4-1

38731 67N



2.4-2

FIGURE 1. SCHEMATIC DRAWING OF THE RADIOMETER SYSTEM

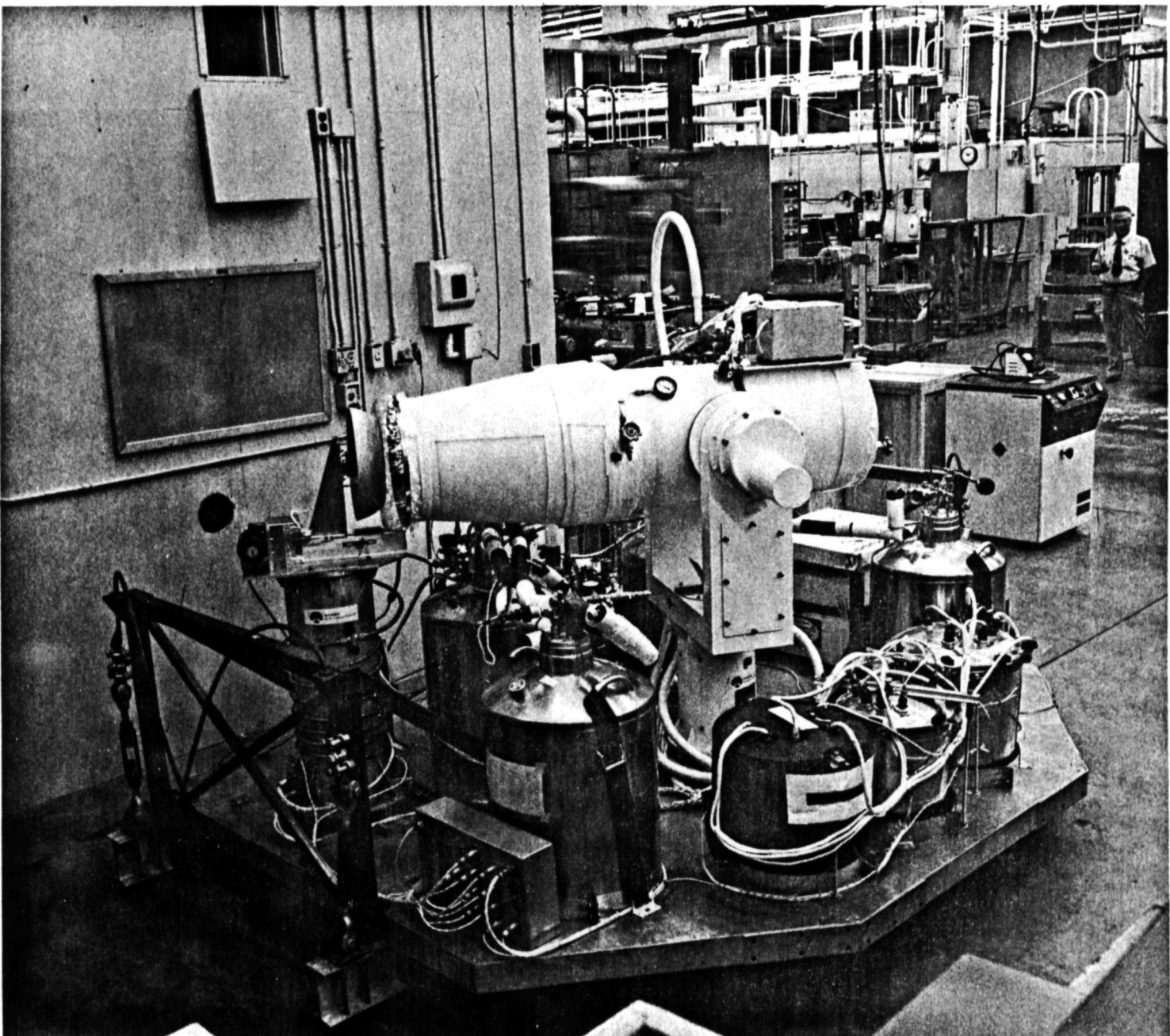


FIGURE 2. SYSTEM MOUNTED ON THE BALLOON GONDOLA
2.4-3

A light gathering system of the radiometer is a well baffled liquid nitrogen cooled Cassegranian telescope with a ten-inch diameter primary mirror. As the telescope's converging beam of radiation approaches its focus it passes through the plane of the rotary chopper. After passing through the Irtran-VI window and the Irtran-VI field lens which seal the vacuum space, the beam passes into the helium gas cooled reimaging cavity. After traversing the two filter wheels the beam comes to focus on a compound stop which contains nine individual openings each twice as large as the corresponding detector mask.

Provisions have been made so that a pair of filters can be placed at each individual field stop aperture. The converging beam(s) continue through the field stop and diverges to imping on an annular almost flat 4th order corrector mirror and still diverging is reflected back to a sphere from which they are imaged on the nine detectors. A linear demagnification of two is accomplished in the reimaging. The Cu:Ge detectors are individually masked to obtain the desired fields of view.

The detectors have FET preamplifiers mounted in close proximity to them and are biased by a feedback circuit to extend the dynamic range and frequency response.

The preamplifier of each detector feeds its signal into parallel linear and logarithmic amplifiers. The linear amplifiers have a wide range of gain settings which are controlled from the ground. The system contains an electronic calibrator which sends signals through the electronics upon command, to check the proper operation of the amplifiers.

Commanding circuitry which operates from Air Force supplied signals provides a means for the following: (1) starting and stopping the rotary chopper in flight and positioning it in a closed or open position; (2) operating the filter wheels to change the filters in the infrared energy paths; (3) changing the attenuator on the signal processing electronics; (4) operating the gaseous nitrogen flow control valves; and (5) operating the liquid nitrogen dump valves.

The sensor is mounted in a gimbal system which is driven by position servos in both azimuth and elevation. The gimbals are caused to position the sensor within their 210 degree azimuth and their 90 degree elevation range by commands from an Air Force supplied programming device.

A sectional view of the radiometer is shown in Figure 3. The radiometer housing is composed of two main sections, the front containing the radiometer telescope and the rear containing the reimaging system, detectors, chopper assembly, and filter assembly. The outer jackets of both sections are machined from aluminum alloy forgings which have been heat treated and cryogenically cycled during the interval between rough and finish machining so that thermally stable structures result. The outer jackets of both sections contain liquid nitrogen, as does the spider which supports the secondary mirror.

The telescope section has been designed so that the metal optical elements are mounted in a stress free fashion and are well cooled both by conduction to liquid nitrogen and by exposure to a purge of gaseous nitrogen at the temperature of the liquid. A heat exchanger, equilibrates the temperatures of the gaseous and liquid nitrogen before the gaseous nitrogen passes through the purge system to cool the mirrors.

The reimaging section contains a liquid helium tank, mounted in a vacuum space for thermal isolation from the outer jacket. It is supported by a fiberglass cylinder to control the conductive heat load. Mounted in this torroidal tank's center are the reimaging optics, detectors, and filter wheel assembly, all maintained at liquid helium temperature. The chopper wheel assembly attaches to the front of the rear section, and operates at liquid nitrogen temperature.

The optical system is designed so that the complete telescope section and the complete reimaging section are, as far as possible, each separate package subassemblies, and could be optically worked and tested as such. The supporting parts were toleranced so that focusing could be performed during the final assembly by optically lapping easily accessible surfaces.

The various demountable gas and liquid seals on the sensor body are accomplished by compressing round indium wire into a rectangular groove which is just a little too small to contain the volume of indium. The resulting overflow is pressed between the mating flat surfaces and forms a tight seal which will withstand cryogenic temperatures.

SENSOR

The sensor radiometer system consists of a paraboloidal primary mirror, a hyperboloidal secondary mirror, a "flat" mirror, an spherical reimaging mirror, an Irtran-VI window, an Irtran-VI field lens, a set of interchangeable filters, a field stop, and various masks and baffles.

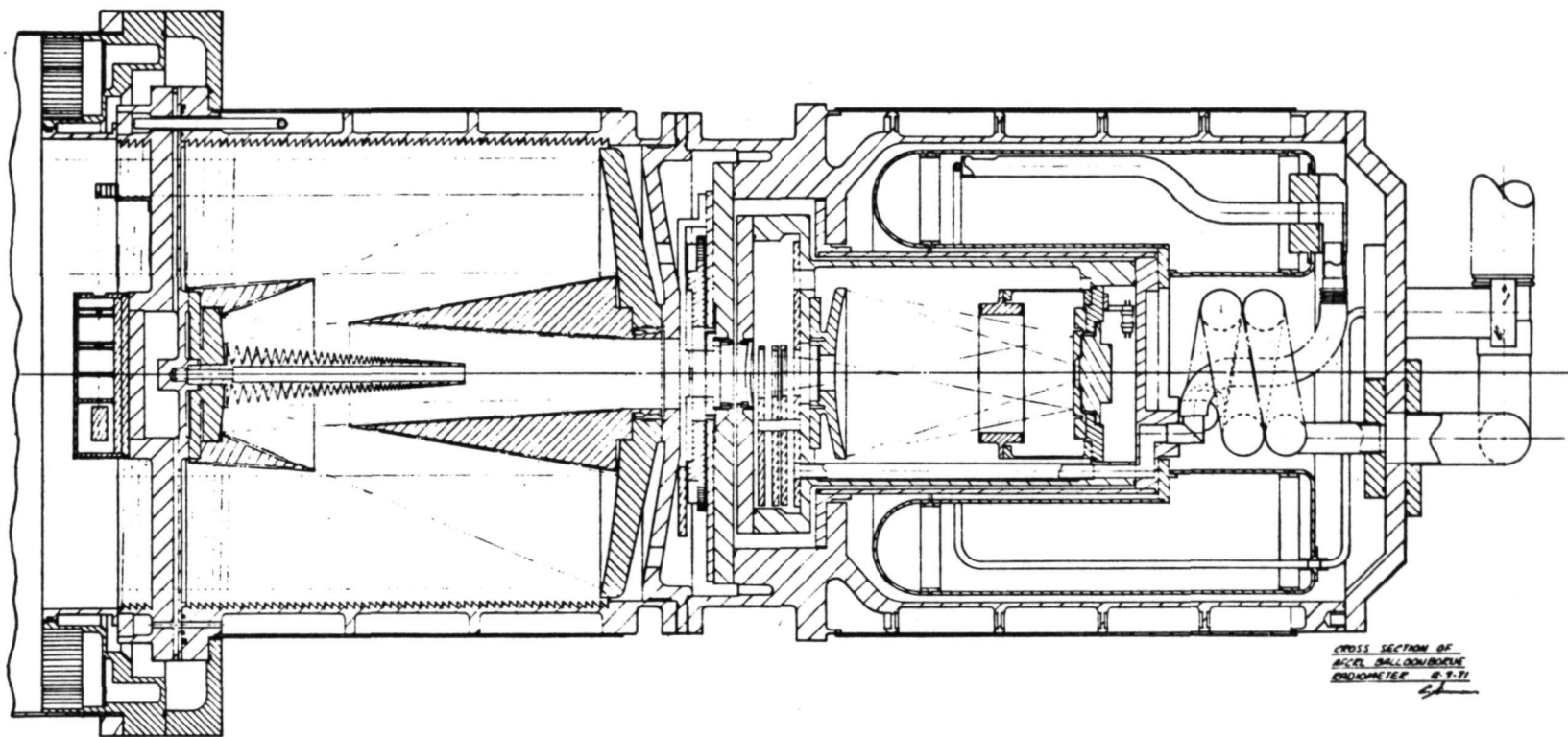
The mirrors were all made from forged billets of aluminum alloy which were cut from the central portions of multi-ton ingots in order to avoid inclusions. The mirror blanks were then heat treated and thermally cycled several times during the process of fabrication so that their shapes remain stable when they are cooled to cryogenic temperatures.

After machining to spherical surfaces close to the optical surfaces required, the aluminum blanks were then ground and lapped to standard optical fabrication techniques to within a thousandth of an inch of the proper figure. Then a thick electroless nickel deposit was placed over the aluminum surface, and the final surface developed by further lapping and polishing of the electroless nickel coating. After testing, the optical surfaces were coated with electroless gold plate for durability and high long-wavelength infrared reflectivity.

The optical system is extensively baffled to reduce the sensitivity of the instrument to radiation from sources from outside of the field of view. In addition to the conventional baffles in the main telescope, additional baffles are included in the reimaging optical system to reduce the effects of diffraction by the spider and central obscuration. These baffles prevent the detectors from viewing these illuminated edges directly.

Figure 4 illustrates schematically the laboratory set up which was used to accomplish the radiometric calibration of the instrument. The laboratory calibrator which is the key piece of equipment used in the calibration is unique and requires description.

REPRODUCIBILITY OF THE
ORIGINAL PAGE IS POOR



CROSS SECTION OF
ACCEL. BALLOONBOOM
ENDOMETER
E.T.T.

FIGURE 3. SECTIONAL VIEW OF RADIOMETER

2.4-6

2.4-7
97

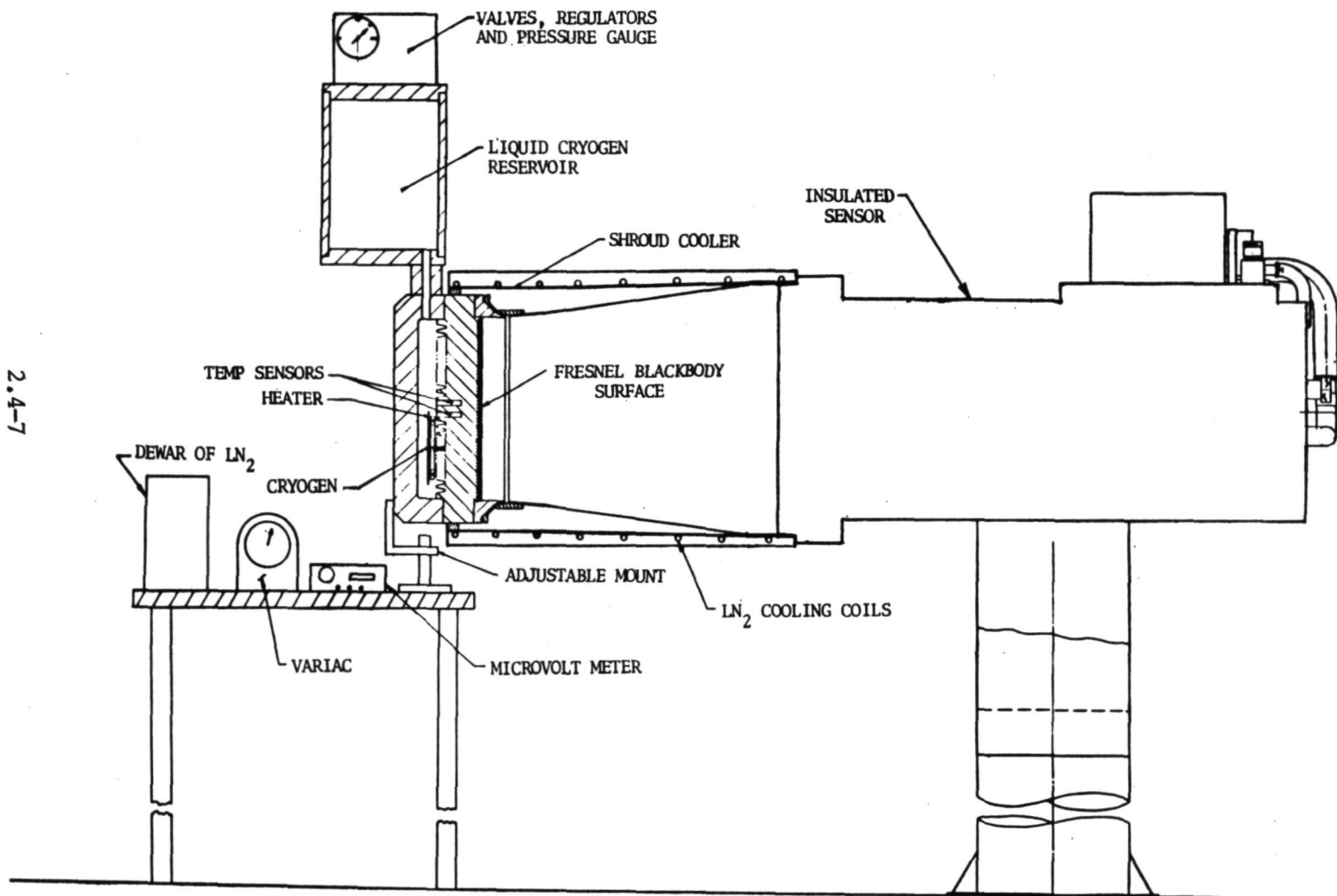


FIGURE 4. SCHEMATIC - RADIOMETRIC CALIBRATOR LABORATORY SET UP

CALIBRATION

The laboratory calibrator is a variable temperature blackbody source which is used for the preflight calibration of the infrared sensor. The device consists essentially of an insulated cryogenic pressure vessel in which the blackbody source, a circular, grooved plate, forms part of the wall. The heavy vessel can be operated at any pressure up to approximately 300 psi. The temperature can be varied almost continuously from under 77K to 300K. Large incremental changes of temperature previously had been achieved by using different cryogens. For a given cryogenic liquid, controlled, continuous changes of temperature are created at present by varying the pressure with the dewar.

In order to proceed expeditiously with the wide range calibration which was required, a 1000 watt calrod type heater was mounted inside the cryogen pressure cavity. When an electrical input to this heater is controlled by a continuously variable transformer, and the cavity contains pressurized gaseous nitrogen or a mixture of gaseous and liquid nitrogen, and the pressure adjusted as required, a wide range of stable temperatures may be obtained much more easily and quickly than by changing cryogens.

Figure 5 is a schematic drawing which shows the calibration device as it appears when attached to the shroud of the infrared sensor. The basic parts are the pressure vessel, calibration source plate, valves and pressure regulators, temperature sensors, and mounting devices. The outside of the calibration source plate is machined with concentric circular grooves, and then sandblasted and black anodized in order to provide a high emissivity.

Concentric circular grooves are also machined on the inside of the plate in order to increase the heat transfer between the cryogen and plate. Mounted on the top of the dewar are a fill valve, vent valve, multi-pin electrical feedthrough connector, burst disk, pressure relief valve, and pressure gauge. The temperature is monitored at a number of points within the source plate by copper constantan thermocouples. The sensor output leads are connected to the multi-pin electrical connector. Rigid attachment of the calibration device to the sensor is accomplished by clamps (not shown) which hold the sensor shroud against the mounting ring. The bottom mount supports the calibration device on a table. The pressure vessel is covered with Armaflex insulating material.

Proper calibration of the radiometer with the laboratory calibration device required that the faceplate of the laboratory calibrator be positioned at the end of the antifrost shroud and that no significant radiant energy be allowed to get into the radiometer except that emitted from the calibrator faceplate. This requires that the antifrost shroud be cooled to 77K, so that any radiance emitted from its inside surface, when reflected by the faceplate into the radiometer, will be very small compared to the emitted radiance of the faceplate itself. For this purpose a shroud cooler has been constructed for use with the laboratory calibrator.

The shroud cooler consists of an aluminum cylinder which fits around the antifrost shroud and attaches to the radiometer and the laboratory calibrator. A coil of one-half inch aluminum tubing is welded around this cylinder. Liquid nitrogen flowing through the tubing maintains the shroud cooler at 77K, and the shroud itself is then cooled by convection and radiation until it reaches an equilibrium temperature near 77K.

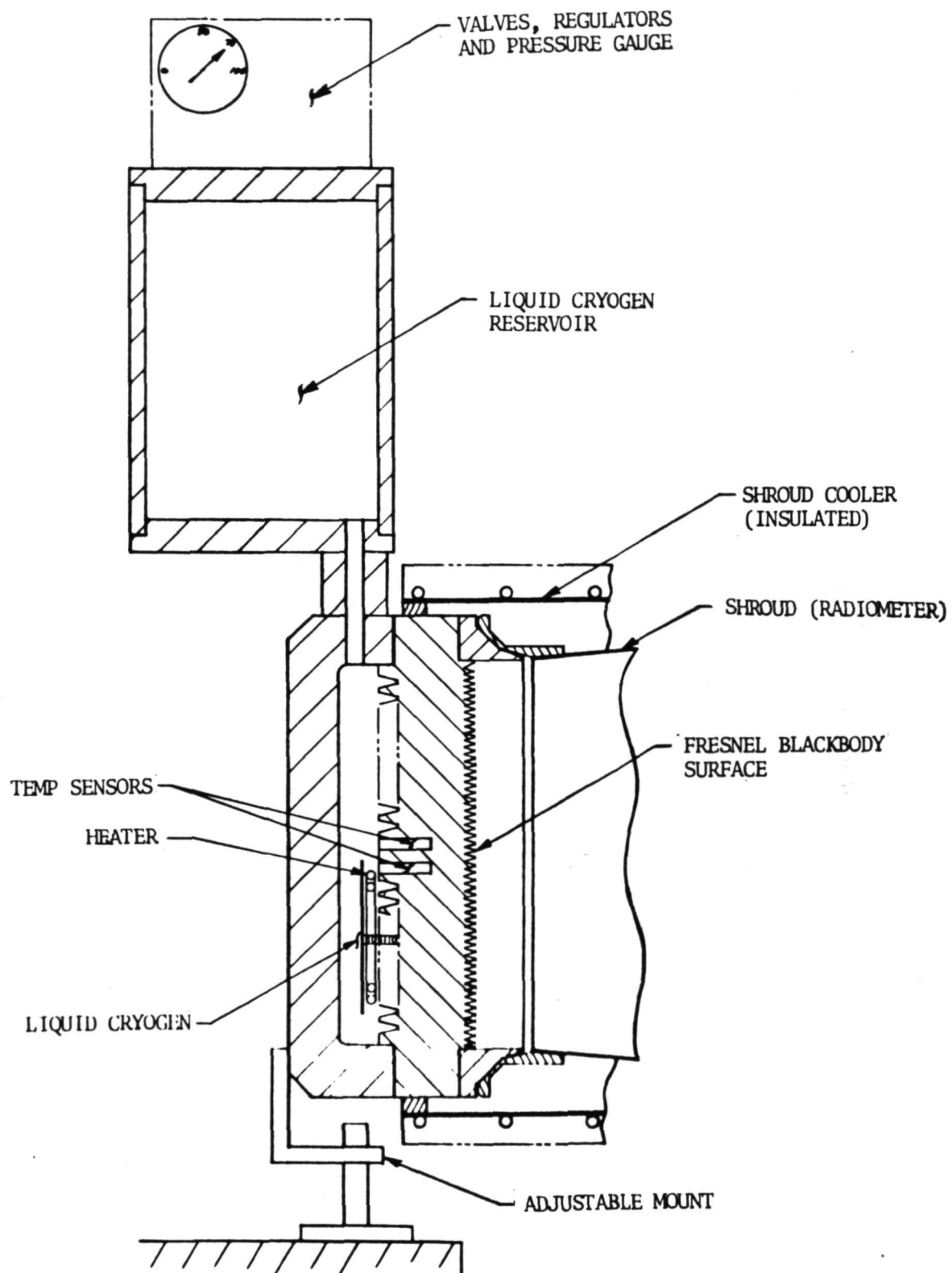


FIGURE 5. SCHEMATIC OF LABORATORY CALIBRATOR ATTACHED
TO SENSOR HEAD

2.4-9

The AFCRL personnel determined the range of radiance over which calibration was desired and then prepared a list of temperatures at which these radiances would be emitted by the blackbody calibrator. Thermocouple EMF's (using a liquid nitrogen reference) were then tabulated for the listed temperatures. A digital microvoltmeter which displayed the thermocouple EMF was used as an indicator as the temperature and the radiance of the blackbody was set at each of the required steps. By manipulating the pressure of the gaseous nitrogen over the liquid nitrogen in the calibrator, and the electrical input to the 1000 watt heater in the calibrator the temperature could usually be held to 1/3 degree centigrade.

At each radiance step (temperature) the output of each detector through each amplifier and with a representative selection of gain steps and filter combinations was recorded. System noise was recorded from a true RMS voltmeter at the point where the radiance of the blackbody equaled the radiance of the chopper.

FILTER WHEELS

The two remotely operated filter wheels are located in planes between the field lens and the field stop. Each wheel has six positions, each position has the capability of containing two filters either spectral or neutral density. The filter wheels (as well as the reimaging mirrors and baffles) are cooled by liquid helium boil-off and operate at about 10K. The filter wheels can be independently rotated by remote control (onboard programmer or telemetry) to change filter combinations. The assembly is illustrated in Figure 6.

Each filter wheel is rotated by a solenoid-driven ratchet which engages teeth around the wheel perimeter. When a filter change command is received, The logic circuitry causes the ratchet mechanism to advance the wheel, stopping it automatically when the next filter is in position.

Signals representing the position of the filter wheels are transmitted to the ground by telemetry. A temperature sensor mounted on the assembly (but thermally isolated from it) reports the temperature of the helium gas surrounding the assembly.

CHOPPER

The chopper wheel is a three-bladed wheel rotating at 2000 rpm, resulting in a signal chopping frequency of 100 Hertz. The chopper is driven by a hysteresis synchronous motor and is capable of being stopped in either a closed or open position. The entire assembly is operated at a temperature of 77K. A photograph of the chopper wheel assembly is shown in Figure 7.

Normally stocked motors available from the vendors will not operate at 77K due to the freezing of their bearing lubricant. The bearings of a small synchronous motor were therefore replaced with special "BARTEMP" low-temperature ball bearings containing a sacrificial lubricating retainer. The motor runs at 12000 rpm and is powered by a 400 cycle inverter.

BARTEMP ball bearings are also used in the chopper wheel and in the idler gear. In addition, the idler gear itself is made of Rulon to avoid the necessity of lubricating the gear teeth.

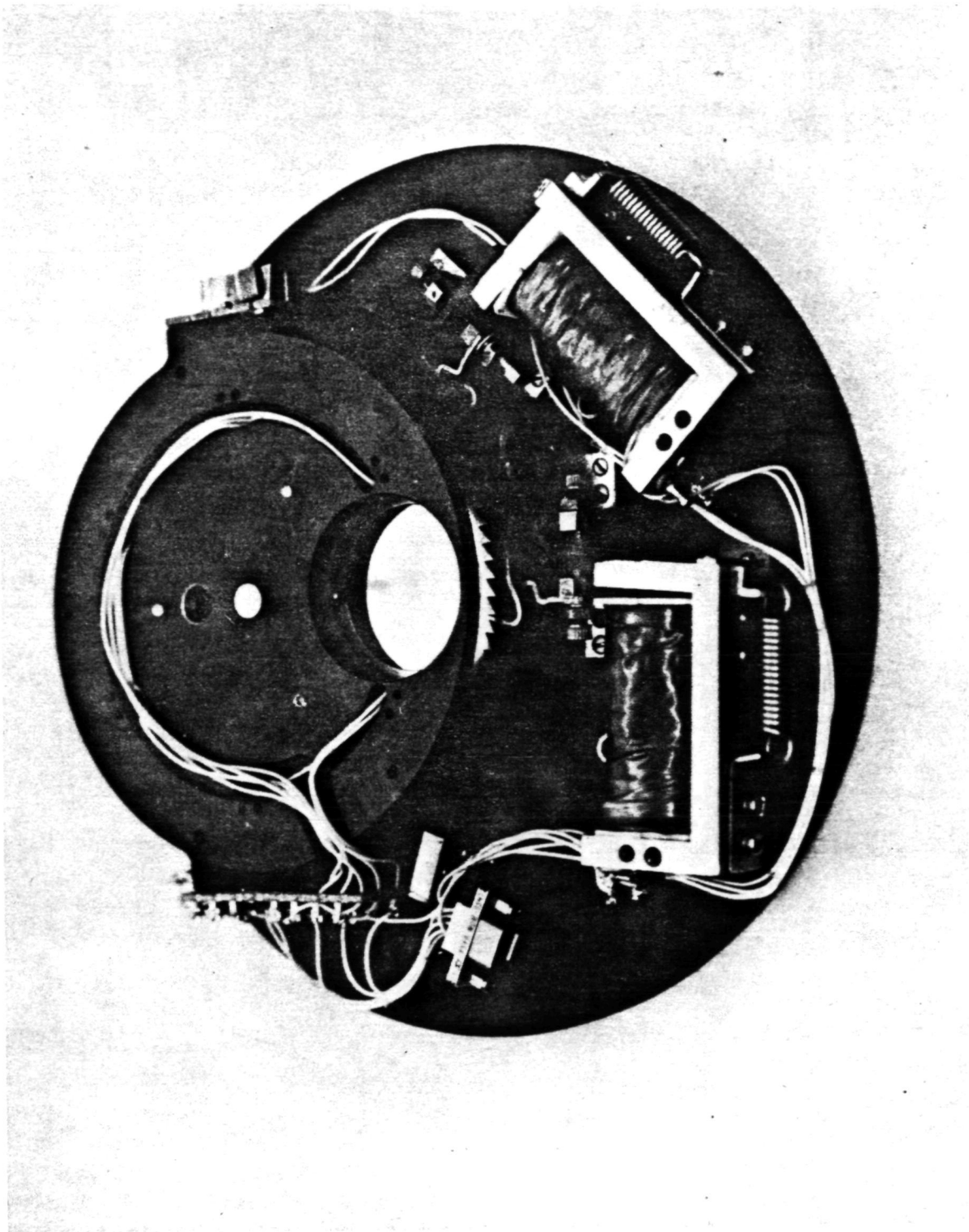


FIGURE 6. FILTER WHEEL ASSEMBLY
2.4-11

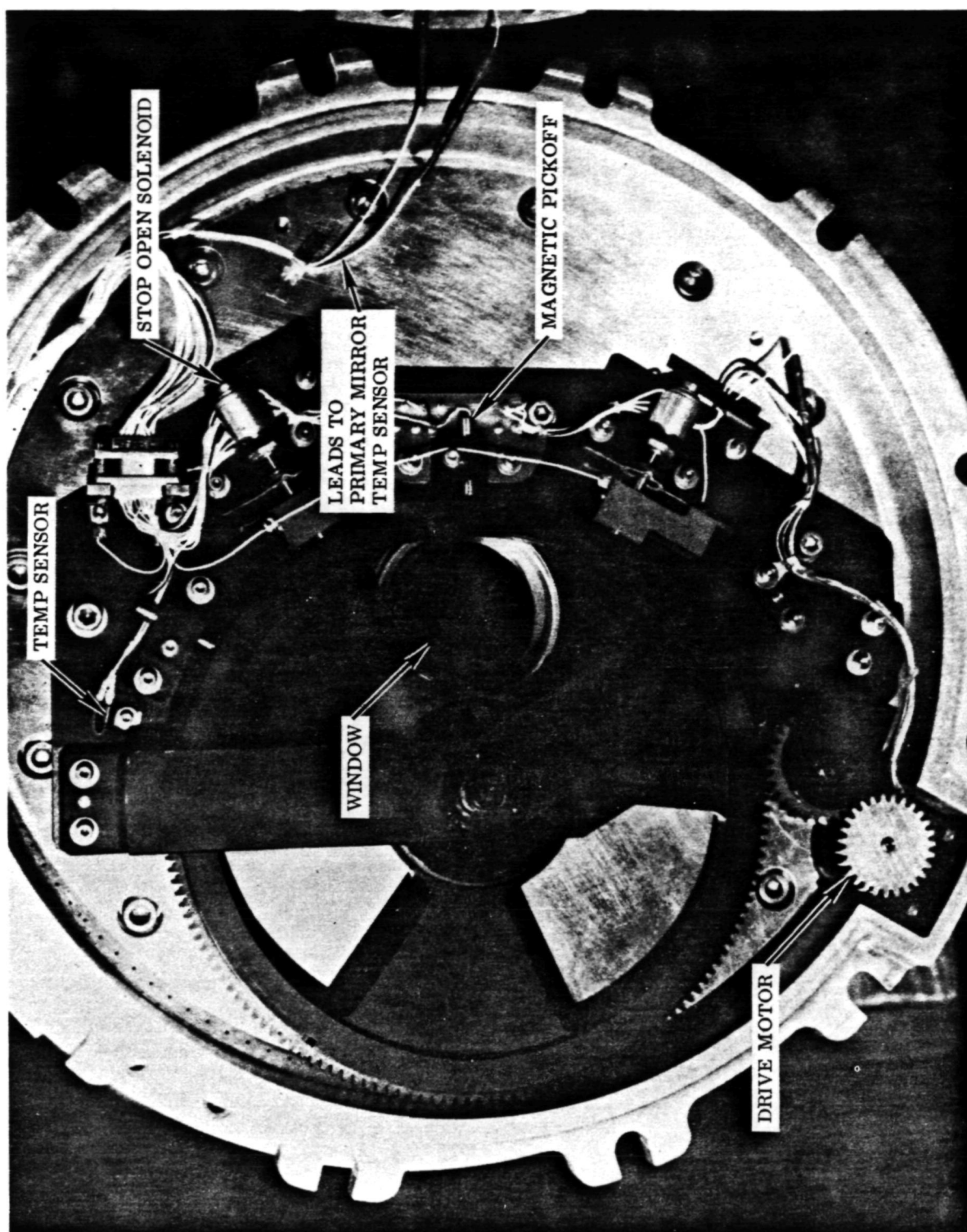


FIGURE 7. CHOPPER WHEEL ASSEMBLY
2.4-12

In the mechanism which was developed to selectively stop the chopper wheel in the open or closed position, a small linear solenoid is used to push a small steel pin into a hole in the chopper periphery. This provides a positive positioning action, and also permits remote verification of proper operation by simply monitoring the position of the locking pin with an electrical contact. Three holes in the chopper wheel allow it to be stopped with any of its three blades in the "closed" position, and a second solenoid angularly displaced from the first and working into the same set of three holes allows stopping in any of the chopper's three "open" positions.

The chopper can be remotely commanded to run or to stop in either the open or closed position. A time delay in the command logic prevents the stopping pins from being pushed into the wheel before it has coasted to a stop. Upon switching from the "running" mode to a stop mode, the following sequence of events is activated automatically: (1) the chopper motor is turned off; (2) after a preset time delay (90 seconds) to allow the chopper to stop, the stop pin is pushed against the wheel rim by the solenoids; and (3) the drive motor is pulsed to rotate the chopper wheel slowly until one of the three holes reaches the pin. Upon completion of this sequence the electrical contact on the solenoid mechanism will signal positive confirmation of chopper position ("open" or "closed").

CRYOGENIC SYSTEMS

The requirement that the radiometer must operate frost free and produce no fog, dictates the use of ambient temperature antifrost gas. A clear aperture antifrost device is fed dry nitrogen at approximately ambient temperature (260K) to prevent the formation of fog. The flow rates required depend upon the ambient pressure which controls the expansion and hence the flow velocity, and whether or not the balloon is ascending and producing a relative wind. In order to conserve the weight of antifrost nitrogen, weight of the water to vaporize it and the container weights, the system has been designed to utilize three different flow rates. Estimates based on laboratory and field experiments indicate that at altitudes between 80,000 and 120,000 feet, ten pounds of gas per hour will be sufficient to keep the aperture frost free. Twenty-five pounds per hour will be sufficient between 50,000 and 80,000 feet, while 50 pounds per hour will be required for operation between 35,000 and 50,000. The low altitude capability adds considerable weight to the system. The system has been built so that these flow rates can be preset before the flight or they can be programmed during a flight to allow measurements at several altitudes.

The gaseous nitrogen supply for the antifrost device consists basically of three liquid nitrogen storage containers, three heat exchangers, two temperature control valves, a gas mixer, and a gas flow control section.

The delivery liquid nitrogen container is vacuum insulated and contains liquid nitrogen at 60 psig. The pressure is maintained by a heater and controlled by a pressure switch and protected by a pressure relief valve and a disc.

The first heat exchanger converts liquid to gas by absorbing heat from a water bath. The heat exchanger is a coil of tubing immersed in a tank of water. The second heat exchanger is a coil of tubing in a smaller tank of water.

The gas flows through this exchanger system depending upon the operation of a temperature control. The third heat exchanger is a coil of tubing exposed to the ambient atmosphere. This exchanger is used to smooth out gas temperature fluctuations and to bring the gas temperature closer to the ambient temperature.

The liquid nitrogen supply system for cooling the telescope consists of a vacuum insulated liquid storage container, a liquid nitrogen delivery control device, and insulated delivery lines. The system delivers liquid nitrogen, on demand, to the liquid nitrogen jacket on the telescope. The telescope jacket is built around the liquid helium tank and acts as a cooled heat shield for the helium. The jacket also cools the telescope optics by conduction. The secondary mirror has a mounting which is in contact with a liquid nitrogen pool in the spider body. The spider pool is fed liquid nitrogen through drilled holes in the spider legs. The boil-off gas from the jacket is used as a continuous low temperature dry gas purge for the telescope, and provides additional cooling to the primary mirror and chopper. Conduction through the jackets foam insulation controls the production rate of the boil-off gas.

To operate the delivery system, the liquid container is filled with liquid nitrogen and pressurized by a heater which boils some of the liquid. The liquid is then transferred to the telescope jacket through insulated tubing, a section of which is flexible to allow telescope movement. The jacket level is sensed by a carbon resistor element in a control circuit which regulates the flow in the transfer line, thus maintaining the correct liquid level in the telescope jacket.

The helium-cooled subsystem consists of the reimaging package and the helium dewar. The reimaging package contains the detector package, the reimaging optics and field lens, and the two filter wheels. The subsystem is supported from its liquid nitrogen-cooled surrounding structure by a low thermal conductance glass epoxy tube, about six inches in diameter. This support cylinder lies within a well which extends the full length of the dewar, and attaches to the dewar at a step in the well somewhat more than halfway through the dewar. The reimaging package occupies the volume within the support tube, and is connected to the support tube and the dewar at the step in the well of the dewar.

The space between the helium-cooled subsystem and its IN_2 surroundings is evacuated to provide insulation for the helium subsystem. (Included in the evacuated volume is the annular space on either side of the support tube.) The IN_2 temperature of the surroundings and the 0.1 emittance of the clean aluminum surfaces of the various components result in a low radiative heat transfer to the helium subsystem. The radiative load is 0.002 watt to the reimaging package and 0.009 watt to the dewar. The primary thermal load is 0.016 watt to the reimaging package via the support tube. The total loads on the system are 0.018 watt to the reimaging package and 0.010 watt to the dewar.

The entire reimaging package is maintained below 10 K by flowing the gas evaporating from the dewar past the detector package, through the body of the reimaging package, and across the faces of both filter wheels before venting the gas from the system. The field lens is vacuum sealed to the front of the reimaging package to prevent the leakage of the helium gas into the vacuum space.

The gas evaporating from the dewar provides cooling equivalent to one latent heat of evaporation for every four degrees K the gas is warmed. Hence, the natural boil-off from the dewar (due to the 0.010 watt heat leak) is slightly less than that required to overcome the 0.018 watt thermal load on the reimaging package while maintaining the detectors below their maximum 10K operating temperature. Hence, a thermal shunt on the dewar has been chosen which will deliver about 0.04 watt to the liquid helium, sufficient to supply enough cold gas to keep the detectors below 7K. These calculations indicate that the dewar will contain sufficient helium for 14 hours operation.

This arrangement for flowing the vent gas through the reimaging package was designed for the express purposes of operating the filter wheels at a temperature specified to be no greater than 40K (and preferably below 35K) and of cooling the filter wheels to operating temperature in a reasonable time. In this design the entire reimaging package, including filter wheels, are rapidly cooled by the large quantities of gas produced during the cool-down and filling of the helium dewar. The filling of the dewar and the cooldown of the reimaging package take one hour. The operating temperature of the spectral and neutral density filters is near 10K.

DISCUSSION SUMMARY — PAPER 2.4

This system was used by the Air Force during four flights to study atmospheric constituents. Typical flight altitude was 90 to 96,000 feet. It was not developed as a shuttle prototype and is now in storage.

The instrument operated between 3 and 25 microns and it uses refractive optics. It includes filters mounted in a filter wheel and achieves 2-micron bandwidths. The performance was characterized as being within 50 percent of the theoretical limit for gallium doped germanium detectors.

Part of this system was cooled with liquid helium and part with liquid nitrogen. Therefore the detectors operated at 8° K, the reimaging optics at about 12° K to 15° K, the filters at less than 40° K and the primary, secondary and housing were cooled to liquid nitrogen temperatures.

A year and a half were used to design and build this system at a cost of \$350,000. \$125,000 was spent for flight operations over the next year and a half.

PAPER 2.6

ULTRAVIOLET STELLAR SPECTROPHOTOMETRY
FROM A BALLOON PLATFORM

Yoji Kondo

Lyndon B. Johnson Space Center, Houston, Texas 77058

Curtis Wells

Lockheed Electronics Company, Houston, Texas 77058

ABSTRACT

A 40 centimeter diameter aperture, balloon-borne telescope and ultraviolet spectrometer is described and selected scientific results are briefly reviewed. The general configuration of the 0.4 angstrom resolution instrument is shown and the utilization of servo-controlled secondary mirror, image dissector detector, and special mirror coatings are discussed. An outlook for astronomical research in the mid-ultraviolet from balloon-borne telescopes is presented together with future development plans for JSC's balloon-borne payload.

I. INTRODUCTION

We wish to outline the scientific program and the existing payload configuration of JSC's Balloon-Borne Ultraviolet Stellar Spectrometer (BUSS) project and outline the plans for the future development of this ultraviolet stellar spectrometer.

The electromagnetic radiation from outside the earth is cut off shortward of about 2000 Å due to the atmospheric absorption. However, if a telescope is taken above the bulk of the ozone layer, it becomes possible to extend astronomical observations to about 2000 Å. From an altitude of 40 km, which is relatively easy to attain today, the entire mid-ultraviolet region becomes accessible; there exists, however, a region of higher absorption near about 2500 Å (Navach, Lahmann and Huguenin, 1973). The extent of the atmospheric attenuation at a given altitude will depend on the time of the flight and the geographic area.

Because of the residual absorption present even at an altitude of 40 km, there exist some difficulties in performing absolute photometry. However, for some types of relative photometry and spectrophotometry, balloon-borne telescopes open up great opportunities. A payload weighing over 500 kg may be taken to this altitude with a balloon of about half a million cubic meters. For those types of observations that can be carried out effectively from the balloon, it provides a basically more economical way (relative to the rocket) to conduct space observations. Compared with the typical few minutes of observing time available for rockets, balloons provide several hours of observing time. Further, it provides an opportunity to utilize the newly developed techniques with the minimum lead time. In contrast, the instrumental design for an orbital experiment must usually be finalized several years prior to launch.

II. ULTRAVIOLET ASTRONOMY FROM THE BALLOON-BORNE PAYLOAD

The types of astronomical observations suitable for a balloon-borne payload in the mid-ultraviolet region (2000-3000 Å) include; (a) relative photometry or spectrophotometry; (b) polarimetry, e.g., project Polariscope by T. Gohrels; (c) imagery, e.g. Project Stratoscope by M. Schwarzschild. In this article we shall discuss spectrophotometry.

The mid-ultraviolet is rich with spectral lines of once- or twice-ionized (and some more highly ionized) metals and provides astrophysical information of much interest. Investigations may be grouped into two basic areas; (1) stellar atmospheres and (2) interstellar media. The study of stellar atmospheres encompasses photospheric lines and "chromospheric" lines, although both types of studies inevitably will overlap with each other.

An investigation of photospheric lines in the mid-ultraviolet is a very useful tool in understanding the atmospheres of intermediate temperature stars (late B to F types) whose surface temperatures are such that many metals are once- or twice-ionized and their strong lines are observable in the mid-ultraviolet. It should prove an especially powerful tool in understanding the physics of the stars with anomalous abundances, such as Ap and Am stars.

The mid-ultraviolet "chromospheric" lines arising from resonance transitions of ionized metals, allowing the word "chromosphere" to include extended atmospheres, will provide exciting opportunities for furthering our comprehension of the outermost layers of stars. Such investigations should also yield valuable information on the mass flow from supergiants of early to intermediate spectral types.

Strong mid-ultraviolet resonance lines, such as the Mg II doublet at 2795 Å and 2802 Å and the Mg I at 2851 Å, provide a vehicle to study the interstellar abundance of these elements in terms of their column density. If, for instance, the interstellar Mg II and Mg I lines are studied together, we can also investigate the electron density and temperature in the interstellar space (e.g. Boksenberg et al., 1972).

III. STUDY OF THE Mg II DOUBLET AT 2795 and 2802 Å FROM THE BALLOON-BORNE ULTRAVIOLET STELLAR SPECTROMETER (BUSS)

The emission of the Ca II doublet component at 3933.7 Å, otherwise known as the Fraunhofer K line, has been employed as a useful tool for studying the stellar chromospheres, e.g., Wilson (1966). However, this emission becomes nearly impossible to detect for stars earlier in spectral type than mid-F. This has been interpreted variously as a result of the disappearance of chromospheres for stars earlier than mid-F or the observational effect due to coupling of the weakening of the Ca II K line and the rising continuum level for the stars in this spectral range.

The Mg II resonance doublet at 2795.5 and 2802.7 Å ($3s^2S-3p^2P^0$) is the ultraviolet magnesium equivalent of the Ca II resonance doublet at 3933.7 and 3968.5 Å ($4s^2S-4p^2P^0$). However, there are reasons to expect the Mg II doublet emission to be more prominent than that of the Ca II doublet, at least for the stars of early spectral types. The cosmic abundance of magnesium is greater than that of calcium; according to Allen (1963) magnesium

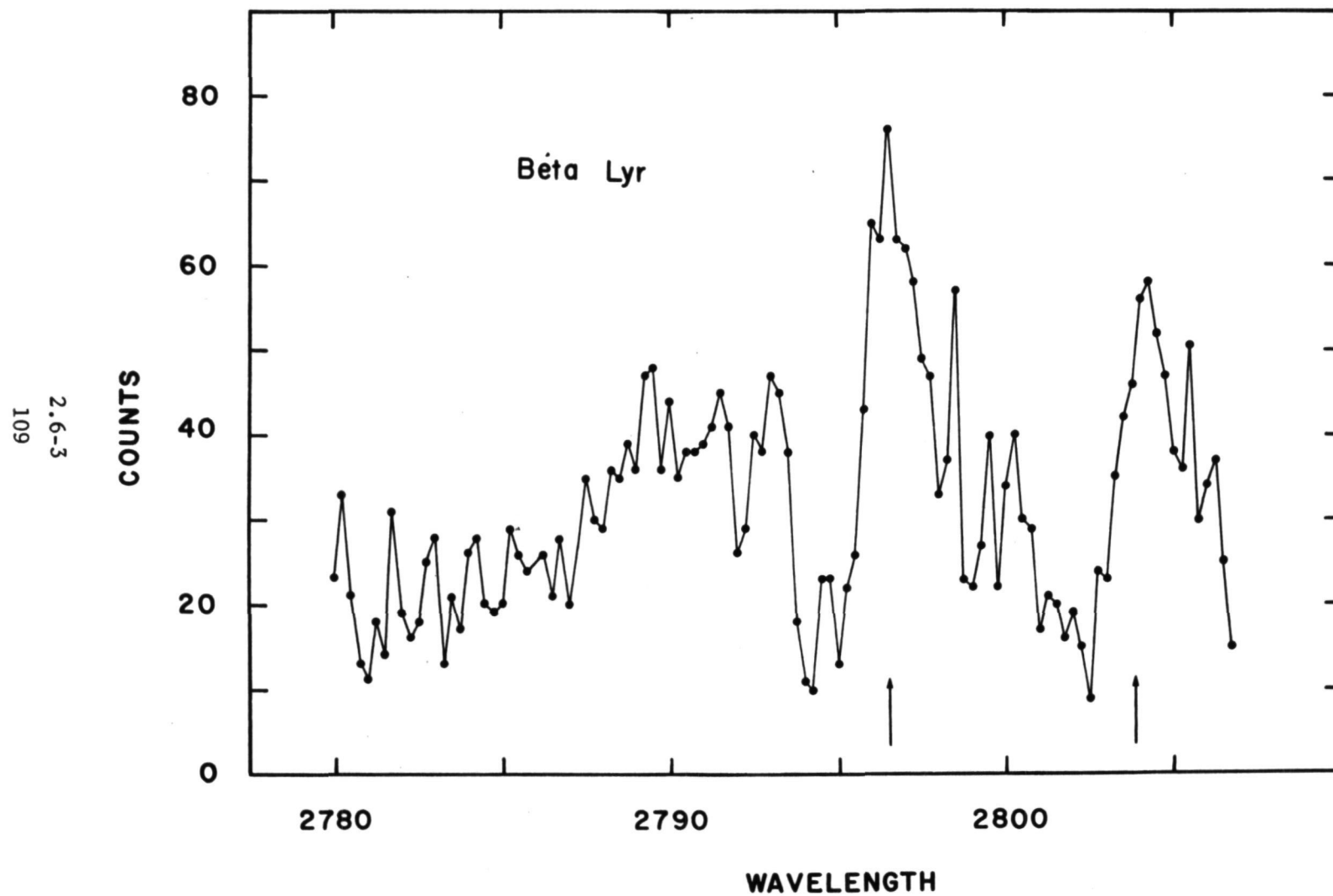


Figure 1. β Lyr Mg II Doublet Emission

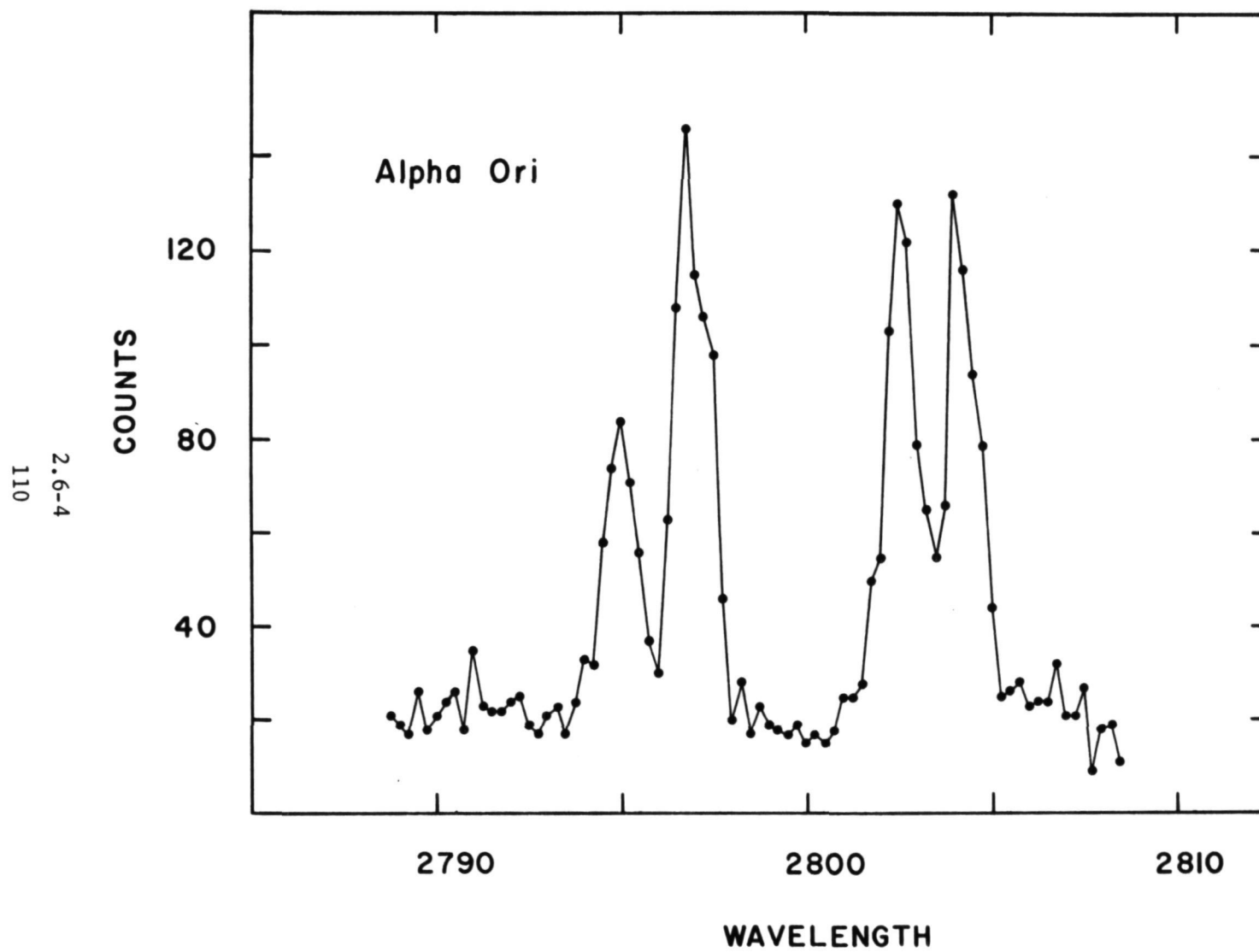


Figure 2. α Ori Mg II Doublet Emission

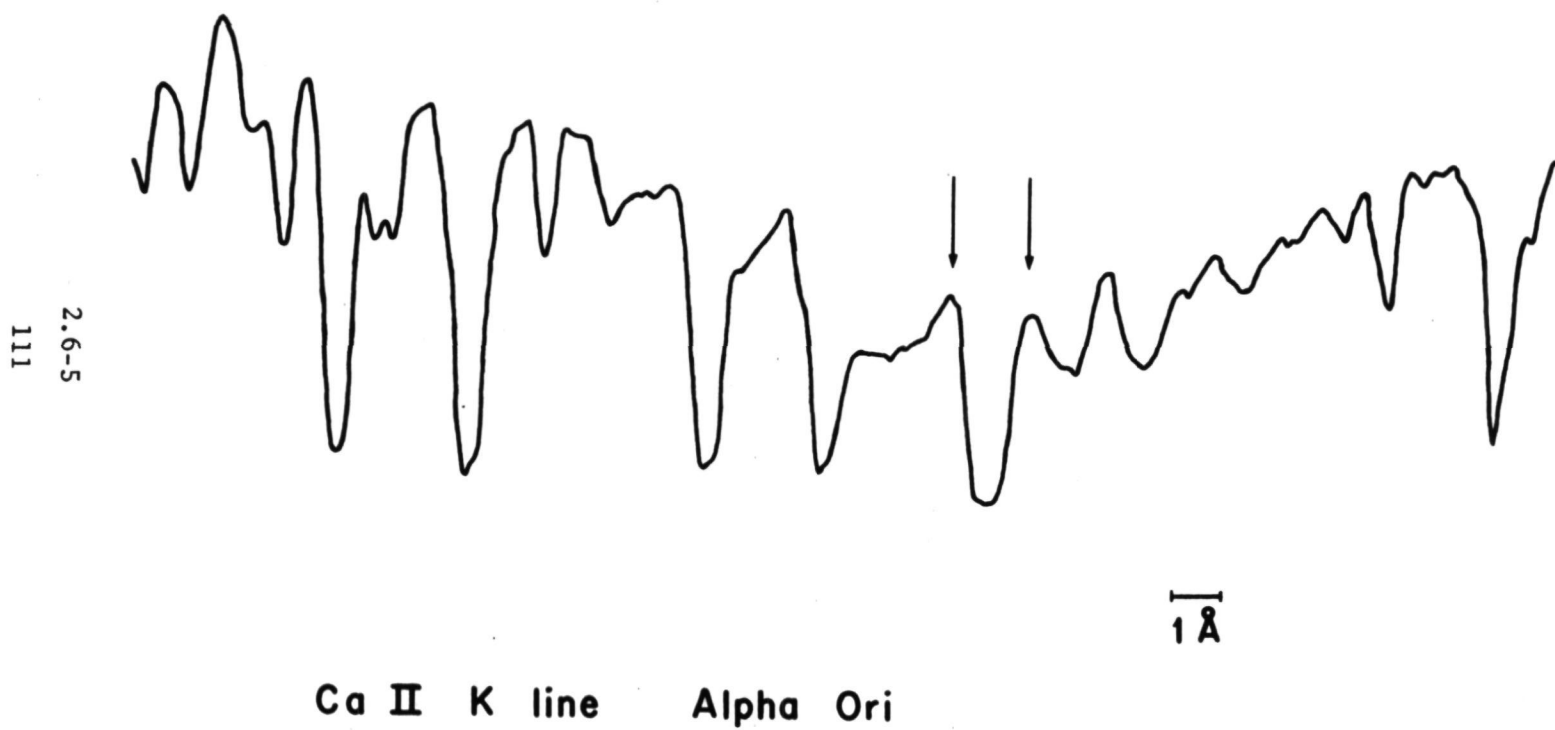


Figure 3. α Ori Ca II "K" Emission

is about 17 times more abundant. The ionization and excitation potentials of these calcium and magnesium lines are such that the Mg II doublet lines are expected to be much stronger than the Ca II doublet, making more feasible the detection of a weak emission at the bottom of the absorption feature. The stellar continuum level at 2800 Å is lower than that at 3900-4000 Å for stars of spectral types later than A. This may be expected to make detection of a weak emission easier.

Indeed, the Mg II doublet absorption features are shown to be the most prominent spectral feature in the mid-ultraviolet by recent observations from orbiting manned spacecraft (Kondo, Henize and Kotila - 1970; Gurzadyan and Ohanesyan - 1972) and satellite (Lamers, et al - 1973).

The Mg II doublet emission observed in β Lyr and α Ori during the past two flights of the BUSS payload are shown as examples in Figures 1 and 2. The slit width employed for the spectrometer was 0.25 Å; the resolution was about 0.4 Å. The Ca II "K" line emission in α Ori is shown in Figure 3 for comparison; it demonstrates clearly that the Mg II doublet emission is the more prominent of the two. A comparison between the observed Mg II doublet emission widths and the Ca II "K" line emission widths (Wilson and Bappu, 1957) is discussed by Kondo et al (1972).

The results thus far obtained demonstrate clearly that the Mg II doublet at 2795 and 2802 Å are indeed the most prominent spectral features in the mid-ultraviolet. The work by Lamers et al (1974), based on the results from the S59 ultraviolet experiment on the TD1 satellite, shows other interesting mid-ultraviolet spectral features in addition to the Mg II doublet. Although the future space observations will probably reveal other astrophysically important spectral features, the Mg II doublet is likely to remain as among the most significant.

IV. DESCRIPTION OF THE BUSS PAYLOAD

We should next like to present a general description of our instrument and discuss some of the more interesting features of the optical and detector systems. The original payload, shown in Figure 4, was designed and built by Ball Brothers Research Corporation of Boulder, Colorado, in 1971. The payload is about 3.5 m in diameter by 2.5 m high and weighs 540 kg, excluding ballast. Crush pads are attached to the four legs of the lower section or gondola, and the roll cage supplies additional protection to the telescope. The suspension train is composed of a 9.5 mm diameter counterwound steel cable extending some 30 m above the gondola to a 20 m diameter nylon parachute. A 420,000 m³ single cell polyethylene balloon lifts the package to an altitude of 40 km. Launches are from the National Center for Atmospheric Research (NCAR) balloon base at Palestine, Texas.

The instrument section consists of the telescope, spectrometer, star trackers, and electronics. The instrument is attached to the gondola through a central drive case which carries the elevation and azimuth shafts and their bearings. The telescope is counter balanced on the opposite side of the drive case by the pointer electronics. Three levels of tracking are employed to achieve an ultimate 3" rms tracking error. Initial pointing by magnetometer in azimuth and potentiometer in elevation brings the target star within

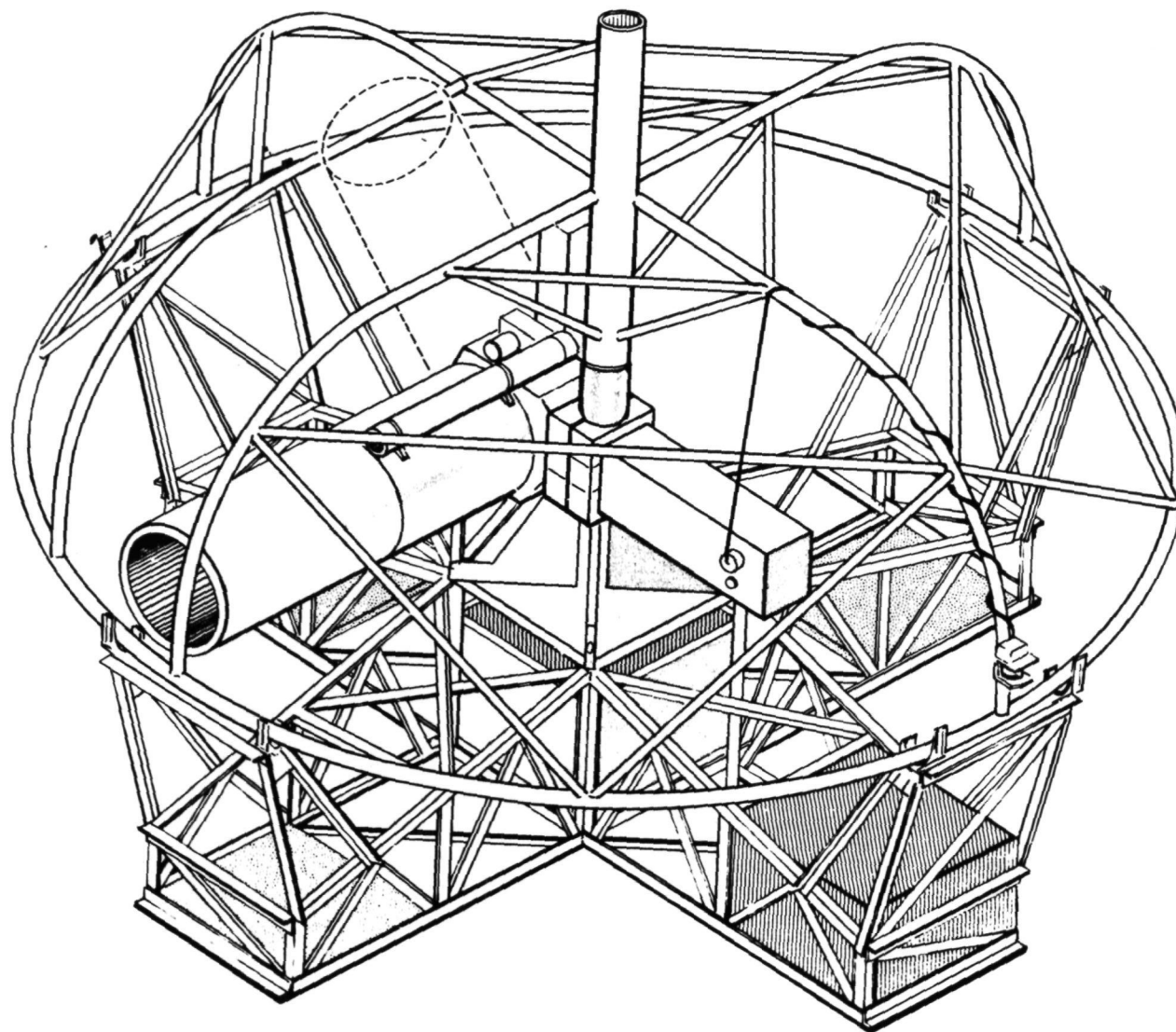


Figure 4. BUSS Payload

the 1° elevation by 3° azimuth field of view of the outer loop star tracker. Payload position data for referencing the magnetometer is provided by NCAR's omega navigation system. The outer loop star tracker is mounted coaxially above the telescope and holds the telescope error to less than $5'$ with respect to the target star. The 16.5 mm aperture outer loop tracker employs an image dissector, has a range of 4.5 stellar magnitudes, a limiting magnitude of +6 and utilizes magnitude discrimination circuitry to select the desired star from the field of view.

Figure 5 shows a cross section of the telescope and spectrometer. Fine tracking is accomplished by tilting the secondary mirror to reduce object errors of up to $5'$ to less than $3''$, effective at the telescope focus. The fine position tracker which controls the secondary mirror is also an image dissector. Control system bandwidths are about 1 hz and 20 hz for the outer loop tracker and the fine position tracker respectively. The telescope is a 40 cm aperture, f/7.5 modified Ritchey-Cretien with servo controlled secondary mirror. The telescope, which uses two hyperboloidal surfaces as in the Ritchey-Cretien, was designed by Bottema and Woodruff (1971) and termed "tilted aplanatic". Object angle errors of up to $10'$ can be compensated by tilting the secondary mirror to return the image to the optic axis while maintaining a $2''$ image size. In this design, third order coma is eliminated at the expense of relatively large mirror eccentricities; -0.58 and -12.5 for the primary and secondary respectively (eccentricity of 1 implies a sphere). This makes the fabrication of the mirrors a relatively difficult task. For example, the thickness of glass to be removed at the edge relative to a sphere, in the case of the primary, is $14\text{ }\mu\text{m}$ for a true cassegrain, $17\text{ }\mu\text{m}$ for a Ritchey-Cretien, and $23\text{ }\mu\text{m}$ for the tilted aplanatic. The mirrors were fabricated by Diffraction Limited, Inc., of Bedford, Massachusetts, and performed to the design goal of $2''$ image size. Both mirrors were made of Cer-Vit and the primary mirror was weight relieved to a weight of 11 kg. The primary mirror is supported on the back side by 3 nylon pads and by 3 spring loaded pads at corresponding points on the front surface of the mirror. About .3 kg is applied to each of the pads on the front surface. The mirror restraints in the radial direction have a slight clearance to allow for thermal changes in the mirror cell. The pads supporting the back of the mirror and the back of the mirror are so shaped that any motion of the mirror is restricted to a rotation about its center of curvature. The secondary mirror is mounted in a flex pivot-gimbal arrangement and controlled by torque motors. The secondary mirror and spider assembly are connected to the primary mirror housing by an invar truss. Mirror alignments have been checked after flight and were found to have remained within the flight limits, through the landing and recovery phases. The fact that the primary mirror was undamaged in an accidental 30 km payload free fall gives a great deal of confidence in the mounting and in the mirror material.

The dichroic filter reflects a 500 A wide band of ultraviolet, centered on 2800 A, into the Ebert-Fastie spectrometer and transmits over 80% of the visible light to the fine position star tracker. The f/7.5, 0.5 m focal length spectrometer is basically an Ebert-Fastie type utilizing a 2160 grooves per millimeter grating in second order to achieve a dispersion of 3.3 A/mm.

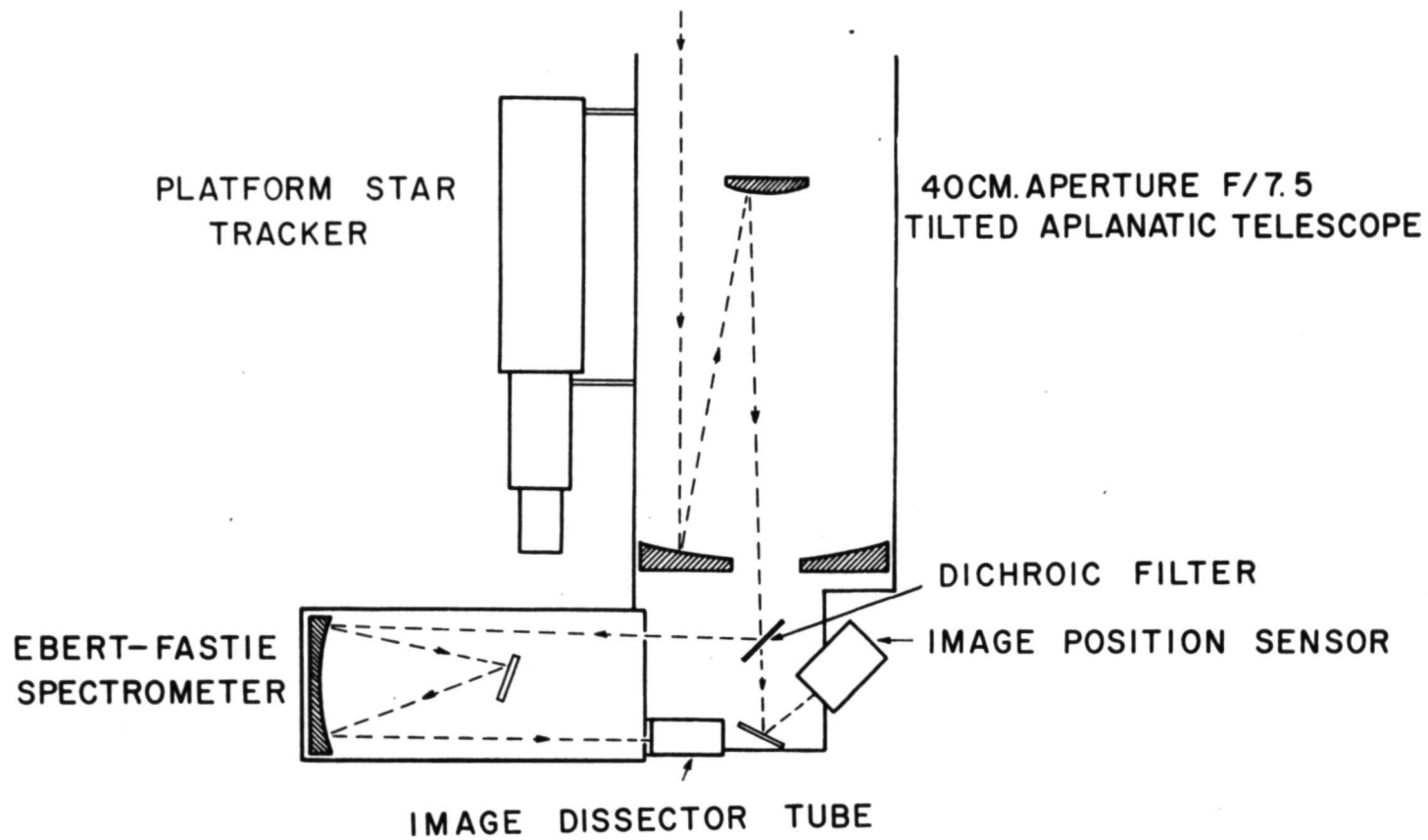


Figure 5. BUSS Instrument

In the spectrometer design a compromise was made allowing a small amount of coma in order to reduce the image height (Bottema, Ray, Wells - 1972). The rectangular envelope of the image is approximately .027 mm by 0.47 mm. A 50 Å wide spectrum, centered on 2800 Å is scanned in 1/4 Å increments by an ITT type F4012 image dissector operated in the photon counting mode. System resolution is about 0.4 Å. An onboard programmer provides several scan routines as directed by telemetry from the ground station. The number of events accumulated in each 1/4 Å channel is telemetered sequentially to a CRT display in the ground station. The image dissector employs a 17.5 mm diameter extended S-20 photocathode on a quartz face plate and a mechanical aperture .072 mm wide by .9 mm long. The length of the aperture is oversized to allow for azimuth tracking errors which are slightly larger than in the elevation or dispersion direction. Advantages of the image dissector are the accuracy and speed of electronic scanning and the low noise resulting from the small effective photocathode area. With discriminators set for 85% counting efficiency, we attain a dark count rate of less than 4 per second at room temperature and less than 0.2 per second at 0°C for our effective photocathode area of 0.065 mm². For our slit dimensions, we have obtained a resolution within a few percent of the theoretical value for a scanning rectangular aperture. This is made possible by high performance magnetic focusing of the photoelectrons. Although we have been pleased with the reliability and performance of the image dissector, there are several features related to the focus coil which require special attention. First, the power dissipated in the focus coil, if not minimized by proper design, can cause the tube to operate at higher temperatures resulting in a larger dark count. With our nominal 2.5 cm diameter tube the power dissipation is about one watt. We have found it undesirable to lower the power by shortening the coil, as the electron optical resolution suffers. Depending on the axial position of the coil, positive or negative electron image magnification may be observed, especially in the case of shorter coils. Since some high performance coils employ slight magnification, this should be taken into account in choosing the size of the mechanical slit. Another characteristic worth mentioning is the necessity of adjusting the focus current as the electron image is deflected, in order to compensate for the curved electron optical focal surface. This compensation typically amounts to a decrease in the focus current of a few per cent. Generally a focus current regulation of better than 0.1% is required if maximum resolution and deflection accuracy are to be maintained. It is also generally helpful to shield against the earth's magnetic field. The only serious disadvantage of the image dissector is that only one data channel at a time is observed. For an extended number of resolution elements, it may be desirable to go to a multichannel detector at the expense of greater cost and complexity.

We should now like to make some brief comments about the reflective coatings on our optics. Because of the generally adverse field conditions encountered in ballooning operations, we have found it highly desirable to use durable, easily cleanable coatings. All of our coatings are multilayered dielectric and comply with military environmental specifications. Reflective coatings on the telescope mirrors have an enhanced ultraviolet reflectivity of greater than 95% and a visible reflectivity of greater than 80%. The dichroic filter and spectrometer mirror have the same coating which

has a reflectivity of 98% within 100 Å of 2800 Å, and less than 15% in the visible spectrum. This provides a rejection ratio of about 300 for visible light. When further reduction of visible light is necessary additional filters can be inserted at the telescope focus. Visible transmission is about 85%.

V. FUTURE PLANS FOR THE BUSS PROJECT

Current plans for improving the BUSS payload lie in three general areas: (A) Extension of the spectral coverage to the entire middle ultraviolet region, i.e. 2000 - 3400 Å; (B) increasing the spectral resolution to at least 0.1 Å and possibly to 0.03 Å; and (C) improving the star tracking capability to track stars as faint as 10th magnitude through the use of off-set guidance techniques.

We expect to realize the indicated range and resolution in a cooperative venture with the Space Research Laboratory of the Astronomical Institute, Utrecht, the Netherlands. They have designed an echelle spectrometer which will be combined with an SEC vidicon detector and attached to our telescope and tracking systems. A television-type sensor, because of its two dimensional format and storage capability, makes possible the simultaneous observation of all resolution elements in the spectral range. This type of detection ameliorates the trade-off among spectral range, resolution and observing time, which has been a major problem in spectrophotometric observations from space.

As an alternative means of obtaining the same, but somewhat less ambitious, objectives, we are investigating the employment of a one-dimensional multichannel sensor such as a silicon diode array.

REFERENCES

- Allen, C. W., 1963. *Astrophysical Quantities*, London: Athlone Press.
- Boksenberg, A., Kirkham, B., Toulson, W.A., Venis, T. E., Bates, B.,
Courts, G. R. and Carson, P. P. D., 1972. *Nature Phys. Sci.* 240: 127.
- Bottema, M. and Woodruff, R. A., 1971. Third Order Aberrations in
Cassegrain - type Telescopes and Coma Correction in Servo-Stabilized
Images. *Applied Optics*, 10:300.
- Bottema, M., Ray, A. J., and Wells, C. W., 1972. Balloon-Borne Ultra-
violet Stellar Spectrometer. *S.P.I.E. Proceedings - Instrumentation in
Astronomy*.
- Gurzadyn, G. A., and Ohanesyan, J. B., 1972. *Astronomy and Astrophysics*,
20:321.
- Kondo, Y., Henize, K. G. and Kotila, C. L., 1970. *Astrophysical Journal*,
159:927.
- Kondo, Y., Giuli, R. T., Modisette, J. L. and Rydgren, A. E., 1972.
Astrophysical Journal, 176:153.
- Lamers, H. J., Hucht, K. A. van der, Snijders, M. A. J., 1973. *Astronomy
and Astrophysics*, 25:105.
- Lamers, H. J., Hucht, K. A. van der, Hoekstra, R., Faragianna, R. and
Hack, M., 1974. *The Astronomical Institute at Utrecht - Internal Report*,
ROF 72, C4.
- Modisette, J. L., Nichols, R. E., and Kondo, Y., 1973. *Astrophysical
Journal*, 186:219.
- Navach, Lehmann and Huguenin, 1972. *Astronomy and Astrophysics*, 22:361.
- Wilson, O.C., 1966. *Astrophysical Journal*, 144:695.
- Wilson, O.C. and Bappu, M. K. V., 1957. *Astrophysical Journal*, 125:661.

71751 27W :

DISCUSSION SUMMARY — PAPER 2.6

The UV spectrophotometer has programmable routines. For example, the dwell time per channel can be programmed for a fixed time or for a fixed number of counts.

It was reported that the 2-percent efficiency referred to in the instrument description was the ratio of photons detected to photons incident within the bandpass.

PAPER 2.7

AIROSCOPE

AMES INFRARED BALLOON-BORNE TELESCOPE

O. L. Koontz
S. G. Scott

Ames Research Center

ABSTRACT

AIROscope is a balloon-borne telescope system designed for astronomical observations at infrared wavelengths. The telescope is gyro-stabilized with updated pointing information derived from television, star tracker, or ground commands.

The television system furnishes both course and fine acquisition after initial orientation using a pair of fluxgate servo compasses.

Command and control is by a UHF link with 256 commands available. Scientific and engineering data are telemetered to the ground station via narrow band F.M. in the "L" band. The ground station displays all scientific, engineering and status information during the flights and records the command and telemetry digital bit stream for detailed analysis.

The AIROscope telescope has a 28-inch diameter primary mirror and Dall-Kirkham optics. The beam is modulated by oscillating a secondary mirror at 11 or 25 Hz with provision for left or right beam fixed positions by command.

A PM tube behind a multi-density target at the telescope focal plane provides information for fine collimation and focusing which is done by commanded adjustments of the secondary mirror.

A star tracker capable of pointing at visual sources to within ± 10 arc-seconds RMS can be switched by command into the gyro control loop in place of the TV for pointing at visual targets.

The primary power source for the gondola is provided by silver zinc battery cells of 80 ampere-hour nominal capacity.

GENERAL

AIROspace is a balloon-borne telescope designed for making astronomical measurements at infrared wavelengths. This system was originally developed at the University of Arizona for operation in the ultraviolet (Frecker 1968, Coyne & Gehrels 1968). It has since undergone extensive modification. Command, control, and data acquisition are by R.F. telemetry. The television system and star tracker are attached to the primary telescope which is gyro-stabilized. Figure 1 is a block diagram of the system. The system weighs approximately 775 kg and is carried to 31 km altitude by a $1 \times 10^5 \text{ m}^3$ balloon. Figure 2 is a photograph of the system at launch. Nominal observation time at this altitude is 10 hours. The gondola is recovered and refurbished after each flight. It can be launched at about 7-day intervals.

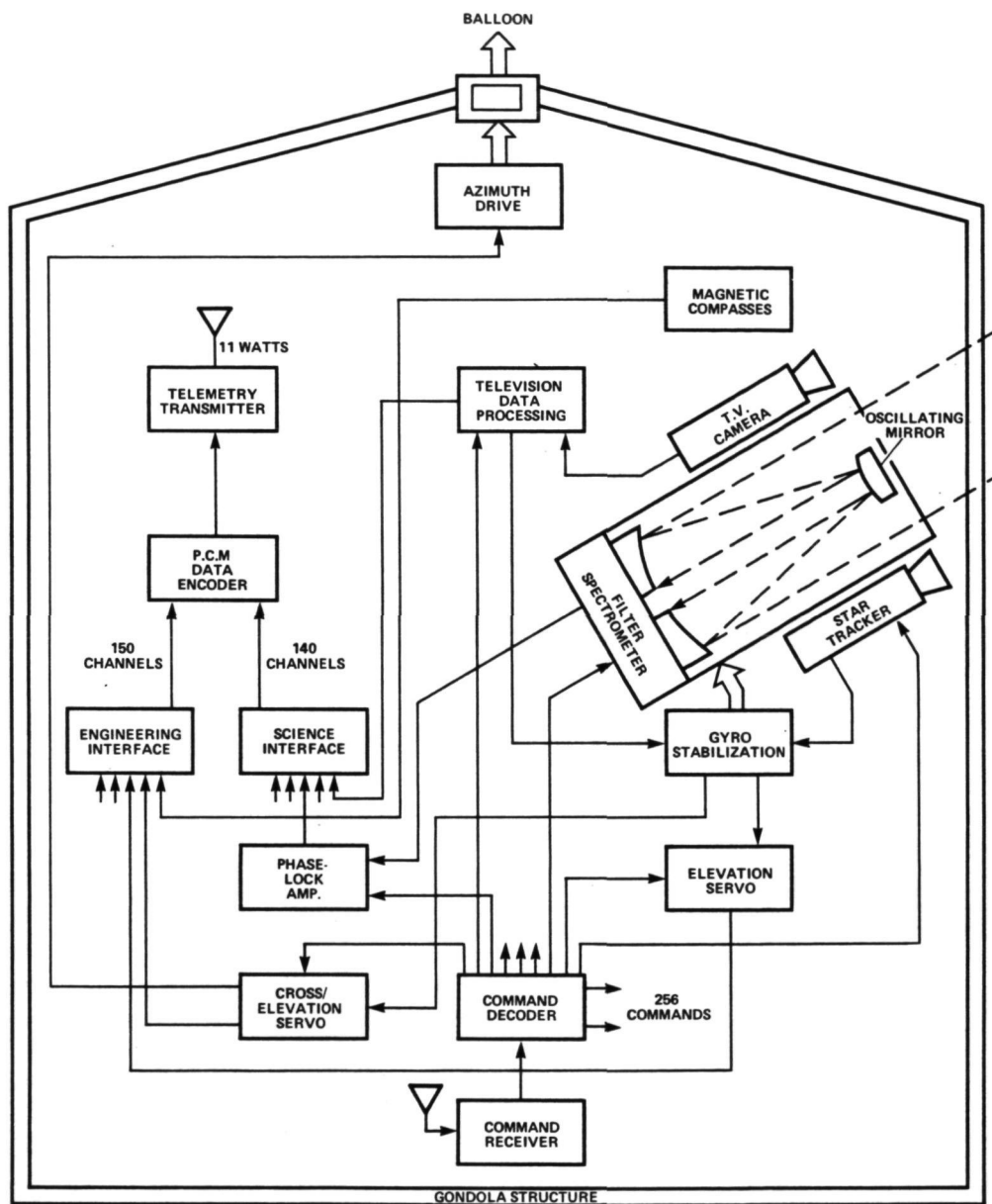


Figure 1. Gondola System Block Diagram

REPRODUCIBILITY OF THE
ORIGINAL PAGE IS POOR

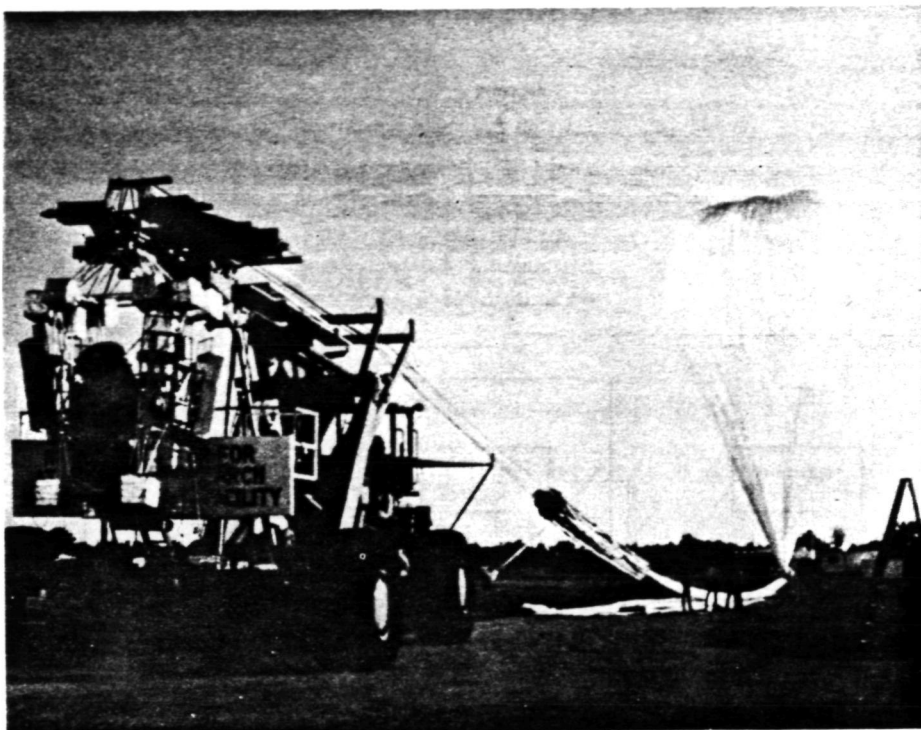


Figure 2. System ready for launch.

OPTICS

The AIROspace telescope has an elliptical primary and a spherical secondary (Dall-Kirkham optics). This arrangement permits selecting focal ratios to match different requirements by choosing from a group of inexpensive spherical secondary mirrors. With our infrared astronomy program the resulting deficiency in image quality is tolerable even for objects several minutes off-axis.

The primary mirror is 71 cm in diameter but is slightly underfilled by the 13-cm diameter secondary. With the current secondary mirror the f number is 11.2 and the plate scale is 0.4 min/mm. An aperture at the detector limits the field-of-view to 5 minutes of arc. Source modulation at 11 and 21 Hz is produced by oscillating the secondary mirror in a spatial chopping mode often used in infrared astronomy. Each beam position (left and right) is 3.5 minutes off the optical axis. Thus, the movement of the secondary will cause the telescope to first look at the object in the right beam and then to look at the background sky symmetrically to the other side of the optical axis. The resulting modulated signal reaching the detector is primarily from the source since the background noise sources including sky and telescope structure are nearly equal in the two beams. Figure 3 is a diagram of the AIROscope optical system.

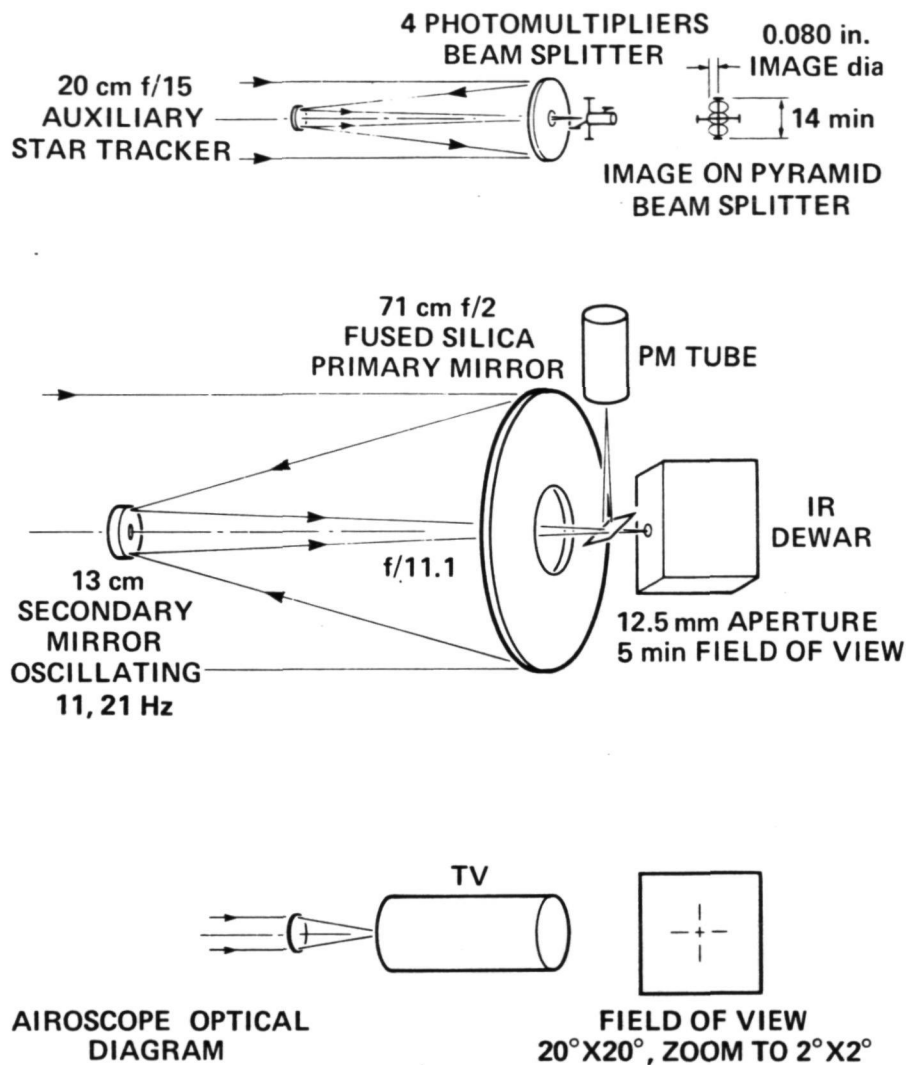


Figure 3. AIROscope Optical System.

Image quality with the present optics is poor by optical standards, but it is entirely satisfactory for use in the infrared. It is believed that geometrical distortion is introduced in the hub mounting of the main mirror. Image size for an on-axis point source is 1 mm in diameter or less. An interesting comparison with the ideal on-axis and off-axis image can be made by considering the results of a ray tracing computer program by Erickson and Mathews. On-axis and 3.5 minute off-axis image sizes for the AIROscope Dall-Kirkham mirrors are about 0.04 mm and 0.2 mm diameter. At wavelengths beyond 10 microns the on-axis image size is determined mainly by diffraction. The diffraction circle at 100 microns is 3.2 mm corresponding to 1.4 minutes of arc. The image quality, then, with the 5 minute field-of-view clearly causes no measurement problem.

SECONDARY MIRROR ASSEMBLY

The separate functions of mirror oscillation and focus-collimation are built into the secondary mirror assembly. The mirror can be moved axially for focus or tilted for collimation by three stepper motor-driven cams. Cam position data is included in the AIROscope data format. Precision potentiometers for the three cams can resolve mirror position to better than 20 seconds of arc. Axial movement permits refocus of the telescope at float when the structure cools off, shortening the distance between the primary and secondary.

An oscillating mirror mechanism is driven by two solenoids in a square wave mode. Adjustable stops for angular throw are built into the solenoid housings. Figure 4 is a photograph showing the mechanical arrangement of the drivers and how the solenoid base plate is spring loaded and tilted by the underlying cam push rods. Mirror throw is 17 minutes which results in a beam travel of 7 minutes of arc. Each beam position, left and right, is 3-1/2 minutes of arc off the optical axis.

Vibration damping was an early problem. This mechanical noise was transmitted through the structure to the detector electronics. Silicon rubber pads in the solenoid stops and resilient washers at the secondary mounting points reduced this noise considerably. A decrease in solenoid driving voltage to about 16 volts from the bus voltage of 27 quieted the system even more. The mirror is mounted at its center to the oscillating plate. The space between

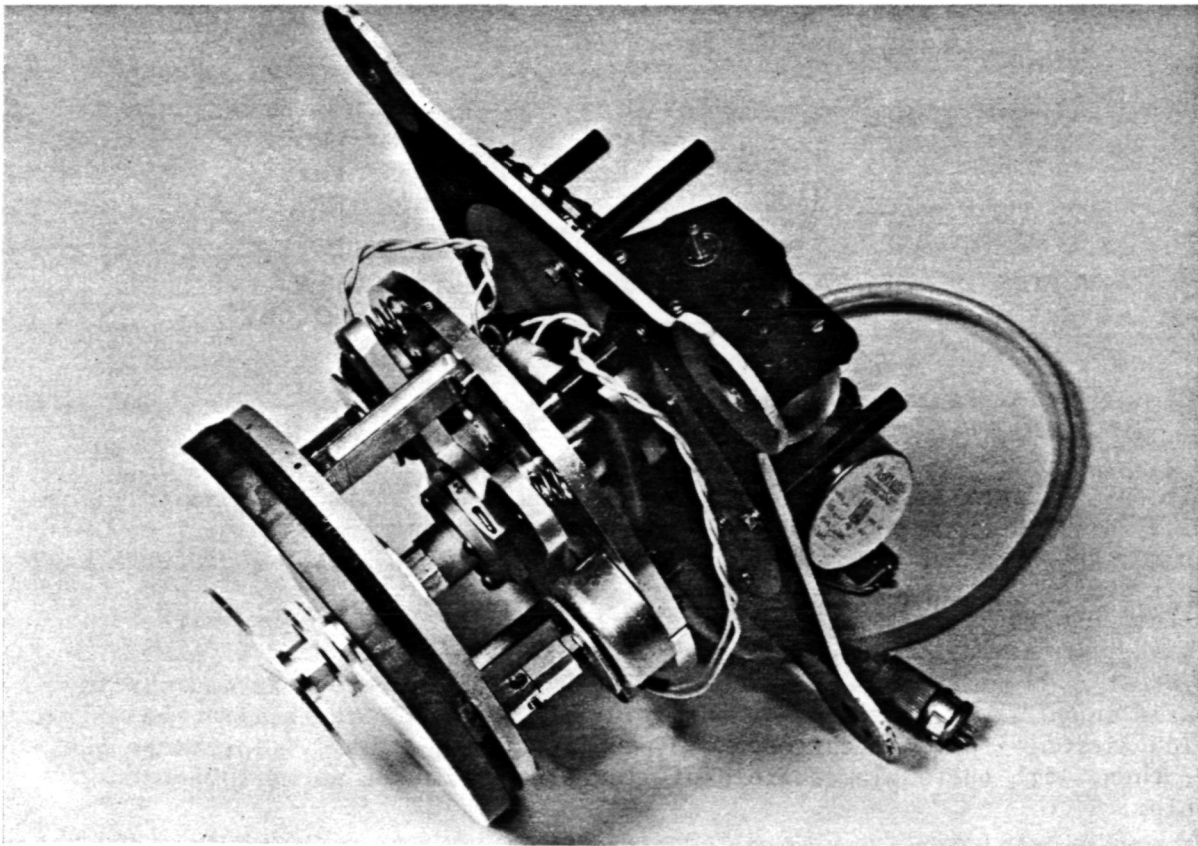


Figure 4. Secondary mirror assembly.

2.7-5

the mirror and the aluminum backing plate is foam filled to dampen mirror vibration. Mirror bounce and mirror mechanical resonances that affect the optical beam are negligible. The only deviation has been a small bounce that amounts to about 1 minute of arc of mirror oscillation which at the detector amounts to less than 30 seconds of arc change or 1 mm of spot oscillation.

This secondary assembly has accumulated about 120 hours of operation with no failures. Changes in chopper throw have been negligible.

The original secondary support structure for this telescope was a source of background IR because of the structural protrusions into the field-of-view. This was redesigned using a tubular truss structure of 1-1/2 inch aluminum tubing stiffened by two thin annular rings with a slip-in magnesium shroud and an 18-inch shroud extension, both of which are easily removed or installed. All of this structure is out of the field-of-view of the detector. The secondary mirror assembly is installed on a spider structure made of roll-flattened aluminum tubing, which gives a superior rigidity and a small cross section to the light beam. All material exposed is gold plated. Figure 5 shows old and new structures and installation of the spider.

COMPASSES

Initial orientation is accomplished using compass heading information telemetered from the gondola to the ground. Since the success of the mission depends so heavily on this initial heading information, there are two compasses onboard for redundancy.

These compasses use fluxgate magnetometer sensors and generate second harmonics as a cosine function of the azimuth angle and the earth's magnetic field. To avoid the ambiguity normally associated with such a system, the D.C. voltage output from the second harmonic synchronous detector is amplified and utilized to drive a closed loop servosystem that attempts to drive the sensor to a null position at all times. This servo also drives a precision potentiometer upon which a 10-volt reference signal is impressed. The potentiometer wiper voltage is telemetered so that the gondola heading is known at all times.

TELEVISION STELLAR ACQUISITION SYSTEM

The television system of AIROscope is a highly sensitive standard scan system used for initial acquisition and offset tracking (Deboo, 1974). The normal video bandwidth of the camera is compressed by onboard data processing. This data compression ratio is approximately 300 to 1 and the effective bandwidth on the telemetry downlink is about 20 KHz.

The field-of-view of the camera's "zoom" optics is about $20^\circ \times 20^\circ$ maximum and $2^\circ \times 2^\circ$ minimum. The sensitivity, zoom position gates, etc., are fully controllable by command from the ground station.

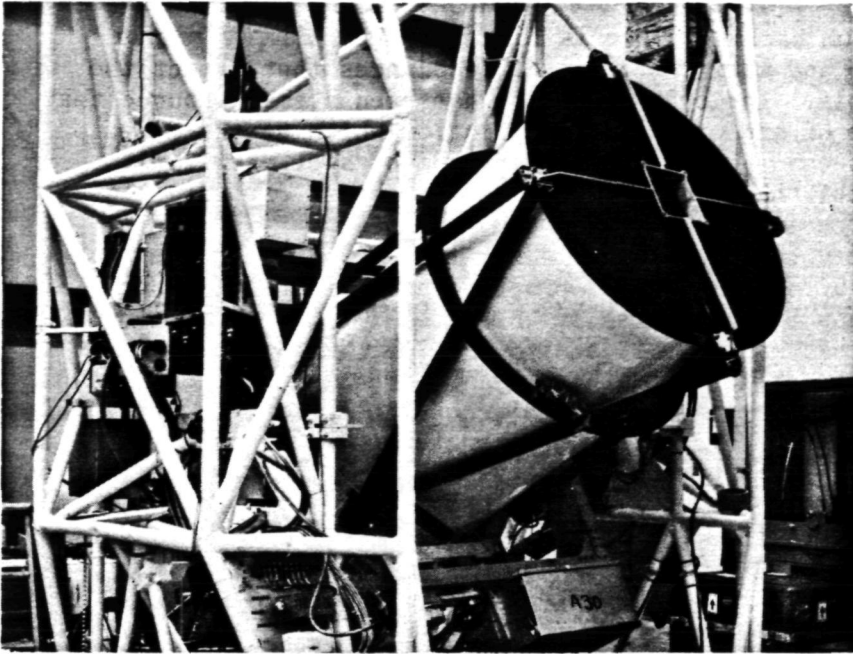


Figure 5a. Present secondary support structure.

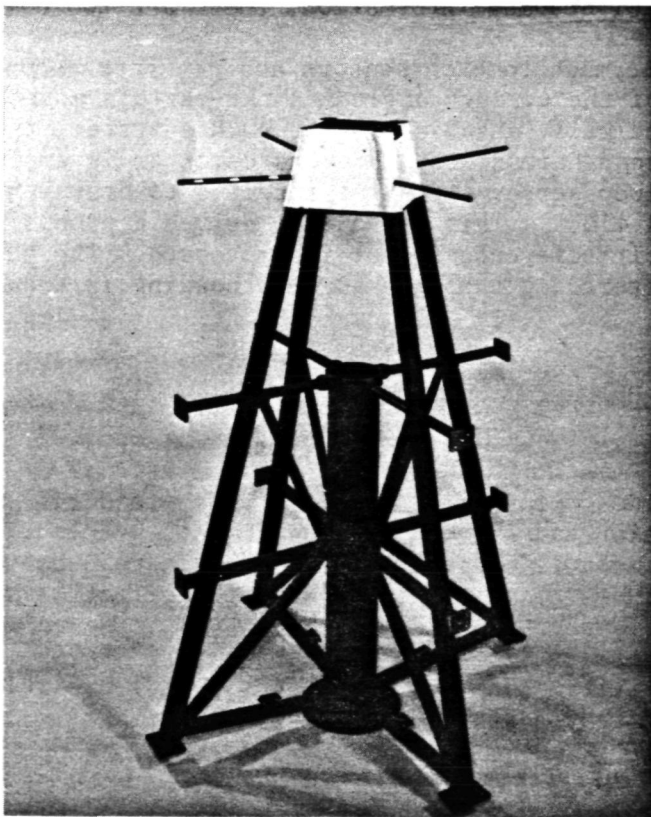


Figure 5b. Original secondary support structure.

STAR TRACKER

A star tracker will be used as a backup to the main TV-controlled offset tracking system. It offers no offset tracking capability. The star tracker optical axis is aligned 3-1/2 minutes of arc from the telescope optical axis such that its axis corresponds to the right beam of the telescope which occurs when the oscillating secondary mirror is in its designated right position. The image of the celestial object is then centered in the aperture.

Light enters the star tracker through a small Cassegrain telescope with a 20 cm f/15 primary. The slightly defocused image of about 2 mm diameter is centered on a pyramid beam splitter which is viewed by four PM tubes. When commanded into the stabilization system loop, the deviation of the image from the centered position produces unbalanced output from oppositely placed PM tubes. In this way the tracker will acquire and lock on a star down to about fifth magnitude. Field-of-view is 14 minutes of arc and the pointing capability is ± 10 seconds-of-arc peak and about 3 seconds-of-arc RMS.

FOCUS AND COLLIMATION AT FLOAT

Prelaunch optical alignment includes aligning the control TV optical axis 3-1/2 minutes of arc to the right of the primary optical axis. Then, an object on the TV cross hair will be focused on the detector when the secondary is in the right beam position. The star tracker is also aligned 3-1/2 arc-minutes to the primary axis. Normally, inflight measurement can proceed based on these ground alignments. That is, when the object is at the reference center of the TV screen and the secondary mirror is in the right beam, the object would be focused on the detector.

In addition, a means is available to accomplish inflight collimation and focusing. A 2-inch diameter end-on PM tube with a field-of-view of 20 arc-minutes is housed in a sealed can along with a programmable high voltage supply. A 45° mirror, by command, diverts the beam to focus onto a 2-inch diameter glass target whose area is divided into rings of different optical transmission. Figure 6 shows the arrangement of this collimation and focusing device. The mirror mechanism is driven by a stepper motor. The output of this photomultiplier is conditioned and then telemetered and recorded in the ground station. Obviously, when the beam is accurately collimated the signal is a maximum.

The procedure for optimizing the beam collimation has several steps. First, while locked onto a star in right beam, the image is focused using the signal from the photomultiplier. Then, while viewing the blank sky (secondary mirror oscillating) the secondary mirror is adjusted slightly to minimize the imbalance, if any, in the infrared background signal. The next step is to lock onto a planet (visual and infrared source) and adjust the tracking angles electrically until the photomultiplier and infrared detector signals are maximized.

Figure 6 shows also how focusing and boresighting are accomplished and the effect on the scan slopes of spot size. The well-focused spot of 1 mm or less should give sharp knees from one band to another while a defocused spot will produce a rounded edge and greater slopes. The beam should be boresighted

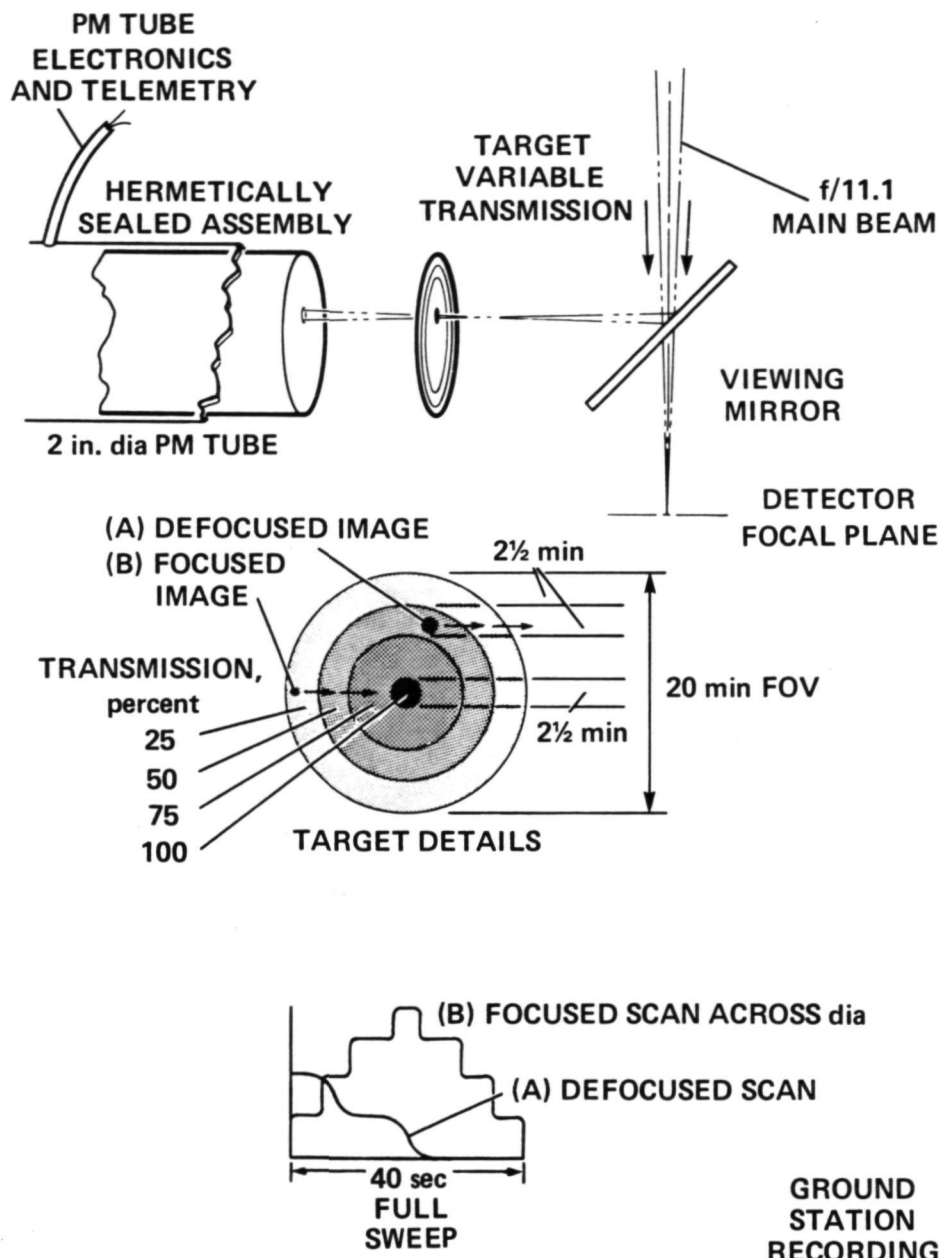


Figure 6. Inflight collimation and focus arrangement.

quickly after a few trial and error scans. Focus should never be far off as corrections for structure temperature can be calculated quite well and the necessary axial adjustment made. For example, at an average temperature of -40°C , the secondary will move about 1.5 mm closer to the primary from where the original prelaunch focus at 20°C was determined. This dimensional change can be corrected for by moving the secondary out from the primary accordingly. The actual uncorrected defocusing of the f/11 beam because of temperature amounts to a change in the focal point of about 4.5 cm.

GONDOLA

The AIROscope gondola is fabricated of thin wall aluminum tubing. This frame weighs about 70 kg. Refurbishment and repair of broken thin wall tubing requires a high degree of metal working competence and a great deal of time is required for the cutting, fitting and welding of such tubing. Ames Research Center (ARC) is now in the process of designing and fabricating a new gondola. This gondola will be larger and heavier than the present one. The lower portion is being constructed of aluminum channels and L's. Thus, in addition to lower initial costs, it will be stronger and relatively simple to repair in the field. The outboard equipment bays will furnish adequate room and protection and insure ease of integration of different experiments such as those dictated by shuttle payload development requirements. This, along with improvements in the electronic subsystems, will allow several users to share in the opportunity of flying at 31 km on a stabilized platform.

TELESCOPE GIMBAL SYSTEMS

The gondola is suspended from the servo-driven azimuth drive. By torquing against the parachute shrouds the gondola turns and may be considered as the outer gimbal. The inner gimbal rotates about a horizontal axis within the outer gimbal and furnishes elevation angular movement. Suspended inside the inner gimbal is the telescope, pivoted to rotate about an axis perpendicular to the axis of the inner gimbal. For balance and minimum deflection, these gimbals are each driven by two torque motors. At present, the gimbals are driven by 12:1 toothless friction gears as developed by the Lunar and Planetary Laboratory, University of Arizona and pioneered by G. Newkirk of the High Altitude Observatory (Frecker, 1968). In the future, AIROscope will use direct drive servo motors on all gimbals (Murphy, 1974). The inner gimbal, telescope, star tracker, television and present experiment weigh approximately 160 kg. Other weights associated with AIROscope includes electronic packages, about 120 kg, the batteries, about 100 kg and about 300 kg of miscellaneous hardware and ballast making the total launch weight of about 800 kg. When the new gondola is installed, weight is expected to be 1300 kg.

COMMAND SYSTEM

Commands are transmitted to the AIROscope on a frequency of 405.4 MHz. The transmitter power output is approximately 10 watts of narrow band FM utilizing Bi-phase-L modulation technique (Barrows, 1974). The basic command word is 8 bits making available 256 commands. This number could be easily increased by paralleling two of the present systems.

Parity checks and complementary techniques are used to insure command security for the system.

TELEMETRY

The AIROscope telemetry system operates on 1483.5 MHz. The transmitter power output is approximately 10 watts of narrow band FM utilizing Bi-phase-L modulation techniques (Pitts, 1974). PCM, pulse code modulation, with 10 bit words is used and the encoder provides 140 data channels for analog signals and 150 discrete digital channels.

Frame length, sync, word length, clock rate, bit rate and other operating parameters of the PCM encoder are controlled by a read-only-memory (ROM) program board. In the ground station, the PCM decommutation equipment may likewise be programmed by IBM punched cards. These boards and cards can easily be changed to accommodate future scientific experiment requirements and insure maximum system flexibility. Furthermore, this system will allow the investigator to reprogram the PCM decommutator or word selectors while the mission is in progress.

SCIENTIFIC INSTRUMENTATION CAPABILITIES

A volume of about 0.25 m^3 is available at the Cassegrain focus for scientific instrumentation. Since this mass is gyro-stabilized, a weight limit of about 40 kg exists. Other instrumentation of much larger size and weight can be mounted at other locations on the gondola.

Helium cooled bolometers, filter spectrometers, preamps, and phase-locked amplifiers exist for the system.

Power (150 watts), commands (50), discrete digital words (50), and analog channels (30) are readily available at the focal plane for use of experiment integration when changing to any other scientific investigation.

GONDOLA PRIMARY POWER CONSIDERATIONS

Most balloon payloads requiring substantial electrical energy use nickel cadmium or silver zinc batteries. These premium batteries are chosen for several reasons, the primary one, in the case of AIROscope, being the reliability of the basic power system. Although simple, it is the one system that is key to the rest of the gondola electrical performance.

AIROscope uses a rated 80 ampere hour, low rate, silver oxide-zinc cell. At the low inflight discharge rates, 10-15 amps, usable capacity is at least 110 amp hours. The silver oxide-zinc cell gives the highest energy to weight ratio of commercially available couples, and has superior low temperature performance with acceptable low rate delivery down to -25°C . Several manufacturers with years of aerospace experience have developed battery cells of outstanding reliability. Charge retention, a flat voltage response through most of its discharge schedule, considerable recharge capability, and ease and safety in charging are additional features noteworthy in this kind of cell. The only drawback is high initial cost, about \$700/kWh versus, for comparison, a commercial lead-acid type at about \$30/kWh.

AIROscope batteries are carefully maintained between flights. The cells are discharged completely and stored at -20°C which retards deterioration of the plates and separators. It is expected that the cells can be used up to two years, with 3-4 flights a year.

AIROscope batteries are given a charge-discharge test prior to final constant-current charging. Individual cell voltage is monitored carefully near the end of charge to prevent overcharging. An automatic charger with continuous cell monitoring and appropriate controls would be a valuable piece of equipment in an active balloon program.

AIROscope batteries are unsealed for flight, but boiling and loss of electrolyte is avoided by maintaining batteries at low temperature. Figure 7 shows the saturated vapor curve for water and for a solution of potassium hydroxide (KOH). At 30 km, the batteries may be safely operated vented if held below about 20°C . Slight pressure drops through the cell vent, insulation, and case give an additional safety factor. AIROscope batteries in flight reached a cell case temperature of about -10°C after 8 hours aloft. In future flights, the target low temperature will be raised to around 0°C .

One special problem with silver oxide-zinc cells is the peroxide over-voltage that exists during the first 15-25 percent of discharge. The elevated voltage, between 1.60 and 1.75 V/cell, produces an unacceptable bus voltage of

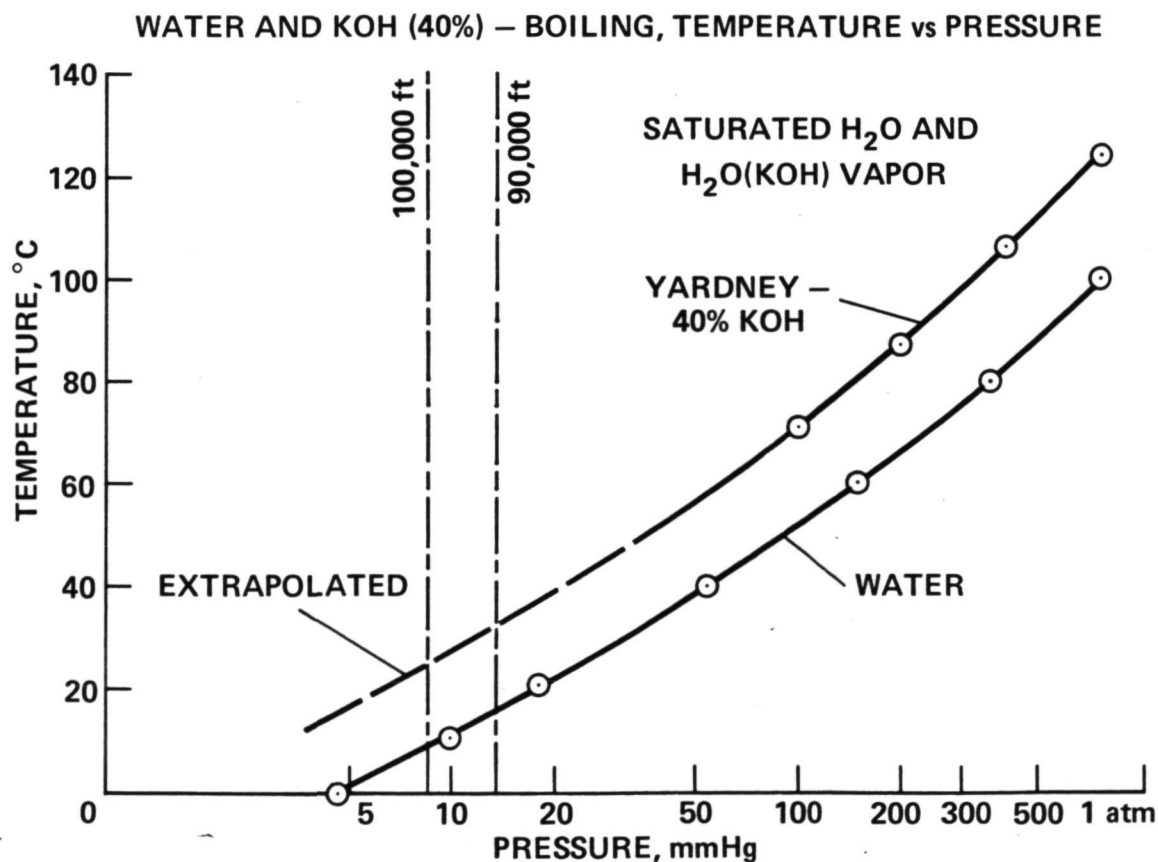


Figure 7. Vapor curve.

up to 31.5 volts compared with the plateau voltage of 27.0 volts. AIROscope bus voltage specification is 24-29 volts. The peroxide overvoltage must be dissipated down to 29 volts before bus connections are made and this means a loss of 12-18 percent in available amp-hours. Since battery energy increments can be made only by new packaging with larger cells or by the addition of another \$2000 of battery, it is important that maximum possible utilization be made of existing batteries.

AIROscope employs a battery connection scheme that results in two separate bus voltage levels, isolates one of the two batteries from the other, and actually utilizes all of the peroxide portion of the battery energy in one battery. In one battery one cell has been removed leaving 17 in series, and a diode is located in the return line from the bus. Nominal voltage of this battery is then 24.5 volts instead of the 27 for the other battery, and maximum initial voltage cannot exceed 29 volts. Benefits from this arrangement include elimination of the preflight power dissipation procedure from one battery, two distinct bus levels for ascertaining roughly the energy remaining, and some saving in overall energy. This latter comes about because 15-20 percent of battery amp-hours are saved and bus current remains fairly constant at the lower bus voltage. This will translate into net 8-10 percent savings when a time factor is included in the power demand. A saving of 10 ampere hours would provide an additional 45 minutes of experiment time.

RECOVERY AND DESCENT PROTECTION

The AIROscope gondola is constructed so as to absorb a maximum amount of shock and damage while providing protection to the experiment, telescope and gimbal system. (See Figure 2.) The crash pads utilized by the AIROscope are aluminum honeycomb. It is expected that aluminum pads will generate considerable less moisture contamination at altitude than paper.

The thickness of the honeycomb material pad area and stroke length are dictated by the following landing constraints:

Maximum "g" loading	10 g
Maximum vertical velocity	6.5 m/sec
Maximum horizontal velocity	6.5 m/sec
Maximum slope	15°

To date, AIROscope has flown four times and has incurred little or no damage on descent and landing.

CONTROL STATION

Figure 8 is an external view of the van housing the primary ground control station. Figure 9 is a conceptual view of the control center. The van is configured internally to support and transport the complete AIROscope system. The rear portion of the van provides ample work area once the gondola and antenna are removed at the launch site. The van has been modified by the installation



Figure 8. AIROscope control van.

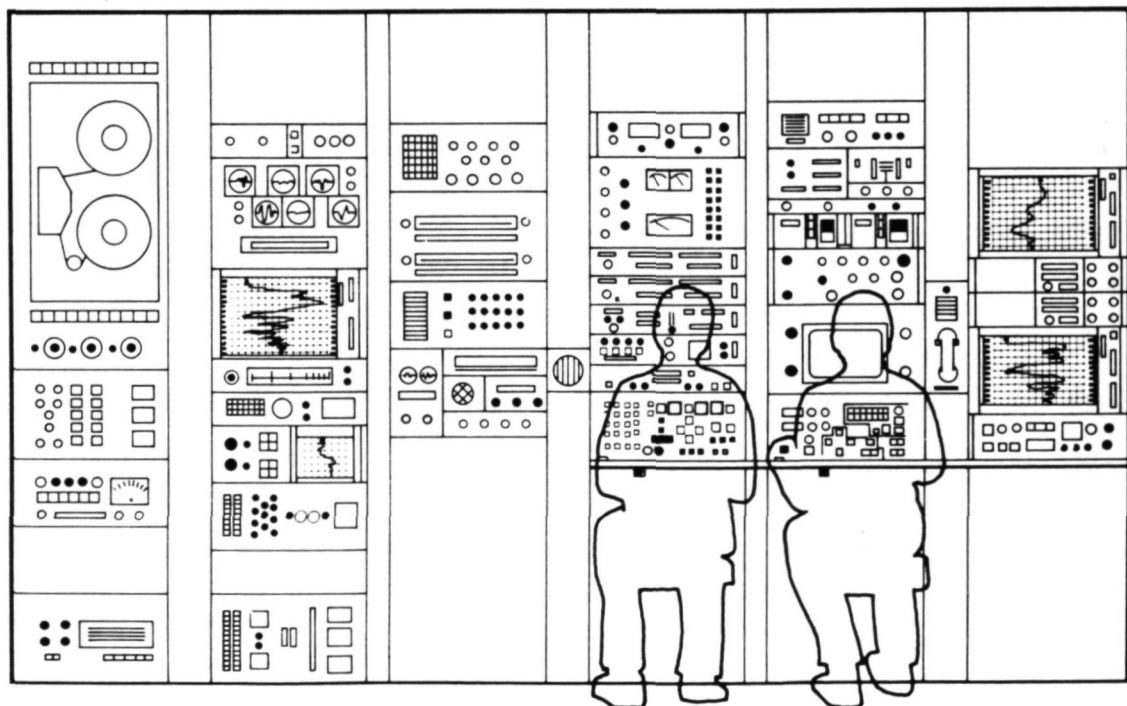


Figure 9. AIROscope control station.

REPRODUCIBILITY OF THE
ORIGINAL PAGE IS POOR

of an Air-Ride suspension system to further protect the rack-mounted electronic equipment during transit.

CONCLUSION

The AIROscope system offers scientific investigators a highly flexible vehicle for astronomical observation while at an altitude of 31 km. Observations for periods of ten hours are possible while above nearly all of the telluric water vapor and carbon dioxide. The unique television system affords offset viewing of infrared sources over long periods of time. The command, control and telemetry subsystems have been designed for satisfactory operation with different experiments and to afford easy and quick integration of various instruments.

REFERENCES

- Barrows, W. AIROscope command system. Proceedings, Symposium on Telescope System for Balloon-Borne Research. To be published, 1974.
- Coyne, G. V., and Gehrels, T., Feb. 1968. Polarimetry from high-altitude balloons. LPL Communication No. 108.
- DeBoo, G. The AIROscope stellar acquisition system. Proceedings, Symposium on Telescope System for Balloon-Borne Research. To be published, 1974.
- Erickson, E., and Mathews, S. Evaluation of Aberrations in a Cassegrain-Type Telescope with an Oscillating Secondary Mirror. To be published, 1974.
- Frecker, J., Feb. 1968. The polariscope balloon-borne servo system. LPL Communication No. 109.
- Murphy, J., and Lorell, K. The AIROscope pointing and stabilization system. Proceedings, Symposium on Telescope System for Balloon-Borne Research. To be published, 1974.
- Pitts, K. AIROscope telemetry system. Proceedings, Symposium on Telescope System for Balloon-Borne Research. To be published, 1974.

84751 55W

DISCUSSION SUMMARY.— PAPER 2.7

During discussions it was reported that AIROscope had a sensitivity threshold of 10^{-24} watts/m²Hz in the wavelength band of 27-90 microns. This was based on observations of Venus during one flight.

The operating procedure for acquiring celestial objects was described. This consists of first reading an onboard magnetic compass for azimuth, then pointing at a prescribed elevation. Next, information from an onboard TV is used for star field recognition and for star tracking. This TV star tracker should be capable of tracking 8th magnitude stars. Finally, the telescope is collimated and focused by command.

It was estimated that the AIROscope system will cost \$200,000 to complete, exclusive of salaries and launch costs. This system will be made available for collaborative investigations in the future if sufficient interest and funding exists.

The present system has a 5-minute of arc field-of-view. In the future, it may be possible to utilize a 1-minute of arc field-of-view.

A background limitation of the AIROscope system was described. The AIROscope uses spatial chopping in cross-elevation by oscillating the secondary mirror. This spatial chopping is horizontal only when the telescope is centered in the gondola. Torsional oscillation of the gondola introduces a vertical component into the spatial chopping and therefore introduces a modulation of the background. This effect is zero at the horizon and becomes significant above 45° elevation. Steps are being taken to limit this effect by limiting the torsional oscillation of the gondola.

The mirror for this system was made at the University of Arizona, it is fused silica and weighs 90 lbs. Mounting is by the central hub which causes an image distortion which has so far not been a problem for infrared work. The mirror by itself has a figure good to one arc-second in visible light.

BALLOON PLATFORM FOR EXTENDED-LIFE ASTRONOMY RESEARCH

L. T. OSTWALD
BALL BROTHERS RESEARCH CORPORATION
BOULDER, COLORADO

ABSTRACT

A configuration has been developed for a long-life balloon platform to carry pointing telescopes weighing as much as 80 pounds (36 kg) to point at selected celestial targets. A platform of this configuration weighs about 375 pounds (170 kg) gross and can be suspended from a high altitude super pressure balloon for a lifetime of several months.

The balloon platform contains a solar array and storage batteries for electrical power, up and down link communications equipment, and navigational and attitude control systems for orienting the scientific instrument.

A biaxial controller maintains the telescope attitude in response to look-angle data stored in an on-board computer memory which is updated periodically by ground command. Gimbal angles are computed by using location data derived by an on-board navigational receiver.

High instrument data rates necessitate increased electrical power consumption and directional antennas for transmission to a data satellite. The maximum usable real-time data rate within weight limitation is about 1000 bps with a 100 percent duty cycle. Higher data rates would be used with reduced duty cycles.

An extended-life balloon platform for astronomy missions appears to be basically feasible; however, the effectiveness of the mission is strongly dependent on the availability and location of ground control and data acquisition facilities.

DISCUSSION

Observation times for instruments lifted by conventional balloons are usually limited to a maximum of two days because the fill-gas is vented as the balloon is subjected to day-to-night temperature fluctuations, and because the balloons usually drift out of range of the ground stations.

Recent flights of "super pressure" balloons, have demonstrated the feasibility of keeping payloads aloft for extended periods. During a lifetime of three months, the balloon might encircle the globe several times, at a rather constant latitude, at an altitude of about 100,000 feet (30 km).

A brief investigation has been conducted to configure and size a balloon gondola to provide electrical power, attitude control, and data handling capability for an X-ray telescope used to observe selected celestial targets while it is suspended from an extended-life balloon. The basic characteristics of a typical balloon-borne instrument are given in Table 1. (The data for the table were supplied by James Kurfess, Naval Research Laboratories,

Washington, D. C., who also supplied many of the systems concepts which influenced the gondola configuration.)

Table 1

TELESCOPE INSTRUMENT CHARACTERISTICS AND REQUIREMENTS

Size:	2 by 2 by 2 feet (60 cm)
Weight:	80 pounds (36 kg)
Electrical power:	15 watts
Data rate:	2,000 bps minimum
Pointing accuracy:	1-1/2 degrees
Pointing modes:	Fixed point and raster scan

Important auxiliary networks are required to maintain control and retrieve the data from the scientific instrument and gondola which may be situated at any longitude during its life-time. Furthermore, the problem of determining the location of the balloon and instrument platform requires a system with nearly global coverage.

A conceptual view of the systems involved is shown in Figure 1.

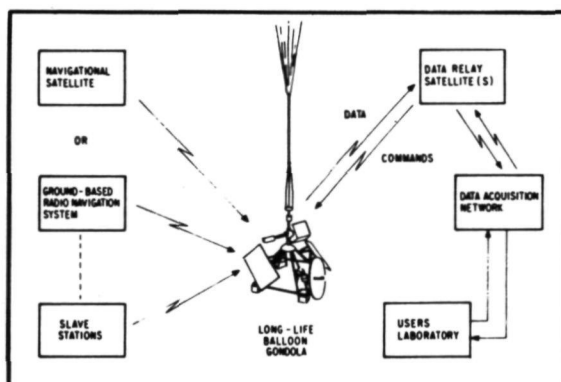


Figure 1. Extended Life Balloon Navigation and Communications Systems

Data are retrieved through a communications channel on one or more data relay satellites, orbiting the earth at synchronous altitudes, stationary with respect to the earth.

Position determination is made from signals received by equipment on the balloon gondola from either ground-based navigational systems such as the OMEGA system or from orbiting navigational satellites such as TRANSIT. Similarly, ground control of the instrument and gondola also uses a time-shared data relay satellite channel or ground-based command network.

The basic configuration of the instrument gondola is shown in Figure 2. The arrangement of the subsystem parts is dictated primarily by the telescope's need for an unobstructed view of the celestial hemisphere, a line-of-sight path from the data link antenna to the data relay satellite orbiting above the earth's equator, and the position of the solar cell array panels to maximize the energy available from the sun.

The coarse orientation of the gondola platform is maintained by an azimuth controller so that the solar array panels are to the east and west. The solar array panels are attached to the structure with mission-selectable brackets so that the normals to the panels are nearly in the ecliptic, and thus maximizing the available energy.

The high gain data transmission antenna is oriented by a biax gimbal located on the north side of the gondola, for flights in the southern hemisphere. Full 180° movement of the antenna is required in the east-west direction, but the north-south excursion is quite small.

The telescope instrument is oriented to selected stellar targets in azimuth and elevation by a biaxial controller located on the main azimuth stem above the gondola base structure.

The gondola suspension system is a ladder formed by three cables spaced in the shape of a triangle. By also spacing the shroud lines on the folded recovery chute in the same manner, the suspension system torsional stiffness is increased.

Weights of the gondola components are given in Table 2. To minimize the structural weight, no roll cage was included in the structural framework. The crushable pads were widely spaced to lessen the likelihood of upset on landing.

NAVIGATION AND CONTROL

Orientation of the telescope instrument and data relay antenna involves the use of an on-board computer to compute gimbal angles from stored data loaded by ground based command data, and geo-position data obtained from a navigational system.

Figure 3 is a simplified diagram of the control and navigational system. Target sequence and coordinate data are entered in the storage by the command receiver when the gondola is within range of ground command stations. The navigational receiver and initial processor supply geo-position coordinates for the balloon based on the signals from ground-based transmitters such as the OMEGA system. The on-board computer performs the coordinate transformations required to derive gimbal angles in the gondola coordinate system.

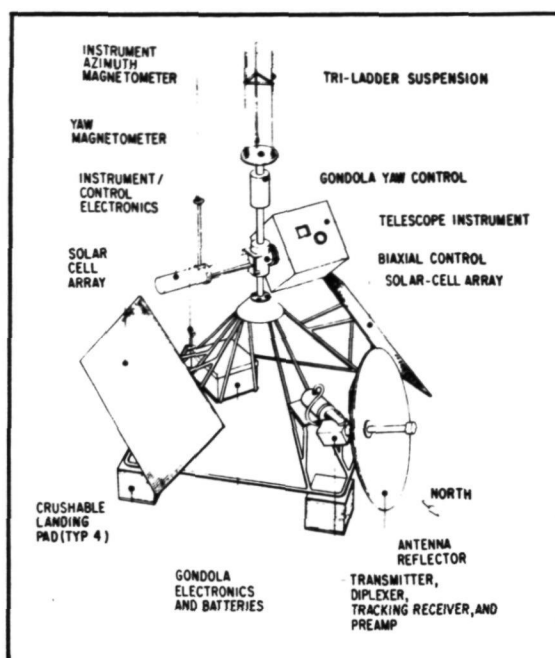


Figure 2. Gondola Configuration

Table 2
WEIGHT BREAKDOWN

	<u>Wt-kg</u>	<u>Wt-Pounds</u>
EXPERIMENT TELESCOPE ASSEMBLY	36	80
COMMUNICATIONS		
• Command Receiver-Decoder	.91	2
• Navigation Receiver	.45	1
• Communications Antennas	.91	2
• Housekeeping Data System	2.72	6
• L-Band Antenna (5-foot diameter) and Feed	2.27	5
• Tracking Receiver and Preamplifier	1.36	3
• Diplexer	.45	1
CONTROLS		
• Telescope Attitude Cont Elec	1.36	3
• Computer	3.6	8
• Antenna Att Cont Elec	1.36	3
• Magnetometers	.91	2
• Yaw Control Electronics	.45	1
POWER		
• 2 to 15 ft ² Solar Array Panels	13.6	30
• Battery - 40 amp/hr Capacity	18.1	40
DRIVES AND MECHANISMS		
• Telescope Biaxial Gimbal	7.26	16
• L-Band Antenna Biaxial Gimbal	4.08	9
• Yaw Drive Assembly	2.72	6
MISCELLANEOUS		
• ATC Transponder	1.81	4
• Altitude Transducer	.45	1
STRUCTURE		
(Cage, Bracketry, Crushable Pads)	<u>34</u>	<u>75</u>
TOTAL BASIC GONDOLA AND TELESCOPE	~135	298
BALLOON SUSPENSION	4.5	10
RECOVERY PARACHUTE AND CUTDOWN ASSEMBLY	10.4	23
LAUNCH ASSIST BALLOON AND BALLAST BOTTLE	<u>4.5</u>	<u>10</u>
TOTAL GROSS WEIGHT	~155	341

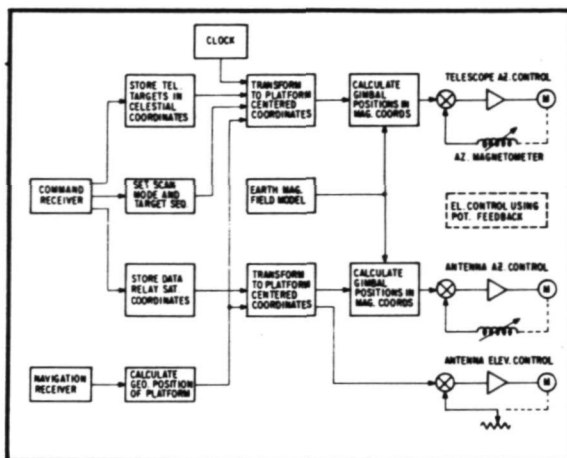


Figure 3. Gondola Navigation and Control System

Azimuth angles are expressed in terms of the local magnetic field and command signals are synthesized for the azimuth servos scaled to the output of the azimuth magnetometers. Elevation angles relative to the local vertical are derived from geo-position data and the stored commands from the ground operator.

The coarse azimuth orientation of the gondola is maintained by a yaw servo with a dead band of several degrees. The yaw controller applies a small, limited torque between the gondola frame and the relatively stiff balloon suspension, rotating the gondola until the output of the yaw

magnetometer nulls a synthesized command signal from the on-board computer.

The gondola remains in the dead band until disturbances from the balloon or gondola cause the gondola yaw position to drift outside the dead band.

The biaxial gimbal systems for both the telescope and antenna control are similar to those used in numerous balloon and spacecraft pointing control applications. The gondola frame and fixed components provide a relatively large inertia against which the azimuth and elevation controllers may react.

The stability and accuracy of azimuth control is limited principally by the limits with which the magnetic field can be resolved on board. Since elevation control is "open-loop", motions of the gondola also affect pointing accuracy. It is predicted that absolute pointing accuracies of better than $1\text{-}1/2$ degrees can be achieved. A method of reducing the uncertainty resulting from errors in resolving and modeling the magnetic field might be to calibrate the azimuth magnetometers at sunrise using signals from an azimuth solar sensor.

Gimbal rates for the data relay antenna will be quite low once acquisition is complete. Since the antenna beamwidth will be about $1\text{-}1/2$ degrees, some means of semi-active tracking of the data relay satellite will probably be required.

One method of mechanizing a semi-active tracking system would be to detect the housekeeping data signal originating at the data relay satellite, using a receiver located in the balloon gondola. The gondola data transmission antenna would be positioned initially by using computer-derived gimbal data. Then a scan would be initiated over a raster several degrees in width. When the signal level from the data relay satellite housekeeping telemetry channel became sufficiently strong, the raster scan would be interrupted. As the look angle to the DRS drifted and the signal level decreased below a predetermined level, the

raster would be automatically reinitiated, and the acquisition sequence repeated.

POWER

Power requirements for the gondola subsystems and components are given in Table 3. Total energy requirements are affected sharply by the data rate employed because of the increased bandwidth and RF power required as shown by the items in the lower part of the table.

Table 3
POWER BUDGET

<u>Component/Subsystem</u>	<u>Power-Watts at 28 Volts</u>
COMMUNICATIONS	
• Command Receiver-Decoder	2
• PCM Telemeter and Subcom	3
• OMEGA Receiver	.5
• Tracking Receiver and Preamplifier	3
CONTROLS	
• Computer	10
• Telescope Att Control	3
• Magnetometers	2
• Antenna Control Elec	3
• Yaw Controller	1
POWER DISTRIBUTION AND CONTROL	3
TOTAL CONTINUOUS LOADS	30.5
ALTERNATE OR DUTY CYCLED LOADS	
• X-Ray Experiment	15
• L-Band Transmitter at 100 bps	10
• L-Band Transmitter at 1000 bps	67
• L-Band Transmitter 25 K bps	240
• ATC Transponder	6
• Tape Rec - Rec Mode	8
• Tape Rec - PB Mode	14.5

The solar cell array panels are tipped inward at an angle of 45 degrees, so that the energy obtainable during the day is relatively constant. The "effective" efficiency of the array panels, when positioned so their normals are parallel to the ecliptic is shown in Figure 4 to be about 54 percent.

Another important determinant of total gondola weight is the energy consumed during the night hours, since battery capacity and the corresponding weight must be increased to enable storage of energy for night operation. The effect of various duty cycle

modes on the total gondola weight is shown in Table 4.

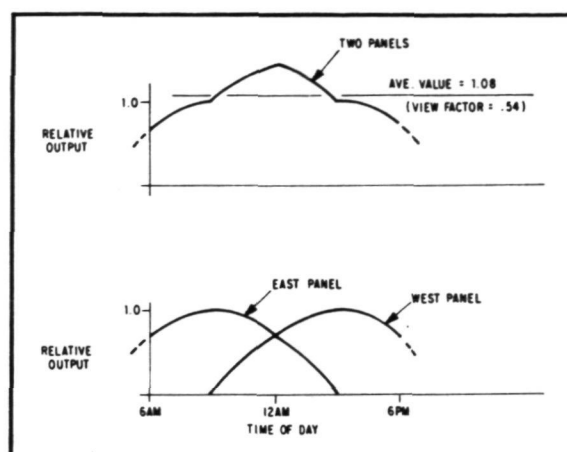


Figure 4. Relative Output of Solar Array Panels

Table 4

IMPACT OF DATA RATES ON SYSTEM WEIGHT

Case	Day Duty Cycle (Percent)	Rate (bps)	Night Duty Cycle (Percent)	Rate (bps)	On-Board Data Storage	Solar Array Area		Battery Capacity (amp/hr)	Total Payload Weight	
						Ft ²	Mtr ²		KG	Pounds
1	100	1000	100	1000	No	34	3.1	48	170	375
2	100	1000	50	1000	No	31	2.9	43	162	357
			50	100						
4	100	250	100	100	No	48	4.4	40	167	379
6	50	2500	100	100	No	35	3.2	32	163	359
	50	100								
7S	80	100	80	100	Yes	27	2.5	40	165	364
	20	250	20	2500						
8S	100	2500	100	2500	Yes	35	3.2	54	177	389
9S	50	100	50	100	Yes	32	3.0	17	175	386
	50	2500	50	2500						

DATA HANDLING

Different data rates and various duty cycles have been evaluated to determine their effect on electrical energy requirements and system weight. The results shown in Table 4 and Figure 5 include cases 7S, 8S, and 9S which involve the use of an on-board tape recorder for data storage.

Without on-board data storage, real-time data rates in excess of 1000 bps require TWT transmitters, and the required DC electrical power takes a step increase over that required for more efficient solid-state units. When on-board data storage is used, the real-time data rates are moderate except during "play-back" when the DC power requirements increase drastically.

However, due to the short duty cycle, typically ten percent, the higher power level does not result in a large increase in the total energy consumed.

For the duty cycles and data rates of case 7S the use of an on-board recorder results in a net saving in weight; for other conditions, the weight of the recorder just about offsets any saving in power system capacity.

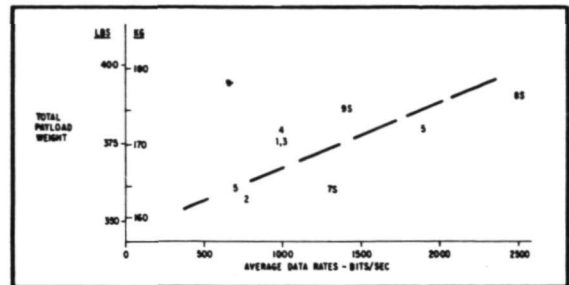


Figure 5. Payload Weights For Various Average Data Rates

CONCLUSIONS

It appears feasible to construct, using current technology, a balloon gondola for extended life astronomy research for altitudes in excess of 100,000 feet (30 km). Thus, many observations could be made over extended periods of time which were previously thought possible only from orbiting satellites, at a substantially greater cost.

Significant further effort is required to implement practical and economical, world-wide communications and navigational systems. Navigational communications may be provided in the future by orbiting satellites. This type of system would be inherently more accessible from remote areas such as the southern latitudes than are the stations of the existing ground-based navigational systems.

Time-sharing of data relay satellite communications channels could be an answer to the need for economical data retrieval and command control of extended life, balloon-borne payloads.

DISCUSSION SUMMARY — PAPER 2.8

The trade-offs associated with using a satellite link for data transmission were considered. It was estimated that a continuous rate of 17 bits per second would cost \$10,000 per month.

Since the Omega system is not complete in the Southern Hemisphere, it is of course not satisfactory for this system.

Further discussion of this topic developed during panel discussion 3.3 on February 22.

LOW-BACKGROUND FAR-INFRARED TELESCOPE FOR BALLOON-BORNE INFRARED ASTRONOMY

Frank J. Low
Wade Poteet
Robert Kurtz
University of Arizona

ABSTRACT

The design and performance of a new type of far-infrared telescope is discussed. The instrument is only 20cm in diameter, but its performance exceeds that of other telescopes at 100 μ .

The performance of far-infrared telescopes is limited not only by size but also by design and environment. The 30cm infrared telescope flown in the Nasa-Ames Lear Jet (Aumann, Low and Gillespie 1970) was limited by the large background originating from the atmosphere at 50,000 feet and from the telescope itself. The work of Hoffmann and his group has indicated that sky background levels of 1 or 2% are possible at balloon altitudes. We therefore undertook to design an instrument whose internal background would be small enough that its performance would be limited primarily by the atmospheric background at balloon altitudes.

Figure 1 shows the principal features of the off-axis (Herschelian) design. The single 20cm diameter mirror is gold-coated to achieve an emissivity at 100 μ less than 1%. Note also the baffle surrounding the mirror. Its emissivity is also about 1% and it insures that the detector sees only the sky after a single reflection.

Not shown in Figure 1 but essential to the operation of this system is the dewar window. This consists of a Mylar membrane only 4 μ in thickness. At low altitude it is protected from ambient pressure by a housing which is removed at altitude. These windows produce negligible background and have proved quite reliable when used in this manner.

Within the dewar a 3mm diameter composite silicon-germanium bolometer (Infrared Laboratories, Inc., Tucson, Arizona) is mounted at the focus of a crystalline quartz field lens which images the detector onto the primary mirror. The cold far-infrared filters follow the design described by Armstrong and Low (Armstrong and Low 1973; Armstrong and Low 1974).

Table 1 summarizes the specifications of the telescope system. It should be noted that at altitude the background loading of the bolometer was insignificant and the performance was determined essentially by detector noise alone. This indicates that further improvements in sensitivity are possible.

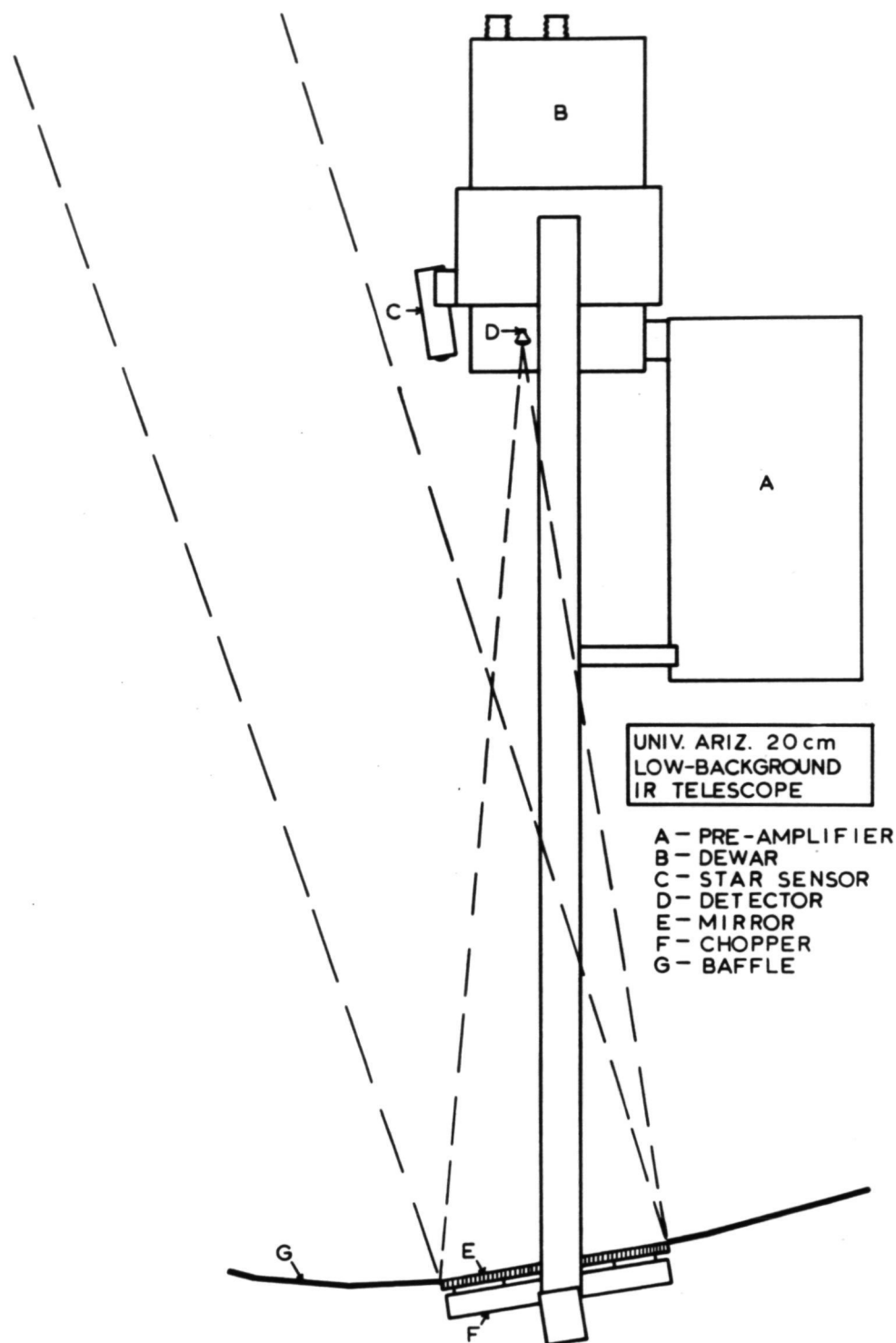


Figure 1. Principal features of the off-axis (Herschelian) design.

Specifications

Mirror dia. = 20cm
Beam dia. = 15[†]
Chopper throw = 15[†]
Chopper freq. = 7.6 Hz

Instantaneous sensitivity = 400 Jansky(10^{-26} w/M²/Hz P.T.P., 1 sec)

Weight

Scientific payload	- 235 lbs.
Instrumentation + tel.	- 119 lbs.
32' parachute	- 54 lbs.
Ballast, crush pad, etc.	- 65 lbs.
500,000 ft. ³ balloon	- <u>194 lbs.</u>
TOTAL	- 667 lbs.

Total power consumption = 15 watts
Chopper power = 2 watts
Flight altitude - 90,000 ft. MSL

Table 1

The 3-axis mounting is shown in Figure 2. The polar axis is oriented by means of a magnetically controlled azimuth stabilization system. An optical encoder permits read-out of the declination and hour angle in steps accurate to better than 0.1°. With this system it is possible to track celestial objects in a manner quite analogous to conventional ground-based telescopes. Long integration times are possible. It should be noted that the instrument itself is extremely lightweight and can easily be taken to much higher altitudes to achieve even lower background levels.

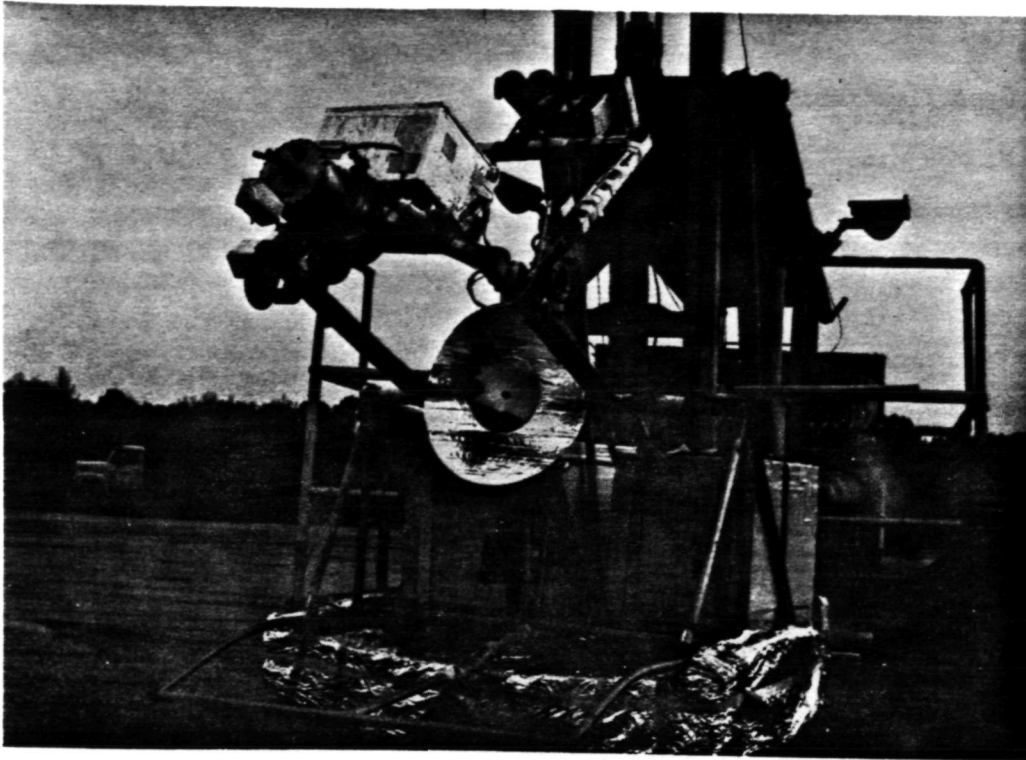


Figure 2. 3-axis mounting.

This system was flown from Palestine, Texas on two successful flights in January, 1974. Mars and Saturn were used as calibration sources and observations were made of HII regions W 3, Orion A, NGC 2024, and the bright infrared galaxy M 82. We believe this is the first detection of an extragalactic source by a balloon-borne telescope. Preliminary data reduction shows a 100μ flux density for M 82 of about 1000 Jansky, in agreement with the results published by Harper and Low using the Lear Jet system (Harper and Low 1973).

This program is supported by the National Aeronautics and Space Administration. We would also like to acknowledge the excellent support obtained from the personnel at the NCAR balloon facility at Palestine, Texas.

REFERENCES

- Armstrong, K., and F.J. Low, 1973. New Techniques for Infrared Filters. App.Opt. 12:2007.
- Armstrong, K., and F.J. Low, 1974. Far-Infrared Filters Utilizing Small Particle Scattering and Anti-Reflection Coatings. App.Opt. 13:425.
- Harper, D.A. and F.J. Low, 1973. Far-Infrared Observations of the Galactic Nuclei. ApJ 182:L89-L93.
- Low, F.J., H.H. Aumann, and C.M. Gillespie, Jr., 1970. Closing Astronomy's Last Frontier--Far Infrared. Astro. & Aero. 26-29.

DISCUSSION SUMMARY — PAPER 2.9

Stabilization of this system utilizes a "dumbbell" shaped inertia bar for the azimuth torque motor to work against. Two schemes were tested for coupling to the balloon. Both worked equally well. It was found that within a few arc-minutes of pointing accuracy, motion of the balloon has no effect.

Corrections to the observations were made to compensate for changes in the magnetic field, latitude and longitude caused by the balloon shift. In this way source positions were known to better than one tenth degree.

This system was used for observations of W-3, Orion, NGC 2024, M 82, Mars and Saturn. The flux observed for M 82 was approximately 1,000 to 1,200 flux units.

SKY SURVEY AT FAR INFRARED WAVELENGTHS
USING A BALLOON-BORNE TELESCOPE

M. W. Friedlander
J. Goebel
R. D. Joseph*
Department of Physics
Washington University, St. Louis, Missouri
(*Now at Imperial College, London)

ABSTRACT

Localised sources of far infrared radiation ($\lambda > 50\mu$) have been detected during a high altitude balloon flight with a 40 cm telescope and silicon detectors. The flight system is described and preliminary results are presented.

I. INTRODUCTION

A large area of the sky has been scanned for localised sources of far infrared radiation, using a balloon-borne system that was sensitive to wavelengths beyond about 55 microns. Two Molelectron silicon bolometers were used, with a Newtonian telescope having a 40 cm primary. The telescope was driven in azimuth at a fixed elevation; this mode of scanning was carried out for the duration of each of two balloon flights from the N.C.A.R. Balloon Facility in Palestine, Texas, in September 1973. The flight system is described in this paper, and preliminary scientific data will be presented at the meeting.

II. FLIGHT SYSTEM

a) Optics.

The primary mirror had a diameter of 40 cm and a focal length of 100 cm; the flat secondary was used as the chopper and was rocked at about 8 Hz. The dewar with the detectors was located at the one side of the telescope, with focus in the entrance plane of two brass light-pipes. The field of view is defined by the ratio of the focal length of the primary and the front aperture of each light pipe, and is a rectangle of 0.65° in azimuth and 1.0° in elevation. The amplitude of the chopping motion was adjusted so that the two fields of view that were to be compared were separated by 1.0° .

Each light-pipe was of square cross-section, starting with 1.8 cm side and tapering over a length of 10 cm to a square exit aperture with 0.5 cm sides, leading to a spherical cavity of 0.95 cm diameter, in which the silicon chip was suspended. The light-pipe assemblies were made of brass; the spherical housing and a mounting plate were made of oxygen-free copper, and mounted to the underside of the liquid-helium container. The two light-pipes were arranged with the one beneath the other. The

02731 27H
silicon detector elements were each 5 x 5 x 0.4 mm, manufactured by Molelectron Corporation.

Wavelength selection was set by the filters: 2 mm crystal quartz on the dewar (0.5 mm of clear polyethylene was used for one flight); 1.8 mm of teflon on the aperture in the radiation shield within the dewar; and 2 mm of crystal quartz plus 6 mil black polyethylene at the entrance to the light-pipes. The overall spectral response of the system was compared to a Golay cell at the University of Missouri-Rolla, using a Fourier-transform spectrometer. The response is fairly flat from 60 microns to the longest wavelength checked, 600 microns; the response falls to half by about 55 microns and is not measurable below 50 microns. A preliminary estimate yields 10% as the overall transmission of the filter combination at 100 microns and 20% for $\lambda \geq 200\mu$.

b) Orientation

The telescope was locked at 26.5° elevation, and then driven continuously in azimuth during the flight. The instantaneous direction of the telescope was obtained through the use of a magnetometer and sky cameras. A Schonstedt magnetometer was used as a sensor to serve two cameras to continuously follow Polaris. These cameras were operated with open shutters and continuously-moving film, so that Polaris was recorded as a trace. (Time markers were supplied by an Accutron watch.) The azimuthal difference between the cameras and the telescope was monitored with a 9-bit shaft encoder, and corrections were later included based on the actual position of the Polaris trace, the local time, and the balloon drift in longitude. The moon was detected by the bolometers several times in each flight, and these sightings provide a calibration of the co-ordinate measurement. The accuracy of other source positions is then about 0.4° in azimuth and $\pm 0.5^\circ$ in elevation; the corresponding uncertainties in R.A. and declination vary somewhat in different parts of the sky but generally do not exceed $\pm 0.5^\circ$.

c) Signal Processing

The preamplifiers were located in a shielded box immediately adjacent to the dewar. The output of the preamps was both telemetered directly and also processed further on board after which it was recorded on-board and telemetered. On-board, lock-in amplifiers were used in conjunction with a reference signal provided by the chopper, and each detector output was recorded in high-gain and low-gain channels. The on-board recording was intended as a back-up system, and consisted of the continuous photographing of meters that displayed the outputs. In parallel, these outputs were telemetered via the NCAR FM/FM system.

During the first flight, a major DC offset was observed which was attributed to differences in emissivity of the two fields that were viewed during the successive halves of the chopping cycle. Before the second flight, all parts of the

telescope that could be 'seen' by the light-pipes were covered with aluminum foil; these included the areas behind the primary mirror and on the inside of the telescope tube behind the secondary and directly opposite the entrance of the light-pipes. The result was a noticeable reduction in offset for the second flight. The offset was still large, but some celestial sources could still be seen on both flight records.

Electronically, the saturation effects of the large DC offset occur in the lockin amplifier, and these could be obviated after the flight. A new lockin amplifier was constructed; the inputs for this were the directly telemetered preamp output and the reference signal (both of which had been recorded). Far larger signals could not be handled, although the lunar signals still completely saturated the system.

Two further electronic filters were introduced and proved to be of major use in cleaning up the signals. These comprise our 'notch' filter: one pass-band is centered at the chopping frequency of 8.3 Hz and the other at 3.1 Hz. At the lower frequency, persistent noise had been detected, and was attributed to beating from the chopping of the secondary mirror.

The post-flight record shows an average noise level recorded at $60 \text{ nv/Hz}^{1/2}$. Extensive pre-flight calibration of the detector had yielded a value of 50 Kv/watt responsivity. With 20% as the filter transmission, this leads to a minimum detectable signal of $\sim 6 \times 10^{-12}$ watt at the entrance to the light-pipe, or an incident intensity $\sim 10^{-23} \text{ W/m}^2 \cdot \text{Hz}$.

It should be pointed out that the minimum detectable signal could be considerably reduced if an oriented system were used. This would permit a much smaller field of view with consequent smaller apertures in the dewar and radiation shield.

d) Scanning Mode

It was decided to adopt the unusual arrangement of the two detectors to allow a check on the sighting of celestial objects. If an infrared source is detected in the east it may first be seen by the lower detector. Four minutes later, when the gondola has returned to the same azimuth, the source will have risen in the sky and should be observed in the upper detector. For a source first seen in the west, the order of sighting in the two detectors will be reversed. Without repeated sighting of an object, there will usually be a residual suspicion that one might instead have noted an instrumental glitch, and the two-detector system is designed to obviate this problem. It might, of course, happen that a source is first viewed in the upper detector but this should happen only for those objects that are already too high to be seen with the lower detector, and one might then expect to observe such objects twice more (one with each detector) later in the flight.

The elevation angle of the telescope is adjustable on the ground, and was set at 26.5° for the September flights, to give us the possibility of sweeping through the galactic center.

The rate of scanning was chosen at 4 minutes per revolution, and the drive system was provided by NCAR.

e) Balloon flights.

Both flights were successfully carried out from N.C.A.R.-Palestine, in September 1973. Data for the second flight (Sept. 20-21) is being analysed first because of the reduced offset problem. Both flights were at float altitudes of about 97,000 ft, for about 9 hours.

III. RESULTS

Only preliminary results were available at the time of the meeting. The upper detector record shows a total of 82 events that at first sight appear to be possible signals, while the lower detector show 78 such events. With only a preliminary analysis so far available, detailed listings of possible sources and their locations are not being included with the present paper. Even at this early stage, it can be seen that the moon was detected four times and that these observations provide a calibration of the co-ordinate measurements. Several other sources were seen more than once. Small corrections in co-ordinates still need to be included.

Acknowledgements

As always, we are grateful to the crew at N.C.A.R. Palestine for their flight operations. Thanks are also due to A. Gorman, M. Jones, J. Borgwald and L. Lissak for assistance at various stages of the preflight and postflight work. This program has been supported by N.A.S.A. under grant NGR-26-008-069.

12751 27N

DISCUSSION SUMMARY — PAPER 2.10

The discussion was concerned with the identification and intensities of the sources observed in the Washington University investigation.

It was reported that the stronger sources observed had intensities of 10,000 to 20,000 flux units. Some sources observed were within one or two degrees of known pulsars but it will be necessary to process the photographs from the onboard star camera before identification is completed.

"THE NATIONAL SCIENTIFIC BALLOON FACILITY"

Robert S. Kubara
National Scientific Balloon Facility

ABSTRACT

More than 12 years ago the National Scientific Balloon Facility was established to improve capabilities of scientific ballooning. In 1963 the first balloon was launched from the facility's launch pad. During this period payloads have increased from 400 pounds (181 Kg) in 1963 to 1500 pounds (680 Kg) in 1973. Average balloon volumes have increased during the same time period from 3.0 MCF (84,951 M³) to 9.5 MCF (269,012 M³) in 1973.

The facility offers complete operational support to its users including launch, tracking, recovery and electronic support. Various launch techniques and electronics are described.

OPERATIONAL SUPPORT

More than 12 years ago a decision was reached at a conference of research scientists interested in or experienced in ballooning to establish a scientific balloon support group within the National Center for Atmospheric Research.

Rapid progress in the atmospheric sciences and astronomy required improvement in ballooning capabilities. The NCAR National Balloon Program was designed to help spur that advance and to make it easier for scientists from the scientific community as a whole to use the improved capabilities as they were developed.

Initially the facility was expected to focus its principal attention on the support of individual complex, beyond the state-of-the-art projects. As physical facilities, instrument systems and "know-how" were developed as by-products of the initial intent of the facility, they were made available to the scientific community as a whole to simplify the ballooning problems facing the individual scientist.

On the 28th of May, 1962, the National Center for Atmospheric Research and the National Science Foundation announced the establishment of the year round NCAR Scientific Balloon Flight Station in Palestine, Texas.

In August of 1963 the first balloon lifted off the facility launch pad. Since that time we have served 55 universities, 6 research organizations and 17 government agencies with more than 900 balloon flights from Palestine, Texas, and several other U. S. launch sites, as well as from nine foreign countries. During this period the average payload has increased from 400 pounds (181 Kg) in 1963 to 1500 pounds (680 Kg) in 1973. The average balloon volumes have increased during the same time period from 3.0 MCF (84,951 M³) to 9.5 MCF (269,012 M³). Balloon capabilities have steadily advanced; in 1968, a 15 MCF (424,755 M³) balloon was the largest operational balloon flown, and in 1974, flights are planned using 53 MCF (1,415,850 M³) balloons.

Payloads ranging in weight from less than 100 pounds (45 Kg) to over 10,000 pounds (4,536 Kg) have been launched by the facility's personnel. Altitudes of over 156,000 feet (47.5 Km) with a payload of more than 800 pounds (363 Kg) have been achieved. Average flight duration has tripled over a ten year period.

The NSBF provides complete operational support to its scientific users; this includes balloon consulting services, pre-flight rigging, launch, tracking,

and recovery services, electronic and meteorological support, plus flight services from locations where the scientific objectives are best achieved.

It would take many pages to discuss in detail the many techniques and services required for the NSBF to fulfill its mission so I will just briefly describe the major portion of the NSBF operational support.

Numerous launch techniques are used by the facility, dependent upon experiment weight and the balloon system used.

The most common technique is the dynamic launch using a single cell balloon with a launch vehicle that supports the scientific gondola prior to launch. The inflated balloon bubble is constrained by a spool, and when the bubble is released from the spool, the launch vehicle maneuvers the payload directly under the ascending balloon. When the balloon is fully extended above the payload it is released from the launch vehicle. This technique permits compensation for changes in surface wind directions thereby providing some flexibility during the launch. The wind constraint for a dynamic launch is normally 10 knots. This may vary with length of the system, maneuvering area and type of vehicle used. Several launch vehicles are used by the facility for dynamic launches. The largest is Tiny Tim, a 52 ton (51,891 Kg) vehicle specially designed for balloon launching. Gondolas as tall as 33 feet (10m) and weighing up to 6155 pounds (2,791 Kg) have been successfully launched from Tiny Tim.

Very heavy payloads are launched by the static technique usually using tandem systems consisting of a top balloon and a main balloon separated by a transfer tube. The top balloon contains enough gas at launch to lift the entire system. During ascent the expanding gas from the top balloon is transferred to the main balloon. Prior to launch the entire balloon system is erected over the payload under continuous control of a winch vehicle. The main balloon is sheathed in a plastic reefing sleeve to prevent sailing prior to launch. The winch vehicle used at the NSBF has a capacity of 3460 feet (1.05 Km) of 5/8 inch (1.6 cm) cable and can safely handle cable tensions as great as 40,000 pounds (18,144 Kg). Gross loads of 14,000 pounds (6,350 Kg) have been launched by the facility using this technique.

For electronic support the facility provides balloon control and scientific telemetry, altitude sensors, telecommands and ground support equipment. In the near future a new generation Consolidated Instrument Package (CIP), will be placed into operation and will include a single command system for both balloon control and scientific commands, plus a telemetry system which has the capability to handle data transmissions on the flight over an L-Band RF carrier. The ground station associated with the CIP will record scientific data and flight parameters including time, altitude and balloon position, on incremental magnetic tape for post-flight processing.

The CIP will contain the following equipment:

1. PCM Data Encoder
2. PCM Command Receiver-Decoder
3. Rosemount Pressure Transducers
4. Omega Receiver
5. Twelve Subcarrier Oscillators (when required)
6. "L" Band FM Transmitter

The ground station at Palestine is equipped with PCM data decommutation and real-time display equipment, omega processor, time code generator, time receivers (Loran and WWV), Analog tape recorder, PDP-11/20 computer with incremental tape recorders, and PCM command encoders/transmitters. A down-range station is maintained with the same equipment except for the computer.

Data may be recorded on analog tape and replayed through the computer at Palestine to generate an incremental tape.

Complete meteorological service is located at the facility for the sole purpose of providing weather information for balloon flights. The weather briefings for each balloon flight include the forecasts for the launch, ascent track to float altitude, the trajectory, descent track to impact, and the recovery area weather.

Accurate position reports of the balloon's trajectory have become essential for many of the scientific experiments flown on balloons. We provide continuous tracking. This is accomplished by several methods including radar, radio direction finding and electronic navigation techniques. Two twin-engine tracking aircraft are operated by the facility to provide the necessary balloon position reports.

The safe recovery and return of scientific equipment to the Balloon Facility is of prime concern to operations personnel, and is accomplished by experienced technicians using specialized equipment.

As many of you are aware, balloon operations has evolved into a very complicated exercise and interface of technicians, machines and electronics. A typical balloon flight of today involves launch vehicles as large as the heaviest earth movers, multi-engine aircraft, the most sophisticated electronic equipment and special recovery vehicles.

The new 2000 ft diameter launch area at the NSBF will be inaugurated in May of 1974. This is only one of the many improvements that the facility is making to keep pace with the ever increasing requirements of the scientific ballooning community.

15725 15725

DISCUSSION SUMMARY — PAPER 3.1

Questions were asked about how NCAR is financed and what share of the budget the user pays. The speaker noted that NCAR is financed inherently by the National Science Foundation. All users are charged for the balloons and helium that they use. Foreign users are charged an additional \$11,000 fee for each successful flight. The user receives complete operational support including launch, tracking, recovery, weather forecasting, use of electronic ground station and other ground facilities. The \$11,000 charge for foreign users is not levied in an unsuccessful flight if the failure is attributable to NCAR equipment.

The possibility that the facility might be overcrowded was addressed. It was noted that all users are treated with equality whether foreign or U.S. The instrument that is ready first is generally the one that flies first. It is possible to fly two separate gondolas at the same time. Plans to fly four on December 27, 1974, are being worked out.

AIR FORCE CAMBRIDGE RESEARCH LABORATORIES BALLOON OPERATIONS

Thomas J. Danaher
Air Force Cambridge Research Laboratories

ABSTRACT

AFCRL scientific ballooning is unique in the Air Force and provides the only Department of Defense in-house capability. A general information base is provided to familiarize the reader with the Air Force organization, research efforts, facilities and balloon flight operations.

INTRODUCTION

The USAF Balloon Program is managed by the Aerospace Instrumentation Laboratory, one of nine Air Force Cambridge Research Laboratories, located at L. G. Hanscom Field, Bedford, Massachusetts. The Aerospace Instrumentation Laboratory is composed of a balloon group and a sounding rocket group. The primary mission of the balloon group is to support the research, development, test and evaluation and operational needs of our sister laboratories in AFCRL and of other elements of the Air Force. Our other objective is to extend the capabilities and versatility of balloons as atmospheric platforms. To carry out this mix of research and operational work, the balloon group of ninety-two people consists of physicists, meteorologists, engineers, and operationally trained personnel.

I will touch only briefly on our research efforts since the topic of this paper is concerned with our balloon operations. The research can be characterized by the following work efforts:

(1) Free Balloons - materials studies directed primarily towards increasing the load-carrying and altitude capabilities of polyethylene balloons.

(2) Tethered Balloons - development of improved tethered balloon cables, improved balloon designs and materials, and studies of balloon dynamics.

(3) Powered Balloons - advanced systems design, power source studies and flight test of prototype models.

(4) Air Launched Balloons - studies of systems launched from aircraft and rockets.

(5) Climatological studies - flight dispersion and operational analyses for proposed programs.

(6) Instrumentation and Tracking - development of navigational systems and command and control instrumentation.

Balloon flight operations conducted at our permanent launch sites located at Holloman AFB, New Mexico and Chico, California utilize and evaluate the research and development products of the balloon group. Thus, there is a closed loop between theory, development, and application, providing the setting wherein theory can be quickly tested and future research needs readily identified.

BALLOON FLIGHT OPERATIONS

As mentioned in the introduction, our mission is first to support Air Force needs. We also provide balloon flight support to other Dept. of Defense agencies and government organizations. Within the latter category, for example, the AFCRL has acquired the responsibility of providing support to the Atomic Energy Commission's Ash Can project, for which about 30 flights per year are conducted. Flights are made from New Mexico, California, Alaska and Panama. The Panama and Alaskan series are conducted once a year. With the impending retirement of the WB-57 aircraft, the Ash Can project will be expanded to include additional air sampling flights within the 40,000 to 60,000 ft (1.2×10^4 to 1.8×10^4 m) altitude range.

Measurements are made of Carbon 14 and radioactive particulate concentrations. After the samplers have performed their functions the payloads are separated from the balloons and aerielly recovered by C-130 aircraft. We are working to extend the present capability of snatching payloads of 450 lbs (2.0×10^3 N) to loads on the order of 700-1200 lbs (3.1×10^3 to 5.4×10^3 N). In order to do this, a new recovery parachute system is under development. We expect that prototype systems will be tested this summer. The advantages of air snatching the balloon payloads are obvious because terminations may occur over water, jungles or the arctic tundra. Since we have been involved in the Ash Can program, the aircrews have not failed to bring a payload home.

NASA has frequently utilized AFCRL balloon flight support. The Planetary Entry Parachute Program, PEPP, and the Balloon Launched Decelerator Test Program, BLDT, for the Viking Program, were major balloon programs conducted for NASA during the past few years. This past year we concluded a balloon-borne laser flight series for NASA-Goddard which provided data on the atmospheric effects on laser beams transmitted from a balloon at 90,000 ft (2.7×10^4 m) to a receiver on the ground.

In summary, in regard to whom balloon flight support is given, first priority is to the Air Force, followed by organizations which have programs from which the Air Force may derive benefit. For example, the NASA PEPP and BLDT programs resulted in the development of new, heavy-payload balloon capabilities which can be directly utilized in Air Force systems testing.

The Air Force has on occasion been accused of being the prime polluter of the lower stratosphere and of doing little to determine the effects on air quality of its aircraft operating at these altitudes. In the balloon sampling program the Air Force is presently doing something about this problem. In the next few years the balloon group and other AFCRL scientists will be engaged in stratospheric pollution research, building on the results of the recent CIAP, Climatic Impact Assessment Program. In particular, we will be conducting balloon flights for AFCRL's Aeronomy Laboratory to obtain data on chemical reactions resulting from jet aircraft emissions in the lower stratosphere.

FACILITIES

Permanent AFCRL balloon launch facilities are located at Holloman AFB, New Mexico and at Chico, California. Both locations also have a remote operations capability for performing flights wherever a need may exist. The balloon launch facility at Holloman AFB has access to the use of precision radar, optical instrumentation, telemetry, and restricted airspace on the White Sands Missile Range. Nuclear blast simulations, high altitude prototype parachute tests, hardware evaluation, high altitude tethered balloon operations-any test involving free-fall can be conducted by the Holloman facility. Each launch site has a completely equipped and staffed weather station, machine shop, instrumentation laboratory, parachute shop, and a small environmental test chamber. The Holloman facility has the use of an environmental test facility with a working volume of 8x8x11 ft (2.4x2.4x3.4m), an altitude range from sea level to 225,000 ft (6.86x10⁴m), and a temperature range of minus 100°F to plus 200°F (minus 73.3°C to 93.3°C).

TETHERED BALLOON FACILITY

AFCRL first became involved in tethered balloon operations when it provided support to NASA's testing of the Surveyor lunar lander. Subsequently, the immediate and potential capabilities of tethered balloons became better appreciated and it became obvious that a permanent facility was essential for these operations. Consequently, Fair Site was established on White Sands Missile Range solely for the purpose of supporting tethered balloon operations. The criteria for the selection of this site were that it should:

- (1) be capable of routinely handling payloads of 500 pounds (2.2x10³N) or more to altitudes in excess of 10,000 feet (3.1x10³m) above ground.
- (2) be unencumbered by other programs.
- (3) be in a restricted air space area to permit flight durations of hours to weeks, and
- (4) be suitable for future expansion, to accommodate development testing and operations of tethered systems of much greater payload altitude capabilities.

Fair Site is located in the northwest corner of restricted area, R-567-B, on the White Sands Missile Range. It is approximately 70 land miles (1.1x10⁵m) from Holloman AFB. Here, there is no restriction upon the flight altitude of tethered balloons. Meteorological conditions have been investigated fully, and the climatology indicates a good year-round flight capability.

The site has the advantage of a fully instrumented range to provide data essential for interpreting the results of many scientific experiments flown on tethered balloon systems. Position data for our tethered balloon flights can be obtained using either FPS-16 radars or cinetheodolites or both. If radar is used, a position display can be set up at the Balloon Control Center at Holloman AFB or at some Range Control Station. Velocities, accelerations and balloon altitude data can be

obtained from both cinetheodolites and on-board instrumentation. Data reduction is provided through WSMR. In addition to the cinetheodolites and radars, facilities for receiving a wide variety of telemetered data are available.

The heart of the tethered balloon facility is the permanently fixed winch which has the following capabilities:

- (1) Line pull capabilities of 30,000 pounds ($1.3 \times 10^5 \text{ N.}$) maximum at a maximum speed of 200 feet (61 m.) per minute;
- (2) Line pull capabilities of 6,000 pounds ($2.7 \times 10^4 \text{ N.}$) at line speeds of 1,000 feet ($3 \times 10^2 \text{ m.}$) per minute;
- (3) Variable speed control in each of the above modes;
- (4) Fail-safe brake system;
- (5) Interchangeable sheave and capstan shoes;
- (6) Drum capacity to 30,000 feet ($9.1 \times 10^3 \text{ m.}$) of $\frac{1}{2}$ -inch ($1.3 \times 10^{-2} \text{ m.}$) diameter line;
- (7) The capability of accommodating line sizes from 3/8-inch through 3/4-inch diameter ($9.5 \times 10^{-3} \text{ m}$ through $1.9 \times 10^{-2} \text{ m.}$).
- (8) Level wind system capable of storing 3/8-inch through 3/4-inch diameter ($9.5 \times 10^{-3} \text{ m.}$ through $1.9 \times 10^{-2} \text{ m.}$) line sizes uniformly on the winch drum, and adjustable for these line sizes with 1/16-inch ($1.6 \times 10^{-3} \text{ m.}$) variation in diameter.
- (9) Instrumentation consists of a line-load measuring device, line-footage counting device, line-speed and direction measuring device.
- (10) Other instruments include those items necessary to monitor the operation of the power source and the hydraulic drive system.

FILMS OF AFCRL BALLOON OPERATIONS

In closing, I will show a short film which gives a general view of some of the equipment we use in our balloon operations and the retrieval of an Ash Can payload by C-130 aircraft over Panama.

DISCUSSION SUMMARY — PAPER 3.2

In answer to questions about expected cost and performance of a tethered balloon operating at 60,000 ft, the development cost was estimated at \$750,000. The French already have flown a 250-pound tethered balloon this high. The possibility of flying a 500-pound device at 90,000 ft was considered good if money were available.

PAPER 3.3

SPECIAL PANEL DISCUSSION ON LONG DURATION BALLOONING

DISCUSSION SUMMARY — PAPER 3.3

Panelists: Dr. Ricker and Dr. Lewin of M.I.T., Mr. Pavey, Mr. Snider and Mr. Shipley of NCAR.

During the panel discussion on long duration balloon flights several points were covered. These points included the importance, effectiveness and some details of such systems, a proposed NCAR program to develop required capabilities and finally the current funding situation.

Two types of long duration balloon systems were considered. One approach uses a zero pressure balloon launched in Europe and recovered after 5-8 days in the United States. The second system would involve launching a superpressure balloon from Australia that would circumnavigate the globe during flights lasting several months.

It was stressed that development of these systems is the important next step in scientific ballooning. The basic advantage of course, is the increased observing time afforded by these long flights. Satellites and balloon-borne instruments were compared to illustrate this time advantage. The sensitivity in many investigations improves as the square root of the observing time available. Therefore, long duration balloon flights are perhaps 10-20 times more sensitive than one day flights, but satellites are perhaps only twice as sensitive as long duration balloon flights. It was estimated that satellites cost one hundred times more per pound than balloon-borne instruments. Therefore, balloon-borne investigations are more cost effective.

During discussion it was pointed out that although the trans-atlantic flights are not as long as the flights around the southern globe there are compensating factors. The most important is the much larger payload capability of the zero pressure trans-atlantic flight. This payload makes possible larger instrument apertures. Since sensitivity depends on aperture, this compensates for the shorter flight duration.

Other advantages of long duration balloon flights were noted. Opportunities to fly instruments on balloons are far more numerous than opportunities for satellite flights. The lead time for balloon-borne investigations is short. Therefore, research concepts can be pursued at a satisfactorily rapid pace. In addition, instrumentation changes required to meet new requirements are possible through most of a balloon flight program.

There was some discussion concerned with dangers to air traffic. Since these balloons float well above commercial air corridors, the only times of concern are during launch and recovery. Safety measures to cover these periods have been well developed during conventional balloon programs. Furthermore most of the long duration flights are planned for far south latitudes where air traffic is very light.

15751 274

NCAR summarized a proposal to the National Science Foundation covering the development of a long duration balloon flight program. The instrument considered would weigh 400-500 pounds and float at 130,000 feet. During discussion various estimates were made of the fraction of this weight available for the scientific instrumentation. These estimates varied from 80-300 pounds. It was felt that this size payload represented a useful and practical first step. The program would cover a two year period and would include both balloon development and test flights. As part of the balloon development, NCAR will analyze the various aspects of the dynamics of mylar balloons. Other balloon materials and balloons will be developed by U.S. companies under contract. There are five (5) test flights included in the program. Three (3) will be in the United States and two (2) in Australia.

Estimates of the costs involved in future research flights were presented. These estimates were based on a projected program including fifteen (15) flights per year. Superpressure balloons suitable for long duration flights will cost about \$50,000 each. Operations costs including launch, tracking, recovery, and operation of four (4) ground stations were estimated at \$75,000 for the fifteen (15) flights. Cost of the flight control electronics was not included since it is expected to be recovered.

Some of the general aspects of the present funding situation were discussed. NASA provides some support for research and development, but not enough to fund the two (2) year development program. Most of the NASA funding is for operations costs involved in current research flights.

For this development project to proceed it must have National Science Foundation funding. There has been an endorsement of the project by the National Academy of Sciences. The problem is that the required funding is in competition with other research programs and with current balloon operations funding.

PAPER 4.1

THE STELLAR AND SOLAR TRACKING SYSTEM OF THE
GENEVA OBSERVATORY GONDOLA

Daniel Huguenin
Geneva Observatory, Sauverny, Switzerland

ABSTRACT

Sun and star trackers have been added to the latest version of the Geneva Observatory gondola. They perform an image motion compensation with an accuracy of ± 1 minute of arc. The structure is held in the vertical position by gravity; the azimuth is controlled by a torque motor in the suspension bearing using solar or geomagnetic references. The image motion compensation is performed by a flat mirror, located in front of the telescope, controlled by pitch and yaw servo-loops. Offset pointing is possible within the solar disc and in a $3^\circ \times 3^\circ$ stellar field. A T.V. camera facilitates the star identification and acquisition.

PLATFORM

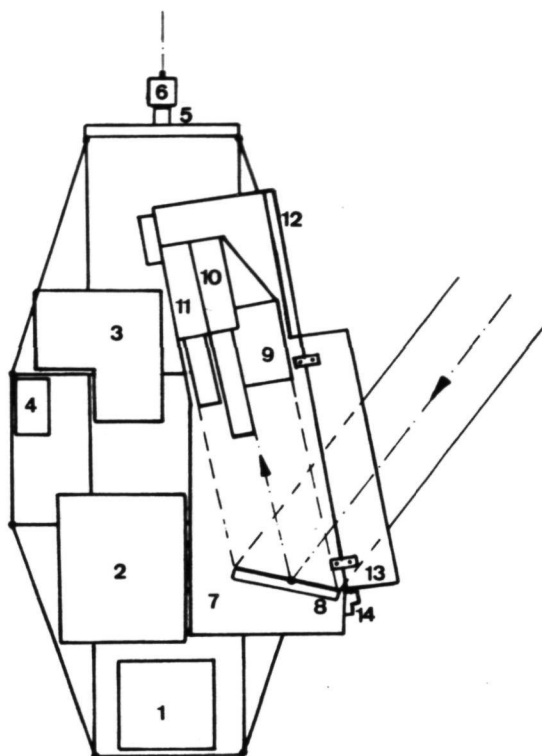
The platform has been conceived as a multi-purpose and light instrument with a moderate pointing accuracy of 1 minute of arc on the sun and on stars down to the 6th magnitude. It can carry a $.5 \text{ m}^3$, 60 kg scientific payload. The fine pointing system is completely independent of the payload (heliostat or siderostat). The structure contains the necessary housekeeping systems, i.e.:

- 28V / 40Ah battery with 9 power buses.
- Quartz time base with power outputs.
- PCM telemetry encoders with 70 analog and digital channels.
- On-board punched tape programmer with momentary, latching and numerical commands.
- Coarse attitude control ($\pm 1^\circ$) for multiple observations to any point of the celestial sphere.
- All the interface wiring mounted on a removable harness for quick change of the scientific payload.
- Weight: 200kg without scientific payload.

Figure 1 gives the disposition of the modules in the gondola. The lay-out is practically the same for solar and stellar flights.

SUN TRACKER

The motion compensation flat mirror is made of "Haeräus" alveolate quartz foam for thermal stability. Two sun sensors, using silicone solar cell bridges, control the pitch and yaw axes of the mirror. They are mounted on the side of the scientific telescope and aligned with its optical axis. The azimuth axis of the gondola is held within $\pm 1^\circ$ of the sun's azimuth by



1. Battery
2. Housekeeping electronics
3. Instruments electronics
4. Magnetometer
5. Universal joint
6. Azimut bearing
7. Instruments compartment
8. Siderostat mirror
9. Telescope
10. Star tracker
11. TV camera
12. Instruments cover
13. Doors
14. Doors mechanism

Figure 1. Schematic outline of the gondola.

auxiliary sun sensors. Sun search is made by a slow rotation of the flat mirror around its pitch axis. When the sun presence is detected, the servo-system switches to the track mode. This equipment was designed by Compteurs Schlumberger in Paris, and made three flights.

STAR TRACKER

The keystone of the stellar acquisition and tracking system is the AD-104 photon counting detector developed at the Geneva Observatory. This unit includes a photomultiplier, signal conditioning electronics with pulse shaping, discriminator and transmission line driver, and a H.V. power supply. It counts up to $6 \cdot 10^6$ photoelectrons per second. It is corona free at all pressures and consumes 2 watts. With this detector, it has been possible to use essentially digital electronics for the star tracker and for the T.V. camera.

The optical schematics of the star tracker is given in figure 2, and the block-diagram in figure 3. The modulator is a classical rotating knife edge driven by a D.C. motor at 8000 RPM.

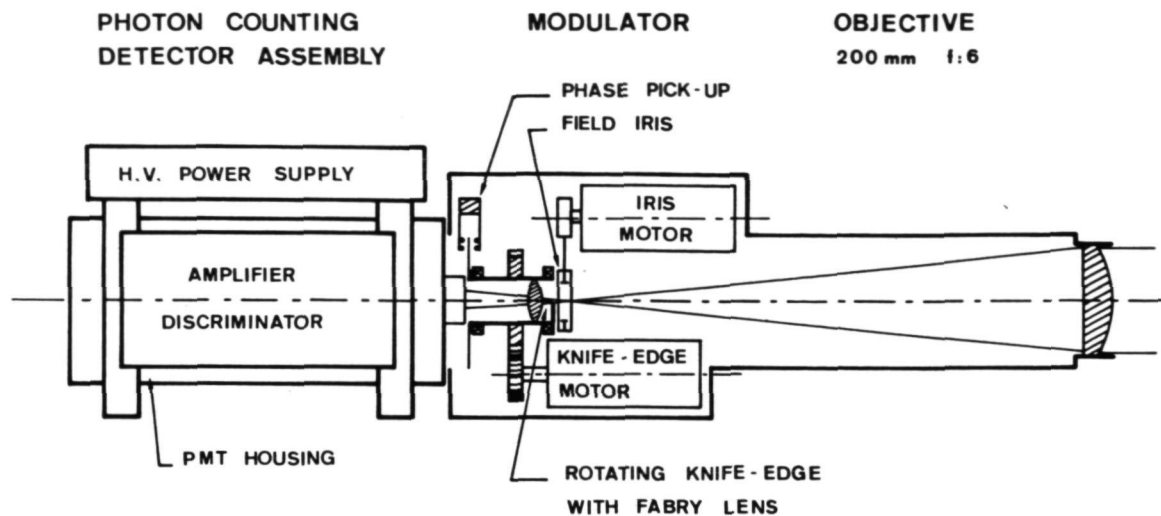


Figure 2. Schematic view of the star tracker.

In the acquisition phase, the field iris defines a 2° circular field of view. When the tracking mode is initiated by tele-command, the field iris reduces slowly the field of view, in five seconds, down to 22 arc minutes, thus lowering the sky noise by a factor 30 and occulting background stars. The rotating knife edge is mounted slightly behind the focal plane, thus creating a linear zone, 6 minutes of arc in diameter, in the center of the field of view. The magnitude counter integrates the photoelectric signal over 4 revolutions of the modulator. The content of the counter at the end of the integration time is proportional to the star magnitude. The result is stored in a buffer memory and updated after every fourth revolution. In the tracking mode, the content of the magnitude memory is frozen. The signal applied to the rate divider is constantly divided by the star magnitude. Therefore, the instantaneous signal is independent of the star brightness in the range $m_V = 0$ to $m_V = 6$. The signal is then integrated over four 90° rotations of the modulator. Thus the field of view is divided in four orthogonal pseudo-quadrants, called up-left-down-right, defined by a photoelectric pick-up mounted on the hollow shaft of the modulator. The up-down and left-right signals are subtracted from each other respectively by the pitch and yaw up/down counters. The result of these subtractions are the pitch and yaw error signals. This type of modulation and axes separation has two advantages. The star follows a short radial path directed toward the center of the field of view. The detector sensitivity is kept constant over the field of view by a Fabry lens and by the quadrant by quadrant photon integration, thus target ambiguity caused by background stars is eliminated. We found that the guide-star is acquired without ambiguity if it

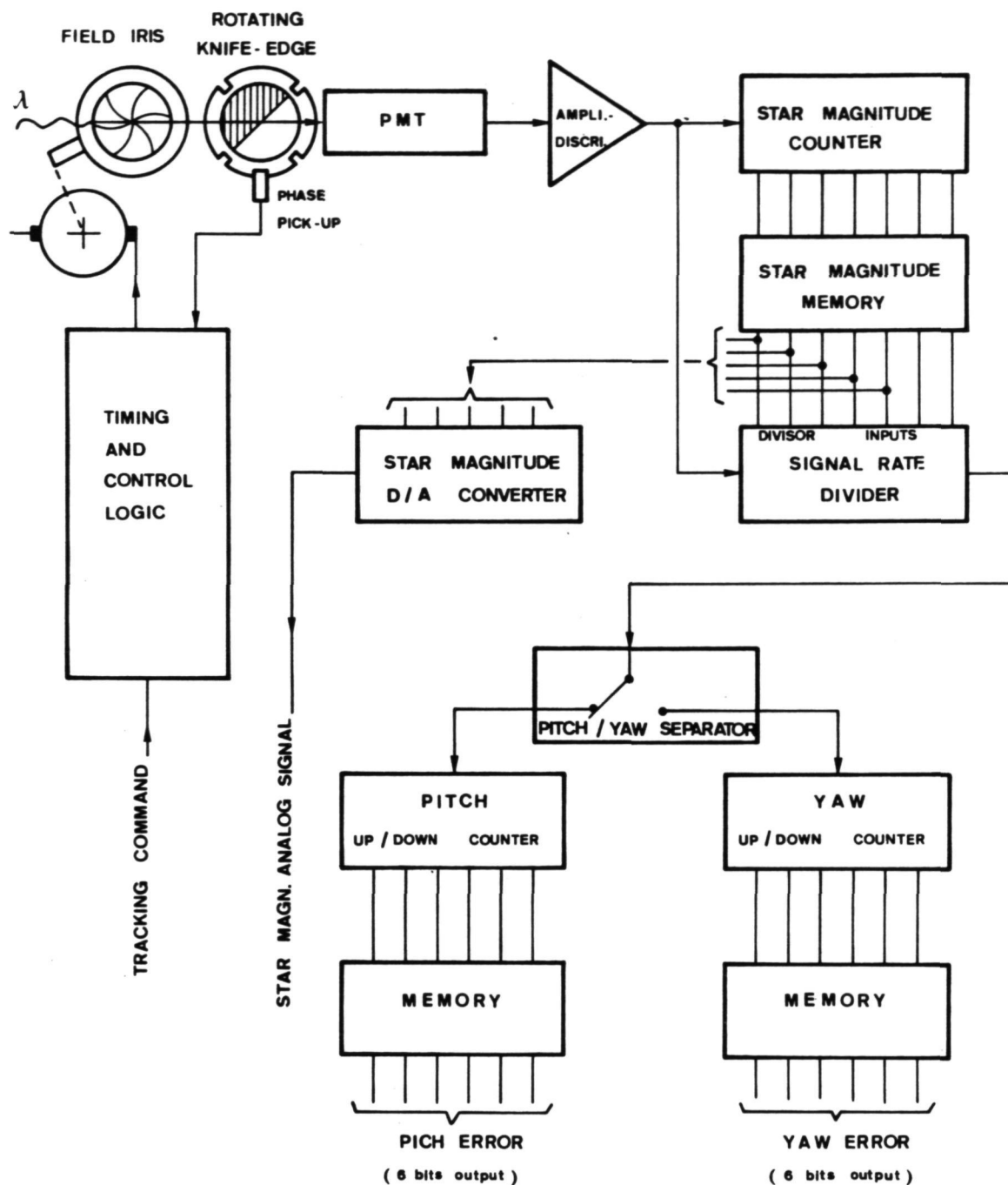


Figure 3. Block diagram of the star tracker electronics.

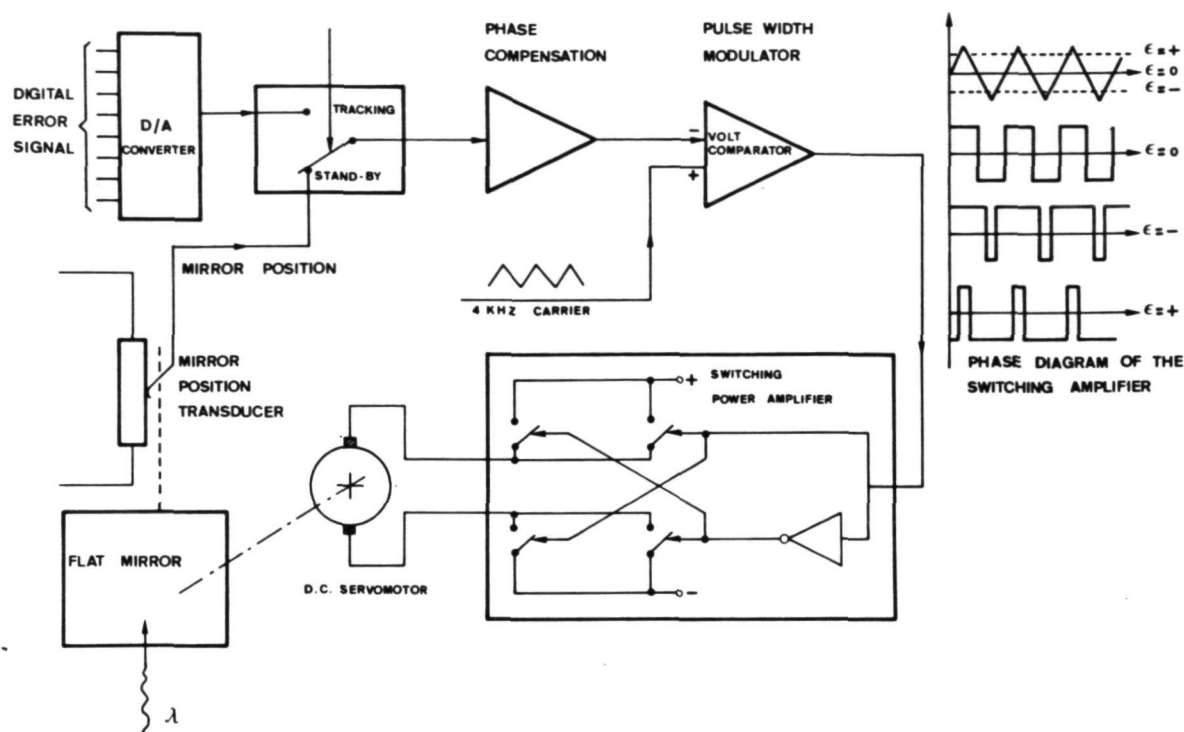


Figure 4. Mirror control electronics.
Pitch and yaw loops are identical.

is 20% brighter than the total brightness of all other objects in the field of view. Bright background stars are occulted by the field iris in the tracking mode if their angular separation from the guide-star is more than 15 minutes of arc.

The flat mirror rests on 3 points defining the pitch and yaw axes. At the intersection of these axes the mirror is attached to its frame by a ball-joint. The two other points are materialized by pitch and yaw precision screw-jacks driven by DC servomotors. A fourth attachment, with four degrees of freedom, prevents the mirror from rotating in its own plane. The angular motion range of the mirror about each axis is $\pm 4^\circ$ (optical).

The mirror itself is made of two 6mm Pyrex plates separated by a bundle of tubular spacers ground and cemented together with epoxy. This construction made the mirror 60% lighter than a solid plate of the same dimensions (31 x 31 x 6cm).

The mirror control electronics is represented in Figure 4. In the stand-by mode, the mirror is maintained in its median position by the error signals of two linear position transducers mounted on the screw-jacks. In the tracking mode, the mirror is controlled by the star-tracker. The star tracker has an offset pointing range of $\pm 1.5^\circ$ with regard to the telescope.

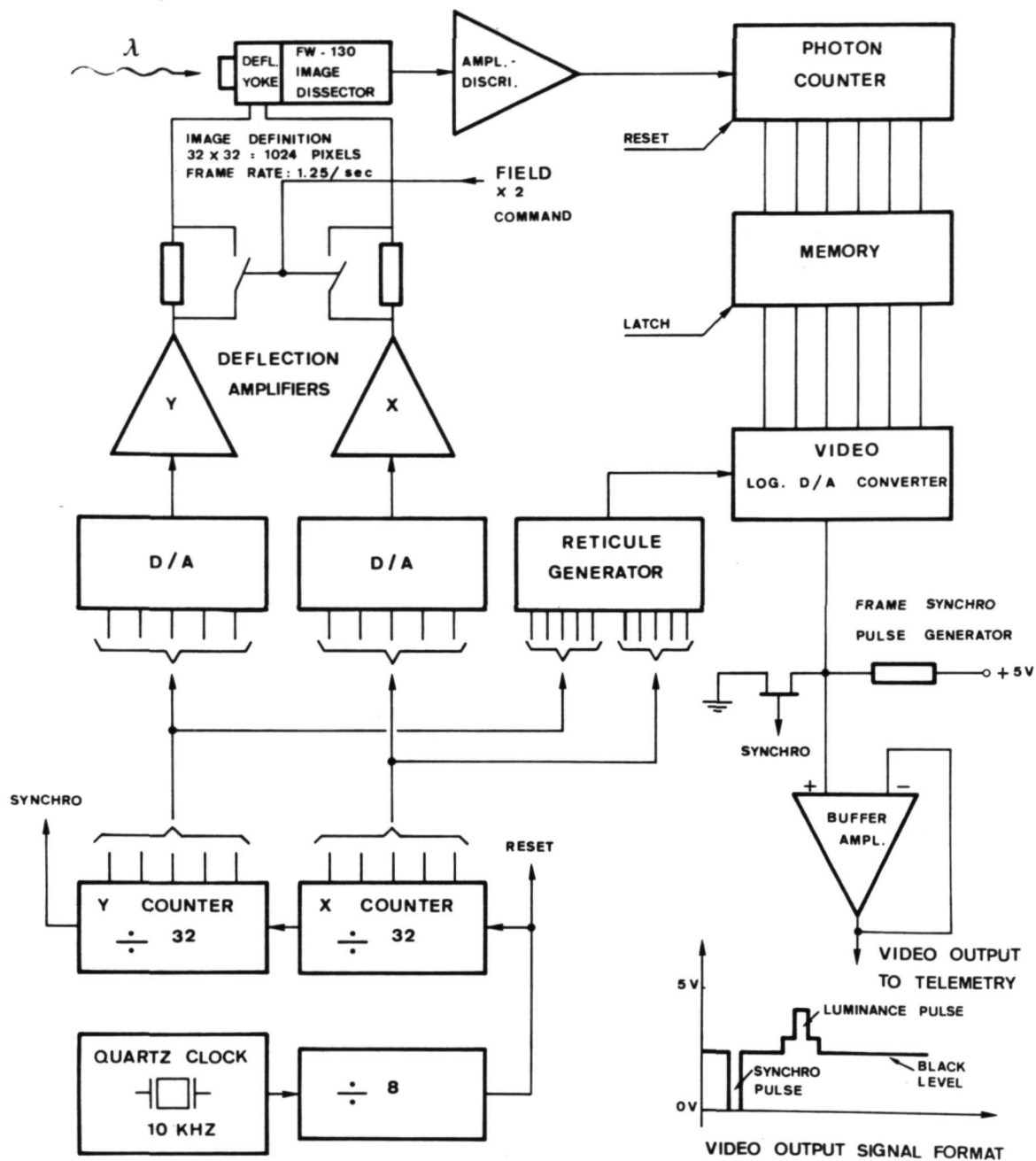


Figure 5. Block diagram of the TV camera.

Coarse pitch orientation is made by rotating the whole mirror assembly around a horizontal axis. Coarse azimuth orientation is controlled by a magnetometer acting on the suspension bearing. Coarse azimuth and pitch angles are programmed on the on-board punched tape and updated by telecommand.

TV CAMERA

The stellar TV camera is used for star identification and acquisition. The tube is an ITT FW-130 image dissector used as a photon counter (Figure 5). The image definition is 32 points per line by 32 lines. The X and Y sweeping signals are produced by digital staircase generators. The exposure time is .8 second per frame. The number of photoelectrons produced by one picture element is stored in a memory and converted into an analog signal after logarithmic compression. With its 50mm ϕ objective the camera covers the magnitude range $m_V = -.5$ to $m_V = 6.5$. The camera generates a reticule (centered cross). The reticule signal is also used on the ground as a luminance reference signal. Each frame begins with a synchronisation pulse. The video signal

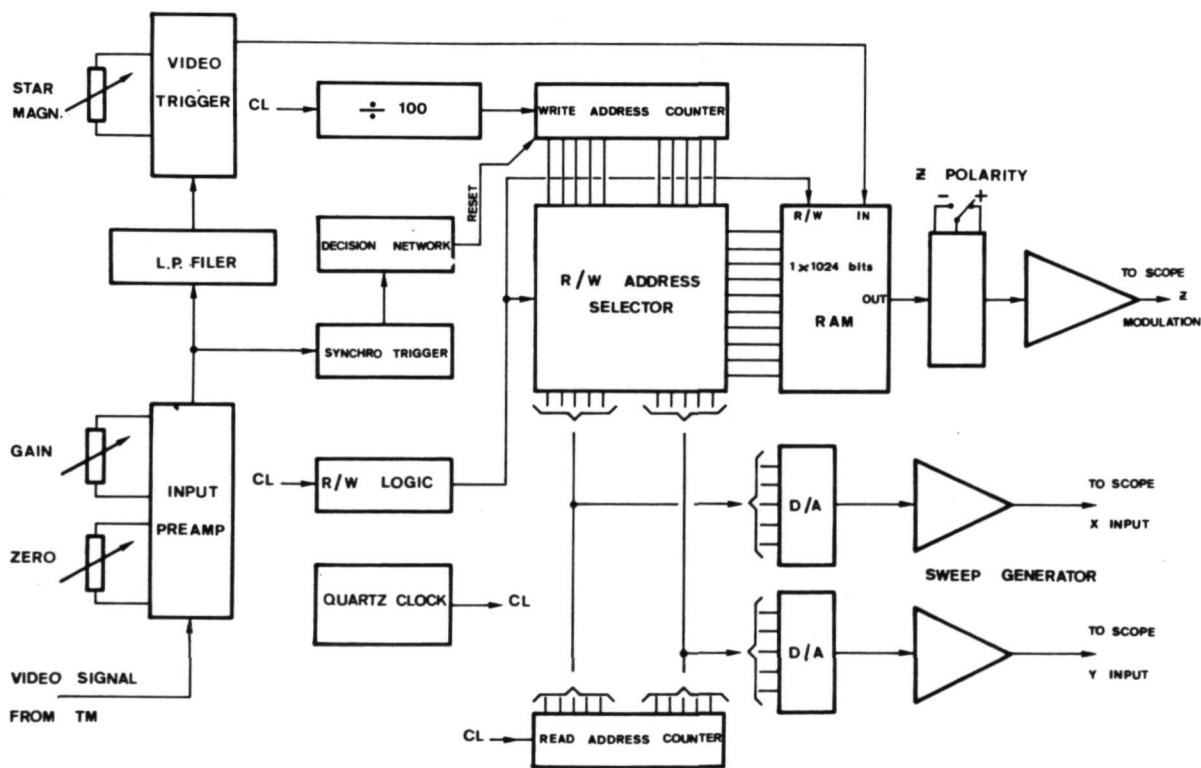


Figure 6. Block diagram of the TV receiver.

can be transmitted to the ground on a regular IRIG FM/FM channel with a 1.2kHz bandwidth.

On the ground the video signal is stored in a random access memory and displayed at the rate of 50 frames per second on any laboratory oscilloscope having a Z modulation input. The star brightness can be measured with a calibrated video amplitude discriminator. Background stars can be eliminated from the picture. The field of view is 100 x 100 minutes of arc. It can be magnified by 2 by telecommand in the star search phase.

FLIGHTS

P. Stettler's solar infra-red interferometer (1972) has been flown three times on this platform with the solar tracking system. Pointing errors never exceeded 1.5 minute of arc in the worst case. The gondola made three stellar flights with coarse attitude control only. Navach et al. (1973) took 50 spectra of hot stars with a prism-objective Schmidt camera. One flight failed because of a short-circuit in the scientific payload. Rigaud and Steiger (1973) studied the effect of ozone absorption in the near-UV spectrum of hot stars. They were able to measure the ozone thickness above the balloon at sunrise. The stellar tracking system and the TV camera were tested in flight for the first time in France, in October 1973; both performed well.

We would like to take this opportunity to thank CNES (France) and NCAR (USA) for their kind assistance and advice since the beginning of this program, in 1963.

REFERENCES

- Huguenin, D., 1973. Model AD-104 Amplifier-Discriminator for Single Photoelectron Counting. Geneva Obs. Publ.: 26p.
- Navach, C., Lehmann, M., Huguenin, D., 1973. Feasibility of UV Astronomy by Balloon-Borne Observations. Astron. and Astrophys. 22: 361-379.
- Rigaud, P., 1973. Mesure de la variation de l'ozone crépusculaire au moyen d'un photomètre stellaire embarqué à bord d'une nacelle stratosphérique. Thesis No. A.O.9045, Université de Paris VI.
- Stettler, P., Kneubühl, F., Muller, E., 1972. Absolute Measurement of the Solar Brightness in the Spectral Range 100 and 500 Microns. Astron. and Astrophys. 20: 309-312.

PAPER 4.2

A HIGH SENSITIVITY BALLOON-BORNE X-RAY
TELESCOPE SYSTEM

M. R. Pelling
Department of Physics
University of California, San Diego
La Jolla, California 92037

ABSTRACT

Despite remarkable advances in the field of low-energy X-ray astronomy during the past few years, the sky remains relatively unexplored in the high energy regime. This situation exists because of the fundamental limitations in performing extensive observations at the required sensitivity. Recent developments in the use of phoswich configured scintillation detectors now allow the attainment of collecting areas on the scale of 1000 cm^2 or more with optimal background and field of view characteristics. Such a system, now under construction at UCSD, will have 1350 cm^2 of sensitive area and allow photometric observations of roughly one order of magnitude improved sensitivity in the 15 to 150 keV energy range. For stronger sources, a modulation collimator may be utilized to obtain angular resolution in excess of .5 min of arc. To support these observations a gondola having an alt-azimuth gimbal with absolute pointing accuracy of 6 arc min and stability of .5 arc min is under development. Azimuthal stability is maintained through a reaction wheel which is referenced to the local magnetic field. Absolute pointing accuracy is obtained by readout of a stellar or solar azimuth sensor. All pointing and control decisions are performed in real-time using results of on-line processed gondola housekeeping data. In order to fully realize the potential of this system, stringent requirements must be imposed upon the balloon control and tracking systems.

INTRODUCTION

Progress in X-ray astronomy in the above 15 keV energy band which is accessible to balloon-borne instrumentation has lagged the lower energy field due to the generally inadequate sensitivity available for observations. The problem is further compounded by the inherent weak fluxes present at higher energies in many sources. High energy observations remain fundamentally important, though, in the study of cosmic X-ray sources since the physical characteristics of a given

15122 22791 22791

DISCUSSION SUMMARY — PAPER 4.1

In answer to a question about the type of circuitry used, the speaker described it as essentially CMOS technology except for the first two stages of the photon counters which used high speed analog circuits.

The scientific objectives were stellar photometry in the mid-UV and measurements of variations in the atmospheric ozone content at sunrise. Both types of measurements are made with a 15-centimeter Cassegrain with six channels between 2,000 and 3,000 angstroms.

source are seldom determined unambiguously by isolated low energy measurements. Other potentially fruitful areas of investigation which remain unexplored in the high-energy regime include spectroscopic and imaging measurements.

In this paper, we describe a new large area, high sensitivity X-ray telescope system suitable for photometric type observations from balloon altitudes. We also describe the balloon gondola system, its performance requirements and the overall performance requirements of the balloon/gondola support system.

HIGH SENSITIVITY BALLOON-BORNE X-RAY OBSERVATIONS

In general, high sensitivity can be defined as the ability to detect a weak source given sufficient integration time or the ability to measure features of a stronger source to some significance level given a limited integration time. For example, the source complex in the Perseus Cluster of galaxies is expected to be weak, though observable, at balloon X-ray energies (Ulmer *et al.*, 1973). Another example, Cyg X-1, may exhibit interesting variability features on sub-millisecond time scales which could only be observed at enhanced sensitivity (Rothschild *et al.*, 1973).

While the above examples represent specific observations, one may more generally evaluate the versatility of an observing system through consideration of its limiting sensitivity as follows. The third UHURU catalog lists 150 sources above the 3.0 counts per second detection level in the energy range 2 to 6 keV. This compilation represents a nearly complete survey of the sky at that sensitivity. Figure 1 indicates the integral number distribution of these sources as a function of source strength. Of these 150 UHURU sources about 20 have been observed in the greater than 15 keV balloon-accessible energy band (Peterson, 1973). Assuming that cosmic X-ray sources can be characterized in some sense by an average spectrum, one can use the relation in Figure 1 to estimate the number of sources observable at an enhanced sensitivity level. By this argument one might expect a total of 55 observable sources in the hard X-ray energy band if sensitivity improves by one order of magnitude. While this is a crude approximation at best, it does serve to indicate the diversity of new observational objectives that are possible with a high sensitivity balloon-borne telescope system.

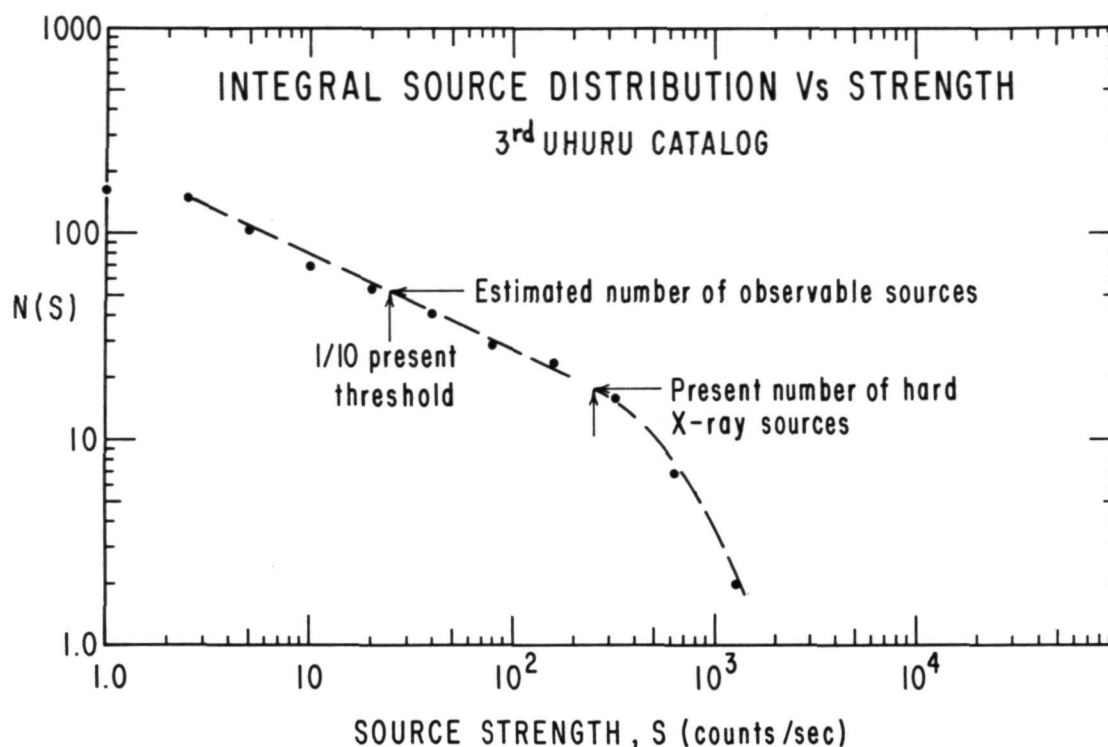


Figure 1. The 20 presently detected high energy X-ray sources have about a 75 percent correspondence to the strongest UHURU sources.

A LARGE AREA LOW BACKGROUND X-RAY TELESCOPE

The sensitivity of a detector system for an observation limited only by counting statistics can be expressed in terms of its specific background rate in the energy interval of interest B (in counts-cm⁻²-sec⁻¹), the effective collecting area, A , the observation time interval, $\Delta\tau$, and the inherent detection efficiency, η .

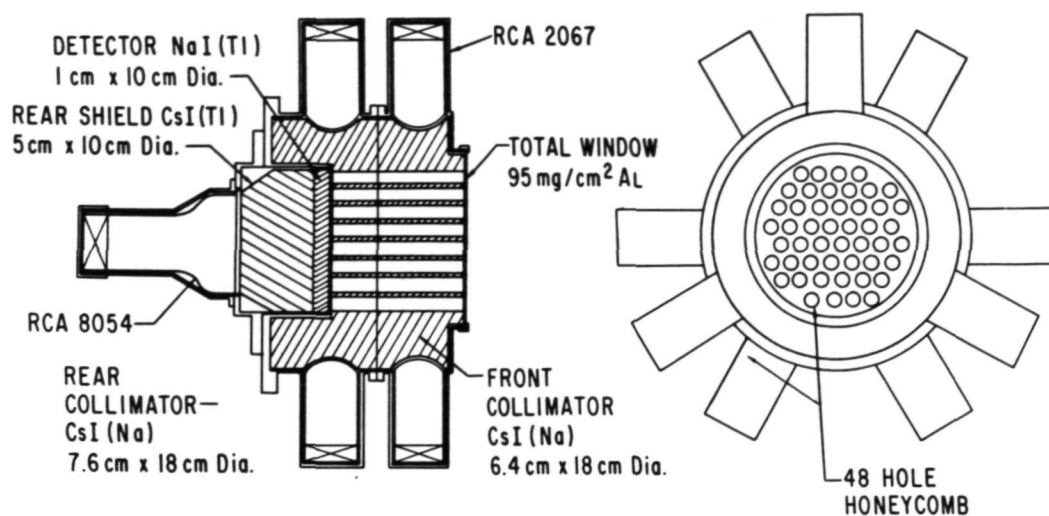
$$S = 1/\eta \sqrt{\frac{B}{A \cdot \Delta\tau}} \text{ counts-cm}^{-2}\text{-sec}^{-1}$$

The detection efficiency is in general a strong function of photon energy but can be taken as unity for observations using scintillator techniques in the 15 to 150 keV range. For attainment of enhanced sensitivity, one's choices are limited, then, to some combination of increased area and observation time or to lowering the specific background counting rate of the detection system. Actually, the choices are more restricted since the observation of time varying X-ray emitters may preclude arbitrarily long integration periods. An additional consideration,

often overlooked when applying the above sensitivity relation, is the implicit assumption that the system background is determined to an accuracy consistent with the limitation of counting statistics. An observation, in fact, consists of a background measurement as well as the integration period on the source. Since the instrument background is subject to a number of variational mechanisms one must design his observational technique to properly compensate for such effects. We will discuss these considerations in more detail later; however, for present purposes we adopt the somewhat arbitrary background integration period limit of one hour.

Thus, to improve detection sensitivity one is limited to either lowering the specific background or increasing the collection area of the detector. The first approach has been the objective of extensive studies at UCSD over the past few years. The culmination of these efforts is the honeycomb phoswich detector shown in Figure 2. The background properties of this configuration are analyzed at length by Matteson and Pelling, 1974. The basic concept of this system is that minimal background can be attained by completely surrounding the primary detection element with active absorbing shield material. In this configuration the forward and lateral shielding are provided by the honeycomb drilled CsI(Na) scintillators. Shielding from the rear is provided by pulse decay analysis of the CsI(Tl)/NaI(Tl) phosphor sandwich (phoswich) combination. Events having significant energy loss in the thicker shield portion of the phoswich are discriminated from desirable events originating in the primary detectors by their longer ($1.0 \mu s$ vs $.25 \mu s$) decay characteristic. The thick absorbing shield allows anti-coincidence of events in the primary detector which do not originate in the forward acceptance cone defined by the honeycomb collimator. For further discussions of the origin of such background effects see Peterson, 1967 and Dyer and Morfil, 1971. For this discussion, though, it is sufficient to note that the extent to which background can be lowered has definite practical limitations due to such factors as detection efficiency within certain regions of the shielding and ultimately the property of the detector crystals to become radioactive in the cosmic ray environment encountered under flight conditions. (Matteson and Pelling, 1974). These factors result in an effective background lower limit in the neighborhood of 5×10^{-4} counts-cm²-sec⁻¹-keV⁻¹ around 30 keV. The present configuration, shown also in Figure 2 consists of a large diameter 3.1 mm thick primary detector crystal CsI(Na) shielded from the rear by a thicker NaI(Tl) crystal. Lateral shielding is provided by a 3.8 mm layer of lead contained within the aluminum crystal housing. Collimation is obtained by modular arrays of tantalum slats of thickness .125 mm. The net field of view characteristics for the telescope is tailored to the specific observational objective by stacking these modules in various relative orientations. A single

ACTIVE HONEYCOMB DETECTOR



LARGE AREA PHOSWICH DETECTOR

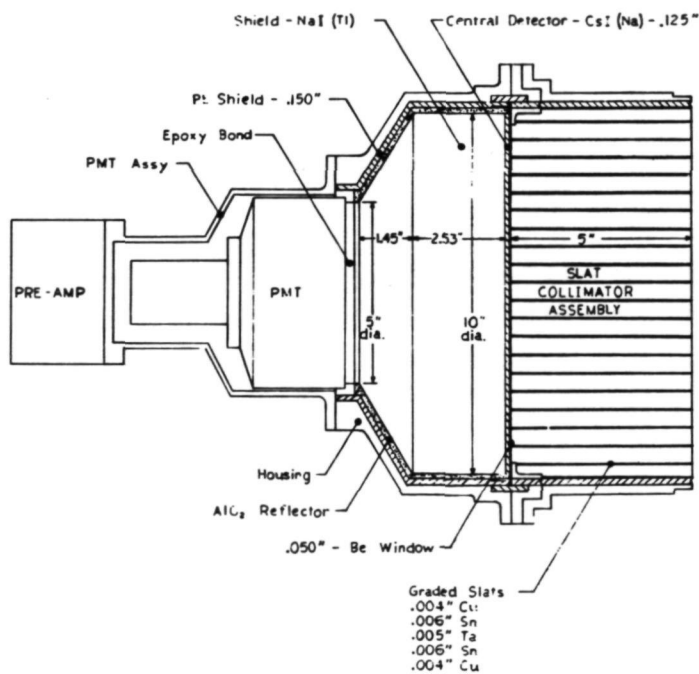


Figure 2. The new large area phoswich module and the detector which it replaces are shown on the same scale.

module has 12.5 cm high slats spaced at 1.25 cm intervals to produce a triangular response pattern along one dimension of slightly less than 6 degrees full width half maximum (FWHM). All housing and collimator surfaces which have direct exposure to the primary detector crystal are plated with successive layers of tin and copper having thicknesses, .1mm and .15 mm respectively. This "graded Z" layering suppresses the characteristic K escape radiation from the higher Z lead tantalum shielding resulting in reduced background in the 80 keV range as well as removal of complicating features in the background spectrum.

Comparing the present configuration with the honeycomb phoswich several significant differences can be noted. The honeycomb drilled CsI(Na) collimator is replaced by entirely passive material. This passive matter is a source of cosmic ray produced secondary background; however, the extent to which this effect lowers the net sensitivity is lessened since the relatively poor light collection efficiency of the honeycomb drilled crystal does not allow efficient background rejection. A second factor in favor of the new design is the improved area efficiency or fraction of the total primary detector collection area that is exposed to a source. Looking at the relation for overall sensitivity, we see that this factor effectively enters twice, once in the useful collecting area and second in the specific background, resulting in the sensitivity varying inversely as the first power rather than the square root of the area efficiency. The new system has an area efficiency in excess of 90% compared to the old system's value of less than 50%. Thus, the use of passive collimation results in increased production background but improved area efficiency offsets this effect and is expected to result in only a small net change in sensitivity.

A second major difference to be seen when comparing the two systems is the reversed role of the phoswich scintillators. The large shield crystal is now NaI(Tl) which is significantly less expensive relative to CsI. Also, the pulse shape discrimination process now accepts the slower CsI pulses, automatically rejecting photomultiplier noise at low energies and possible spurious fast pulses associated with particle interactions in the crystal surface (Cranell, 1972, Matteson, 1971). In the balance the new detector system is at least as sensitive per unit root detector area than the older honeycomb phoswich while being significantly less complicated and expensive. Table 1 compares the overall characteristics of the two configurations. The complete new system will be modular, employing three of the large phoswich modules for a net collecting area of 1350 cm². This system will be roughly one order of magnitude more sensitive than the one which it replaces.

COMPARISON OF DETECTOR PROPERTIES

	Honeycomb Phoswich	New Detector (3 Modules)
Collecting Area	34 cm ²	1350 cm ²
Background Flux at 3.0 gm-cm ² residual depth (counts/cm ² -sec-keV)	8x10 ⁻⁴ at 30 keV 1.5x10 ⁻⁴ at 100 keV	5x10 ⁻⁴ at 30 keV 5x10 ⁻⁴ at 100 keV
Field of View	6° FWHM (Circular)	3°x6° (Rectangular)
Weight	27 kg	50 kg
Envelope	30cm dia x 37cm length	33cm dia x 66cm length

Table 1.

THE POINTING AND CONTROL SYSTEM

The modular detector array weighing roughly 400 lbs is carried in the gondola shown in Figure 3. Pointing control is obtained through an elevation-azimuth gimbal system with the upper suspension support providing the azimuth pivot (gondola rotor) and telescope elevation being controlled by a simple horizontal axis pivot driven by a lead screw.

Under normal flight conditions the telescope azimuth is maintained by torquing against a reaction wheel located in the lower part of the gondola with the upper suspension pivot acting as a free bearing. The wheel has a mass of 25 kg on a radius of .5 m and is driven by DC torque motor having a maximum output of 1.28 kg-m²-sec⁻² and a maximum speed in the neighborhood of 600 rpm. Under the assumption that the most significant external torque operating on the gondola is the bearing friction of the upper suspension rotor, the system can operate for more than 30 minutes before the reaction wheel reaches the saturation point. If the wheel should attain this saturation speed, circuitry within the gondola will switch the azimuth control to a DC torque motor located within the gondola rotor while simultaneously causing the reaction wheel to despin. Thus, the angular momentum accumulated and stored within the reaction wheel is unloaded via azimuth rotor coupling through the suspension to the balloon. These control operations can also be initiated by ground command should observational conditions demand.

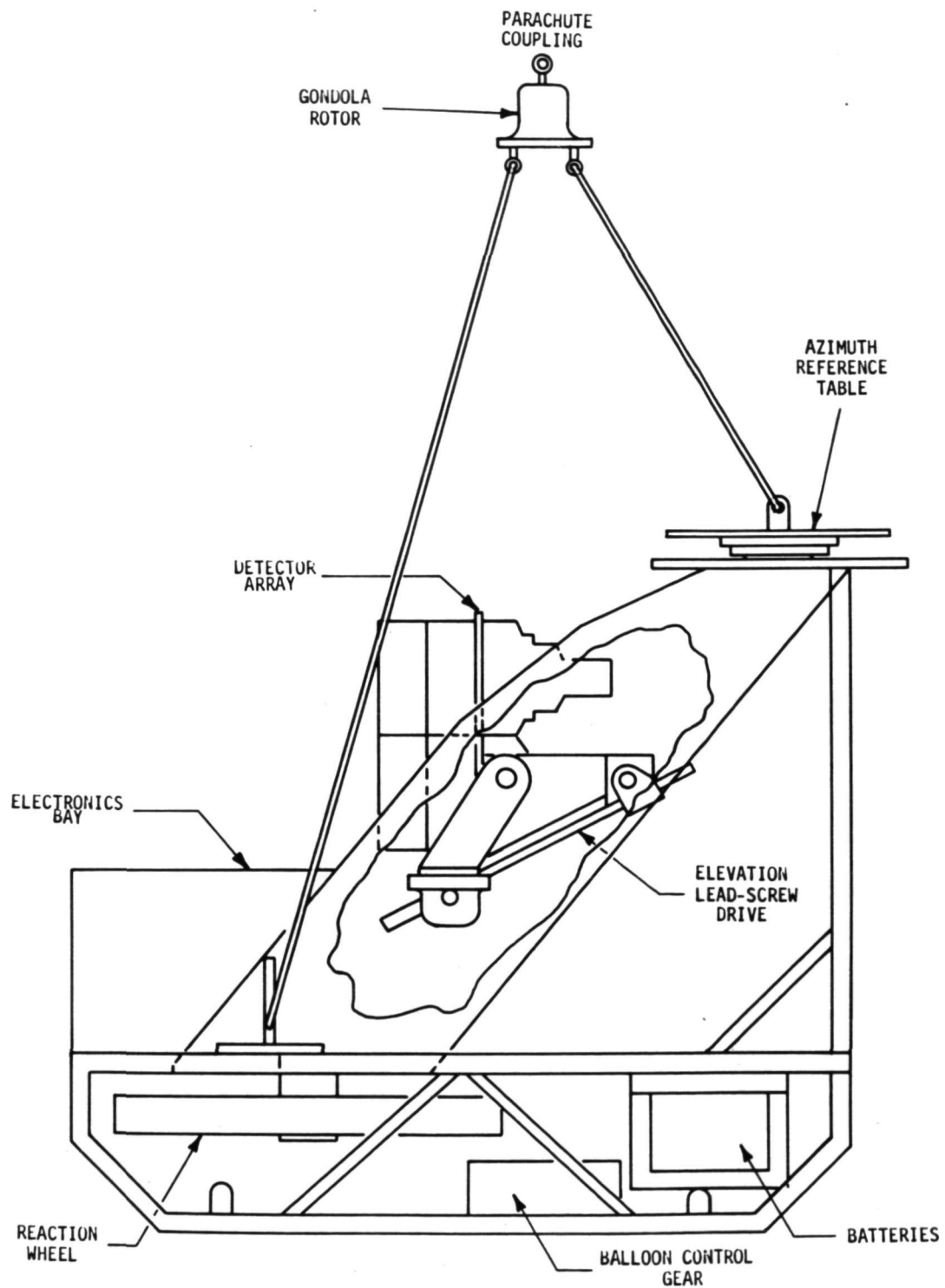


Figure 3. Side view of the gondola. The height of the apparatus to the parachute coupling is approximately 12 ft.

The azimuth servo uses a null sensing reference magnetometer to maintain a given azimuth angle. Absolute pointing accuracy is maintained by periodic update of the magnetometer null angle through use of a solar sensor for day or star sensor for night operation. Additional aspect information is obtained at night by continuous photography of the star field. All azimuth control and readout apparatus including the magnetometer, the stellar and solar sensors, and the aspect camera are fixed relative to one another on the azimuth reference table. This platform maintains its orientation relative to the local magnetic field independent of the gondola azimuth orientation. The actual azimuth angle is then determined by the position of the reference table relative to the lower portion of the gondola. In Figure 4 the mechanics of this scheme is indicated by showing the top view of three possible gondola orientations as they might occur in flight. The major advantage of this arrangement is that for night operations the star field moves slowly relative to the local aspect reference and readout apparatus. Indeed, if Polaris is used as an azimuth reference, its position changes less than 10 degrees throughout a typical flight.

The positioning of the azimuth reference table and the elevation gimbal is maintained via a command transmitted reference to 14 and 12 bit digital shaft encoders respectively. This allows positioning accuracy of 1.3 arc minutes commensurate with operational requirements. A command controlled variable speed clocking system will eventually be incorporated to allow tracking of object sources.

In Figure 5 we show additional details of the mechanisms of the gondola. Components requiring precise orientation, the reaction wheel, the telescope gimbal and the azimuth reference table, are contained within a single rigid structure which is suspended via the three cables from the gondola rotor. Other systems such as the control electronics and data systems, the batteries, and balloon control gear are mounted within lighter peripheral structure which may easily be repaired if damage is sustained on descent or landing.

OPERATIONAL REQUIREMENTS

A high sensitivity X-ray observation may, depending upon the specific objective, may impose variously stringent requirements on the performance of the gondola and balloon support systems. As an example, when attempting to observe a weak source, the major problem becomes the determination of background within limits defined by the statistical precision possible with the system. In the case of the system described here, the observation of a source to an accuracy determined by counting statistics in one hour of observation time requires determination of the average background within the observation time interval to a precision of

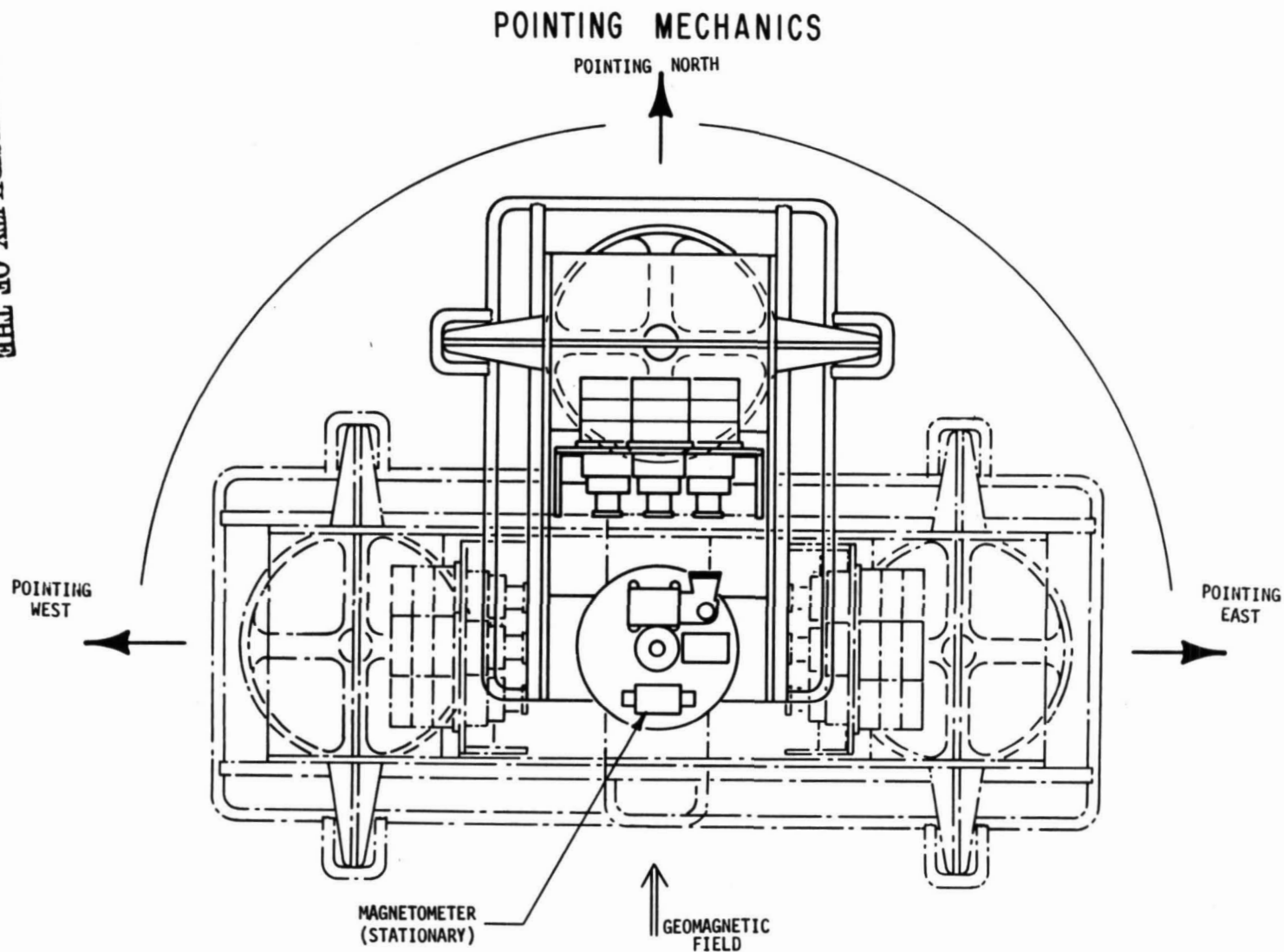


Figure 4. Top view of the gondola. The gondola may be thought of as rotating under the azimuth reference table.

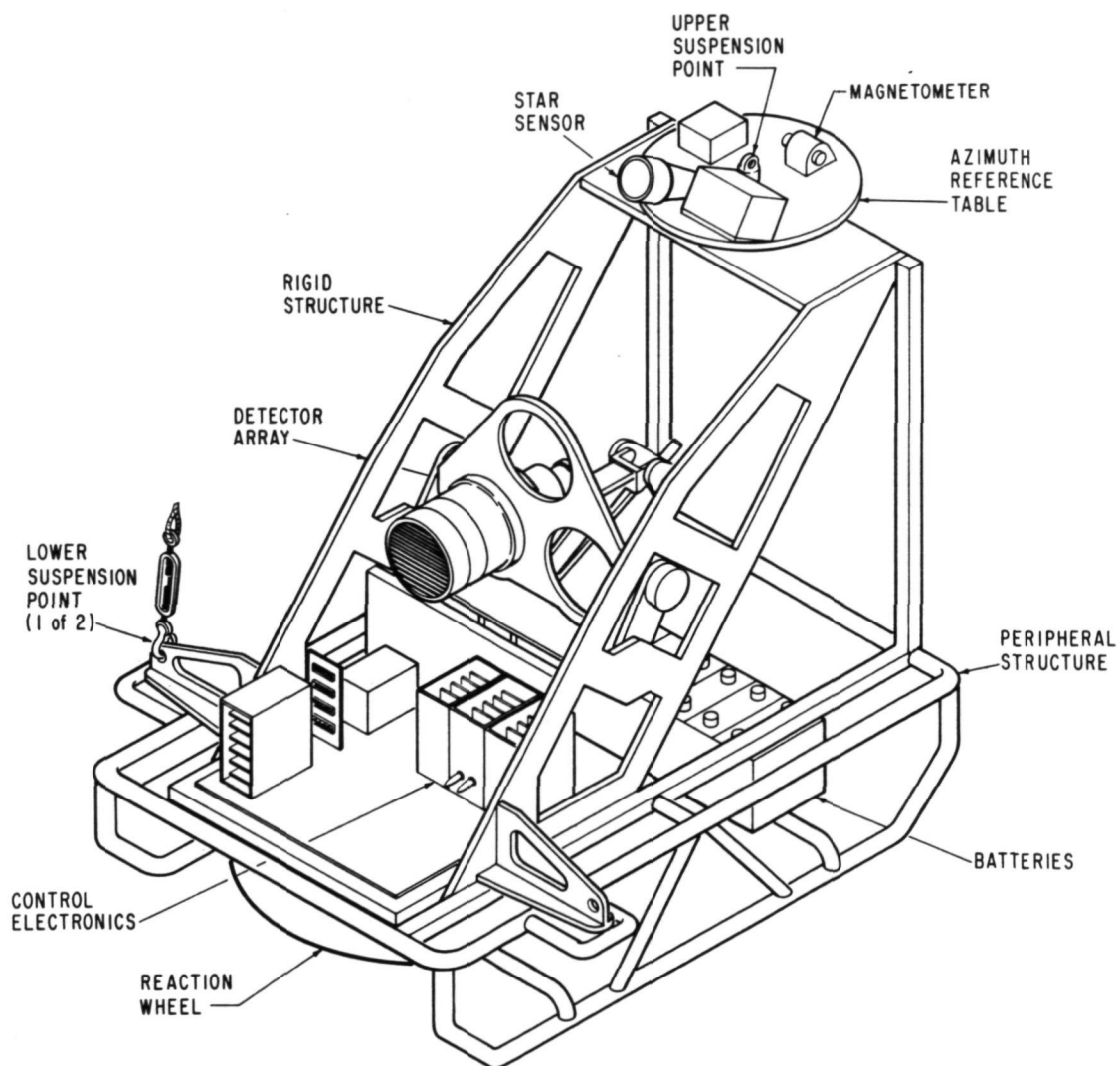


Figure 5. Perspective view of the gondola. The upper suspension pivot is omitted for clarity.

.3 percent. Assuming that one obtains the background measurement by means of a simple scan offset procedure the true background of the detector system must be constant or at least determined throughout the "miniscan" time interval, which might be a few minutes. Background variations significant on these scales may be caused by altitude fluctuations as small as 50 m. This, then, gives rise to a requirement for altitude stability or at least determination precision on this order.

As a second example, one can consider a high precision measurement of spectral variability. The spectral slope of Cyg X-1, for example, can be measured to an accuracy of 5 percent in 2 minutes using the new system. An altitude variation of only 250 m. occurring within the same period could easily mask or simulate such an observation by changing the opacity characteristics of the residual overlying atmosphere.

Finally, we consider the measurement of variability as an objective. In this case the limiting performance characteristics become the aspect control and readout systems. For example, for a source whose nominal strength is equal to the background a .3% variation in apparent intensity will result from an aspect error of only 1.2 arc min if the telescope has a FWHM of 6 degrees. This, then, imposes a requirement for aspect accuracy of this order on the overall system. The aspect requirement translates directly into a requirement for balloon tracking precision of about 1.5 km throughout the duration of the observation. In Table 2 we summarize these general requirements on the performance of balloon and gondola systems.

OPERATIONAL REQUIREMENTS SUMMARY

Gondola Pointing Accuracy	6 arc min
Gondola Pointing Stability	.5 arc min
Gondola Stability Rate	.1 arc min/sec
Balloon Tracking Accuracy	1.5 km
Balloon Float Altitude	39 to 45 km*
Balloon Altitude Stability or Determination	50 to 250 m*
Balloon Float Duration	4 to 16 hours*

* Depending on Observational Objectives

Table 2.

Clearly, as devices of the complexity discussed here are developed, the use of automated data processing systems becomes desirable if not mandatory. The high sensitivity X-ray telescope discussed here will require real-time processing of housekeeping, aspect and in some cases scientific data of its full capabilities are to be realized. Initial flight operations will require only minimal real-time command control of temperature control, power, and aspect systems. Future operations, especially those in which continuous tracking of object sources is performed will require more extensive computer support, eventually tying such systems directly into the command control system.

REFERENCES

- Crannell, C., 1972. "Interim Report on the CsI Detector for Experiment ACR-6 on HEAO-A". Report (GSFC)
- Dyer, C.S. and Morfill, G.E., 1971. *Astrophys. and Space Sci.*, 14, 243.
- Giacconi, R., Murray, S., Gursky, H., Kellogg, E., Schrier, E., Matilsky, T., Koch, D., Tananbaum, H., 1973. The UHURU Catalog of X-ray Sources. ASE-3249, Preprint, American Science & Engineering.
- Matteson, J.L., 1971. "An X-ray Survey of the Cygnus Region in the 20 to 300 keV Energy Range". PhD Thesis, UCSD (Unpublished).
- Matteson, J.L., and Pelling, R.M., 1974. "Design and Performance of a Phoswich System for X-Ray Astronomy". UCSD, In preparation.
- Peterson, L.E., 1967. "Gamma-Ray Production by Cosmic Rays Observed on OSO-I". UCSD-SP-68-1.
- Peterson, L.E., 1973. "Hard Cosmic X-Ray Sources". *Proc. of IAU Symp. No. 55*, Madrid, May, 1972.
- Rothschild, Bolt, Holt and Serlemitsos, 1973. *B.A.A.S.* 5, 473.
- Ulmer, M.P., Baity, W.A., Wheaton, W.A., and Peterson, L.E., 1973 *Ap. J.*, 183, 15.

DISCUSSION SUMMARY — PAPER 4.2

Several questions arose in regard to the pointing system. These and the answers by the speaker are summarized below:

- Q. Do you generate your altitude-azimuth corrections on the ground?
- A. Yes.
- Q. How many commands do you give to keep pointed to one arcminute.
- A. The requirement is six arcminutes. Two digital commands per pointing operation are required. Eventually, within about a year an onboard tracking capability is intended.
- Q. What will be the error in pointing due to pendulum motion?
- A. In a previous performance of the system (in which a reaction wheel was not being used for stabilization) the pendulum motion was less than 0.1 degree. A group from the University of Tokyo used a spheroscopic device to establish that pendulum motion on some of their systems was below an arcminute. The effect on the present system is not yet known and may necessitate a cross-elevation axis.

It was noted that measurements on a gondola of similar size and inertial properties had pendulum motions of two or three arcminutes. The speaker commented that the stability is a strong function of the gain in the system and what you are pointing at.

In a discussion of the X-ray device, the speaker noted that he expected his value of B in the expression for sensitivity

$$S = \frac{1}{\eta} \sqrt{\frac{B}{A\Delta T}} \quad (\text{uncorrected for air absorption})$$

to be lower than on previous flights, particularly at the lowest energies. Tests show that their detector's spectral response is flat relative to the honeycomb detector, so that at lowest energies its sensitivity is lower than other systems. At highest energies, it is higher. The modulation collimator is to be used on the next flight and is the reason for the high stability pointing requirement. The field is five degrees but the highest sensitivity would detect fluctuations below one percent.

PAPER 4.3

BALLOON-BORNE ULTRAVIOLET STELLAR SPECTROMETER:
ACQUISITION, TRACKING AND COMMAND SYSTEMSW. C. Gibson
Lockheed Electronics Company Incorporated

ABSTRACT

The NASA Balloon-borne Ultraviolet Stellar Spectrometer (BUSS) is carried to an altitude of 40 km by a 15 million cubic foot ($4.25 \times 10^5 \text{ M}^3$) balloon for night-time observations of ultraviolet stellar spectra. The BUSS optical system, comprising an 0.40 m aperture Cassegrain telescope and an Ebert-Fastie spectrometer, points at various selected stars and focuses a portion of their spectra on the photocathode of an image dissector tube. The spectral region between 2,775 Å and 2,825 Å is sampled by the detector at 0.25 Å increments using photon counting techniques.

The pointing system for the payload uses a pair of orthogonal magnetometers which sense the earth's magnetic field for an azimuth reference, and a platform potentiometer for an elevation reference. This pointing system places the target star within the 3×1 degree field of view of an "outer" optical star tracker. The outer star tracker is then used to point the entire instrument to within one arc minute of the target star. Finally, an "inner" optical star tracker located near the focal plane of the telescope is used to tilt the secondary mirror sufficiently to bring the star image to within three arc seconds rms of the telescope's optical axis. The acquisition and tracking systems will be discussed as well as the design philosophy behind these systems and the p.c.m. digital command system. Actual performance figures from the June and October 1971 flights will be presented.

Since the development of reliable polyethylene balloons, astronomers have had available to them, at a moderate cost, a vehicle capable of carrying payloads of several hundred kilograms to altitudes from which observations could be made at wavelengths inaccessible to the groundbased observer. To the designer of such an airborne observatory, the problems associated with the pointing and stabilization of telescopes and detectors are formidable. Since each new experiment requires a unique set of pointing specifications, there is little standardization in either the design techniques or the hardware.

The performance requirements for the Balloon-borne Ultraviolet Stellar Spectrometer (BUSS) called for a balloon payload capable of acquiring and tracking at least five 5th magnitude stars during a night flight and recording their spectra in the range 2775-2825 Å with $1/2$ Å resolution and with at least 10% counting statistics in each wavelength resolution element. Real time spectrometer data readout was also required to provide for increased flexibility in the observing program. An additional requirement was to have complete groundbased control of the pointing system and spectrometer to allow freedom of target selection at any time during the balloon flight. Due to physical size and environment

dynamics, a multistage pointing concept was used. Detailed servo design information has been described by Gibson, et al (1972). The resulting hardware has been flown three times with successful results and, in general, all the design parameters and experiment requirements were met. The scientific results obtained from these flights have been reported by Kondo, et al (1972).

The payload is divided into two basic sections. The upper section is referred to as the pointed section and the lower section as the gondola (see Figure 1). The two sections are connected by a semi-rigid support shaft called the azimuth shaft, the upper end of which is connected to the balloon suspension train. The pointed section is mounted to the azimuth shaft by means of anti-friction load bearings. This section contains all the servo electronics, the PCM encoder, and serves as the experiment mount. The experiment is mounted in a cantilever fashion to a large flange on the end of a horizontal shaft/yoke fixture which is referred to as the elevation shaft. There is unlimited rotational freedom around the azimuth axis and 70 degrees around the elevation axis. The pointed section has attached to it a protective roll cage structure that prevents damage to it and the experiment in the event that the payload should turn over on landing. This structure also provides a means of mounting the magnetometer sensor block. The "roll cage" structure was fabricated from thin walled aluminum tubing and welded together in easily assembled sections. Electrical connections made from the gondola section to the pointed section are through a 14-segment brush and slip ring assembly. The gondola supplies power and pre-decoded command signals through the slip ring assembly and the pointed section supplies the PCM encoder output through the slip ring assembly to the RF transmitter located in the gondola.

The gondola section also serves as a reaction mass for the pointed section as well as the mounting area for the battery supply, command RF receiver and pre-decoder, RF telemetry transmitter, power control command circuitry, and balloon launch facility flight gear. In addition, a single centrally located ballast hopper and valve are mounted on the gondola. The ballast hopper is positioned directly in line with a vertical axis through the center of mass of the entire payload. This location reduces to negligible proportions the effect of induced forcing functions on the servo during ballasting operations required for balloon control.

The gondola is a truss structure fabricated from aluminum angle to reduce the cost of repair and refurbishment. Field damage is easily repairable since the damaged piece can simply be replaced with another which is cut and formed using common hand tools. The mass of the telescope, spectrometer, and associated equipment run about 91 kg, and the roll cage, about 58 kg. The mass of the entire pointed section, including all electronics, mechanical pointer structure, star trackers, and counterweights, is roughly 244 kg. The gondola, with batteries and NCAR equipment, has a mass of about 210 kg. To this is added whatever ballast is required by NCAR for flight operations.

Pointing is controlled in three separate stages. The first system, referred to as coarse acquisition, was designed to acquire the target to within the field of view of an "outer" star tracker by referencing to the horizontal component of the earth's magnetic field for an azimuth reference and to local horizontal via a potentiometer for an elevation reference. The second stage of pointing, referred to as the platform tracker loop, is

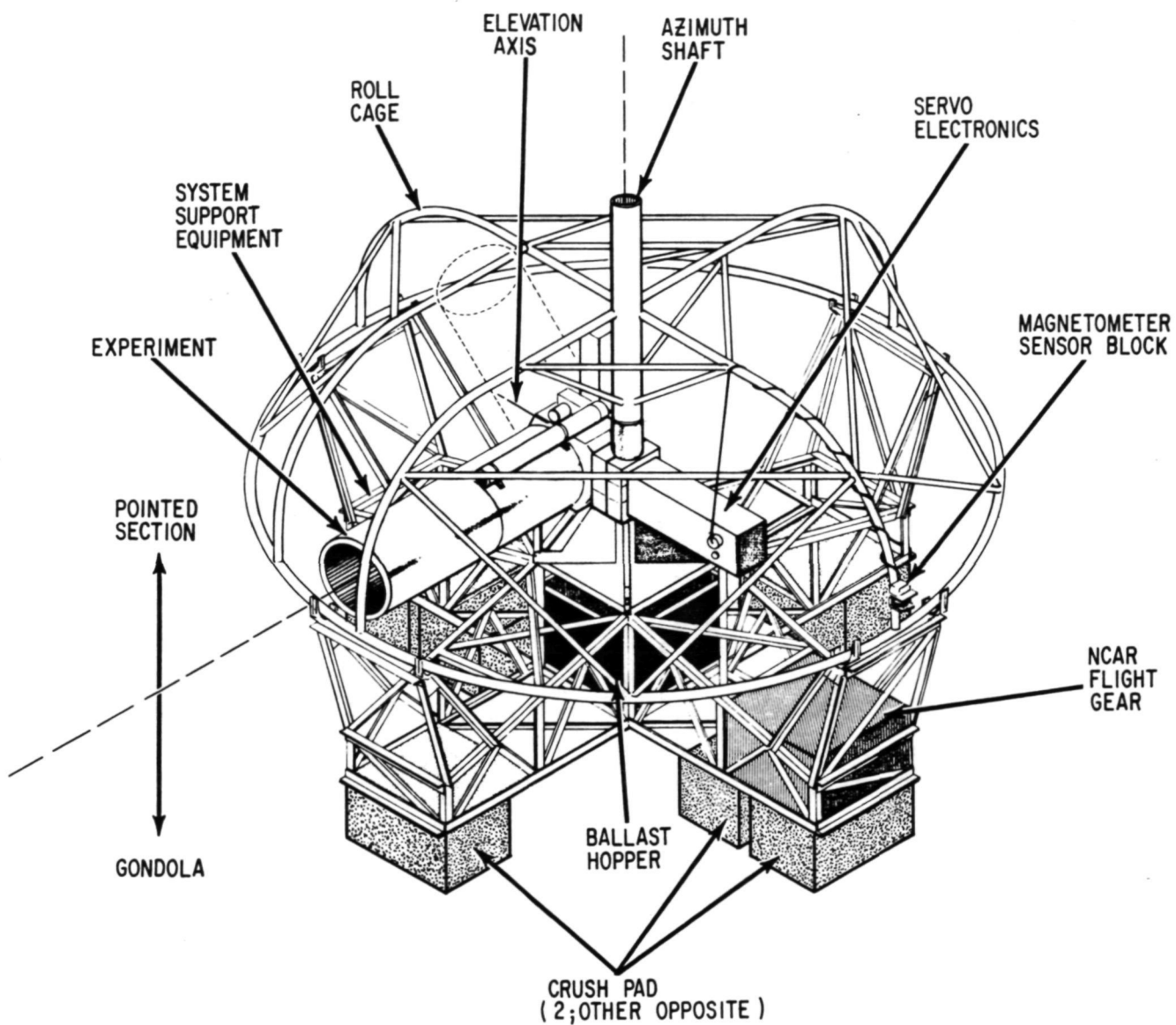


Figure 1. BUSS Payload configuration.

controlled by the outer star tracker, which has a ± 1.5 degree field of view in azimuth and a ± 0.5 degree elevation. The tracker is bore-sighted to the optical axis of the telescope and will drive the control system to a null angle that is within 1-arc minute of the optical axis of the telescope. The third stage, called the inner loop, achieves very fine pointing with an "inner" star tracker located approximately at the focal plane of the telescope. Signals from this star tracker are used to drive two d-c torquers to tilt the secondary mirror about two orthogonal axes so that the off-axis star image is stabilized to within about 3-arc seconds rms of the optical axis. The ultimate accuracy of this loop is limited by the star tracker noise, which is itself a function of star brightness, and the velocity error constant of the control loop. Pointing commands and other operational mode commands are telemetered from the ground through a serial digital PCM command system.

The magnetometer selected for use on the outer acquisition loop is a Heliflux MND-52C-300NB, manufactured by the Schonstedt Instrument Company. The elevation potentiometer is a precision resistive film, one-turn type, manufactured by the Computer Instrument Corporation. As prime movers for both the azimuth and elevation axes, Inland Motor Company T-4036 d-c torquers were selected. The outer loop star tracker was designed and built by Ball Brothers. It was designed to track the brightest star in its field of view below the level set in the remotely set magnitude discriminator circuit.

The outer-loop azimuth control system is mechanized to stow the experiment platform to a potentiometer null referenced to the azimuth shaft. The stow drive is rate limited to approximately five to seven degrees per second. A balloon rotation of 1.0 degree per second can be easily handled in stow; however, acquisition time is increased.

A block diagram of the azimuth loop is shown in Figure 2. Azimuth acquisition of the three-degree target field is accomplished by commanding the experiment platform relative to the local north-south earth magnetic field line. Two horizontal orthogonal magnetometers are used to provide azimuth reference from magnetic north. The magnetometer control loop has a bandwidth of about 0.3 Hz and points the experiment to a stable null provided by the ground commanded angle and the sensed magnetometer angle. The servo loop is proportional plus "limited" integral, thus, no servo loop pointing error is evident for nominal friction torques of 1.7 lb-in. (.197NM). The integral term is limited to prevent poor performance during acquisition.

A target field 180 degrees away from magnetic north can be acquired in about 40 seconds. For the 180 degrees acquisition, rates of 20 degrees per second will occur. This high rate is produced because the rate limiting circuit does not prevent rate build up on the unstable null side during acquisition. For acquisitions of 90 degrees or less, the rate limit is about five to six degrees per second. Acquiring the target star 90 arc-minutes away from Star Tracker null takes approximately seven seconds.

The azimuth acquisition principle is based on generating the trigonometric identity:

$$\cos \psi_A \sin \psi_T - \sin \psi_A \cos \psi_T = \sin (\psi_T - \psi_A)$$

where

ψ_A = magnetometer angle from magnetic north

ψ_T = target angle from magnetic north

(ψ_T is the commanded angle)

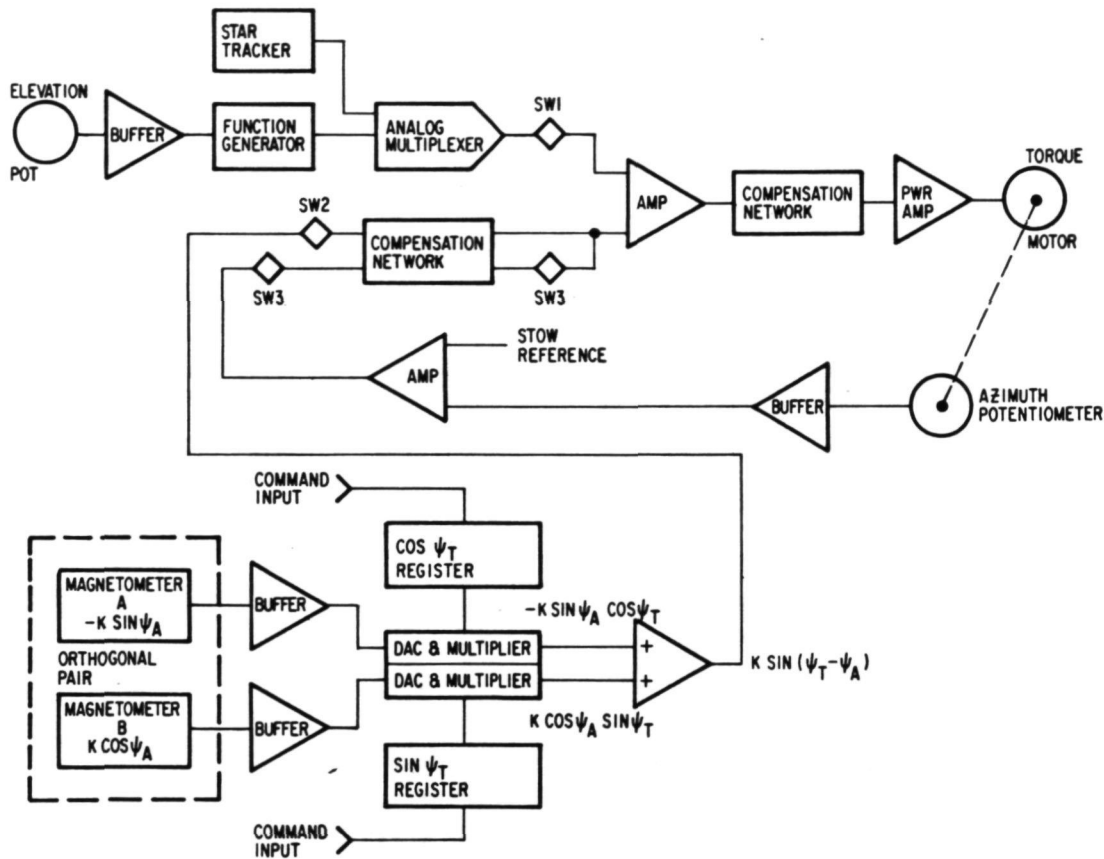


Figure 2. BUSS Azimuth Servo Block Diagram

The azimuth Star Tracker signal is scaled in an analog multiplier by a scaler that is proportional to the elevation angle of the target. The scaling factor is:

$$S_F = K \sec \theta$$

where θ = angle above horizontal.

Scaling is necessary to maintain a reasonably constant servo gain, or otherwise, the effective gain of the azimuth servo will fall off as a function of the cosine of the elevation angle. Scaling of this nature will permit reliable operation up to at least a 70 degree elevation angle.

The outer loop azimuth Star Tracker control system also uses a proportional plus limited integral technique. The "steady-state" pointing error is zero considering the friction torque effects and the integrator action. The azimuth Star Tracker loop has a bandwidth of roughly 0.5 Hz. Transient effects of direction changes for kinetic friction torque and signal noise from tracking targets of 0 to +5 visual magnitude result in less than 0.4 arc-minutes of experiment pointing error. Control bandwidth for this loop which is determined by loop gain and the compensation lead terms must be compromised with torque motor noise output. Battery stored electrical power is consumed proportional to motor noise. The resultant azimuth pointing accuracy is nominally less than 1.0 arc-minute.

A block diagram of the outer loop elevation control is shown in Figure 3.

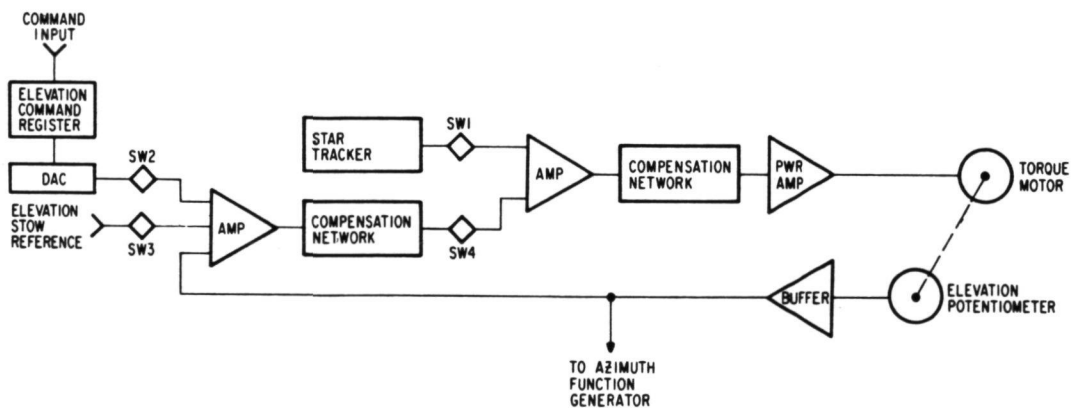


Figure 3. BUSS Elevation Servo Block Diagram

Elevation control was designed to stow the experiment section and point the experiment to a 1.0-degree target field referenced to a potentiometer null. Potentiometer null was set normal to the azimuth shaft. The elevation servo was designed to handle an azimuth shaft oscillation at the simple pendulum frequency with an amplitude of plus and minus 1/3 of a degree. As in the azimuth control loops the elevation control is proportional plus limited integral. The limited integral "washes out" pointing errors in acquisition and track that result from the 1.27 lb-in. (0.144NM) kinetic friction torque

and a maximum 3.0 lb-in. (0.34NM) torque of mass unbalance around the elevation axis. The elevation acquisition of a target field is rate limited at approximately eight degrees per second; thus, acquisition of a target field 70 degrees from start will require about ten seconds. Acquisition of the target star to within the 1.0 degree field of view will be less than eight seconds. Elevation tracker loop bandwidth is about 1.4 Hz. Again, the bandwidth is reduced to decrease torque motor power consumption while tracking the noisy signal from dim targets. Another reason for keeping bandwidth low was to reduce error rate inputs to the experiment section secondary mirror control system. The transient pointing errors in the elevation axis while tracking stars of 0 to +5 visual magnitude are less than 1.0 arc-minute.

Azimuth acquisition of the target star relies upon knowledge of (a) payload geographical position, (b) target ephemeris data, and (c) knowledge of the direction of the horizontal component of the earth's magnetic field. A computer program, derived from data supplied by the National Oceanographic and Atmospheric Association (NOAA), provided the means for determining the direction of the horizontal component of the earth's magnetic field to less than 0.5 degree. Use of the OMEGA system at the NCAR balloon facility in Palestine, Texas, produced geographical coordinates allowing for position determination to less than five miles. However, payload geographical position need only be known to approximately ten miles. Elevation acquisition of the target relies only upon knowing the geographical position of the payload and target ephemeris data. These data, when referenced to payload local vertical, provide the information needed to program a precision potentiometer in the elevation servo loop.

The graphs in Figure 4 are plots of the outer loop Star Tracker pointing error versus time. These data are taken from Flight 2 and are typical of inflight performance. Graphs A and B show initial Star Tracker acquisition in azimuth and elevation respectively. Note the moderately light damping used to permit sufficient gain to be used while pointing on target. Graphs C and D are again respectively azimuth and elevation Star Tracker pointing error versus time after acquisition stabilization. The predominant error appears at about a 0.6 Hz rate. The forcing function for the error input has as yet not been specifically identified. However, there is evidence to indicate a torsional oscillation of the 10-foot long section of the three-cable suspension train. Graphs E and F are examples of the worst case-pointing that occurred for relatively short time periods. The predominant motion is in azimuth and is probably a result of torsional suspension line energy coupling into the servo. This is being evaluated and will be corrected.

Once the outer loop controls have done their jobs and the stellar image is stabilized to within one arc minute of the outer loop tracker's null axis, the "inner loop" star tracker is activated. Telemetry signals from the inner loop tracker verify that the star tracker sees the target star and also give an indication of the apparent brightness of the star. There is no magnitude discriminator circuit in the inner loop tracker. The inner loop control system is an integral plus proportional, d.c. type 1 loop. Error signals from the tracker are processed by the compensation networks, amplified by the CTC model 916 100 watt servo amplifiers and applied to two d.c. torques to tilt the telescope's secondary mirror sufficiently to bring the star image to within approximately 3 arc seconds rms of the tracker's null axis.

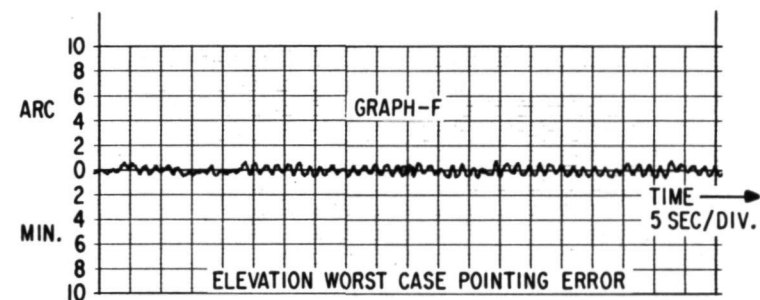
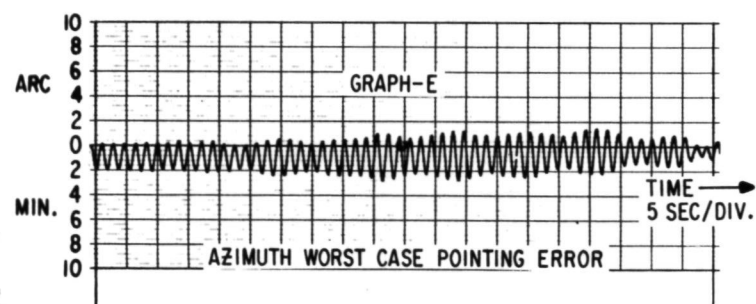
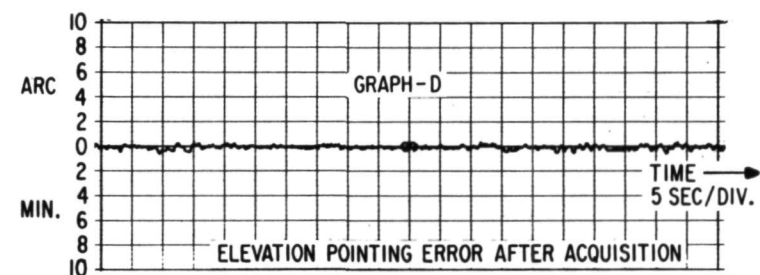
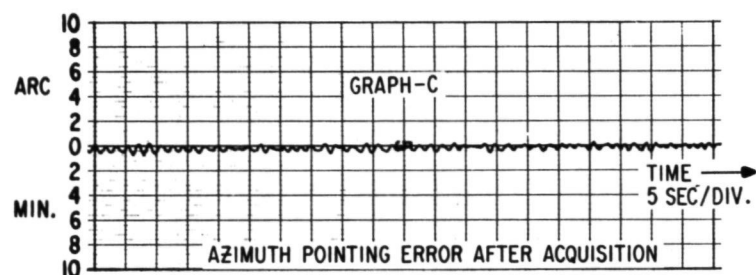
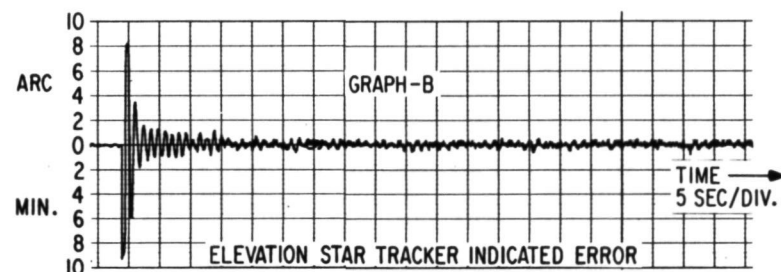
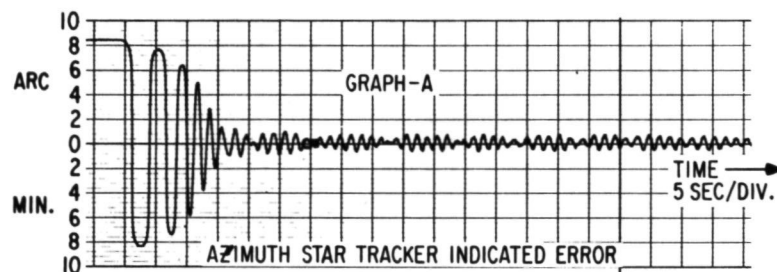


Figure 4. Star Tracker pointing error data.

For the first two flights of the BUSS payload, an EMR 569B-M1 optical star tracker was used for the inner loop. During both flights there were irregularities with the performance of the sensor so that for the third flight a new star tracker was procured from Ball Brothers. The new tracker is in most ways a duplicate of the original outer loop tracker. The reader is directed to reference 1. (Gibson, et al, 1972) for a detailed discussion of the outer and inner loop control systems.

A block diagram of the BUSS command system is shown in Figure 5.

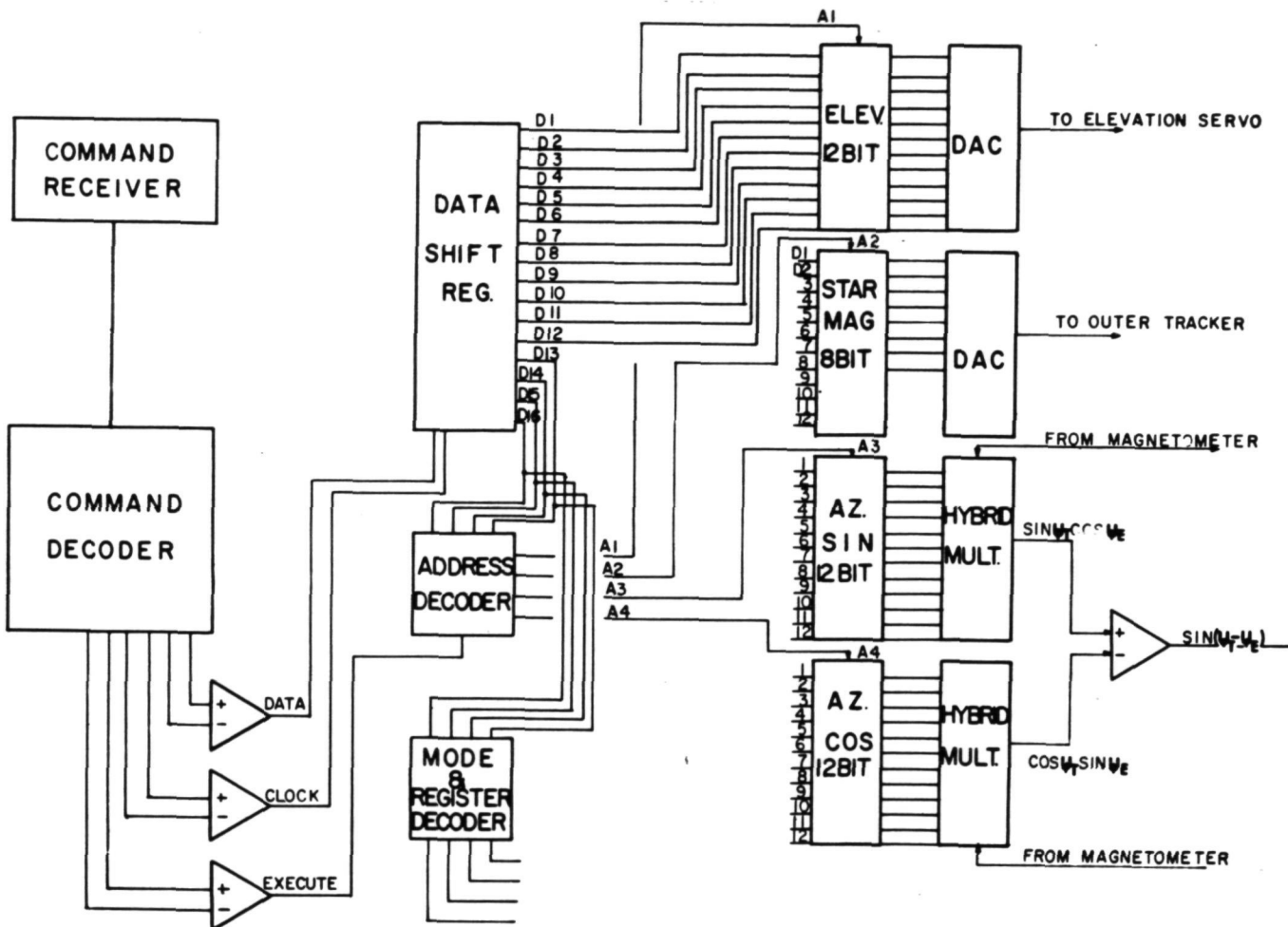


Figure 5. BUSS Command System Block Diagram

The command system is a serial digital p.c.m. type. The decoder section has been recently redesigned because of a failure during the third flight. Commands are encoded on the ground by simply setting the positions of sixteen single pole double throw toggle switches to correspond to the states of the bits of the command word. The digital word thus derived is serialized and used to deviate a voltage controlled oscillator which in turn deviates a 430 MHz FM carrier for transmission to the payload. Each command word actually contains 23 bits. The six least significant bits form a fixed recognition pattern. The seventh bit is a sign flag to inform the airborne decoder whether the command word is an information or discrete type command. Discrete

commands are used for relay closures and other latching functions such as main payload power on and off.

In the ground station command encoder discrete commands are encoded by use of a two digit thumbwheel switch. This switch in turn produces a two decade BCD code corresponding to the decimal value set on the thumbwheel switch. If the thumbwheel is set to any number other than 32 the sixteen discrete switches on the front panel of the encoder have essentially no effect on the command, and the "tag bit" is encoded as a logic zero.

The video signal originating from the airborne command receiver, is routed to a pair of notch filters in the command decoder. These filters function as subcarrier discriminators and reconstruct the digital bit stream as encoded on the ground. The bit stream is then located in one of two twenty-three bit shift registers. The command decoder is designed to require that each command be received twice and that the two commands be identical before it is acted upon. As the second command is received the first command is shifted to a second shift register and the new command is then stored in the location just vacated. Magnitude comparator circuits then decide if the two commands are identical. If the two commands are identical, a routine is executed to multiplex the 16 bit word and transmit it through a line driver to the pointed section of the payload where it is executed. If the command is a discrete type it will trigger a 28 volt, 500 ms pulse, on one of sixteen possible circuits depending on the position of the thumbwheel switch mentioned above.

To turn main battery power on to the payload a separate battery power controller is used. The controller accepts the 28 volts, 500 ms pulse from the command decoder and employs it to trip a one shot multivibrator which in turn sets a J-K flip flop. The output of the flip flop is connected to a hybrid interface gate (Sprague UHP-503). When active, this circuit sinks enough base current from a PNP silicon darlington to saturate the transistor. In the saturated state, the 2N6050 acts as a switch between the payload's silver zinc batteries and the pointed section of the payload.

The author wishes to acknowledge the excellent work done on the BUSS project by the personnel of Ball Brothers Research Corporation. Specifically, Mr. Don Guthals and Mr. Art Ray are to be commended. Other BBRC employees who should be mentioned are Messrs. Jim Jensen, Joe Eccheer and Dave Wartburg.

Employees of Lockheed Electronics, Aerospace Systems Division, who deserve recognition for their years of support to the BUSS field activity are Messrs. R. D. Welch, Glen Teasley, Harvey Vordenbaum and Curtis Wells. It goes without saying that thanks and recognition are due to the project managers, Dr. Yoji Kondo, Dr. Tom Giuli and David White.

REFERENCES

- Gibson, W. C., et al., 1972. Pointing and Guidance of the BUSS Telescope. Proceedings of the Society of Photo-Optical Instrumentation Engineers. 28:249-260.
- Kondo, Y., et al., 1972. Observations of the Stellar Mgx II Doublet at 2795Å and 2802Å. The Astrophysical Journal. 176:153-164.

52751 27H

DISCUSSION SUMMARY — PAPER 4.3

In comparing the usefulness of this system with OAO the speaker noted that it operated near 2,000 angstroms which is not optimum for OAO.

Inquiries were made on several details of the pointing and stabilization system as summarized below:

- Q. How well does the magnetic stabilization system point?
- A. The magnetometer orientation must bring the object within a 3-degree field-of-view.
- Q. How do you couple or decouple your cell to the balloon for pointing?
- A. The instrument is mounted around the azimuth shaft. The shaft is connected onto the balloon suspension line. The coupling to the train is only through the slight friction in the bearings, so we simply react about the gondola and suspension line.

PAPER 4.4

STABILIZATION, POINTING AND COMMAND CONTROL
OF A BALLOON-BORNE 1-METER TELESCOPEN. L. Hazen
L. M. Coyle
S. M. DiamondCenter for Astrophysics
Harvard College Observatory
and Smithsonian Astrophysical Observatory
Cambridge, Massachusetts

ABSTRACT

A 1-meter balloon-borne telescope has been constructed and flown to observe far-infrared radiation from celestial sources. The attitude control systems must perform to the diffraction limit of the telescope (<0.5 arcmin.) for stabilization and have positioning capability for source acquisition. These and associated systems are discussed in detail, as is the command control of the payload as a whole.

INTRODUCTION

The attitude control requirements for the 1-meter telescope balloon gondola developed by the Harvard College Observatory, the Smithsonian Astrophysical Observatory and the University of Arizona (Fazio et al, 1974; Hazen, 1974) are that the telescope line of sight be pointed in the celestial sphere to an accuracy of 0.1 degrees and then stabilized to track the observed object with rms errors below 0.5 arcmin. and DC drift of less than 1 arcmin./minute. These requirements are achieved in an altitude-azimuth mounting utilizing DC torquers and position servos. Figure 1 is a general view of the telescope and gondola.

For the elevation control system the reaction mass is the gondola frame; in azimuth it is a heavy reaction wheel. The azimuth reference for initial positioning (position mode) is a servo-driven null magnetometer which always points to the local north. The elevation reference is the gondola vertical. For tracking stabilization (inertial mode) the control signals are derived from a pair of inertial gyros mounted on the telescope base ring. By switching appropriate DC currents to the gyro torquers, large (1.5×3 degrees) or small (0.5×1.0 degrees) rasters can be executed over the target area. Either gyro can also be torqued by manual command from the ground, thereby performing straight-line scans at rates of 1 degree or 3 degrees/minute. Figure 2 depicts the principal gondola sub-systems in block diagram form.

In addition to the positioning requirements, the design of the control systems must be able to accommodate the oscillatory periods characteristic of balloon suspended payloads (Freckler, 1968; Nidey, 1968). For our payload these include a simple

pendulum period of approximately 20 seconds, a compound pendulum period of about 2 seconds, a suspension train torsional period of about 40 seconds, and a maximum balloon rotation rate of 1 revolution per minute.

A payload which is actively controlled in real time from the ground requires a versatile and reliable command capability. This is achieved by using the relatively simple command interface (provided by NCAR) to enter a command matrix, thus providing many more functions with some redundancy.

Each of these areas is described in detail in the following sections.

AZIMUTH CONTROL SYSTEM

The azimuth system achieves its control by torquing a 20 slug-foot² reaction wheel with respect to the gondola frame. The gearless DC torque motor is an Inland type T-7203 rated at 22 foot-pounds. A system block diagram is shown in Figure 3. It can be seen that the acquisition (position mode) and tracking (inertial mode) loops are completely independent except for the torque motor and its power amplifier.

The position mode reference is derived from the servo magnetometer, an independent servo system that is used to stabilize a table with respect to magnetic north using a null magnetometer (Schonstedt MND-5) as the sensing element. A 13-bit absolute position encoder reads the orientation of the gondola with respect to the magnetometer table and, with suitable correction, with respect to geomagnetic north. A digital subtraction is then performed between the encoder output and a 13-bit position command telemetered from the ground. This subtraction provides the input signal for a D-A converter whose output is the azimuth position error signal. To avoid high rate transients, a rate limiter has been added that uses a clock and the 13-bit command word as inputs and whose output is a 13-bit word that changes at the clock rate (1/2 degree/second) to adjust itself to equal the command word. Thus, when a new azimuth angle is commanded, the error signal is changed at a rate that the servo systems can follow. An addition to the rate limiter compares the difference between the output and input 13-bit words and if this difference is greater than 180° causes the payload to take the shorter path to the new azimuth angle. For increased sensitivity, the D-A converter is of 10-bit capacity and is biased to mid-range so as to avoid a discontinuity at zero error.

The inertial mode reference is a rate-integrating gyro (King C702519007) mounted on the telescope base ring. (The gyro is caged in the position mode and is thus an independent rate sensor in this mode.) This mounting is a complicating factor in that the azimuth gyro sensitivity is reduced by the cosine of the elevation angle. In order to compensate for this effect, the output of the azimuth gyro synchronous demodulator is impressed across a nonlinear pot ganged with the elevation position pot, which has a transfer function of $0.2 \sec \theta_{EL}$ for θ_{EL} between 0° and $\pm 75^\circ$

and the output of this pot is fed to the gyro loop compensation amplifier. The advantage of the gyro mounting is that it provides direct control of the telescope line of sight. The disadvantage is that at higher elevation angles the gyro is increasingly sensitive to payload roll, and with an imperfectly aligned reaction wheel axis induces compound pendulum oscillations. The problem is kept under control by the friction damping in the payload support joint (Figure 4) at elevation angles below 40°. Here, a gimballed three axis (i.e. cross-elevation) mount would have been advantageous but was not used because of cost limitations (Frecker, 1968).

Both position and inertial modes utilize type 2 loops (1 kinematic, 1 electronic integration) and both have output velocity feedback via a 1.20 volts/radian/second tachometer mounted on the reaction wheel drive shaft. In position mode the system has a calculated bandwidth of 4.8 radians/second, while in inertial mode the bandwidth is about 1 radian/second. Reduced block diagrams for the azimuth system when operating in position and inertial modes are shown in Figures 5A and 5B respectively. A Bode plot showing the system response in the two modes is depicted in Figure 6.

MOMENTUM DUMP SYSTEM

Not discussed in the foregoing section was the need to maintain long term control of the reaction wheel angular velocity in spite of wind disturbances and balloon rotation influencing the azimuth system. The momentum dump system accomplishes this by coupling momentum from the gondola into the balloon when the reaction wheel velocity exceeds + 1 radian/second, performing that function by alternately torquing the gondola clockwise and counterclockwise against the balloon shroud lines with a duty cycle determined by the azimuth reaction wheel velocity. The momentum dump motor is a Globe type BL DC motor with an integral gearhead which drives a ring gear attached to the periphery of the main payload support bearing. This bearing has a running friction level of 4 foot pounds under load, and breakaway is assured by means of an inertia bar mounted on the link above the payload support shaft.

As shown in the block diagram contained in Figure 3, the motor is driven continually by a 5 Hz oscillator, causing it to reverse direction twice every 0.2 seconds. When the reaction wheel velocity exceeds 1 radian/second the output of the reaction wheel tachometer is added algebraically to the output of the 5 Hz oscillator, causing the duty cycle to change. The result is a net torque between the gondola and the shroud lines in a direction such that the reaction wheel velocity is reduced. A reduced block diagram is shown in Figure 7.

Figure 8 shows the relationship between momentum dump motor velocity and bearing torque, from which it can be seen that:

$$\dot{\theta}_{md} = (\sin 31 t) + 7.2 \dot{\theta}_w$$

4.4-3

where $\dot{\theta}_{md}$ is motor shaft velocity in radians/second and $\dot{\theta}_w$ is reaction wheel velocity in radians/second.

Torque reversals occur at times t_r , given by

$$168 \sin 31 t_r = -7.2 \dot{\theta}_w$$

$$t_r = 0.032 \arcsin (-.043 \dot{\theta}_w).$$

Since for small arguments $\arcsin x = x$,

$$t_{r1} = 0.032 (-.043 \dot{\theta}_w)$$

$$t_{r2} = 0.032 (\pi + .043 \dot{\theta}_w)$$

$$t_{r3} = 0.032 (2\pi - .043 \dot{\theta}_w), \text{ etc.}$$

The net equivalent torque is the torque function integrated over one complete cycle; i.e.

$$T_{net} \text{ (lb.-ft.)} = 4 \frac{t1 - t2}{t1 + t2} = 4 \frac{(t_{r2} - t_{r1}) - (t_{r3} - t_{r2})}{0.2} =$$

$$0.113 \dot{\theta}_w, \text{ for } \dot{\theta}_w > 1 \text{ radian/second and the total}$$

$$\text{momentum coupled out of the gondola is } \int T_{net} dt = \frac{0.113 \dot{\theta}_w}{p}$$

In the limiting condition, with the reaction wheel at peak angular velocity (saturated), the momentum dump is capable of a constant 4 foot-pounds or alternatively of following a balloon angular velocity ($\dot{\theta}_{md}$) of 2π radians/minute.

ELEVATION CONTROL SYSTEM

The elevation system achieves its control by direct DC torquing at the elevation trunnion between the telescope and the gondola. The torquer is the same as that for the azimuth system and, like azimuth, the position and inertial mode control loops are completely independent except for the torquing function. A system block diagram is shown in Figure 9.

In position mode, the error voltage is derived from a linear, 5,000 ohm, 360° pot mounted on the elevation trunnion concentric with the elevation torque motor. The center tap of the pot is grounded, and with ± 5 volts across the winding; sensitivity is 1.60 volts/radian. Damping is achieved by feedback from a tachometer having a sensitivity of 1.20 volts/radian/second, also mounted on the elevation trunnion. The position loop is calculated to have a bandwidth of 0.4 radians/second and it is a type 1 loop (single kinematic integration) having zero position error.

Position commands are transmitted via the telemetry link as 12-bit words (LSB = 1.3 arcmin.) and converted to analog voltages by an on-board digital-to-analog converter. In order to minimize the effects of acceleration and jerk ($\frac{da}{dt}$) on the system which might excite high-frequency mechanical resonances or compound pendulum motion, the output of the DAC is operated on by a 0.03 radian/second rate limiter and a 2-pole 1.41 radian Butterworth low-pass filter before being fed to the error summing junction. A reduced

block diagram of the elevation position loop is shown in Figure 10A.

In the inertial mode, the error voltage comes from a rate-integrating gyro identical to that used for azimuth. Here, however, the gyro senses elevation angle directly and no compensation of the sort used in azimuth is necessary. The gyro has a closed loop gain (including the gyro pickoff winding) of 35.3 volts/radian, and a nominal drift random rate of 3 arcmin./hour or less. Practically speaking, however, the drift is determined by the gyro control circuitry and is less than 1 degree/hour here and in azimuth (although anomolous higher rates have been observed in flight).

Error-rate damping is used in inertial mode, rather than output shaft velocity damping as in position mode. This choice was made to avoid the possibility of gondola disturbances appearing as velocity error inputs to the inertial loop. (Note that the telescope is intrinsically stable in elevation inertial position, independent of gondola motions except for bearing and cable loads.) A reduced block diagram of the elevation servo system in inertial mode is shown in Figure 10B. This is also a Type 1 system and has a calculated bandwidth of about 6 radians/second. A Bode plot showing the system response in the two modes is shown in Figure 11.

POINTING VERIFICATION

Intrinsic to any attitude controlled telescope is the problem of verifying its performance during actual flight. This is achieved by a variety of means. The elevation position is read out by two independent potentiometers through the telemetry; in azimuth readouts are provided of the azimuth position error (DAC output) and of an independent pair of cross magnetometers. For the inertial mode, readouts are provided of the gyro outputs indicating proper tracking. Overall pointing data are also provided in real time by a photometer, masked by a N-shaped aperture placed in the focal plane of the telescope, which senses the passage of stars down to 9th magnitude. Post flight data are provided by a star field camera mounted on the telescope which records the field of view frequently in automatic response to the various inertial mode pointing activities. These last two systems are discussed in more detail elsewhere (Fazio *et al.*, 1974; Hazen, 1974).

BACKUP POSITIONING

Prompted by payload failures early in the flight program, an independent set of positioning drives has been incorporated into the gondola with enough readouts to be self-sufficient in the case of primary system failures. This backup capability uses the NCAR tone command system for control and is powered by an independent battery pack capable of several hours of continuous operation. The backup system is based on the concept of azimuth drift scanning at controlled elevation angles and is depicted in Figure 12,

including a diagram of the command functions.

The elevation drive consists of a drive ring surrounding one elevation trunnion which upon activation engages a lug on the trunnion shaft. In practice, the operator uses a tone command (6) to enable the backup elevation drive, then uses two other tone commands (1 and 2) to drive the ring up or down, engaging the telescope and positioning it. Position accuracies to about 0.5 degrees can be achieved. Not shown in the figure is that the capture pawl is positively disengaged from the telescope when driven to elevation angles above 80°.

The backup elevation drive serves an additional purpose in providing means to stow the telescope in the vertical position prior to impact after a flight in cases where the primary systems fail or the payload is out of TM range. This is achieved by sending two tone commands (5 and 6) which initiate an automatic drive to the upper stop, or through a timer (set just prior to launch) and baroswitch (set to 30,000 ft.) which spontaneously initiate the same action during parachute descent. Both means serve also to switch off the main flight battery avoiding the problems of a powered payload during impact and recovery. Note also that this means can be used during flight to reset those DC-DC power supplies on the payload that a transient might trigger into crowbar cutoff. Easily cutting off and reinitiating total payload power is essential for resetting systems without going into a very elaborate alternative scheme.

Backup azimuth control is achieved by providing manual control of the momentum dump motor, using tone commands similar to those for elevation to permit torquing against the balloon. Although stationary positioning is difficult to achieve, azimuth rates can be kept sufficiently low to do effective drift scanning in the desired portion of the sky. One tone command (8) is used to clear the drive logic for both elevation and azimuth.

Note in Figure 12 that the primary flight battery is connected to the backup positioning system and, in fact, because of its higher voltage assumes the principal load except for the case of outright battery failure. There are also position readouts: a pot for the elevation and a pair of orthogonal magnetometers that monitor magnetic azimuth of the payload independently from the systems in the main section of the payload. For simplicity's sake, the active devices in the backup system are latching and momentary relays. Power and grounds run through separate paths from the power for the rest of the system.

COMMAND CONTROL

The command interface to which the payload was designed (ca. 1971) consisted of 20 sets of relay contacts, 10 sets momentary and 10 sets latched (thus involving 30 commands). Each momentary command provides a 25 ms connection of the common to the normally open contact. Otherwise, the common is connected to the normally closed contact. In the case of the latch commands,

the common maintains its contact with one of the relay throws until the clear command is sent, when the common is brought into contact with the other throw. The relays are configured to provide TTL level outputs to the payload interface. Each normally open contact is connected to a +5V logic level through a 2.2K resistor. Each normally closed contact is connected to a signal ground. The common is brought to the interface as the command signal.

In addition, eight maintained switch closures were made available via a separate tone command system, where the duration of the switching is dependent on the duration of the tone. Here either ground or 24 volts are switched to the command input depending upon the application.

[Since the construction of the payload, NCAR has updated their commanding system (Snider, 1974). Funding limitations have forced us to retain the old input interface to the payload and to provide the adaption to the new by means of a relay interface box.]

Looking at the payload, a substantial number of functions have to be accommodated by command. The basic two axis positioning information requires 25 bits. In addition a large number of functions must be enabled and cancelled, and subsystems turned on and off. It was evident in the design that many of the commands would have to do multiple duty. A matrixing scheme was established, whereby 4 of the latching commands were used to address particular 13-bit registers and 7 of the momentary and the other 6 of the latching commands were used as signals into all of the registers. The remaining 3 momentary commands are used to control main power and to execute loads into the four registers. Figure 13 shows the scheme of the matrix. The first two registers are used to enter and store positional information for azimuth and elevation. The third register is used to "call" for certain payload functions, while the fourth controls the activation of major systems or functions.

In order to command the payload, the procedure is to address one of the four 13-bit registers, load the inputs to the register as required, execute (thus entering the load into the addressed register) and clear the address and the command load. The loads may, in general, be sent before or after the address, and the sequence of clearing after the execute is generally of no consequence.

To load an azimuth position, for example, the azimuth register is addressed (35), the desired azimuth position (13-bit word) is loaded, an execute is sent (32), then the addressing of the azimuth register is cleared (47) and the azimuth command bits are cleared. It is necessary to clear only the latching commands, since the momentaries are cleared at the last of the sequence that is initiated by the execute command (32). Figure 14 shows the logic to accomplish this and to otherwise achieve a high level of commanding reliability.

As a consequence of the momentary command load being cleared immediately after it has been loaded into its appropriate register, a lockout circuit was added to prevent a multiple execute command

from entering a faulty command load. Thus, if more than one execute signal is received, the first one will perform the function and will block any others. Upon receipt of the command, the execute sequence enables and loads the addressed register, disables all registers to any inputs and clears the loaded momentary commands. In order to reenable the system to act upon an execute command, it is necessary to clear any outstanding register address. When faulty address codes are entered, the command system simply "enables" a non-existent register.

The third, or "call", register is handled a little differently. The desired function is addressed or "called"; then one of two "GO" tone commands is sent to actuate the function in the "plus" or "minus" direction. There are six functions of this sort (focus telescope, balance telescope, azimuth inertial scan, elevation inertial scan, momentum dump override and stow pin), and mutual exclusivity in these operations is advantageous in terms of noise immunity and simplicity of operation. A one-of-sixty-four decoder is therefore used at the output to monitor the status of those register outputs corresponding to the six desired functions. When one and only one of these six input lines is at a logic "1" state, the appropriate logic path is enabled and the "plus" or "minus" tone command will then actuate the function. When more than one function is "called", no system is actuated upon sending either of the GO commands.

Note that there are redundant pairs of GO commands. The tone commands provide immediate short term response (as for the focus drive); the matrix commands provide longer term enabling (as for an azimuth inertial scan). Logic not shown in the figure monitors the relevant outputs and precludes simultaneous use of more than one of these commands.

Unlike the first three registers, the register that turns systems on and off is used simply by addressing and loading, (not requiring execution). The momentary commands that appear as inputs to all of the registers are fed through this register, known as the 44 register, whenever it is addressed; these are used to turn on and off modes and systems by setting bistable devices.

The remainder of the 44 register (using latching commands) controls the power to the major systems in the payload, but since, as mentioned earlier, this register is entered by addressing and loading, it is easy to change its status. This possibility is minimized by means of "securing" the sub-register, whereby it must be separately enabled through one of two other registers in addition to its normal addressing. The functions controlled by the secure sub-register are normally turned on only once at the beginning of a flight for the duration.

Test and flight experience has shown this commanding scheme to be an effective means of controlling a payload of this complexity. Nonetheless, the new NCAR command equipment could provide significant simplification and will probably be utilized in future flights.

ACKNOWLEDGEMENTS

The authors gratefully acknowledge the valuable contributions of many of the staff of the Solar Satellite Project and the Model Shop at the Harvard College Observatory during the design, construction, test and flight phases of this effort.

Sponsorship for payload development came from the Smithsonian Astrophysical Observatory, Harvard College Observatory and the University of Arizona. The last two flights were supported by NASA under grant NGR-22-007-270.

REFERENCES

- Fazio, G., D.E. Kleinmann, R. Noyes, E. Wright, and F. Low, 1974. A Balloon-Borne 1-Meter Telescope for Far-Infrared Astronomy. Presented at the Symposium on Telescope Systems for Balloon-borne Research. NASA-ARC.
- Frecker, J., 1968. The Polariscope Balloon-borne Servo System. Communications of the Lunar and Planetary Lab. No. 109. Vol. 7 (Pt. 1) p. 39-44.
- Hazen, N., 1974. A Stabilized Large-Aperture Far-Infrared Telescope Gondola. Presented at the Seminar Instrumentation in Astronomy II. SPIE, Tucson.
- Nidey, R., 1968. Stabilization and Orientation of Balloon-borne Instruments. National Center for Atmospheric Research, Boulder.
- Snider, J., 1974. NCAR Telemetry and Command System. Presented at the Symposium on Telescope Systems for Balloon-borne Research. NASA - ARC.

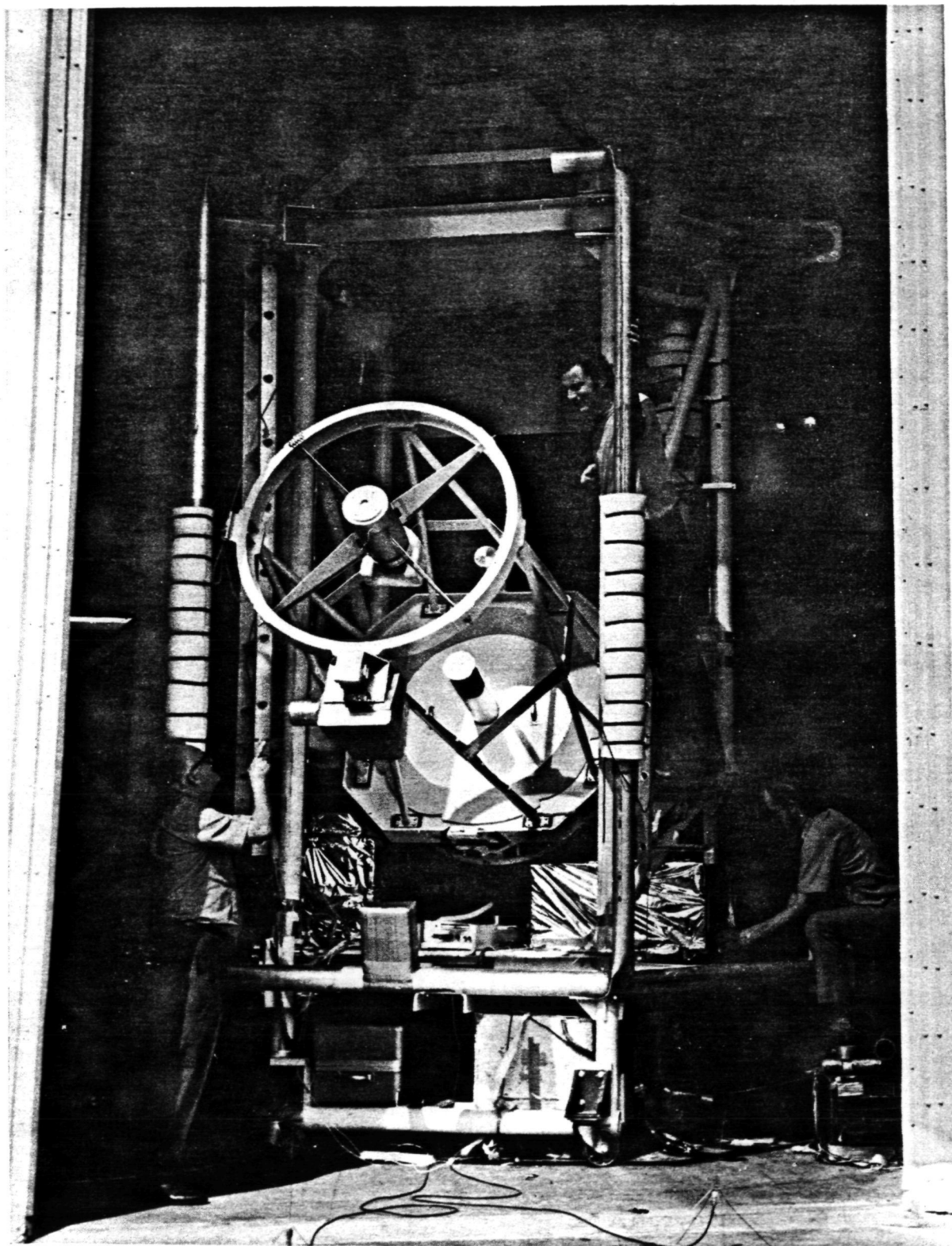


Figure 1. 1-meter IR telescope balloon gondola.

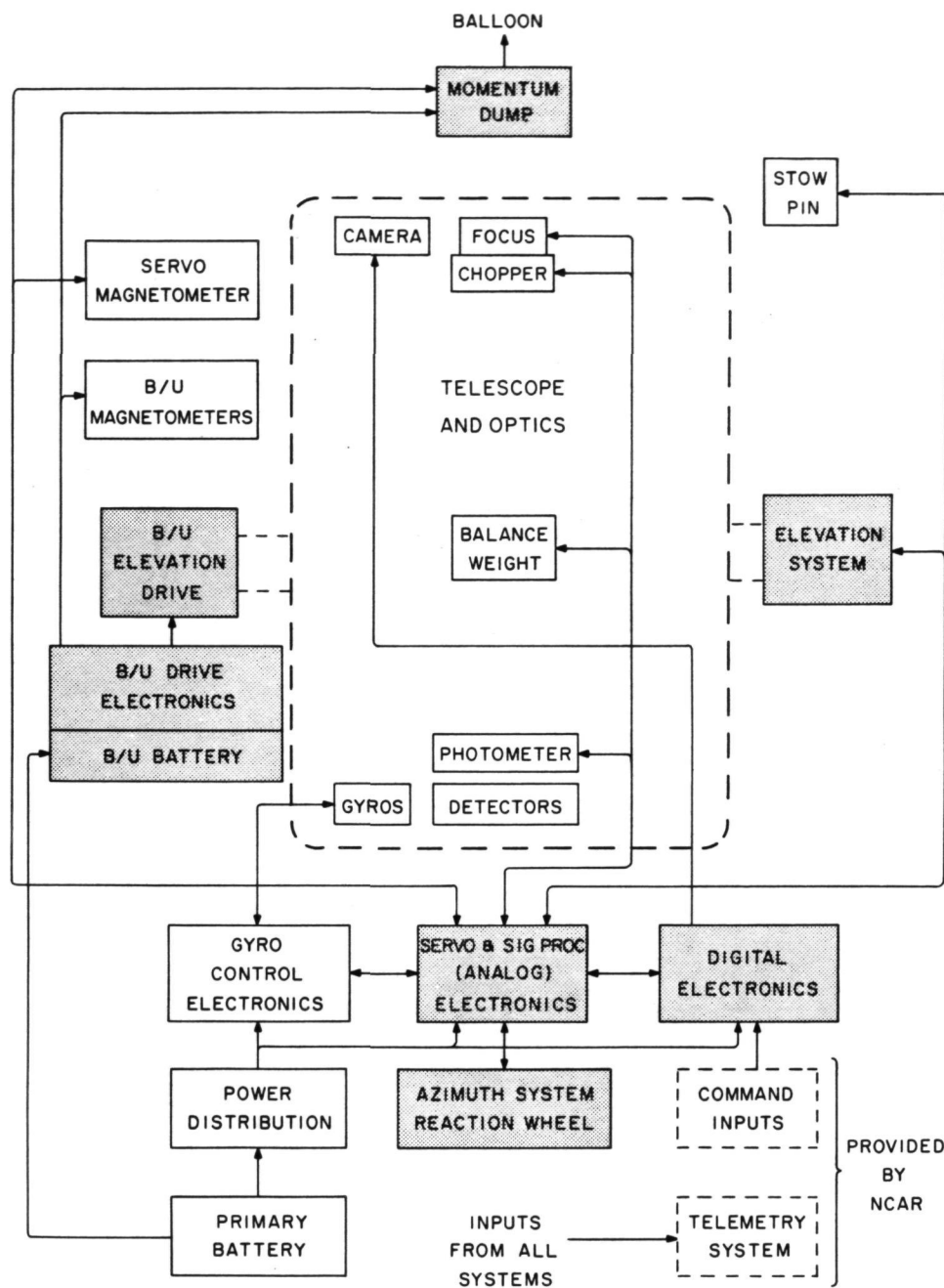


Figure 2. 1-meter telescope gondola - simplified block diagram.

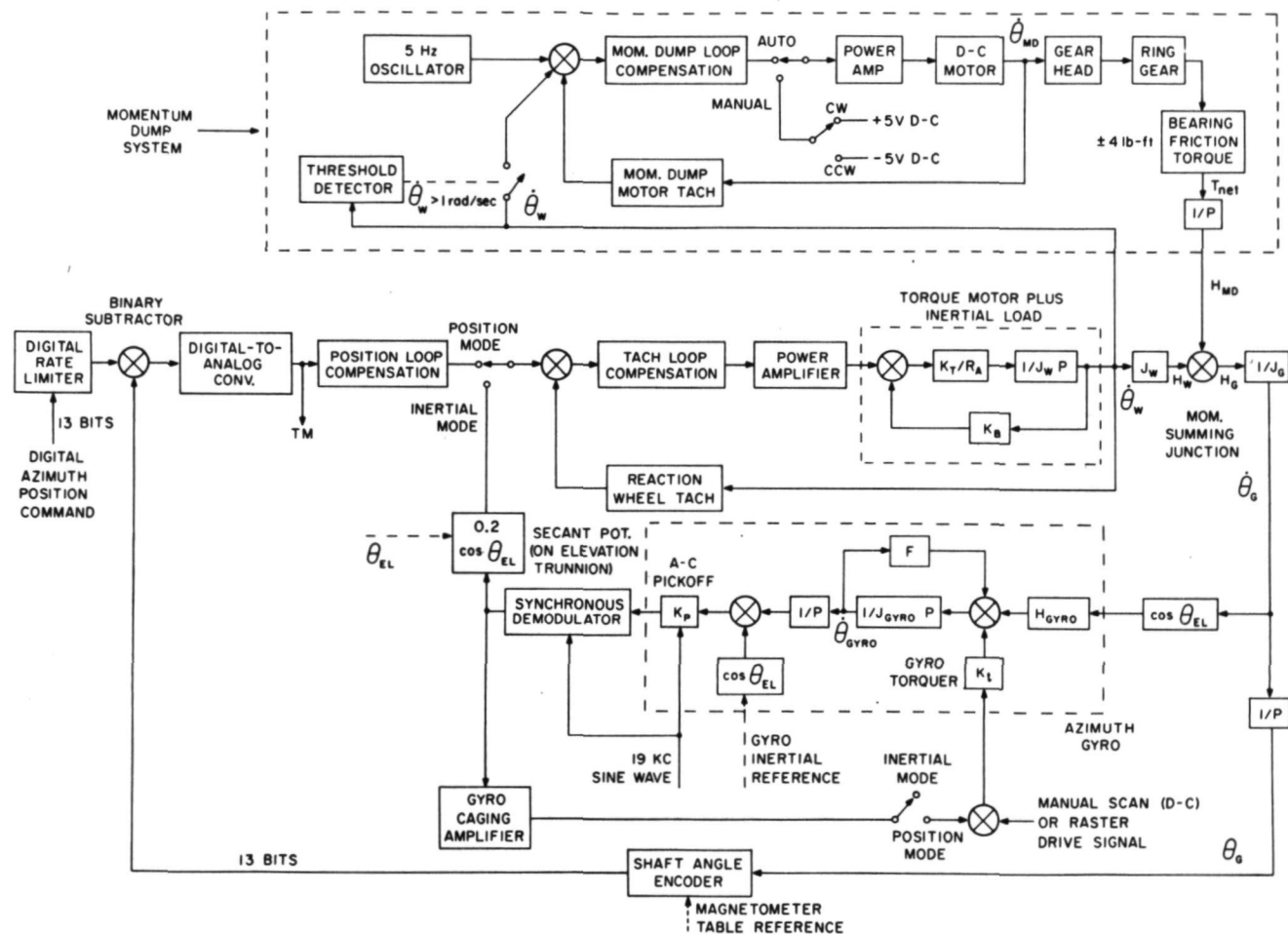


Figure 3. Azimuth control system block diagram.

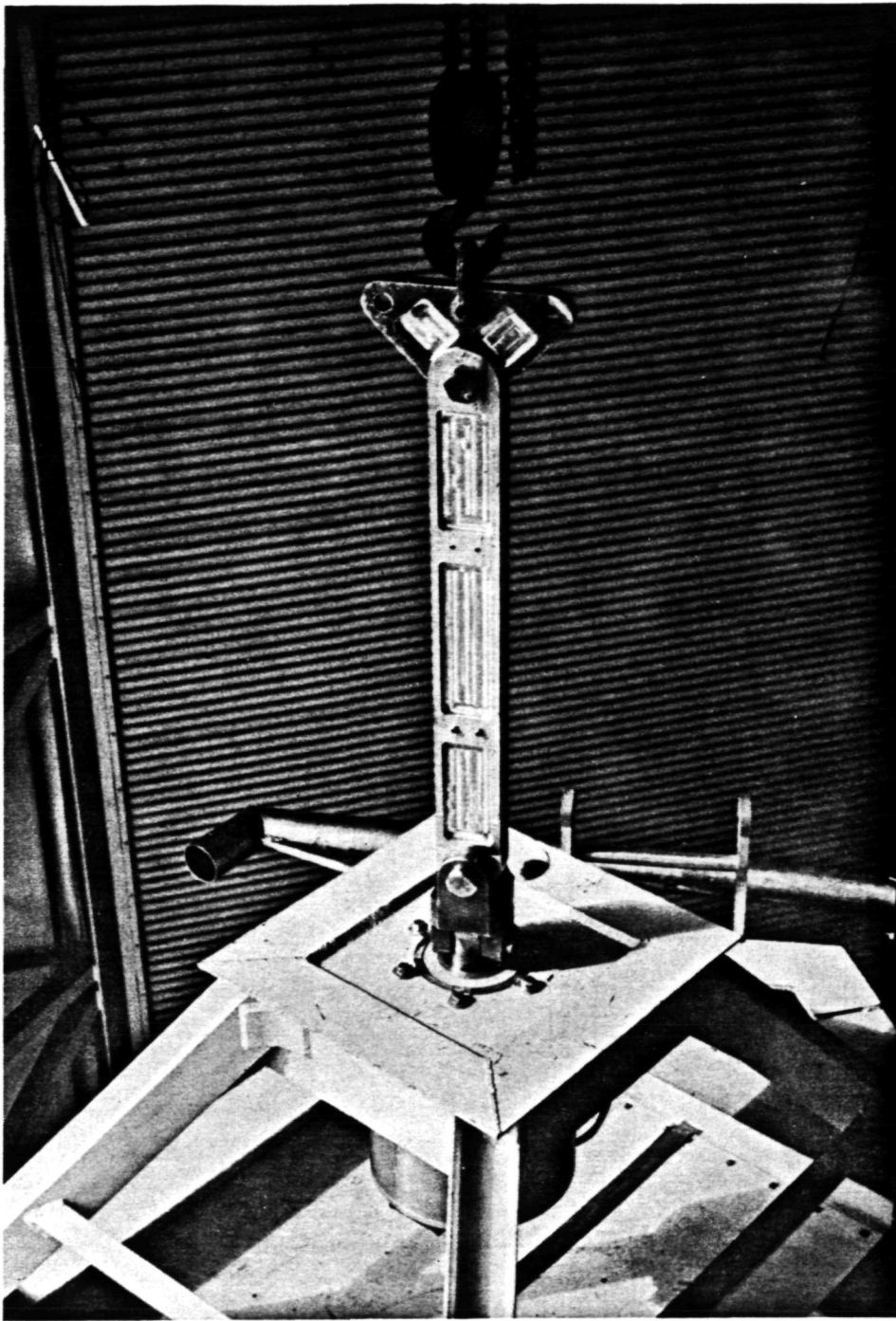


Figure 4. Suspension link (Inertia bar not shown).

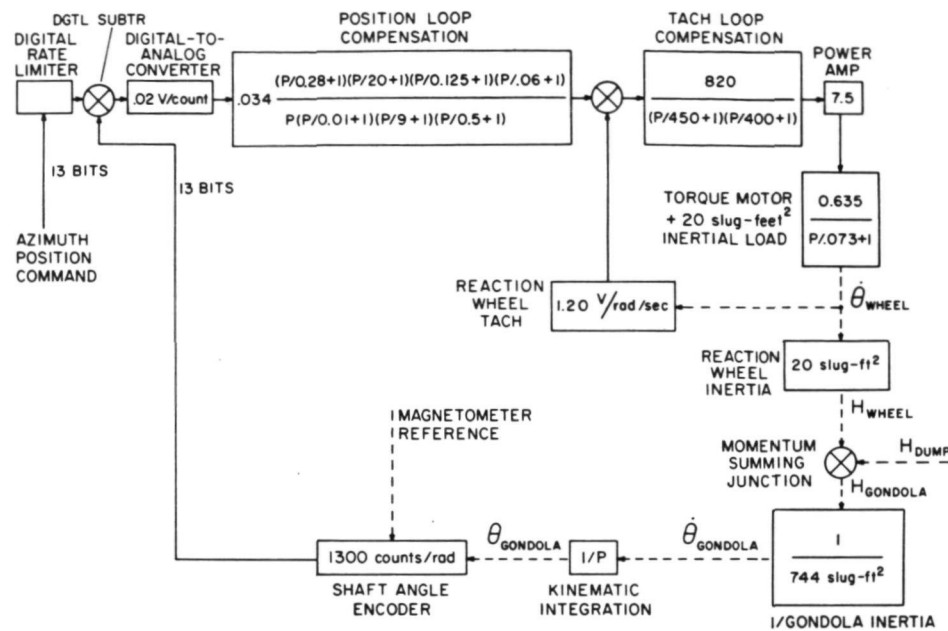


Figure 5A. Azimuth system reduced block diagram - position mode (momentum dump system not shown).

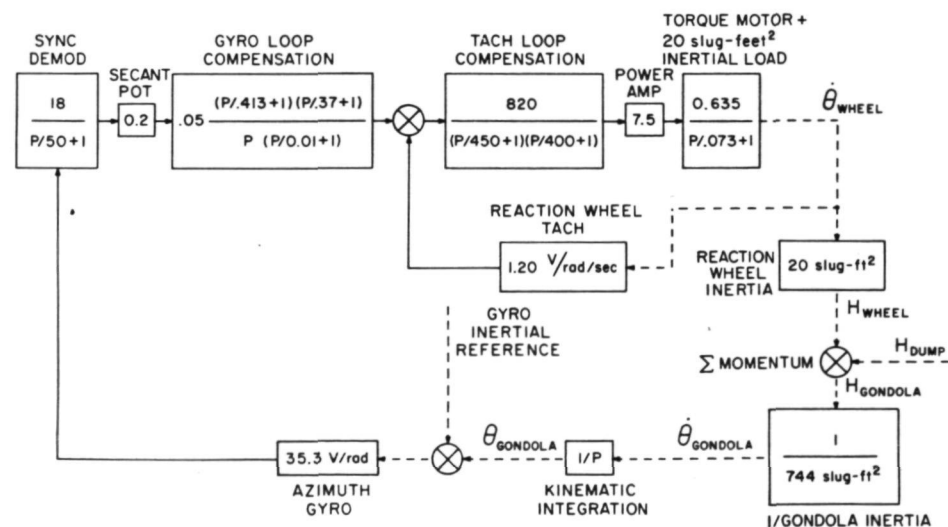


Figure 5B. Azimuth system reduced block diagram - inertial mode (momentum dump system not shown).

REPRODUCIBILITY OF THE
ORIGINAL PAGE IS POOR

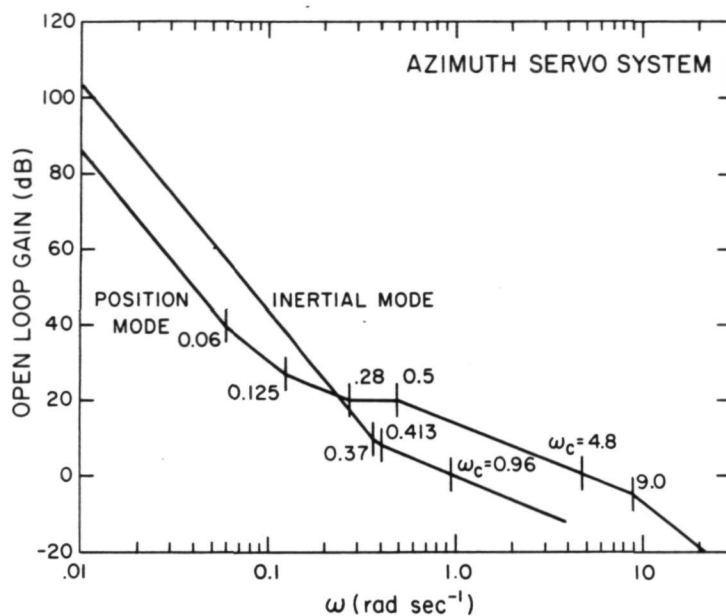


Figure 6. Azimuth servo system response.

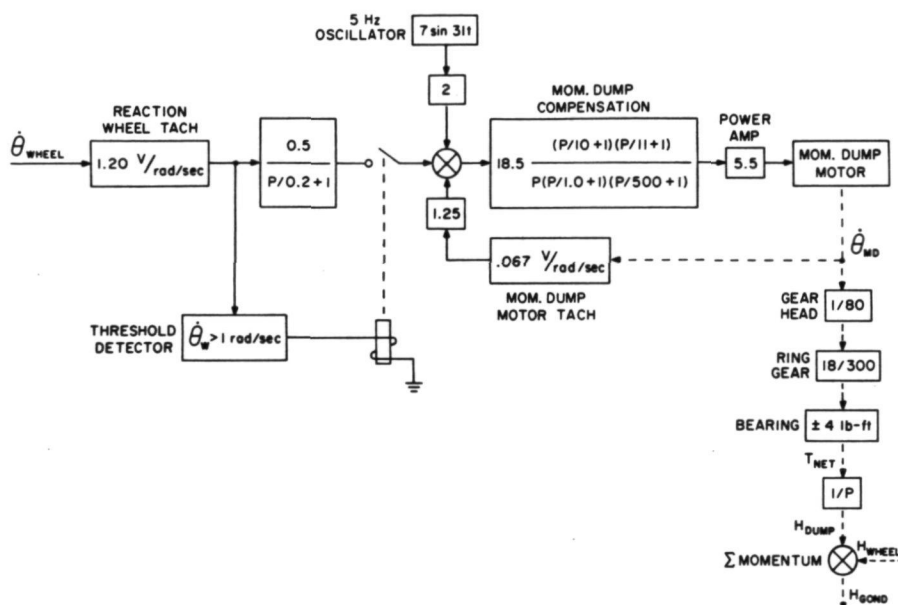


Figure 7. Momentum dump system - reduced block diagram.

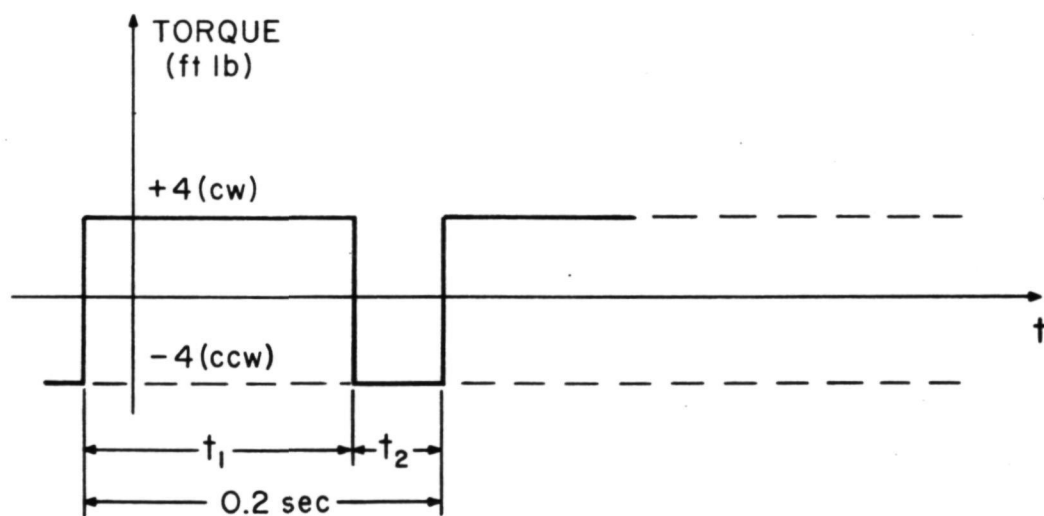
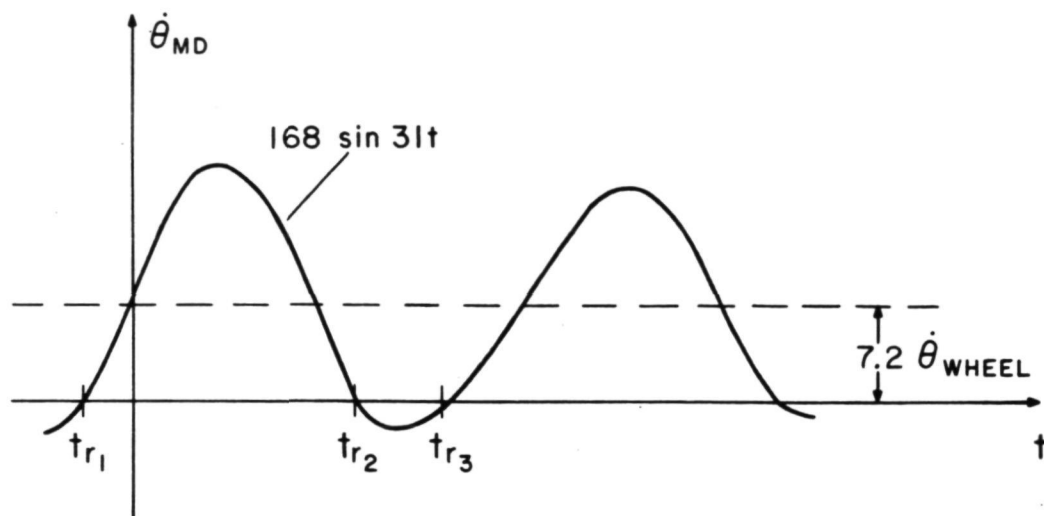


Figure 8. Momentum dump motor velocity and torque.
Output vs. time.

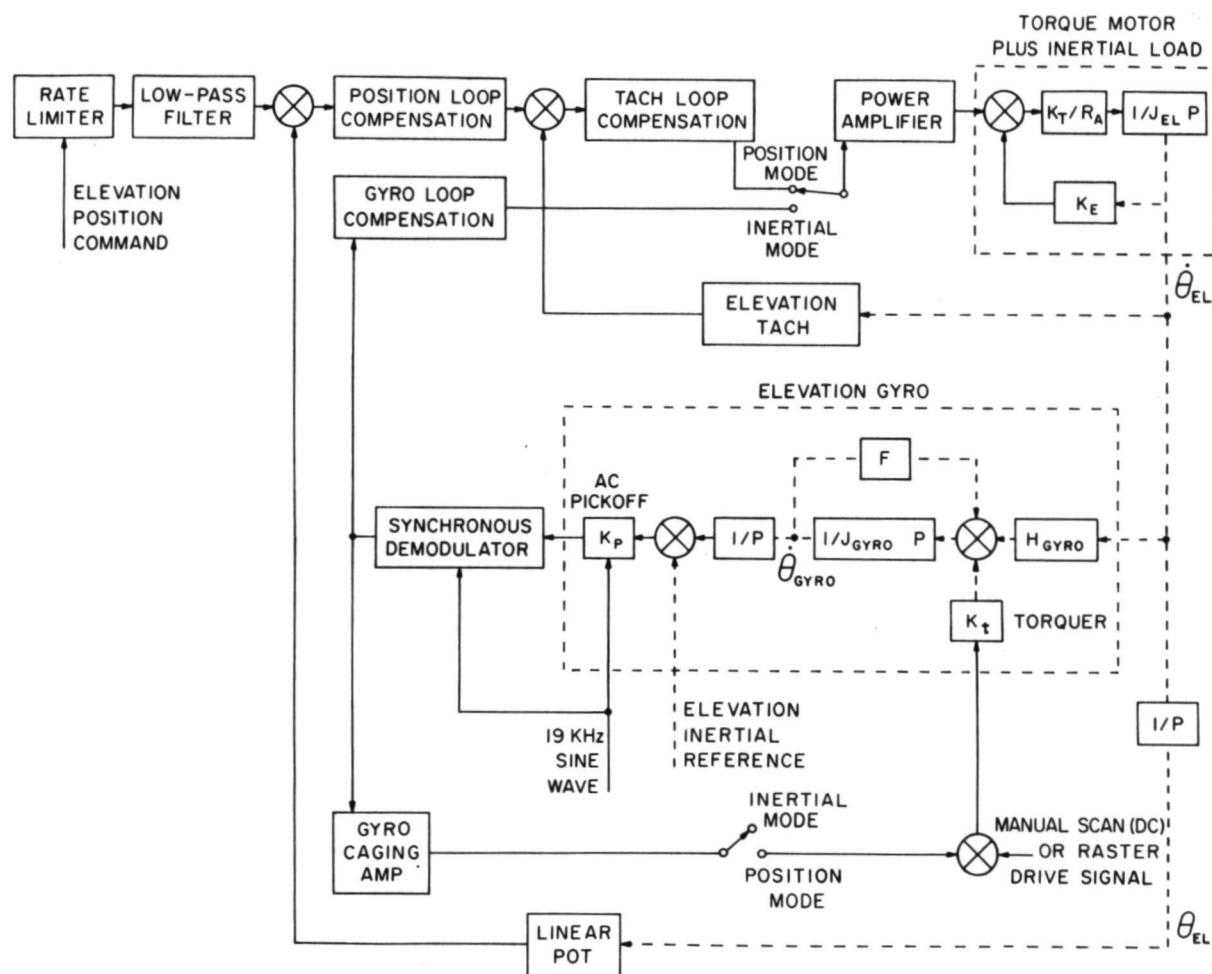


Figure 9. Elevation control system block diagram.

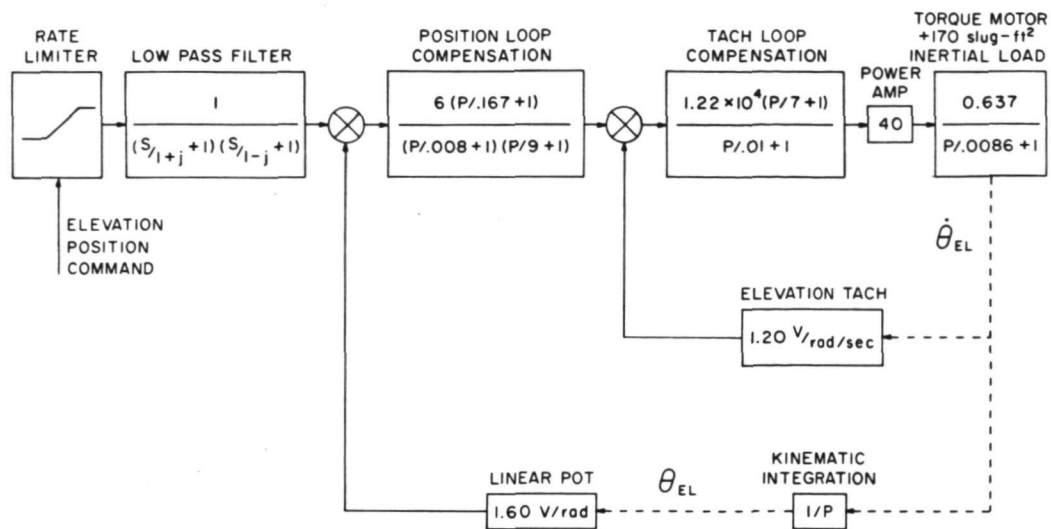


Figure 10A. Elevation system reduced block diagram - position mode.

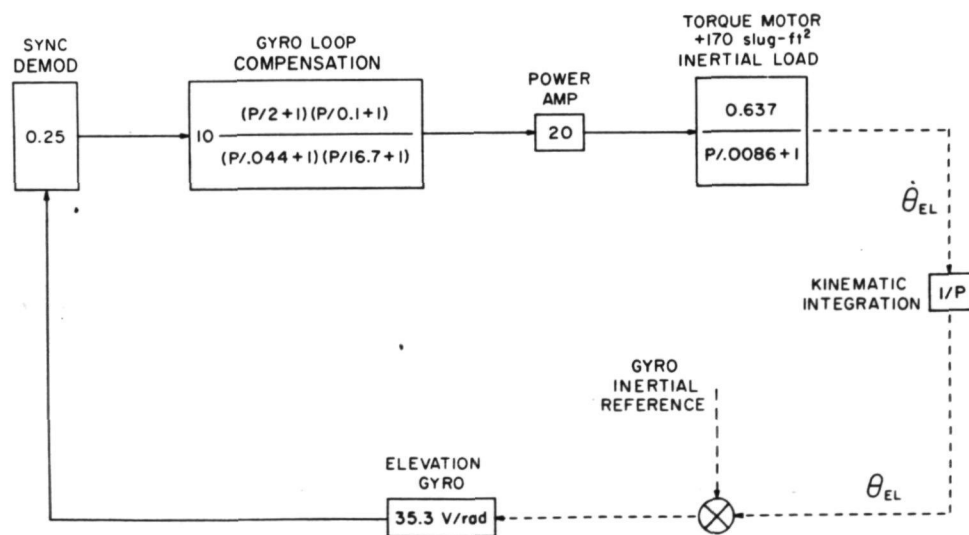


Figure 10B. Elevation system reduced block diagram - inertial mode.

REPRODUCIBILITY OF THE
ORIGINAL PAGE IS POOR

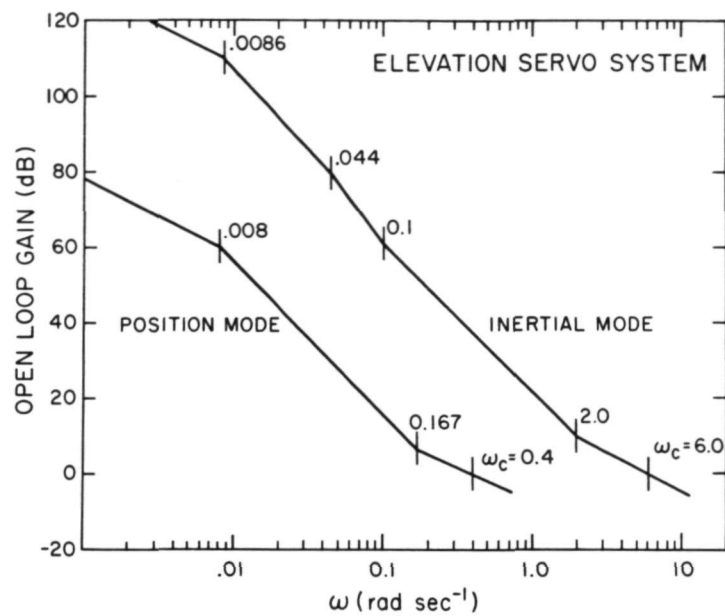


Figure 11. Elevation servo system response.

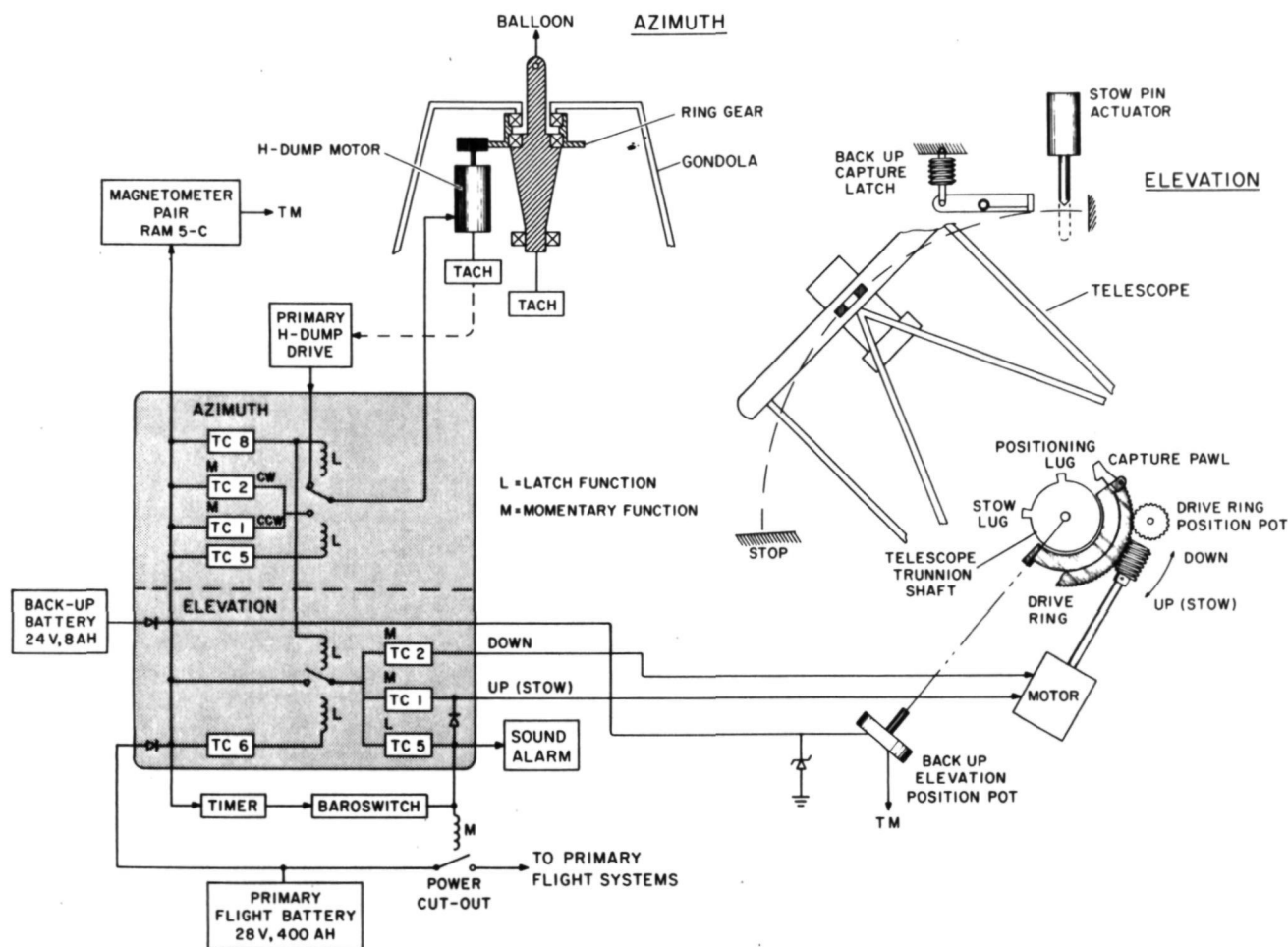


Figure 12. Backup drive and stow system block diagram.

5 & 6 = AUTO STOW
& BATTERY CUT OUT

Figure 13. Functional command matrix.

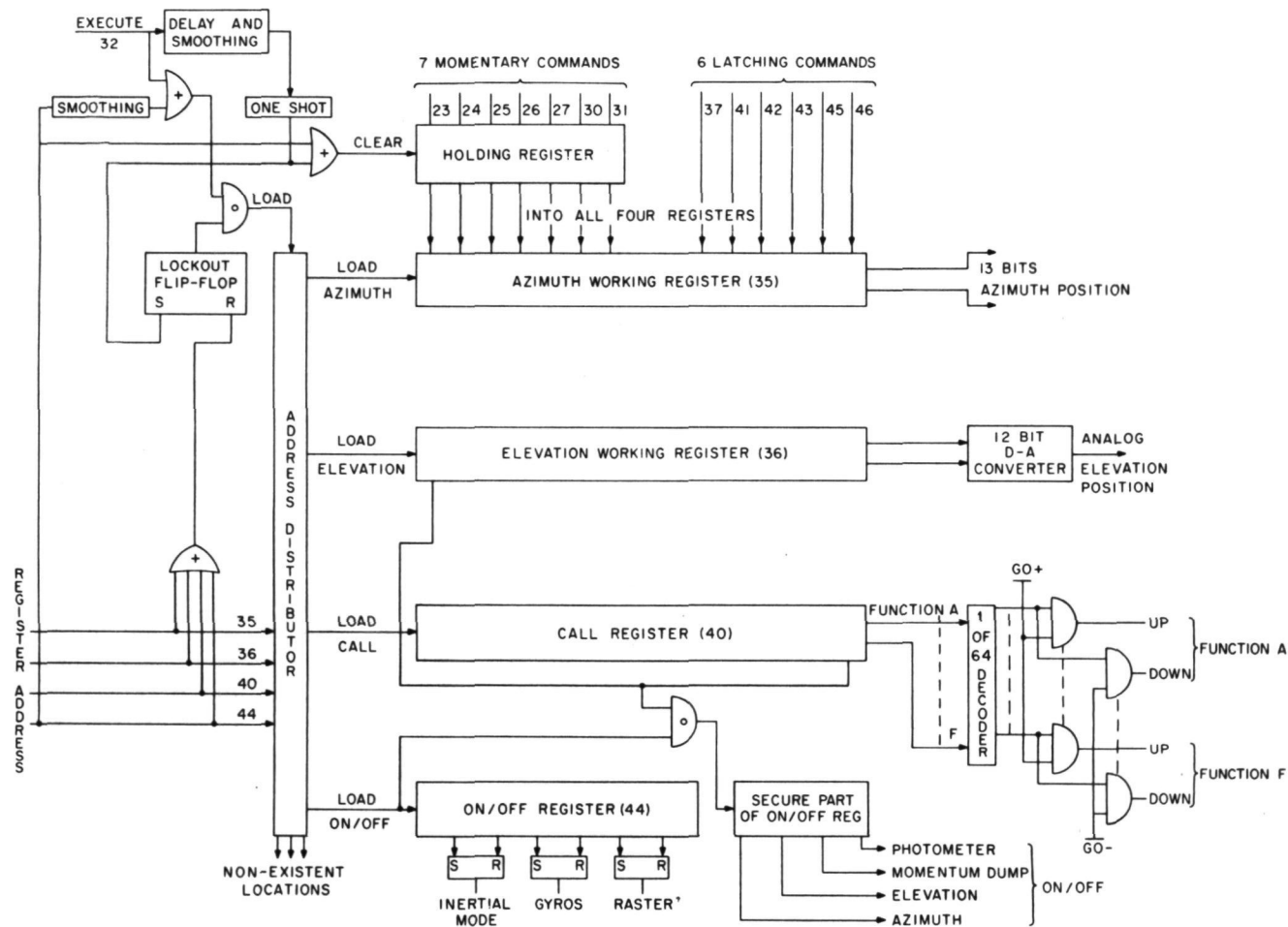


Figure 14. Command system block diagram.

DISCUSSION SUMMARY — PAPER 4.4

Several questions were asked about details of the stabilization and pointing systems. These and the ensuing discussions are summarized below:

- Q. How does the fact that the inertial wheel was not centered relative to the center of gravity of the payload affect the stabilization?
- A. Torquing the reaction wheel causes a counterrotation of the payload around its center of mass. Furthermore, if that counterrotation includes a roll component, then the azimuth gyro will sense that and feed it back into the balloon. Consequently, the system becomes quasi-stable when pointed at high elevation angles. A quasi-stable small amplitude roll is built into the system with a frequency of about half a cycle per second, the component pendulum rate for this system.
- Q. Why do you have a redundant system for pointing the telescope?
- A. One or more of the primary systems failed in the first two flights, so redundancy was built in to ensure getting scientific data.
- Q. Are the gyros good enough to do daylight observations?
- A. The gyros are very good. They have drift rates on the order of 0.03° per hour, DC or random. The stability of the control circuitry is not that good and results in drift rates of about half a minute of arc per minute. This could be improved, but observations have not yet required it. Daylight observations have not been performed.
- Q. Can you slew the telescope to view a non-visible object?
- A. Yes. Inherent in the inertial loops is the ability to put in mission selectable scan rates by torquing the gyro and, therefore, causing the attitude control system to change.
- Q. How good is the position mode (magnetic stabilization) in the presence of friction?
- A. The friction isn't bothersome because the moment of inertia of the payload is such that an oscillating four foot pounds torque produces an oscillation at the five Hertz momentum dump rate of approximately 0.3 to 0.4 arcminutes. Pointing performance has been consistently better than a tenth of a degree in stability (not absolute) for times on the order of five or ten minutes.
- Q. How much friction do you have in the main bearing?
- A. The system was designed to withstand up to 10 g's without damage. The payload weighs 400 pounds, so the bearing is rated at 40,000 pounds. It has two joint tapered roller bearings. Under dynamic conditions their torque (running torque) was measured at four foot pounds. They are oscillated in order to control this. The break-away torque has not been measured but is felt to be significantly higher.

AIROSCOPE STELLAR ACQUISITION

Gordon J. Deboo, Gilbert T. Parra and Roger C. Hedlund
Ames Research Center

ABSTRACT

The acquisition system to be described operates in conjunction with a balloon-borne TV system, boresighted to a telescope. It has two main functions, a star field monitor and an offset star tracker.

The design of the system was strongly influenced by the TV camera, which uses the same interlaced scanning system as is employed in commercial television broadcasting. To reduce power and bandwidth requirements, the star field information transmitted in our system consists only of the horizontal and vertical coordinates of each star and its brightness. As a star field monitor the system provides video thresholding, camera blemish suppression, coordinate digitization in 3 axes, circuitry to recognize as single star the dispersed video signals resulting from one star overlapping adjacent scanning lines and storage of all signals for readout by the telemetry at appropriate times.

The offset tracker generates a set of coincidence gates in the gondola controlled by command from the ground. Coincidences between the gate pattern and the video of the tracking star produce gyro correction signals which force the tracking star to go to and be locked into the center of the gate pattern. The gate pattern is displayed on the ground as a crosshair superimposed on the star field and the operator can move the crosshair to encompass any desired star, which is then forced into the center of the crosshair and, hence the gate pattern. When the operator moves the crosshair, the tracking star and the whole star field move as one. By moving the crosshair, the tracking star can be placed in a predetermined location which positions the object under study in the center of the telescope field.

The acquisition system to be described is part of the Ames Infrared Balloon-Borne Telescope system (AIROscope) introduced earlier in this symposium. It consists of a television camera, a video signal conditioning unit and a gate pattern generator, which combine to perform two main functions. The TV camera and video signal conditioning unit provide signals for a star field monitor, so that an experimenter on the ground can observe and recognize the star field around the field of view of the telescope, which is boresighted to the camera. The purpose of the gate pattern generator is to provide a means for the experimenter to position an IR source invisible to the TV camera, in the center of the camera and telescope fields of view. The camera, the video signal conditioning system and the gate pattern generator are each described below in more detail.

CAMERA

Table 1 on page 4.5-2 summarizes the main features of the TV camera.

The specifications having the greatest impact on the design of the star field monitor and offset tracking circuitry are those relating to the interlaced scanning system employed in the camera, which is the same as is used in

commercial broadcasting and which impose similar bandwidth requirements on the rf portion of the AIROscope telemetry. To transmit a complete television picture, including synchronizing pulses and picture information, requires a bandwidth of approximately 6 megahertz. For balloon applications the transmission distances are larger than those typical of commercial broadcasting, being in the range of perhaps 0 to 400 kilometers. It is evident that the transmitter power requirements would therefore also be larger, being in the hundreds of kilowatts range. The power requirements could be reduced by using a very large, tracking, directional, receiving antenna, but this is not available to us, would be too expensive and is unnecessary anyway due to the bandwidth reduction techniques described below in the section on video signal conditioning.

Camera:	Silicon intensified target type.
Scanning:	Standard 525 line, 2:1 interlace, 30 frames per second.
Sensitivity threshold:	10 ⁻⁵ F.C. on faceplate.
Zoom:	Remotely controlled zoom to provide 2° to 20° field of view. Detector/telescope FOV is 5°.
Spectral response:	350 to 750 nm, peaking at 420 nm.
Iris:	Automatic iris control based on peak illumination to adjust iris and change neutral density filters to give 100,000:1 dynamic range. Manual control is available.
Reticle:	Four points of light forming a square of 1/2 to 1/20th of picture height depending on zoom setting. Can be remotely turned on or off.

Table 1. Camera Specifications

VIDEO SIGNAL CONDITIONING

The main purpose of the video signal conditioning system is to process the video picture and synchronizing pulse information from the camera electronics so that the star field seen by the camera can be reproduced on a ground-based display without the need for a high power, 6 megahertz telemetry system, since only 30 watts of transmitter power and a few kilohertz of bandwidth are available in the AIROscope system.

Our approach takes advantage of the fact that the number of stars seen by the TV camera in our AIROscope applications is small - we consider 10 to be the maximum required - and further, that any apparent motion of these stars is very slow. Therefore we have a small amount of data and a low data rate which, when combined, require several orders of magnitude less bandwidth to transmit than would the conventional TV signal the camera is capable of handling. The x, y, and z coordinates of each star are measured and stored, where x is the distance from the left-hand side of the picture, y is the distance from the top of the picture and z is the star intensity. To transmit the location and intensity of 10 stars requires 10 xyz measurements or 30 data words. x, y and z are transmitted using the 10-bit words available in the telemetry pulse-code-modulation (PCM) system, so the total bit requirement is $10 \times 30 = 300$ bits for a complete star field. In a noiseless system it would require that the 300 bits be transmitted perhaps every second or less to account for apparent star motion, but to help integrate out noise a complete star field is sent down 30 times per second. This requires $30 \times 300 = 9000$ bits per second, a

data rate which is compatible with the gondola PCM telemetry system. The xyz coordinate data are measured digitally, but are available in the gondola in both digital and analog form. We are currently planning to have the PCM system sample the xyz data in analog form because it simplifies synchronization problems between the camera and the PCM system, which have different and random phase clocks, by eliminating the need for synchronization at all. It should be noted also that coding the star locations and brightness as coordinates eliminates any need to transmit horizontal or vertical sync pulses, which again conserves bandwidth and incidently eliminates the need for a raster in the ground display, thereby clarifying the picture of the star field presented to the investigator.

The measurement of the xyz coordinates involve certain complications, some of which are outlined below to indicate the scope of the electronic design problems. They are most easily discussed by referring to Figure 1. Figure 1(a), which is not drawn to scale, shows two stars A and B being scanned by an interlaced raster consisting of lines 1, 2, 3 and so on. Also shown, in Figure 1(b), are the resulting video pulses and their relationship to the camera synchronizing pulses. Notice that a complete picture requires 525 lines (some of which are lost during the vertical retrace period) and is called a "frame." One frame takes 1/30th of a second to write. Each frame has two "fields" each of which contains 262-1/2 lines taking 1/60 of a second to write. The lines from each field are interlaced to form a frame and in Figure 1(a) the lines of the first field of the frame shown are drawn as solid lines, while the lines of the second field of the same frame are drawn as dotted lines. The main problems illustrated by Figure 1 are the dispersion in time of the signals from 1 star and the interleaving in time of the signals from one star with other stars. The degree of the dispersion and interleaving are functions of how many lines it takes to completely scan a particular star. Because a star is a point source of light and because of the high quality of the TV camera and its optics it should theoretically require only 1 or perhaps at worst 2 lines to cover a given star. However, to allow for such contingencies as a partial loss of focus, our system allows for up to 5 lines being required. This is the situation shown in Figure 1(a) in which stars A and B cover 5 and 2 scanning lines respectively.

Notice that line 3, which is in the first field of the frame shown, scans A but not B. Line 3 on the video waveform therefore has a signal due to A only as shown in Figure 1(b). The next line down on the raster is line 264, but this line does not occur, nor do the video signals resulting from the scan of this line occur, until the second field is scanned about 1/60th of a second later. Line 3 is actually followed in time by line 4, which can be seen to scan both A and B, resulting in two video signals on line 4 of the video waveform as shown in Figure 1(b). By noting which lines scan A and B and where A and B occur on the lines the complete video train for stars A and B for both fields of one frame can be drawn as has been done in Figure 1(b).

The design of a system to measure the coordinates of A and B and other stars must be prefaced by an examination of the waveforms in Figure 1(b). Some of the more important conclusions to be drawn from this examination are listed below.

1. The signals from A and B are interleaved with each other and will interleave with other star signals that may exist. Therefore, we do not have the relatively straightforward situation in which one star is represented by a single signal.

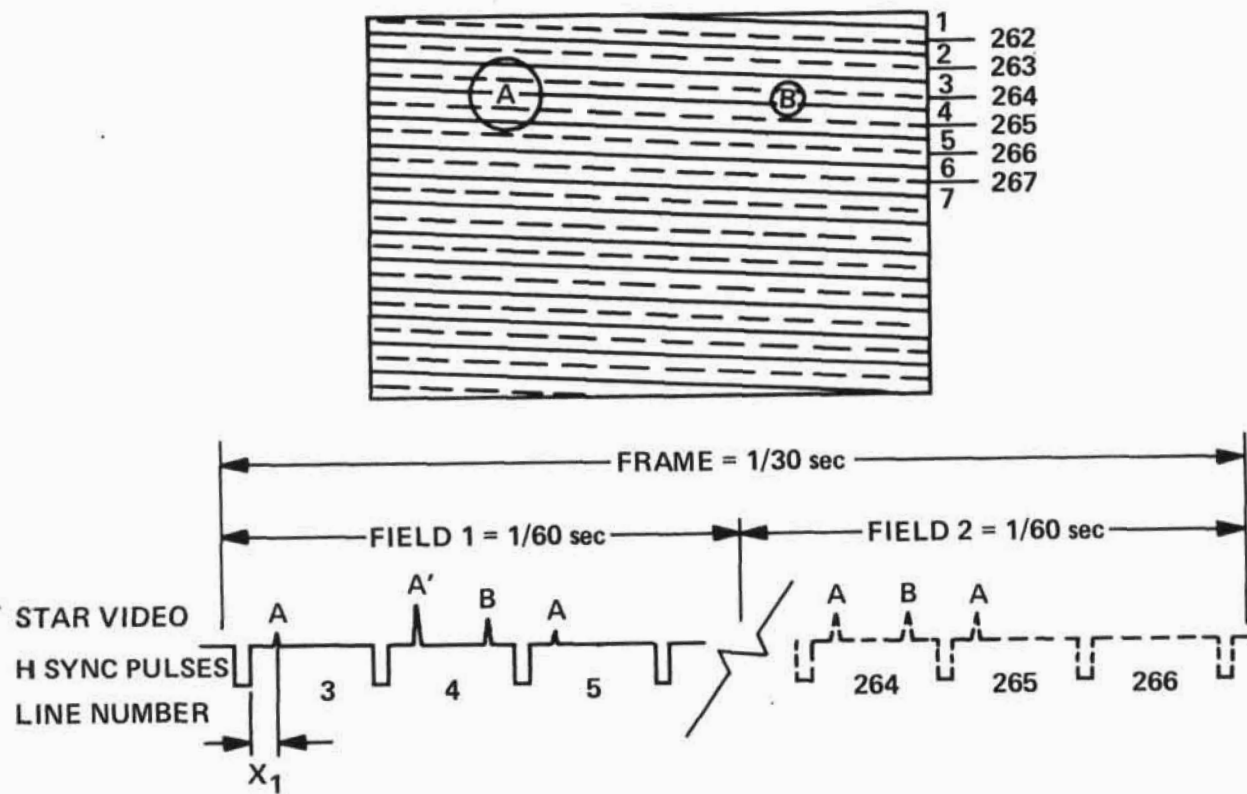


Figure 1. Interlaced scanning of stellar images

2. The amplitudes of the signals from any given star vary depending on how the star happens to be scanned. For the situation shown, the peak of A occurs on line 4, while B has 2 equal peaks on lines 4 and 264, that is, in different fields.
3. To measure the location and brightness of each star we should use only the peak video signal for each star. A has one such peak designated A' on Figure 1(b), while both pulses associated with B are equally large.
4. With a different focus there may be different numbers of lines per star and, depending upon the exact location of a star with respect to the raster lines as it drifts across the screen, the number of lines may change.
5. We must only transmit the location and magnitude of the peak video from each star since to transmit all the A and B signals would require too much bandwidth.
6. We do not know until after we have scanned a star how many lines are required to completely scan it and which line has the peak video.
7. A star with a diameter of one line spacing will have a video signal of a little under 200 nanoseconds duration. Therefore, although the output star field data is slow, on board processing must be fast.

We can infer from these conclusions that we cannot measure the xyz coordinates we need simply by measuring the time between video pulses and synchronizing pulses, thereby obtaining, for example, x_1 in Figure 1(b). The result would be incoherently jumbled data in excessive quantities. To pick a solution to the problem is not difficult, the difficulties occur in picking a solution compatible with the time, money and manpower available and with having to be incorporated in a balloon payload.

A completely detailed discussion of how x, y and z are measured in AIRO-scope is beyond the scope of this paper, but approaches to two problems are outlined here to indicate the general philosophy.

The interleaving problem is reduced if we look only at the data from one field in every frame. For example, referring to Figure 1(b), if we measure only that data in Field 1 of Frame A, we have not only reduced the number of video signals from 7 to 4, but, more importantly from the point of view of simplification, we have reduced the dispersion of the relevant signals from milliseconds to microseconds. However, using the data from only Field 1 of all frames could give rise to certain systematic errors, so we use alternate fields in each successive frame and average the data from them.

If we assume that the largest star image will overlap 5 scan lines, the process of using data from only one field per frame reduces the maximum number of video signals per star per frame from 5 to 3. We can further reduce the 3 signals to 2 by referring to Figure 2, which shows video signal groups from seven possible star/line overlap combinations. Figures 2(a), (b) and (c) are video signals from a star overlapped by three lines of a field. Figures 2(d) (e) and (f) are for two overlapping lines and Figure 2(g) is for a star scanned by only one line.

If there are the maximum of 3 video pulses per star in a field, the second one must be the largest, as is evident from Figures 2(a), (b) and (c), and would be the one we would want to use for an xyz measurement. If there are only 2 video pulses, either the first or second or both could be largest as shown in Figures 2(d), (e) and (f). If there is only one video pulse per star in a field, that is the one one must consider as in Figure 2(g). But we can always be assured of retaining the pulse we need if we adopt the rule that we consider the first one or two pulses per star and not

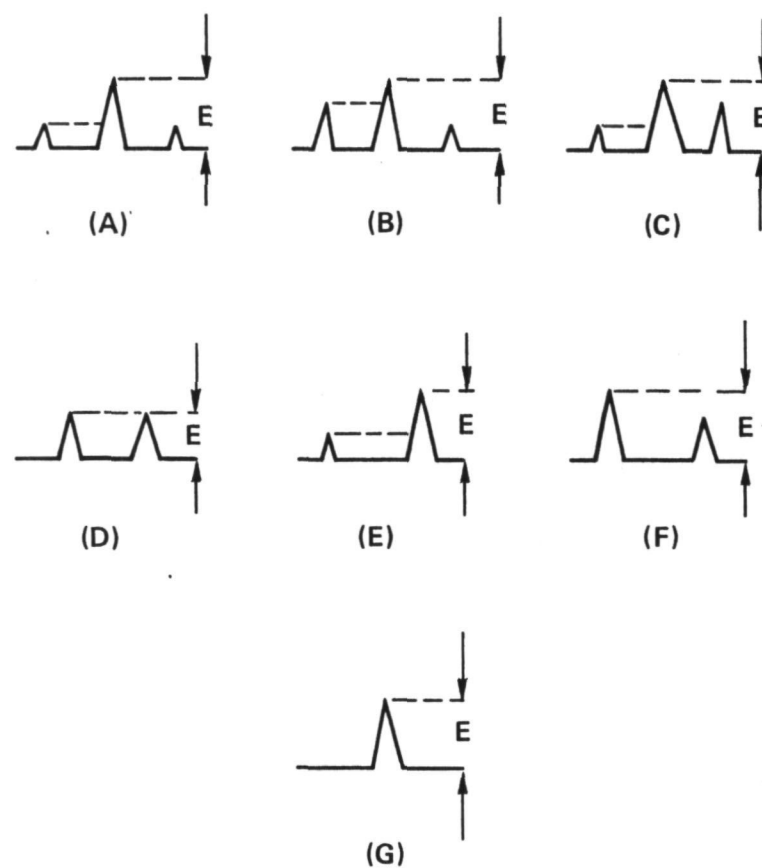


Figure 2. Peak sample and holding

use the third, if it exists. Electronically this can be implemented for the intensity or amplitude measurement z by using a peak sample-and-hold circuit as shown in Figure 2. The peak sampled-and-held voltages E , shown as dotted lines in Figure 2, are always a measure of the largest video signal when that exists.

In addition to the measurement of x , y and z coordinates the video signal conditioning system performs two other main functions - video thresholding and camera blemish suppression.

The video thresholding circuitry permits only video signals above a certain level to be measured. There are eight threshold levels, the minimum being just above the video channel noise level and the maximum being approximately half of full scale. The eight levels are remotely set by telemetered command from the ground and may be used to eliminate extra noise or limit the number of stars displayed.

The silicon intensified target tube has defects called blemishes, which are due to imperfections in the silicon target and their size is expressed in scan lines. For our camera, which uses a 525-line TV system, the blemishes range in size from 1 to 5 lines.

There are two kinds of blemishes - one which does not result in a signal when illuminated and one which produces a signal whether it is illuminated or not. The number of blemishes is small, there being perhaps 10 of each type for the quality of camera we have. The blemishes producing no signal are a minor problem because of their small area and the low probability that a star will image exactly on one of them. Even if this does occur the camera could be zoomed slightly to move the star off the blemish.

The approximately 10 blemishes that produce a signal are more troublesome since they have the effect of producing what look like stars on the ground CRT display. We plan to measure only ten stars and do not have the telemetry bandwidth capability to transmit ten stars plus ten blemishes. Therefore we must eliminate the effect of the blemishes on board the gondola. Since the location of the blemishes is fixed and can be measured, it is possible to arrange for the xyz measurements to be blanked while a blemish region is being scanned. The amount of effective area that must be blanked depends both on the spatial stability of the scanning circuitry in the camera and the accuracy and stability with which a given area can be blanked. We have not completed programming of the blemish blanking circuits, but we are hopeful that we can blank squares having sides of length typically 1% of the screen size. If we can do this, 10 blemishes would result in blanking out only one thousandth of the area of the screen. Again, by zooming slightly, a star could be moved out of one of these blemish regions if necessary.

GATE PATTERN GENERATOR

The purpose of the gate pattern generator is to allow the telescope/detector combination, with its 5 minute field of view, to track an IR source by forcing the boresighted TV camera to offset track a visible star somewhere in its 2 to 20° field of view. Figure 3 helps to show how this is done.

The important parts of the airborne portion of the video/gate system are shown in block diagram form in Figure 3(a). The airborne portion of AIROscope contains, of course, many other systems, but these have been omitted for purpose of clarity. Shown are the telescope and the boresighted TV camera, which has an electronics package whose outputs of interest here are the video signals from stars, blemishes and noise and the various raster synchronizing pulses.

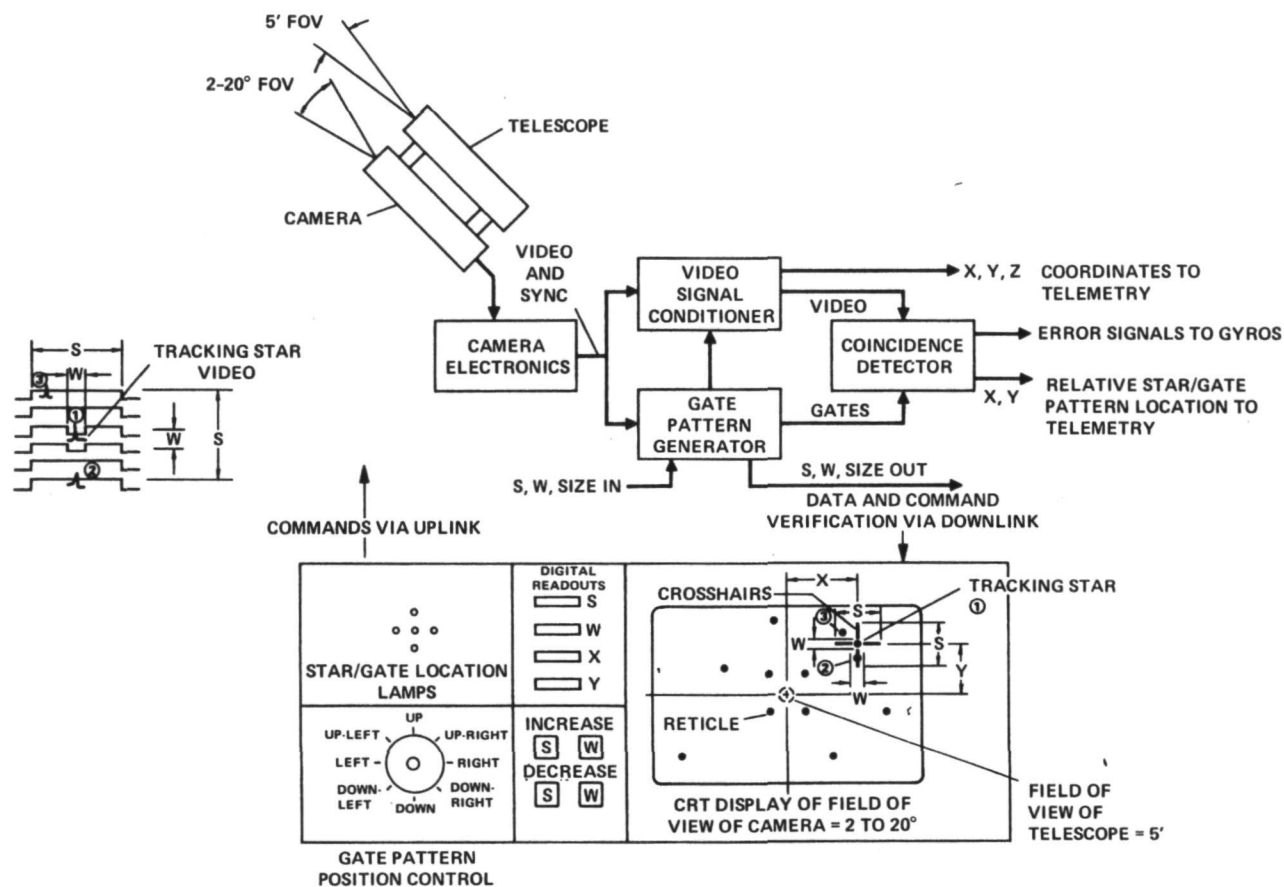


Figure 3. Offset tracking using gate generated crosshair

These outputs go to two systems. One is the Video Signal Conditioner, which digitizes the stellar brightness and location information and which was described earlier in this paper. The other is the Gate Pattern Generator. Each of these two systems has outputs going to a coincidence circuit whose outputs in turn provide error voltages and used to produce gyro correction signals so as to produce the desired tracking.

Figure 3(b) shows some of the ground based parts of the video/gate system. Again the AIROscope ground equipment contains many other systems, controls and displays not shown in Figure 3(b), but they have been omitted for purposes of clarity.

There is a cathode-ray-tube (CRT) display, some controls and some digital and lamp readouts. The CRT is shown displaying two types of data. First, there is an array of 10 stars shown as dots, whose location and brightness are derived from the xyz data measured by the video signal conditioner in the gondola and telemetered to ground. Second, there is a set of what we can refer to as crosshairs surrounding the star selected to be used for offset tracking. The crosshairs have dimensions S and W as shown and coordinates (X,Y,) with respect to the center of the CRT display. Note that the region in center of the CRT display is also the field of view of the telescope and that S, W, X and Y are controlled and monitored on the ground. The position of the crosshair, that is X and Y, is controlled by the joystick in Figure 3(b) and the crosshair can be moved to any location on the display by moving in any of 8 directions, UP, LEFT, UP-LEFT and so on. S and W can be increased or decreased by using the appropriate control shown in Figure 3(b) and X and Y can be read to about 0.2% on the displays shown. These readouts are in plus or minus degrees referred to the center of the display, with scaling provided to allow for camera zooming. W and S are also displayed, but to an accuracy of only 1%. The five-lamp display gives a more accurate indication of where the tracking star is with respect to the crosshairs than can be achieved by observing the oscilloscope. The center lamp comes on when the tracking star is in the center region of the crosshairs and the other 4 lamps come on appropriately to indicate other locations of the tracking star in the crosshair. Of course, in addition to the meter readouts, all quantities can also be monitored by observing the CRT display.

It should be noted that all meter and CRT displays are generated from signals telemetered to the ground from the gondola, not directly from the controls on the command/display console in Figure 3(b). This is intended to give the experimenter some degree of confidence that what he is trying to make happen in the gondola is, in fact, happening.

X, Y, S and W commands are telemetered up to the gondola for reasons other than to inspire confidence in the investigator. These quantities are used to generate a set of gates in the gondola such as are shown in Figure 3(c). Note that the X, Y, S and W commands are all dc-type signals such as "X go LEFT" and "INCREASE S", so that they are all low bandwidth signals and easy to telemeter with the many other commands in the AIROscope time-shared telemetry system. The gate signals they generate in the gondola involve, in some cases, submicro-second pulse-widths and could not be transmitted up with the AIROscope telemetry.

Note in Figure 3(c) that the dimensions of the gates generated in the gondola are designated X, Y, S and W as are the crosshair dimensions on the ground. On the ground CRT display X, Y, S and W have the dimensions of minutes of arc, but in the gondola the dimensions are microseconds, because the

generation of the gates occurs in time synchronization with the raster generated by the camera. The crosshairs on the ground are a readout of the location and size of the tracking gates generated in the gondola with respect to the camera raster.

Coincidences are performed in the gondola between the tracking star video signal from the camera and the XYSW gate pattern from the gate pattern generator as indicated in Figure 3(c), where a typical set of coincidences is shown. In practice only one star is allowed in the gate pattern at any one time and the tracking mode can be switched out until X, Y, S and W have been adjusted to achieve this, which prevents confusing the tracking gyros. Figure 3(c) therefore shows different locations of the same star in the gate pattern.

With the tracking star video located in time such that it appears in time location 1 in Figure 3(c), the ground display would show the tracking star in the center of the crosshair. Because the star is in the "W" region of the crosshairs, no correcting signal is applied to the gyros and the telescope pointing is unchanged.

If the tracking star were located in time location 2 in Figure 3(c), it would appear in location 2 in the ground displayed crosshair region. Further, because of the coincidence between the star video signal and the gate pattern shown in Figure 3(c) an error signal is generated which forces the telescope and camera to move in a direction that will drop the star video into the gate hole W, where correction signals do not exist.

Similarly the coincidence occurring at location 3 in Figure 3(c) produces error signals which force the tracking star video into the center of the gate region in the gondola and the tracking star display into the center of the crosshairs on the ground.

With maximum zoom the camera field of view is about 120 minutes and W can be set to be as little as 1/240th of that or 0.5 minutes of arc. If the tracking star tries to wander outside this 0.5 minute region it is forced back in by correction signals generated by the gate pattern signal/star video coincidence.

Since the experimenter can move the gate pattern around by adjusting X, Y, S and W and observing the crosshair on the ground display, he can position any star selected as the tracking star on the display somewhere in the crosshair region and it will automatically drop into the center of the crosshair display. If the experimenter now adjusts X and Y, that is moves the crosshair, the whole star field displayed on the ground will move as well. If the coordinates of an IR source, not visible to the TV camera and therefore not displayed on the ground, are known with respect to the tracking star, the tracking star can be moved using the gate pattern X and Y controls so as to position the IR source in the center of the CRT display. This also places it in the center of the field of view of the TV camera and in the field of view of the telescope.

In addition to the mode described in which tracking depends on video/gate coincidences, it is possible to switch to a mode in which the gates can be moved through the star field without generating any error signals. Tracking on a visible star with a conventional non-offset tracker and manual tracking modes are also available.

Since the diurnal motion results in a circular motion of the stellar source about the IR source the gate location must be updated by changing X and Y. This can be done with an onboard timer, but also, as in the case of the current AIROscope, by manual command.

The principle used to generate the offset tracking gates may be illustrated with the help of Figure 4. Figure 4(a) is a block diagram of the

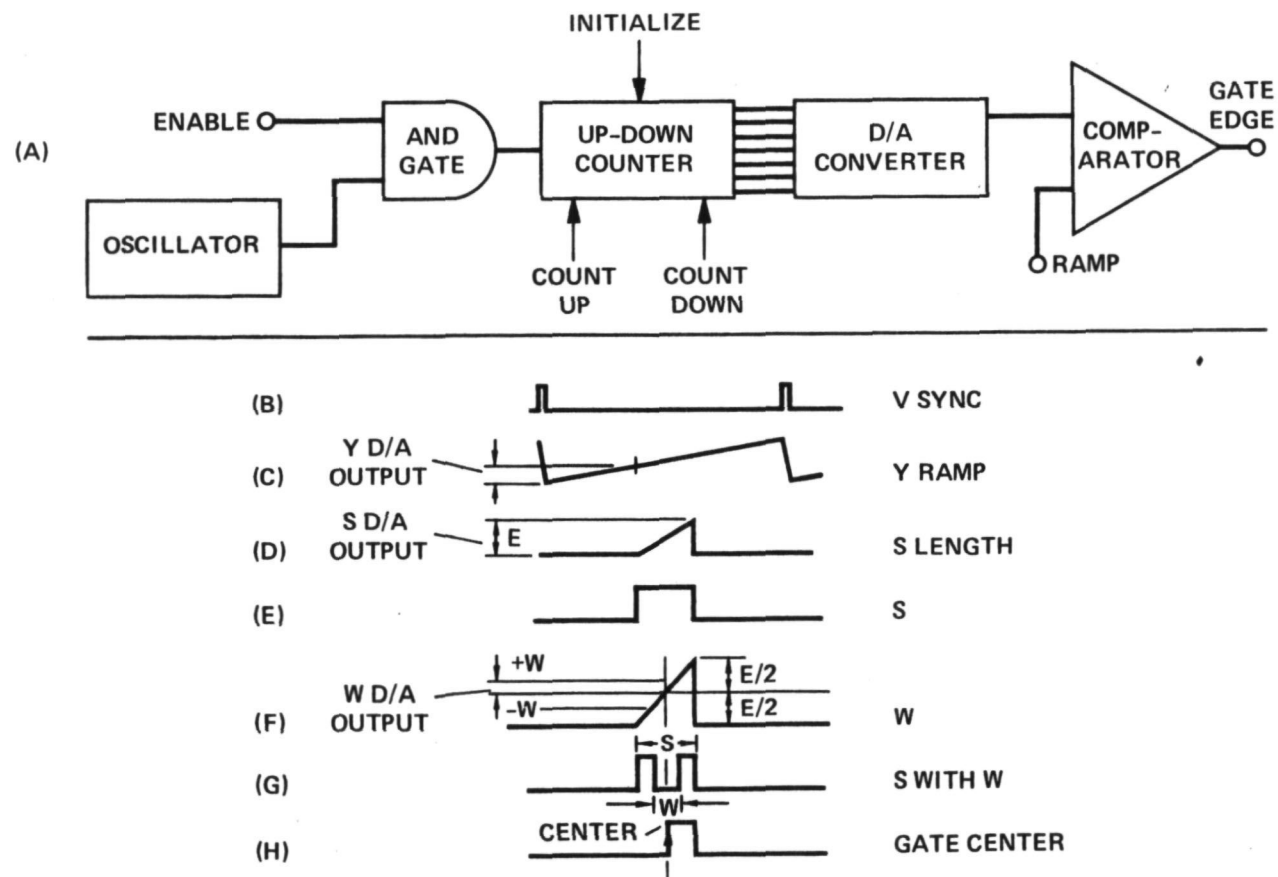


Figure 4. Gate generation

electronics required to generate a typical gate edge and the leading and trailing edges of both S and W gates are generated using similar circuitry. The horizontal and vertical gates used to produce the crosshair pattern are similar to each other, except that the horizontal circuitry is much faster because a vertical sweep takes about 16 milliseconds compared with a horizontal sweep which takes only about 58 microseconds.

An initialize command in the form of a 5-V level change is transmitted to the gondola to set an initial gate position and size. When this command is sent an observer viewing the CRT display in Figure 3(b) would see the gate pattern become centered on the screen with $S=64$ lines and $W=20$ lines. This display is the result of signals telemetered to the ground from the gondola so that a round trip check is provided.

The initialize command is entered into an up-down counter as in Figure 4(a), which causes the counter to feed a preselected count into a digital-to-analog (D/A) converter. The effect of the initialize command is therefore to produce a previously determined voltage at the output of the D/A converter and at the input of the comparator of Figure 4(a).

The other input of the comparator is fed with a ramp such as that in Figure 4(c), which is a sawtooth waveform synchronized with, in the case shown, the vertical sync pulses of Figure 4(b). When the voltage on the ramp input of the comparator equals the preselected Y D/A output voltage on the other input two things happen. A second ramp is started as in Figure 4(d) and the leading edge of S is generated as in Figure 4(e). The second ramp in Figure 4(d) is allowed to sweep up until it reaches a second preprogrammed, preselected level E derived via an S D/A converter from an S up-down counter. At this point the ramp in Figure 4(d) is reset and the trailing edge of S is generated, resulting in the S gate of Figure 4(e). The Y and S up-down counters are preprogrammed in such a way that, in response to an initialize command, waveform S in Figure 4(e) is exactly centered between the vertical sync pulses in Figure 4(b), thereby placing the vertical component of the crosshair in Figure 3(b) in the center of the CRT display.

The W portion of the crosshair display again uses an up-down counter, a D/A converter and a comparator system. The W D/A converter is preset by initializing an up-down counter producing a predetermined voltage $+W$ from which $-W$ is derived so that both plus and minus W are available simultaneously. The ramp in Figure 4(d), whose amplitude is E, is offset by exactly $E/2$ and compared with the $+W$ and $-W$ voltages as in Figure 4(f). The resulting comparator outputs are used to generate a hole in the S waveform of Figure 4(e), resulting in the waveform in Figure 4(g). It is the waveform of Figure 4(g) that is used to generate the vertical component of the crosshair of length S with blanked center portion W in Figure 3(b).

In order to measure the position of the gate for display on the Y digital readout in Figure 3(b) the gate center is required. This is shown in Figure 4(h) and is readily obtained by level comparison from the waveform in Figure 4(f).

In order to change the location of the gate pattern the Y up-down counter is placed in the count-up mode to move down, or the count-down mode to move up, and fed with pulses from the oscillator of Figure 4(a). This changes the D/A reference voltage level at the comparator input and causes the comparison shown in Figure 4(c) to slide right or left, thereby moving the S gate with respect to the vertical sync pulses and the crosshair with respect to the stellar display in Figure 3(b). From the waveforms in Figure 4 it is evident that this motion of the S gate does not result in a change in the lengths W

and S. They are changed by up-down counting of the W or S counters. The gate pattern location and W and S may all be changed independently. S and W are in fact increased or decreased by holding down the appropriate command button in Figure 3(b), and the gate position is changed using the command joystick on the same figure. All these commands result in logic inputs to the up-down counters in the gondola.

For the Y or vertical component of the crosshair we have described the need for Y, S and W up-down counters, Y, S and W D/A converters and Y, S and W comparators. It is only necessary to add an X counter, converter and comparator to generate the X horizontal component of the crosshair, since the S and W circuitry are common to both X and Y directions.

The crosshair can be moved to any region of the CRT display at either 1 or 10 lines per second and stops are provided to prevent it going offscreen. Dimension S can be varied over a range of 5 to 64 lines and W from 2 to 20 lines, both at 1 line per second.

SUMMARY

A system for providing ground display of a star field and offset tracking has been described, which uses a modified standard TV camera as its input. The star field information is telemetered accurately over long distances from a relatively low power transmitter by using digital bandwidth reduction techniques. Offset tracking is accomplished by forcing a selected tracking star into the center of a gate/crosshair system by means of which the tracking star can be moved to a predetermined location so as to position the source under study in the center of the telescope field of view.

ACKNOWLEDGEMENTS

The principle of offset star tracking using a coincident gate system to generate error signals was suggested by Charles Swift of the Astrophysics Branch at Ames Research Center.

DISCUSSION SUMMARY — PAPER 4.5

In answer to questions about the sensitivity of the television camera, it was noted that the system is expected to be able to guide on stars as faint as eighth magnitude. Since there are, on the average, 0.25 eighth magnitude stars per square degree and the smallest field-of-view is two-degrees across there would usually be a bright enough star in the field-of-view. In cases where this is not true, the zoom capability (to twenty-degrees) would presumably bring an eighth magnitude star into the field-of-view.

A number of questions about details of the camera and the responses are summarized below:

Q. What is the power consumption of your camera?

A. Thirty watts.

Q. Has the SIT been tested in the balloon environment?

A. It has not been tested by us, but the camera manufacturer gave the whole camera an environmental test. It is hermetically sealed in an enclosure at one atmosphere pressure.

Q. Is the TV system being constructed here and what is its cost?

A. The TV acquisition and stabilization system was designed and built at Ames. The electronics are completed. The cost of the parts for the electronics was \$7500 and for the camera itself, \$22,000. The latter includes the cost of the tube which was \$6000. It was pointed out that cheaper tubes are available. The cost of the tube depends inversely on the number of blemishes.

Q. What is a blemish?

A. A blemish is a defect in the silicon lattice which is used in the intensification process in the tube. There are two kinds of blemishes. One kind fails to give you a signal when you illuminate it. The other kind gives you a signal whether you illuminate it or not.

Q. How many bits of information are used to determine brightness of stellar images?

A. We transmit 10 bits, but we can't use that many because the cathode ray tube is the limiting factor, probably at 64 to 1.

Q. What is the deadband of the servo control?

A. It is about a half a minute of arc.

PAPER 4.6

THE AIROSCOPE POINTING AND STABILIZATION SYSTEM

James P. Murphy
Kenneth R. Lorell
Ames Research Center

ABSTRACT

The AIROscope pointing and stabilization system is described. The system is configured with three gimbal axes and rate integrating gyro stabilization to provide a stable platform for infrared astronomy. Error signals for on and off-axis pointing are derived from a video sensor which also drives a ground station display. Other features of the system include direct drive torque motors and electronic suspension damping. Results of analysis and simulations used to design the control loops, and a pointing error analysis are presented.

INTRODUCTION

The AIROscope pointing and stabilization system has been designed to allow a variety of infrared investigations. The system has the capability to scan selected sky regions and to point for extended periods of time at visible infrared (IR) objects (on-axis pointing) or at IR objects that have no visible counterpart (off-axis pointing).

Key features of the system hardware include rate integrating gyro (RIG) stabilization of three gimbal axes; azimuth, elevation and cross elevation. Direct drive dc torque motors control the elevation and cross elevation axes, and a dc torque motor and tachometer are used for suspension damping and control of the azimuth axis. A unique video sensor and associated electronics provide error signals for on and off-axis pointing. A control panel in the ground station commands the pointing and stabilization system and includes a CRT display for presentation of the video sensor output and a joystick for commanding slew rates to the elevation and cross elevation RIG's.

The system has two primary pointing modes that can be selected at the ground station, manual and TV auto. In the manual mode, the CRT display and joystick are used to control pointing of the telescope; in the TV auto mode, error signals from the video sensor control the pointing of the telescope. While pointing accuracy in the manual mode depends on the ability of the operator, the system has the capability to move minutes of arc in a controlled fashion. In the TV auto mode for on-axis pointing, pointing accuracy is expected to be less than 0.51 arc minutes, and for off-axis pointing, pointing accuracy is expected to be less than 1.29 arc minutes for time periods up to 1 hour.

SYSTEM CONFIGURATION

The system has been configured to satisfy the requirements of infrared astronomy. Since off-axis pointing is essential, the effect of gondola

disturbances on the rotation of the telescope axis is important. While a simpler two gimbal platform (Greeb et. al., 1974) could have been used, a three gimbal platform, with RIG stabilization for each gimbal axis, was selected to provide better isolation of the telescope from suspension and gondola disturbances such as pendulation. Figure 1 shows the AIROscope gimbal arrangement and the location of the primary pointing and stabilization hardware on the azimuth, elevation and cross elevation gimbals.

The mounting location of the RIG's on the gimbals has been chosen as a compromise between complexity and performance. All three RIG's could have been mounted on the telescope to provide complete stabilization similar to an inertial platform, however, this would require a complex coordinate transformation to derive the error signals to drive the torque motors. In addition, a singularity would exist when the cross elevation and azimuth axes are parallel at low elevation angles. Consequently, the elevation and cross elevation RIG's are mounted on the telescope, and the azimuth RIG is mounted on the azimuth gimbal. The RIG's chosen for the system are surplus units which can be trimmed electronically to have drift rates below 1 degree/hour and which have a noise level of 2 to 3 degrees/hour rms.

Direct drive dc torque motors supply control torques for the three gimbal axes. Even though direct drive torque motors require more power than geared dc torque motors, the direct drive motors allow more isolation from gondola disturbances and better pointing stability. A toothless gear train has been used (Freckler, 1968) in a previous balloon system to eliminate the backlash associated with standard gears, however, the gimbals are still directly coupled to the gondola because of the necessity to accelerate the gear train. With the direct drive motors, the only coupling to the gondola is through bearing stiction and motor back-emf. Pairs of dc direct drive motors are utilized for both the elevation and cross elevation axes to reduce the effect of mechanical resonances (Freckler, 1968). A single dc torque motor is used for azimuth and torques against the suspension. Since the suspension acts as a lightly damped spring inertia system, a tachometer is used to measure the relative rate between the suspension and gondola, and control logic is implemented which increases the damping of the suspension.

The primary attitude sensor for the system is a unique video sensor whose error signals control the elevation and cross elevation RIG's for the TV auto pointing mode and provide information for the CRT display in the ground station. A complete description of the video sensor system is given by Deboo et. al. (1974). As a backup to the video sensor, a star tracker is available which can be used for on-axis pointing. Alignment of the video sensor and star tracker to the telescope is done prior to flight and experience has shown that the alignment can be accomplished and held during flight to within 0.5 arc minutes (Scott, 1974). While the primary reference for the azimuth gimbal is a RIG, it is not a satisfactory long term attitude reference. Consequently, a compass is mounted on the azimuth gimbal and a readout of azimuth attitude with respect to magnetic north is provided in the ground station.

A control panel in the ground station is used to command the pointing and stabilization system and includes a visual presentation of the video

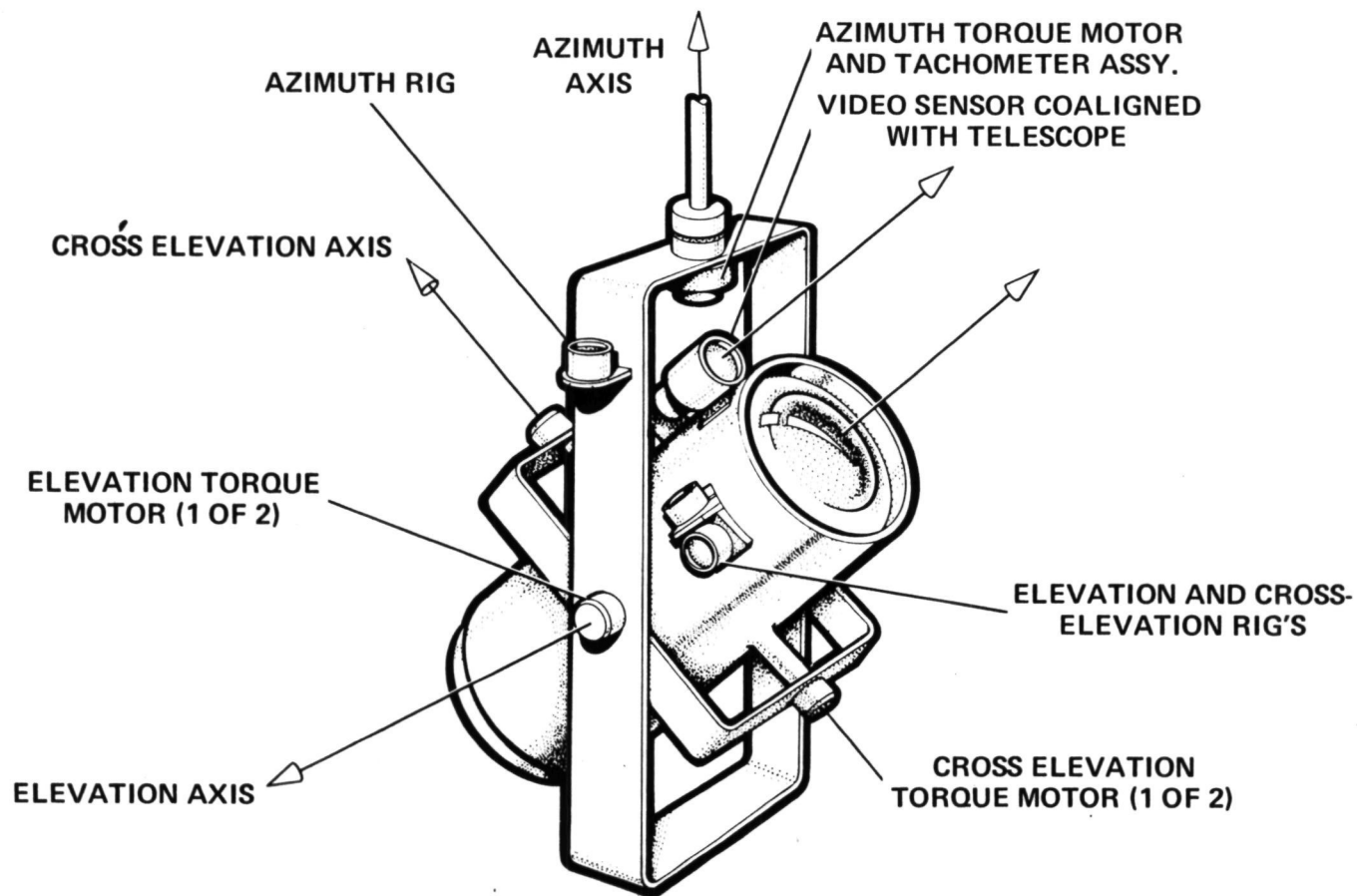


Figure 1. AIROscope Gimbal Configuration

sensor output. A joystick commands slew rates to the elevation and cross elevation RIG's for manual pointing, and is used with the TV auto mode to control the gate positions in the video sensor's gate electronics. A rotary switch selects the pointing modes and thumbwheel switches control the selection of bias currents for compensating the RIG drifts. A thumbwheel switch also commands the desired azimuth attitude.

AZIMUTH CONTROL LOOP

Coarse acquisition of IR targets is accomplished by slewing the azimuth gimbal with reference to magnetic north. Once the gimbal has stabilized at the commanded angle, a stabilization mode, which isolates the telescope from axial motion of the balloon and suspension, commences. Small adjustments (approx. 1.5° - 2°) may be made during stabilization but the control must be returned to the slew mode for large angle changes. The primary attitude sensor is a RIG, located on the gimbal, whose sensitive axis is coincident with the azimuth axis. A reference to the earth's magnetic vector is provided by a magnetic compass.

The design of the azimuth gimbal pointing and stabilization loop was influenced by a number of considerations arising from both the disturbance-torque environment in which the system operates, and the system configuration. Primary among these are the need to damp the motion of the suspension and to compensate for the combined effects of balloon rotation and bearing friction, both viscous and static. Additional design constraints derive from the need to decouple the motion of the suspension from the gondola as much as possible during stabilization and to provide an angular reference during the slew mode.

There are two major physical phenomena with which the azimuth controller must contend: first, disturbances transferred from the suspension to the gondola through the azimuth gimbal bearing; and second, the large amplitude oscillations of the suspension excited by torque motor impulses. At float altitude, the balloon attains a relatively steady state rotation, the sense of the spin being unpredictable, of $.25^{\circ}/\text{sec}$ to $1.0^{\circ}/\text{sec}$ (Morris, 1969), which results in a steady rotation of the suspension as well. This motion of the suspension is translated into a relatively constant body-fixed torque on the gondola azimuth axis through the action of viscous bearing friction, damping terms in the control law, torque motor back-emf and the non-negligible amount of stiction in the bearing (Nidey, 1969, Nidey, 1966). The use of a conventional rate-plus-position control law to stabilize the azimuth gimbal, while providing adequate damping and slewing control, results in steady-state errors in the commanded azimuth angle proportional to body-fixed moments applied to the gondola. Therefore, in order to maintain little or no offset, some additional compensation is necessary.

Control torque along the axis of the azimuth gimbal is provided by a torque motor acting directly against the cables used to suspend the gondola from the balloon. The suspension behaves like a very lightly damped torsional spring-mass system when excited by the azimuth torque motor. In order to keep from "wrapping up" the suspension (i.e., causing the cables to cross, thus reducing the effective spring constant to zero) and eliminate

the large oscillations that result from torque pulses, a control law that includes terms to damp motion of the suspension should be employed.

Precise pointing of the telescope requires that the effects of disturbances to the gondola be minimized. Thus, during the stabilization mode, it is desirable to decouple the gondola from the suspension as much as possible. This is in contrast to the requirement that the suspension be damped to avoid wind-up and large-amplitude oscillations. Therefore, the controller should be mechanized in a way that provides two levels of suspension damping in order to satisfy both slewing and stabilization requirements.

For reasons discussed earlier, a RIG was selected as the primary attitude sensor for use during stabilization. It would be desirable to use the RIG as the attitude sensor during the slew mode as well, thereby conserving weight, power, and complexity. However, most RIG's have only limited (usually less than 10°) motion about the sensing axis precluding their use for slewing through large angles. Thus, an additional consideration is the modification of the characteristics of a RIG during acquisition of targets through large angles.

Figure 2 shows the AIROscope gondola suspended from the balloon by two cables 55.8m in length. The axial reaction moment of the suspension-gondola system is a function of the cable length L , the gondola mass m , the angle through which the suspension is twisted relative to the balloon θ_r , and the distance separating the two cables d .

$$\text{Thus} \quad K_\theta = \frac{2mgL}{\theta_r^2} \left[1 - \left(1 - \frac{d^2}{L^2} \sin^2 \frac{\theta_r}{2} \right) \right]$$

where K_θ

represents the classical spring "constant." A curve of K_θ vs. θ_r assumes the shape of a parabola with the maximum occurring around $\theta_r = 0$. For the purposes of this analysis, K_θ will be considered a constant, its value calculated at $\theta_r = 45^\circ$. A design goal is to constrain θ_r from exceeding $\pm 30^\circ$.

A simple model of the system to be controlled is illustrated in figure 3.

For a linear system:

$$J_1 \ddot{\theta}_1 = -K_\theta \theta_1 - K_B (\dot{\theta}_1 - \dot{\theta}_2) - M_C + M_{D1}$$

$$J_2 \ddot{\theta}_2 = -K_B (\dot{\theta}_2 - \dot{\theta}_1) + M_C + M_{D2}$$

A conventional method of providing damping for the suspension would be to use $\dot{\theta}_1$ as part of the control law. Although it is not practical to measure $\dot{\theta}_1$ directly, by putting a tachometer on the torque motor shaft, $\dot{\theta}_2 - \dot{\theta}_1$ can be measured. θ_2 and $\dot{\theta}_2$ are available from the sensor on the azimuth gimbal, so a rate-plus-position linear control law would give:

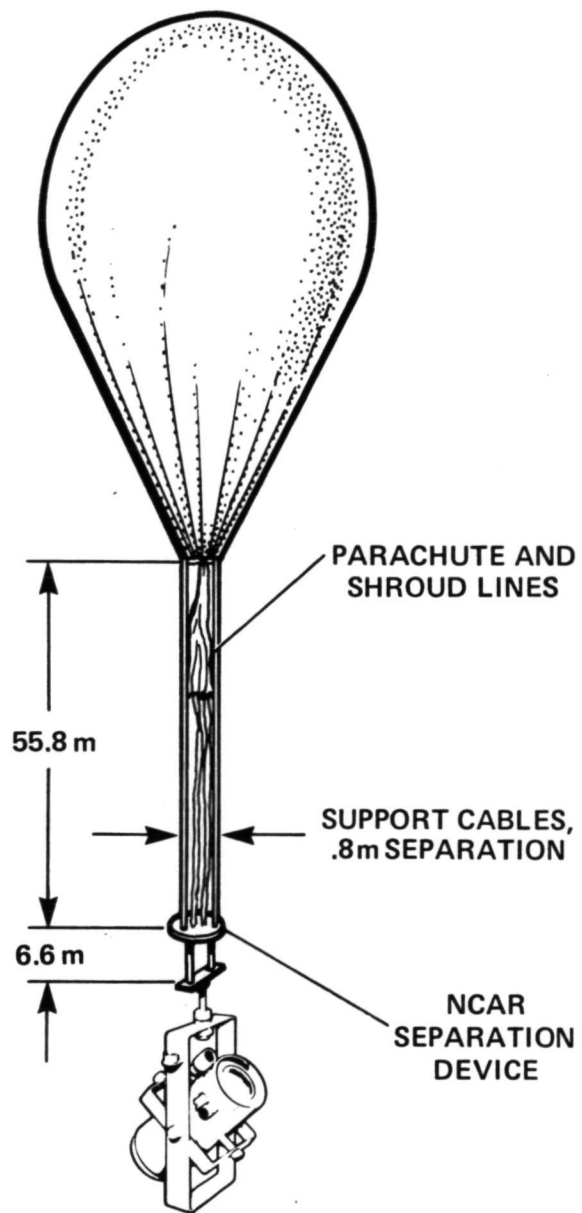


Figure 2. AIROscope Suspension Configuration

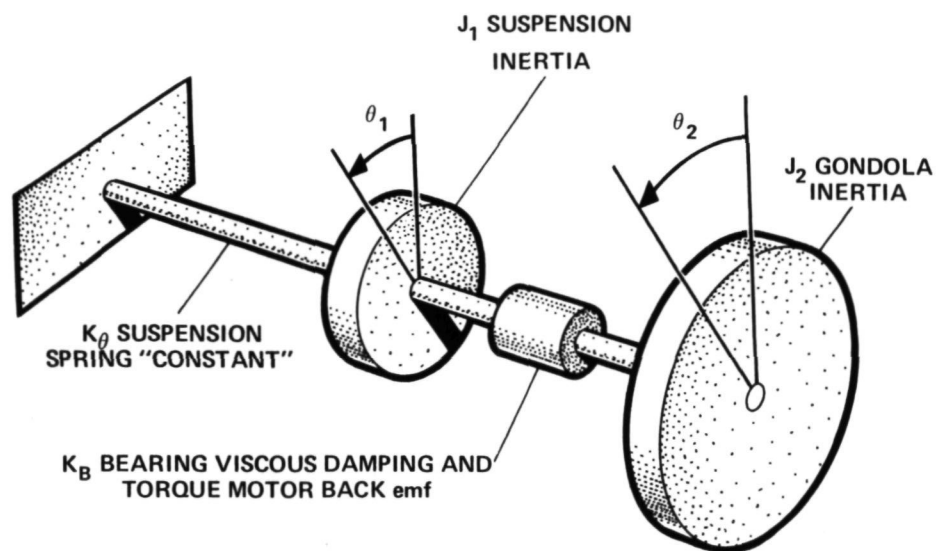


Figure 3. Simple Dynamic Model of AIROscope Suspension Coupled to Gondola

$$J_1 \ddot{\theta}_1 + (K_B + K'_B) \dot{\theta}_1 + K_\theta \theta_1 = (K_B + K'_B + K_V) \dot{\theta}_2 + K_P \theta_2 + M_{D1}$$

$$J_2 \ddot{\theta}_2 + (K_B + K'_B + K_V) \dot{\theta}_2 + K_P \theta_2 = (K_B + K'_B) \dot{\theta}_1 + M_{D2}$$

We can control suspension damping through K'_B and adjust the azimuth damping coefficient through $(K_B + K_V)$. The response of the two systems cannot be controlled arbitrarily because of the coupling, so gain selection requires a compromise between fast response of the gondola and adequate damping of the suspension.

The steady-state rotation of the balloon may be modelled as a ramp torque acting on the suspension. Bearing stiction is a disturbance of fixed magnitude whose sign depends on the sign of $(\dot{\theta}_1 - \dot{\theta}_2)$. So,

$$M_{D1} = K_\theta (K_R t) - \text{SGN}(\dot{\theta}_1 - \dot{\theta}_2) M_S, \quad M_{D2} = \text{SGN}(\dot{\theta}_1 - \dot{\theta}_2) M_S$$

Substituting M_{D1} and M_{D2} into the equations above and Laplace transforming them, we can obtain steady-state solutions for θ_1 and θ_2 .

$$\theta_1(t \rightarrow \infty) \rightarrow \infty$$

$$\dot{\theta}_1(t \rightarrow \infty) = K_R$$

$$\theta_2(t \rightarrow \infty) = \frac{(K_B + K'_B) K_R + M_S}{K_P}$$

As expected, the quality of the bearing between the suspension and the azimuth gimbal is a major factor influencing the pointing performance of the system. If an estimate of the offset torque $(K_B + K'_B) K_R + M_S$ could be made, it would be possible to eliminate the offset.

In order to provide azimuth rate and position information during the slew mode, some form of reference other than the azimuth gimbal RIG must be used for reasons stated earlier. A rate gyro whose output is integrated to provide position will satisfy this requirement. However, rather than add a rate gyro to the system, the RIG may be made to behave like a rate gyro by electronically closing the loop between its output-axis position pick-off and torquer. By selecting K_G in

$$J_3 \ddot{\phi} + K_Z \dot{\phi} + K_G \phi = \dot{\theta}_2 H$$

so that the gyro has the appropriate step response as well as steady-state error to ramp inputs as given by

$$\epsilon(t \rightarrow \infty) = \frac{K_Z}{K_G} \cdot K_a,$$

(where K_a is an arbitrary constant acceleration), a rate gyro of relatively low but sufficient bandwidth for this system is produced.

Angular reference is provided by integrating the output of the rate gyro. A digital integrator, consisting of a voltage-to-frequency converter, an up-down counter, and a digital to analogue converter is employed. This mechanization has the advantages of low drift, wide dynamic range, and the capability of accepting command angle inputs directly from the command system.

When a two mode system is used, mode I for slewing to the commanded azimuth angle and mode II for stabilization, the problems of dual suspension damping coefficients and RIG vs. rate gyro operation are alleviated. While slewing, a large damping coefficient K_{B1} is provided to keep the suspension motion relatively subdued. The RIG gimbal is always nulled by closure of the pickoff-torquer loop converting it to a rate gyro. An integrator connected to its output supplies the attitude reference. After $\dot{\theta}_2$, the angular velocity of the azimuth axis measured by the rate gyro, has remained below some low threshold value for an appropriate length of time, the controller can be switched to mode II for stabilization.

In mode II operation, the damping gain for the suspension can be decreased by an order of magnitude (K_{B2}) to give adequate damping for the low levels of torque motor activity while improving the isolation of the suspension from the gondola. The gyro is returned to the RIG configuration by disconnecting the gain K_G . Control signals are taken from the RIG output and compensated by a lead-lag network.

A conventional controller would also bypass the integrator, since its output is no longer necessary with the RIG in the loop. However, such a system with the integrator disconnected will exhibit a steady state error in mode II of up to 6° for a balloon rotation rate of $.6^\circ/\text{sec}$ and typical values of K_B , K_{B2} , K_p and M_S . This is clearly unacceptable in view of the $\pm 10^\circ$ angular freedom of the cross elevation gimbal.

An earlier equation shows that $K_p \theta_2(t \rightarrow \infty) = (K_B + K_{B1}') K_R + M_S$, or that the steady state value of the position error signal is an estimate of the disturbing moment. Further, the value of θ_2 stored in the integrator subtracted from the commanded azimuth angle represents the pointing error of the control system attained during mode I. Thus, two changes to a standard control loop can correct this pointing offset. First, after the integrator input is disconnected, the integrator output is retained as part of the control signal. Second, the output of the RIG, which in mode II supplies position information, can be biased with the error value of $\theta_2(t \rightarrow \infty)$ stored in the integrator in order to point the gondola back towards its original commanded azimuth angle. If $\theta_2^I(t \rightarrow \infty)$, $\theta_2^{II}(t \rightarrow \infty)$ represent the steady state values of θ_2 at the end of modes I and II respectively, then

$$\theta_2^I(t \rightarrow \infty) K_{p1} = (K_B + K_{B1}') K_R + M_S$$

and

$$\theta_2^{II}(t \rightarrow \infty) K_{P2} = (K_B + K'_{B2}) K_{R+M_S} - \theta_2^I(t \rightarrow \infty) K_{P1} - K_{P2} \theta_2^I(t \rightarrow \infty)$$

so that

$$\theta_2^{II}(t \rightarrow \infty) K_{P2} = (K'_{B2} - K'_{B1}) K_R - K_{P2} \theta_2^I(t \rightarrow \infty)$$

By the addition of a sample-and-hold device, the only component not required in a conventional controller without the pseudo-integral control feature, the steady state value of the suspension rotation rate K_R can be obtained to compensate for the change in the damping value from K'_{B1} to K'_{B2} . This addition produces

$$\theta_2^{II}(t \rightarrow \infty) K_{P2} = (K'_{B2} - K'_{B1}) K_R - (K'_{B2} - K'_{B1}) K_{R(\text{measured})} - K_{P2} \theta_2^I(t \rightarrow \infty)$$

or $\theta_2^I(t \rightarrow \infty)$ is biased to an equal and opposite value of the mode I pointing error.

Figures 4, 5, 6 illustrate the details of the azimuth controller. Figure 4 is a block diagram of the system showing the switches required to implement two-mode operation. Figure 5 is a simulated response of θ_2 to a 10° step slewing command. Note the 20-second timeout for $\dot{\theta}_2$ below the $.05^\circ/\text{sec}$ threshold and the correction of the attitude error in mode II. In Figure 6, θ_1 is shown for the same case of a 10° step slew command. The behavior is well damped at all times and does not exhibit the large angular excursions usually associated with slewing torques. Transition to mode II is characterized by a transient disturbance which is quickly removed with the K'_{B2} damping term. The steady state motion of the suspension is indicated by a line whose slope is K_R .

ELEVATION AND CROSS ELEVATION CONTROL LOOPS

The elevation and cross elevation control axes are identical except that cross elevation has a smaller inertia. In the manual pointing mode, slew commands enter the control axes as RIG torquing currents commanded with the joystick in the ground station. For the auto pointing mode, torque commands are provided to the RIG's from the video sensor. The output of the RIG is demodulated, filtered and then enters the RIG stabilization loop compensation. The control signal is then converted to a high power signal in the power amplifier and used to drive the torque motors. Figure 7 shows a block diagram of the elevation control axis. Simulations have been performed to design and evaluate the performance of the elevation and cross elevation control axes.

Figure 8 shows a bode plot of the RIG stabilization loop. The compensation is designed so that the open loop bode plot has a crossover frequency midway between the estimated mechanical natural frequency of the gimbal and telescope, and the estimated frequency of the pendulation disturbances. The compensation is complex and includes an electronic integration. Figure 9 shows a response of the RIG stabilization loop to

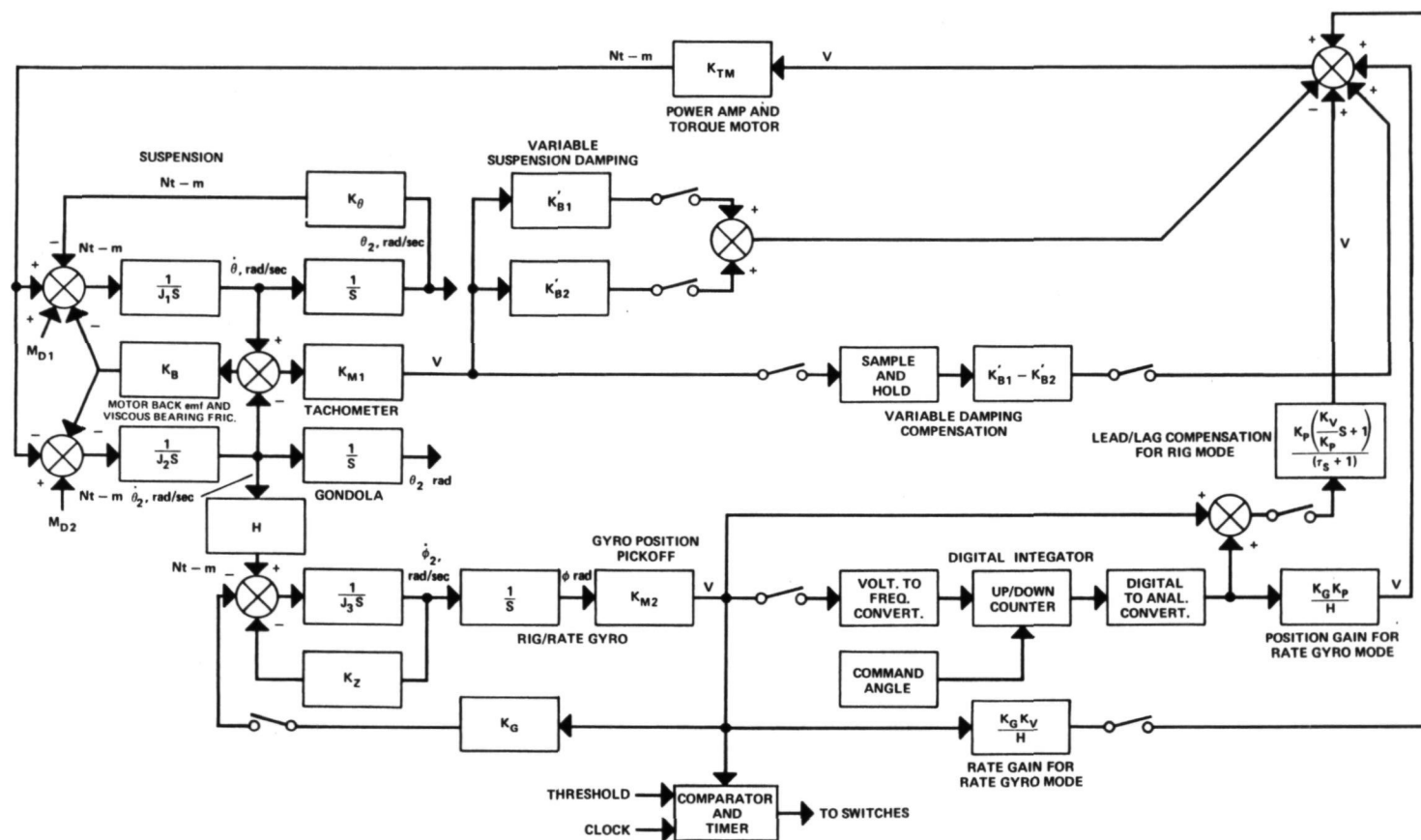


Figure 4. Azimuth Control System Block Diagram

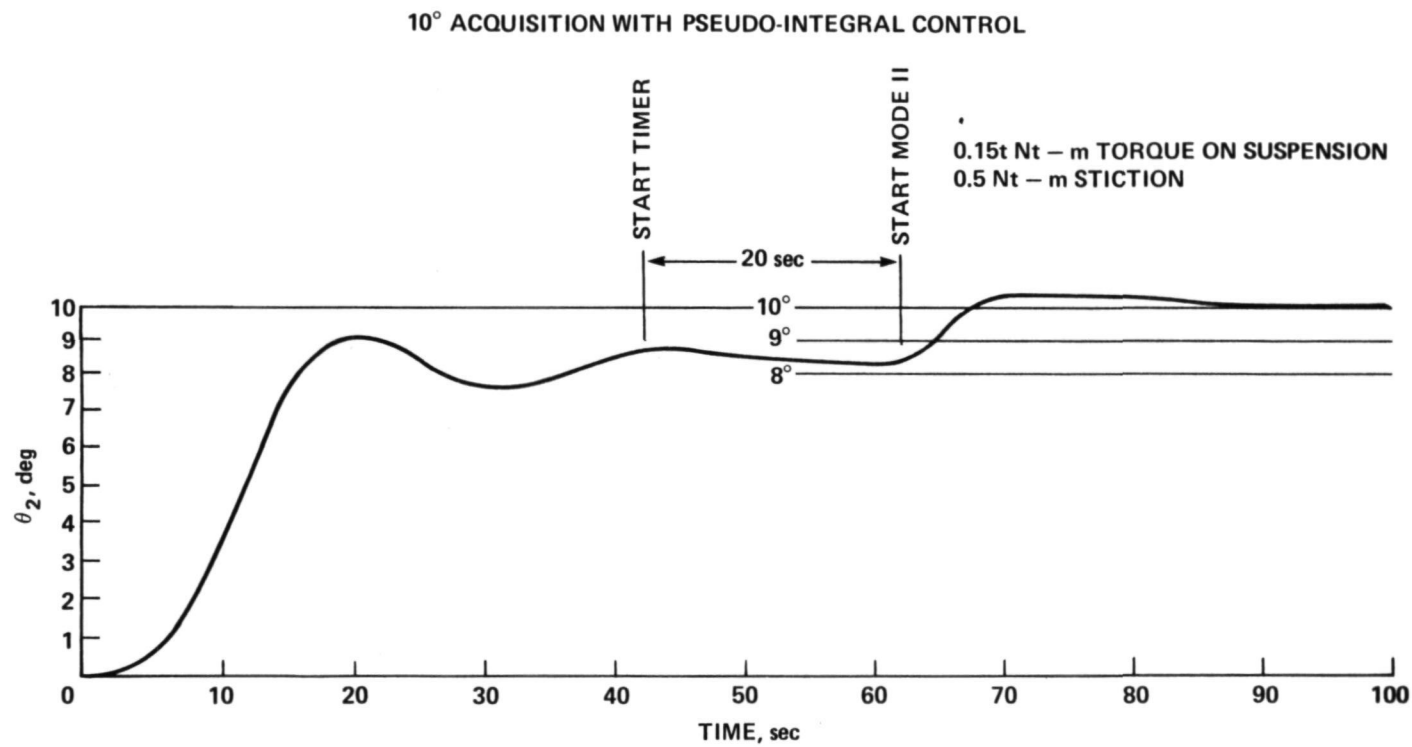


Figure 5. θ_2 versus Time

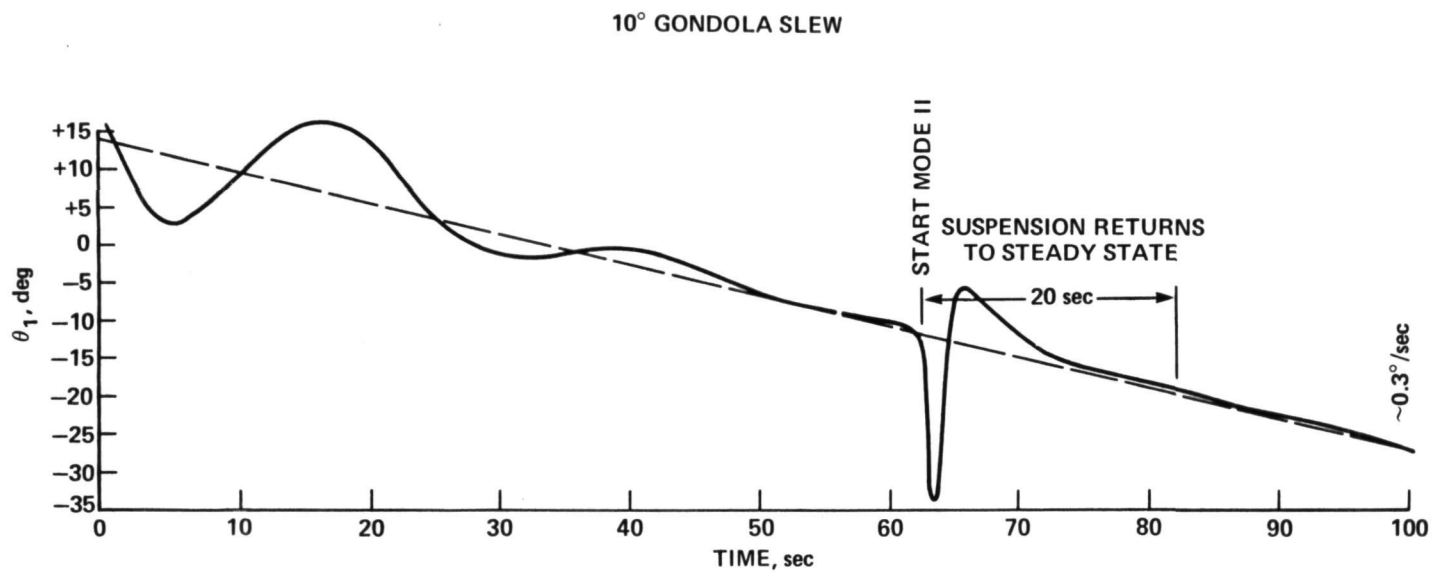


Figure 6. θ_1 versus Time

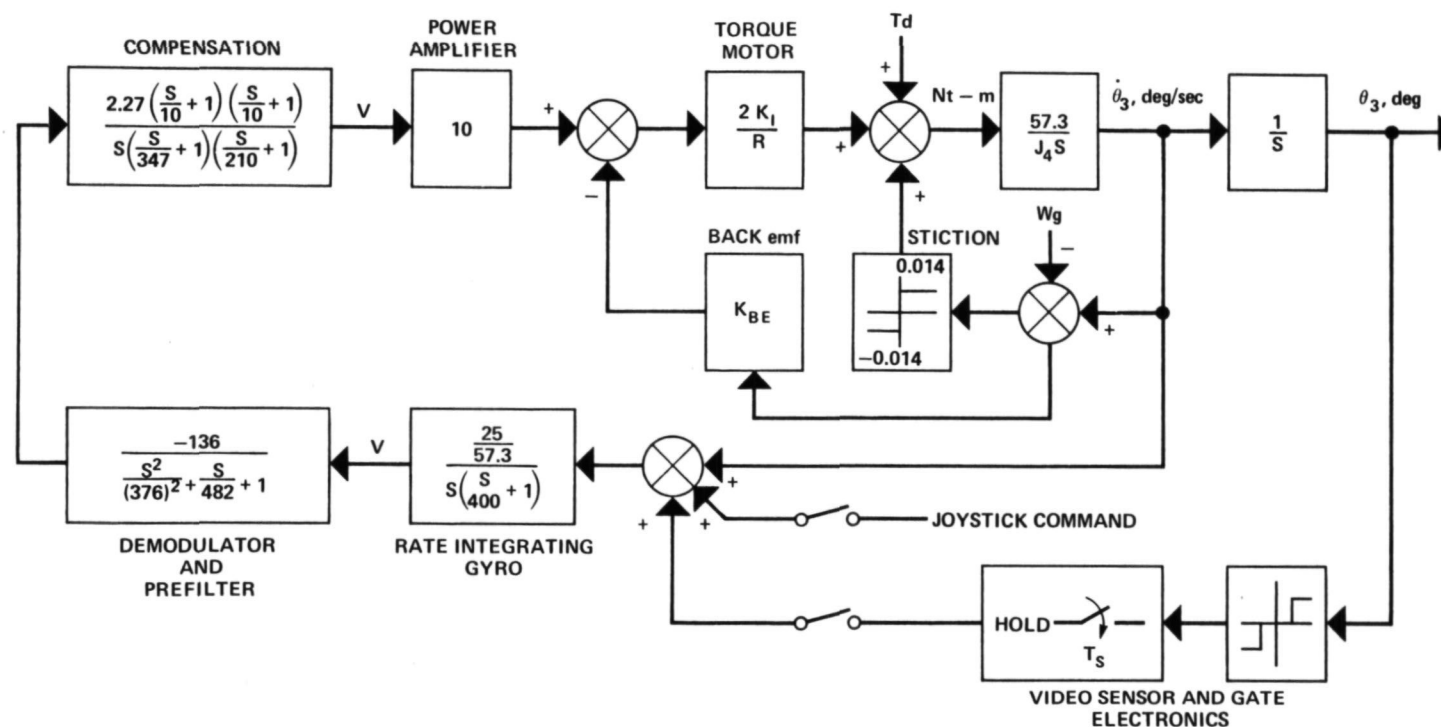


Figure 7. Elevation and Cross Elevation Control System Block Diagram

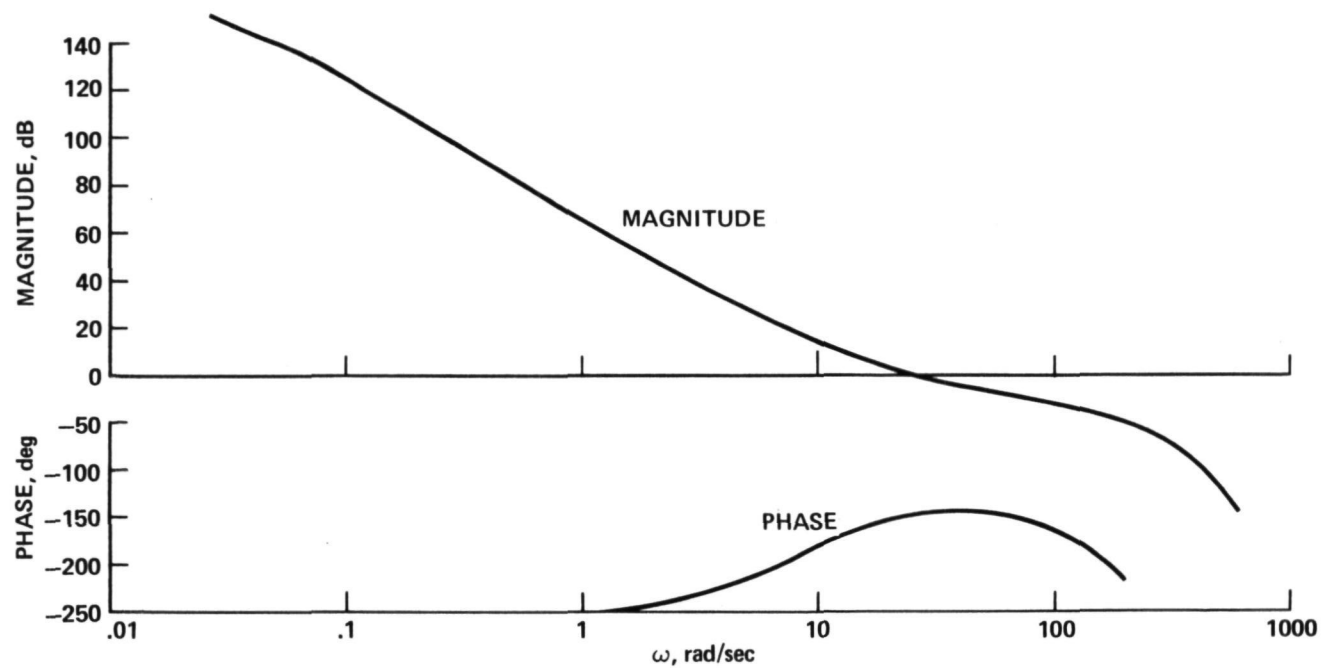


Figure 8. Bode Plot of RIG Stabilization Loop

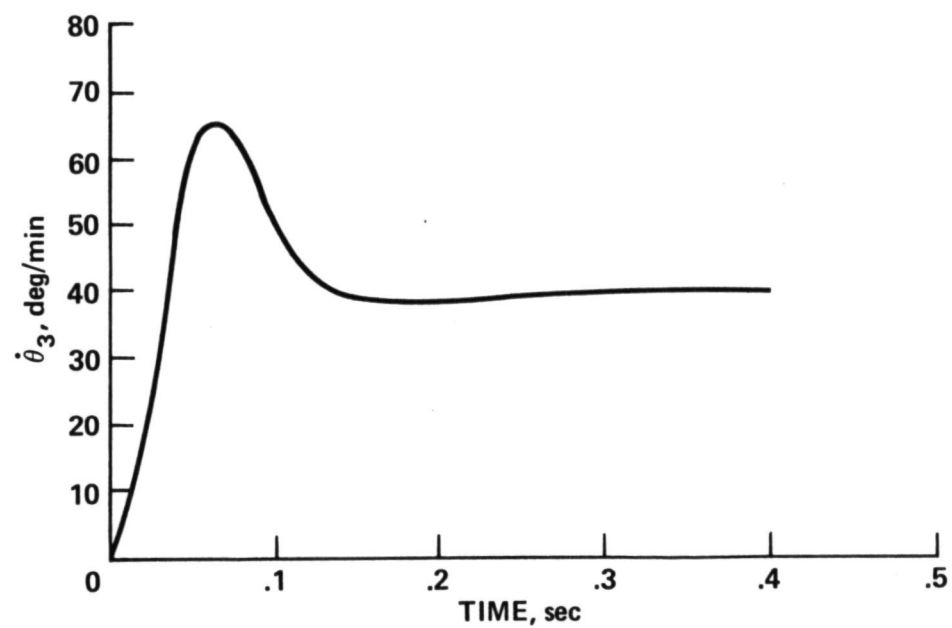


Figure 9. Response to Joystick Command

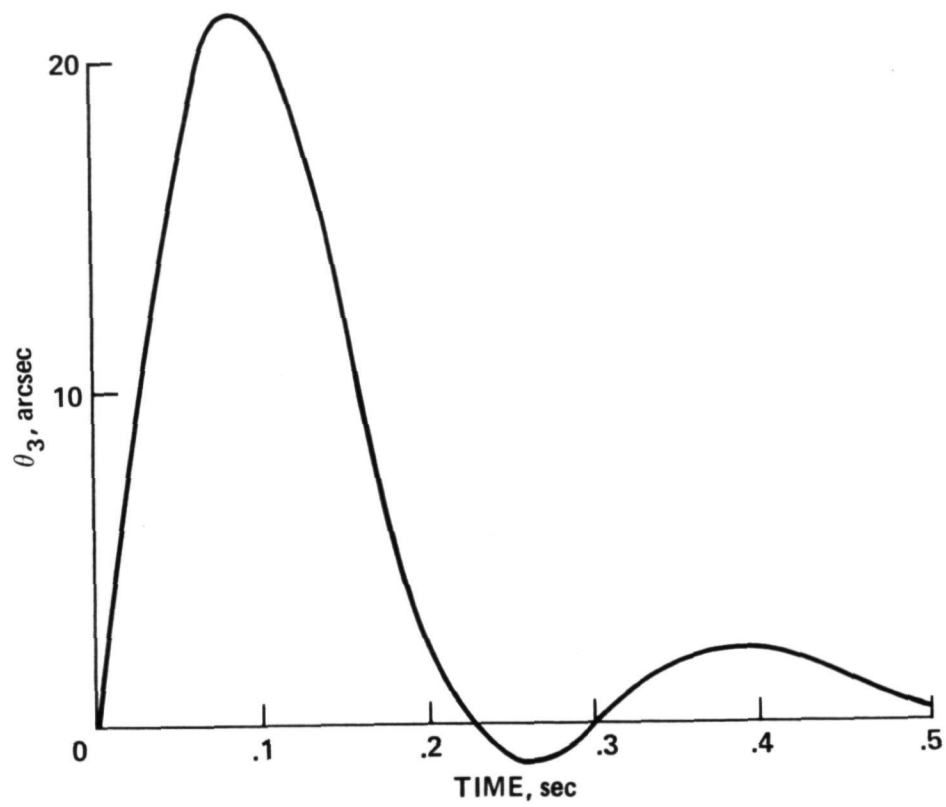


Figure 10. Response to Step Disturbance Torque

a step joystick command of 40 degrees/minute, while Figure 10 shows a response to a step disturbance torque of 1.4 nt.-m. A short time after application of the disturbance torque, the system returns to its original attitude. This effect is a result of the electronic integration in the compensation. Without the electronic integration, a steady state attitude change would result from the disturbance torque.

Since isolation of the telescope from the disturbances of the gondola is important for good stabilization performance, the RIG stabilization loop was tested for its ability to reject these disturbances. As shown in Figure 7, the primary coupling of the elevation or cross elevation axes to the gondola is through the motor back-emf and through bearing stiction. Figure 11 shows the response of the RIG stabilization loop to an oscillatory disturbance rate representing a pendulous motion of the gondola. At the lower pendulation frequency, the primary disturbance effect is caused by the bearing stiction; while, at the higher frequency the torque motor back-emf is the primary disturbance effect. Since the estimated compound pendulation frequency should be less than .5 Hz., the pointing stability caused by the stiction and back emf should be less than 5 arc seconds peak to peak.

A simulation was also performed of the RIG stabilization loop with RIG commands coming from the video sensor. This simulation was used to evaluate the performance of the TV auto mode with disturbance torques and RIG drift, and to choose a value for the torque commands from the video sensor. As shown in Figure 7, the video sensor has been simulated as a deadband with a sample-and-hold. The deadband corresponds to the adjustable gate size while the sample-and-hold results from the camera scan rate. With the simulation, RIG commands up to 120 degrees/hour were used with a deadband as small as ± 0.5 arc minute and no problems were experienced. With a RIG drift, limit cycle operation results and the frequency of cycling depends on the size of the drift. The result of a step disturbance torque is to cause a momentary RIG command; after a short period of time the system returns to normal. Figure 12 shows the acquisition from an initial condition of 6 arc minutes with a deadband of ± 0.5 arc minute and a RIG command of 120 degrees/hour. At $t=4$ seconds a step of disturbance torque is applied and results in a momentary RIG command; at $t=10$ seconds a RIG drift of 15 degrees/hour is applied and results in a periodic application of the RIG command.

POINTING ERROR SOURCES

A number of factors related to the mechanization and operating environment of the pointing and stabilization system contribute to the system pointing accuracy.

When the system is in the manual mode, i.e., joystick commands to the elevation and cross elevation RIG's, pointing accuracy is not as important as the ability to change the telescope attitude by very small amounts. The basic slow RIG command from the joystick is 1 degree/minute. Since the minimum command pulse time through the command system is approximately 0.1 second, a momentary joystick command would result in a telescope movement of 0.1 arc minutes. In addition, the low value of system jitter and stability provided by the direct drive motors and RIG stabilization, and the small trimmed RIG drift rates (below 1.0 degrees/hour) are also important for good performance in the manual pointing mode.

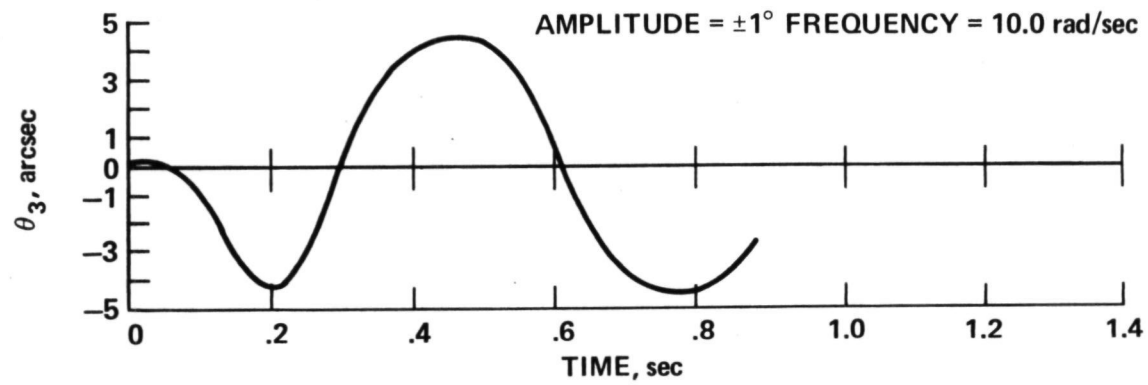
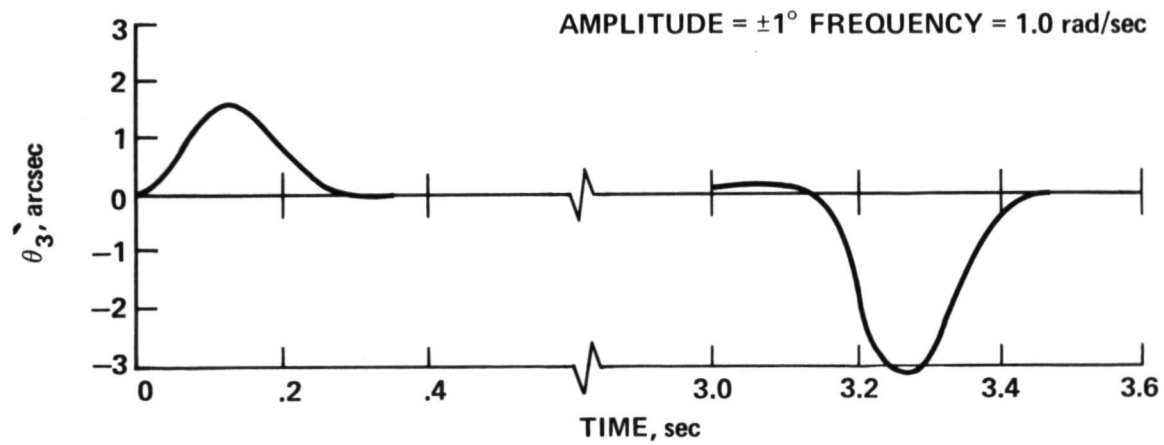


Figure 11. Response to Pendulation Disturbance

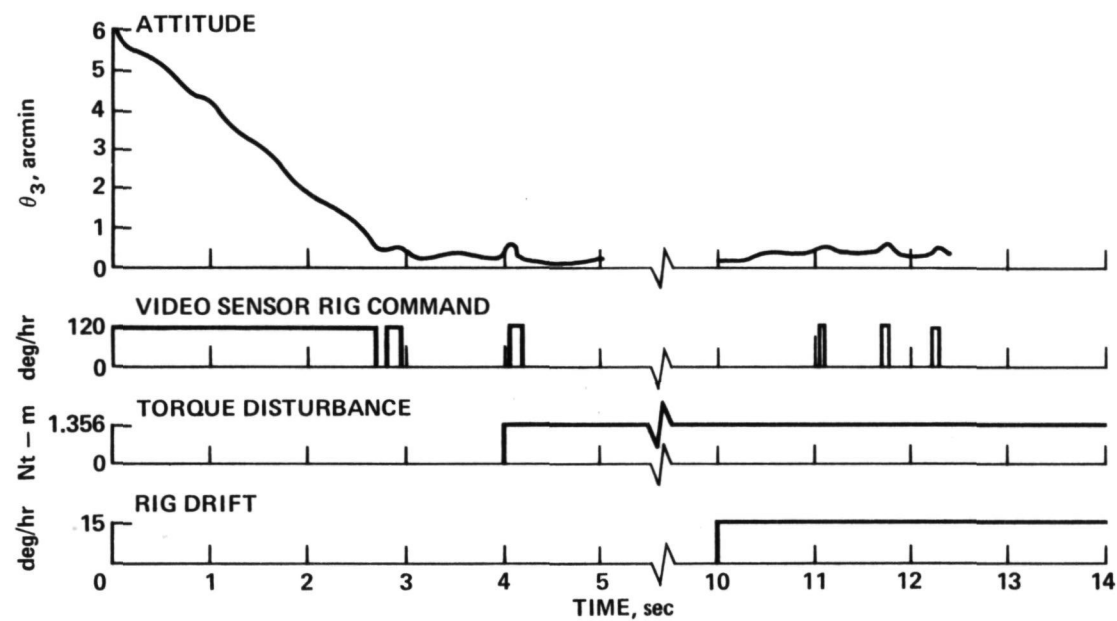


Figure 12. Attitude Response with Disturbance Torque and RIG Drift

In the TV auto pointing mode, pointing accuracy depends on whether the object can be tracked on or off-axis. If an IR object has a visible counterpart so that it can be tracked on-axis, the primary pointing errors are the misalignment of the video sensor to the telescope and the size of the deadband set in the video sensor's gate electronics. Since misalignments can typically be kept less than 0.5 arc minutes and the deadband can be set as small as ± 0.25 arc minutes, the worst case pointing error is less than 0.85 arc minutes. Figure 13 shows the error sources for on-axis pointing in the TV auto mode. Figure 14 shows the addition of the misalignment and deadband errors in a probabilistic sense and shows that the error will be less than 0.51 arc minutes 68 percent of the time.

For off-axis pointing at IR objects in the TV auto mode, the video sensor gates must be positioned about a guide star in the field of view of the video sensor. While the same error sources for on-axis pointing affect the off-axis pointing accuracy, there are additional errors caused by nonlinearities in the video sensor and diurnal motion of the guide star.

To initiate off-axis auto pointing, the joystick and video display are used to position the desired object in the telescope field of view. When a sufficient indication of the object is obtained from the output of the experiment, the RIG's are used to hold the pointing position momentarily while the operator positions the video sensor electronic gates about a suitable guide star with the joystick. Since the video display in the ground station will have its own nonlinearities and null offsets, a set of lights in the ground station indicate whether the guide star is centered in the video sensor gate deadband on board the gondola. When the lights indicate that the gates are centered about the guide star, the TV auto mode is initiated. Consequently, pointing errors at the start of off-axis pointing are similar to the errors for on-axis pointing.

The guide star will appear to rotate about the desired object due to diurnal motion. The ability to move the null position of the gates to account for the diurnal motion will introduce additional errors over the time period required to obtain data from the science instrument. In addition, the diurnal motion will introduce errors due to linearity of the video sensor.

There are three methods that can be used to update the position of the gates due to diurnal motion. The first method would use sidereal time, right ascension and declination of the object and guide star, and latitude information to generate tables that could be used to obtain the position of the guide star relative to the target object as a function of time. Due to variations in time and latitude and the three gimbal angles associated with the gondola, it is apparent that the table look up method is somewhat cumbersome and inaccurate. A second, more precise method would use current information about the gondola gimbal angles, latitude, and time, combined with the right ascension and declination of the guide star and object to calculate in real-time the video sensor gate positions. This method, while very accurate, would require a computer in the ground station with an electrical interface to the command and data systems.

A third method was developed which provides a compromise between hardware complexity and accuracy. This method uses the current gimbal angles, azimuth, elevation and cross elevation and latitude to find the component of earth rate about the telescope axis. This rate, the instantaneous rate at

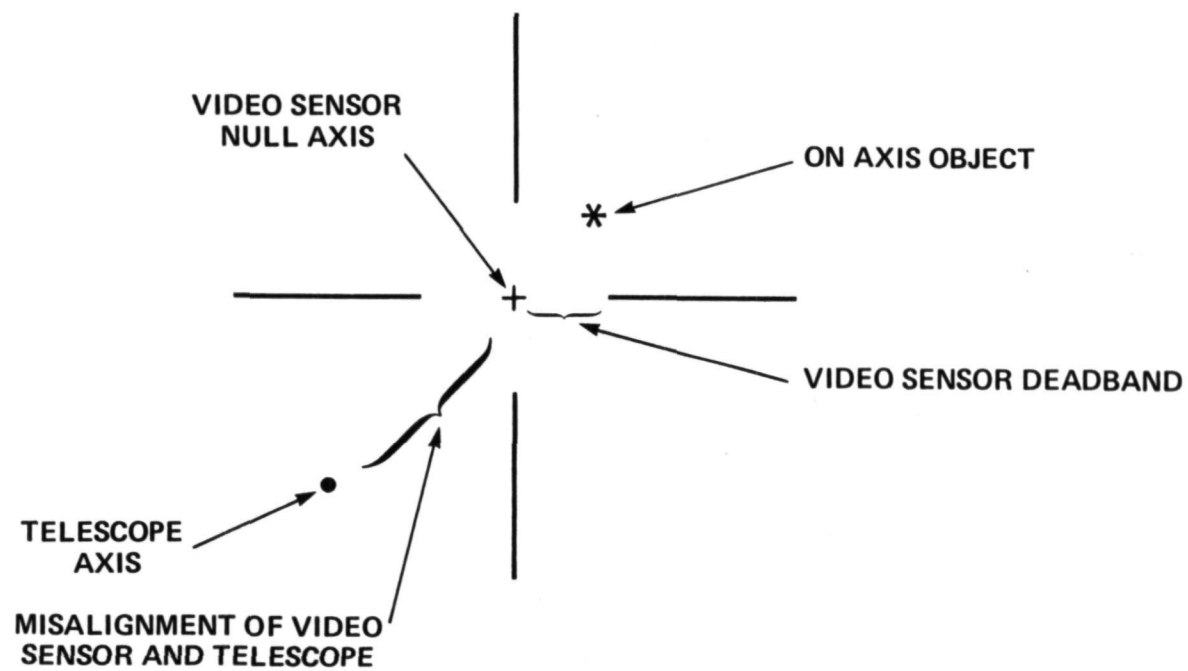


Figure 13. On-Axis Pointing Error Sources

ERROR SOURCE	arcmin	CONFIDENCE	1σ
MISALIGNMENT	0.50	1σ	0.50
GATE DEADBAND	0.35	3σ	0.12

1σ RSS TOTAL = 0.51 arcmin

Figure 14. On-Axis Pointing Error

which the guide star is rotating about the pointing axis, is small (less than $15^\circ/\text{hour}$) and changes slowly. Knowledge of the present gate location combined with the value of the guide star rotation rate, allows the gate positions to be updated incrementally and these calculations can be rapidly performed with a small hand-held programmable calculator.

Figure 15 shows a summary of the sources expected to contribute to pointing error during off-axis pointing when the gate positions are updated at one minute intervals. The misalignment and gate deadband are similar to those associated with on-axis tracking. The bias or uncertainty in the calculation of the guide star rotation rate will cause an error that will build up during the pointing interval and this is shown as the rate estimate uncertainty error. The time increment error represents the motion of the guide star between gate position updates and is independent of the pointing interval length. The video nonlinearity error arises from the motion of the guide star from the initial position; gondola pendulation will cause a small apparent movement of the guide star and is shown as the gondola disturbance error. Figure 15 shows that the pointing error during a one-hour interval with the guide star two degrees from the object will be less than 1.29 arc minutes.

Examining Figure 15 reveals that if the more complex method of updating the gate positions with an on-line ground station computer were used, the rate estimate uncertainty and time increment errors would be removed. The one sigma pointing error would then be 0.73 arc minutes for the one-hour interval.

CONCLUSIONS

The AIROscope pointing and stabilization system has been configured with rate integrating gyros, direct drive torque motors and three gimbals to provide a very stable platform for infrared astronomy. Since the azimuth torque motor uses the suspension for reaction torque, a tachometer and control logic have been implemented to increase the suspension damping. The use of an electronic integrator, in the elevation and cross elevation RIG stabilization loops, aids in the rejection of disturbance torques and minimizes the effect of pendulation disturbances coupling through bearing stiction and torque motor back emf. A unique video sensor provides error signals for on and off-axis pointing and information for a CRT display in the ground station. Results of the pointing error analysis show that the on-axis pointing error should be less than 0.51 arc minutes, and that the off-axis pointing error should be less than 1.29 arc minutes for pointing intervals up to one hour.

ERROR SOURCE	arcmin	CONFIDENCE	1σ
MISALIGNMENT	0.50	1σ	0.50
GATE DEADBAND	0.35	3σ	0.12
RATE ESTIMATE UNCERTAINTY	3.14	3σ	1.05
TIME INCREMENT 1 STEP/min	0.52	3σ	0.17
VIDEO NONLINEARITY	0.20	1σ	0.20
GONDOLA DISTURBANCE	1.40	3σ	0.47

GUIDE STAR 2° FROM OBJECT

1σ RSS TOTAL = 1.29 arcmin
FOR 1 hr INTERVAL

Figure 15. Off-Axis Pointing Error

SYMBOL

d	Suspension cable separation
H	RIG angular momentum
J_1	Suspension inertia
J_2	Azimuth inertia
J_3	RIG gimbal and wheel inertia
J_4	Elevation inertia
K_a	Acceleration constant for evaluation of rate gyro errors
K_B	Coefficient of azimuth bearing friction and torque motor back emf
K_{BE}	Coefficient of elevation torque motor back emf
K'_{B1}	Coefficient of azimuth damping during slewing
K'_{B2}	Coefficient of azimuth damping during stabilization
K_G	RIG position feedback gain
K_I	Elevation torque motor scale factor
K_{MI}	Tachometer scale factor
K_{MZ}	RIG scale factor
K_P	Position scale factor
K_R	Balloon rotation rate constant
K_{TM}	Azimuth torque motor scale factor
K_V	Rate scale factor
K_Z	Coefficient of RIG gimbal damping
K_r	Coefficient of suspension torque
L	Suspension cable length
M	Gondola and telescope weight
M_c	Control torque
M_{D1}	Suspension disturbance torque
M_{D2}	Azimuth gimbal disturbance torque
M_s	Stiction torque
R	Elevation torque motor winding resistance
T_d	Elevation gimbal disturbance torque
T_s	Video sensor sample rate
W_g	Gondola pendulation rate

θ_1	Suspension angle
θ_2	Azimuth gimbal angle
θ_3	Elevation gimbal angle
θ_r	$\theta_1 - \theta_2$
γ_s	Time constant
SGN	Signum function

REFERENCES

- Deboo, G.J., Parra, G.T., and Hedlund, R.C., 1974. The AIROscope Stellar Acquisition System. Symposium on Telescope Systems for Balloon-borne Research. To be published.
- Frecker, J.E., 1968. The Polariscope Balloon-borne Servo System. LPL Communications No. 109.
- Greeb, M.E., and True, G.A., 1974. Balloon Infrared Astronomy Platform (BIRAP). Symposium on Telescope Systems for Balloon-borne Research. To be published.
- Koontz, O.L., and Scott, S.G., 1974. AIROscope Ames Infrared Balloon-borne Telescope. Symposium on Telescope Systems for Balloon-borne Research. To be published.
- Morris, A.L., and Stefan, K.H., 1969. High Altitude Balloons as Scientific Platforms. NCAR, Boulder. 85p.
- Nidey, R.A., 1969. International Orbital Laboratory and Space Sciences Conference. International Academy of Astronautics, Cloudcraft. 9p.
- Nidey, R.A., 1966. Stabilization and Orientation of Balloon-borne Instruments. Kitt Peak National Observatory, Tucson. 36p.

DISCUSSION SUMMARY — PAPER 4.6

Information about the weight, cost and power consumption of the rate integrating gyros was requested. The gyros used on AIROscope are surplus units costing \$400 each. They were bought from commercial surplus dealers. They weigh approximately one-half kilogram. Their power consumption is less than 10 watts. Most of this power is for the heaters.

It was noted that the gimbal arrangement does not allow for correction of field rotation.

A question was asked regarding a comparison of calculated performance with the performance of the gyroscope. This, of course, depends on how one corrects for drift in the gyroscopes. If this is done with a star tracker (observing an on-axis object) as in the original Polariscope, 15 arcseconds pointing accuracy could be expected. In the infrared where off-axis tracking is often necessary the TV camera is used for the drift correction, but it is less accurate than on-axis tracking.

The speaker noted that many of the ideas used on AIROscope, such as the three gimbals, the video display and the ground station were basically features of the Polariscope system. Since they were considered to be good features, they have been carried over to the new system. The difference in the tracking systems stems from the fact that so many strong IR sources have faint visible counterparts, so that the star tracker is not always useful.

PAPER 4.7

BALLOON INFRARED ASTRONOMY PLATFORM (BIRAP)

M.E. Greeb

G.A. True

Ball Brothers Research Corporation

ABSTRACT

Our goal was to develop a balloon borne attitude control system for infrared astronomy studies using flight proven hardware and/or techniques as much as possible. The resulting BIRAP system is the realization of that goal. BIRAP will be used to study sources that emit little or no energy in the visible spectrum. Existing technology in tracking sensors does not permit the direct pointing method. Development of a sensor for direct sensing of the IR sources was discarded immediately as nonfeasible from a cost consideration. The use of existing technology and hardware design, therefore, became the challenge for the BIRAP development. The BIRAP uses "electronic gimbaling" for the offset pointing which eliminates a set of mechanical gimbals. Guide stars with visual magnitudes as low as +6 are used for fine tracking assuring that all areas of the sky can be covered. The BIRAP control concept uses a closed loop system in the airborne equipment with automatic update through a command link that can be operated either manually or automatically by a ground based computer. The first flight of this unique platform is scheduled in mid 1974.

INTRODUCTION

Observation of astronomical targets emitting little or no energy in the visible spectrum poses several unique problems for the attitude controller. The state of the art in infrared sensors makes direct sensing of the IR source infeasible. In fact the size and shape of many of the IR sources themselves make precise direct pointing difficult even if an IR sensor was available. We chose to sense a visible star and offset the IR instrument to the target of interest as an alternate to direct sensing for BIRAP.

Because it has the basic stellar acquisition and pointing capability, The Balloon Astral Pointing System (BAPS) became the natural baseline for the BIRAP design. BAPS was developed for NASA/MSC, Houston, Texas, and has been flown successful several times from Palestine, Texas.

The BAPS system has been described previously by Gibson et al (1972) and Guthals et al (1973). Both of these papers are referenced several times in this paper.

The primary differences between BAPS and BIRAP are the offset pointing requirement, the IR Telescope interface differences and the operational aspects of the balloon launch. All of the

differences are minor in nature but are necessary for the BIRAP missions. Compatibility to European as well as U.S. launch sites was a major requirement for the BIRAP configuration.

The switch of star trackers is the most significant change for BIRAP. The BAPS tracker was replaced by an existing star tracker design currently being used in the SASS-C spacecraft. The BIRAP tracker permits tracking dimmer stars and provides greater offset accuracy capability than the BAPS tracker.

The two axis gimbal configuration is actually a third generation design. The same basic gimbal configuration was used in the Balloon Borne Solar Pointer designed and built for the Air Force Cambridge Research Laboratories (AFCRL). This pointer is described by Toolin et al (1973), and Greeb (1965). The stellar version of that system (BAPS) is an outgrowth of the BBSP. Both the BAPS and BIRAP systems are by necessity more complex than the BBSP, primarily because the acquisition of a stellar target is more difficult than acquiring the sun and more than one target is normally observed during each stellar mission.

Addition capability has been incorporated into the BIRAP system to allow introduction of offset commands, permit automatic ground computer update of the offset signals through the command link, compensate for instrument cryogen loss and measure the payload pendulation.

A brief description of each of the major subassemblies is given in a later section. The emphasis in this paper will be on the concepts, problems and hardware unique to BIRAP. Since control electronics and command system for BAPS and BIRAP are nearly identical and an excellent description of the BAPS system is contained in papers by Gibson et al (1972) and Guthals et al (1973), we will not address these areas in great detail. However, a sufficient general description has been included to allow the reader to visualize both the operation and physical appearance of the system.

SYSTEM CONCEPT AND OPERATION

The basic purpose of the BIRAP system is to point a telescope towards an IR source with a design goal accuracy of ± 30 seconds. A summary of the major BIRAP specifications is listed in Table 1. To appreciate the fine sensor requirement and to understand the offset pointing method, it is necessary to understand the basic gimbal set that is used. The system shown pictorially in Figure 1, and as a two view sketch in Figure 2 is made up of the landing platform and the pointed section. The upper half of the unit including the tubular structure makes up the pointed section. This entire section is fastened to a suspension tube. The suspension tube serves as the couple between the balloon and the landing platform, and the azimuth shaft for the pointed section. When the payload is properly balanced, the action of gravity holds the suspension tube parallel with local

Table 1
BIRAP SYSTEM CAPABILITY

<u>Parameter</u>	<u>Capability</u>
<u>POINTING ACCURACY</u>	
Acquisition - Elevation Axis	$\pm 0.5^\circ$
- Azimuth Axis	$\pm 2.0^\circ$
Fine Pointing Accuracy (Neglecting Penulous Motion)	
Maximum	$\pm 1 \text{ min R.S.S.}$
<u>ACQUISITION TIME (Slew Rate)</u>	
Maximum Time from Initiation to On Target Pointing (90° angle change)	<300 sec
<u>TARGET RESTRAINTS</u>	
Number of Objects to be Observed	Limited only by observation time
Guide Star Magnitudes	+6 to +2
Maximum angle between guide star and experiment target	5°
<u>SCAN RATE</u>	10 min/min
<u>ASCENT AND DESCENT INSTRUMENT POSITION</u>	
Azimuth - Ascent	Caged to Landing Platform
- Descent	Uncaged
Elevation	Caged to Horizontal
<u>INTERFACE</u>	
<u>Mechanical</u>	
Maximum Instrument Length	150 cm (59 in.)
Outside Diameter	80 cm (31 in.)
Maximum Instrument Weight	95 kgf (200 lb.)
<u>Electrical</u>	
Commands Available	16 discrete, One 16 bit serial digital word
Power	150 AH
<u>GIMBAL FREEDOM</u>	
Azimuth Axis	Continuous
Elevation (Zenith Angle)	30° to 100°
<u>TOTAL WEIGHT INCLUDING INSTRUMENT</u>	410 kgf (900 lb.)

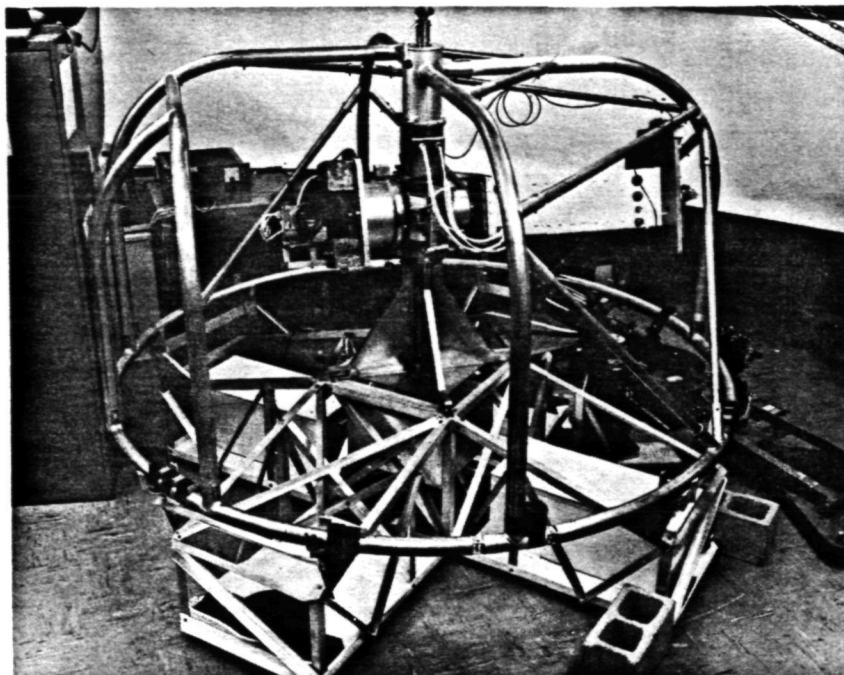


Figure 1 BIRAP System Configuration

vertical. The landing platform provides the inertia for the azimuth servo to react against. The pointed section has unlimited freedom about the suspension tube (azimuth axis) as it rotates in a plane perpendicular to local vertical. The IR Telescope and the star tracker are mounted to another axle attached to the pointed section. The telescope and the star tracker are free to rotate about this axle (which is defined to be the elevation axis) in a reference plane that is perpendicular to the azimuth plane. During initial acquisition, the pointed section is rotated about the azimuth axes until the target star lies in the reference plane. The proper rotation about the elevation axis will then align the telescope and star tracker optical axes toward the target star. Initial acquisition of the target star is complete when the center of the star tracker FOV is pointed directly at the star. This initial acquisition is accomplished to an accuracy of $\pm 2^\circ$ in azimuth using the earth's magnetic field as a reference. The elevation acquisition is accomplished to within $\pm 0.5^\circ$ using a position potentiometer mounted to the elevation axle.

The star tracker mount is designed so that the center of the star tracker field of view is aligned to the optical bore-sight axis of the IR Telescope. Therefore, during the initial

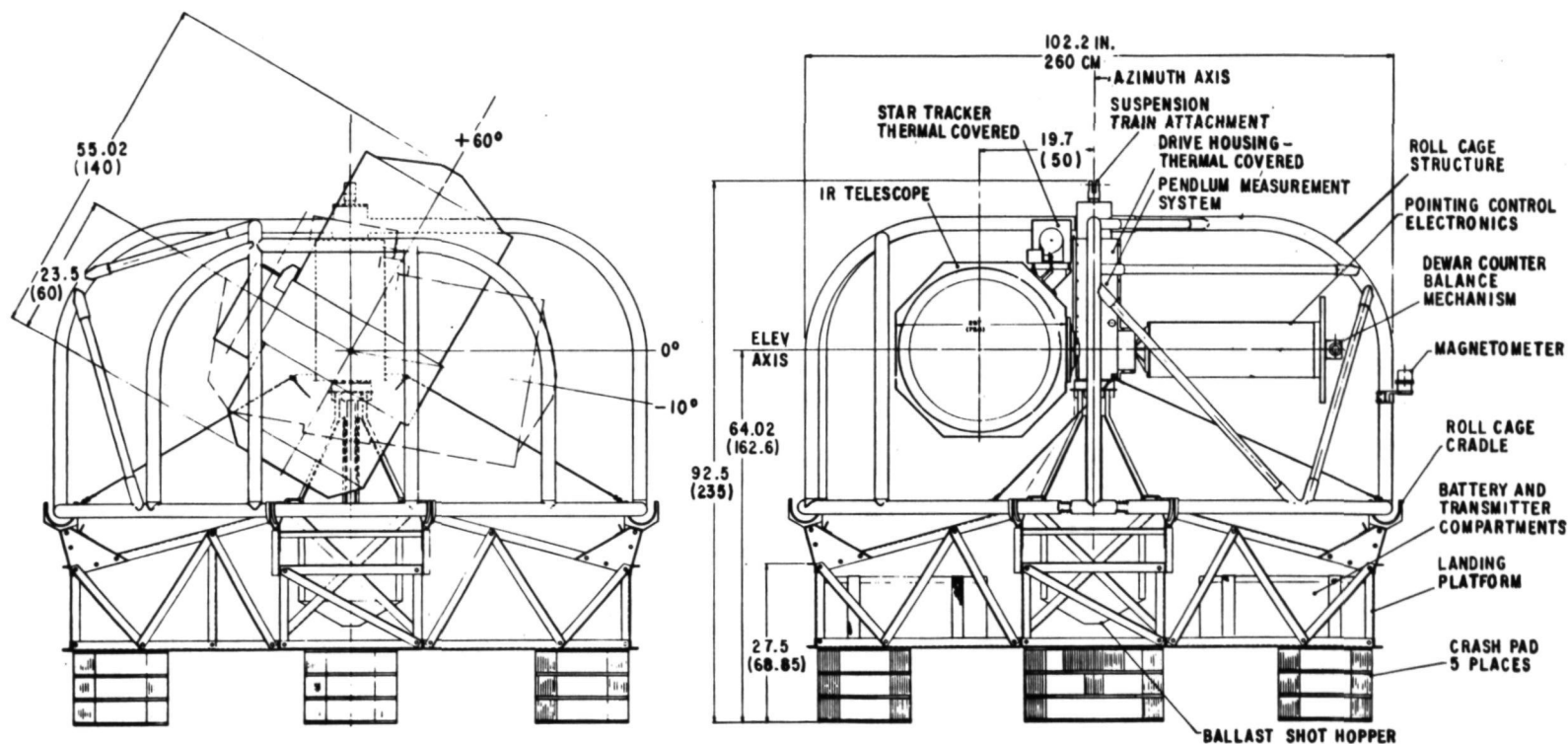


Figure 2 BIRAP Layout Drawing

acquisition both the tracker and the IR Telescope are pointing at the target star. Offset signals are introduced to orient the experiment telescope towards the IR source after the star tracker is allowed to acquire the target star and control has been switched from the magnetometer and elevation potentiometer to the tracker.

We chose the "electronic gimbaling" method to offset the star tracker to avoid another set of mechanical gimbals. Electronic gimbaling is accomplished by simply inserting electrical bias signals into one or both of the servo control loops. Error signals are then required from the star tracker to satisfy the servo null condition. The control system, therefore, rotates about each of the gimbals until the tracker output error signals are equal and opposite in sign from the input bias signals.

In order for the IR Telescope to be pointed at the desired IR source, both the target star and the IR source must be in the star tracker FOV. The BIRAP tracker fits the requirement very well since it has a minimum 8° square FOV and can track stars as dim as +6 magnitude. This combination assures that at any launch site at least one target star will appear in the tracker FOV regardless of the position of the IR source in the celestial sphere.

Two very important considerations were addressed during the feasibility study of this 2 axis, single star tracker approach for BIRAP. They were the effects of payload pendulous motion, and the apparent rotation of the IR source about the target star during long time exposures.

The offset error due to pendulous motion grows to a maximum when that motion occurs in a plane which is parallel to the elevation axis. The pendulation will result in a roll motion about the star tracker line of sight. The roll motion results in a scanning motion of the IR Telescope across the IR source. For small pendulous motion the error signal can be shown to be as follows:

$$\Delta\theta_E = \theta_P \frac{\sin \beta}{\cos \theta_T}$$

where

$\Delta\theta_E$ is offset error

θ_P is pendulous amplitude of oscillation

β is the offset angle

θ_T is the elevation angle

Our information on pendulation after the payload reaches float altitude indicates a maximum excursion of less than ± 10 arc minutes; therefore, the largest error due to pendular motion with a zenith angle of 30° and offset angle of 5° is 1.5 minutes.

Since the BIRAP gimbals are tied to local vertical and local horizontal the apparent movement of the stars during a long

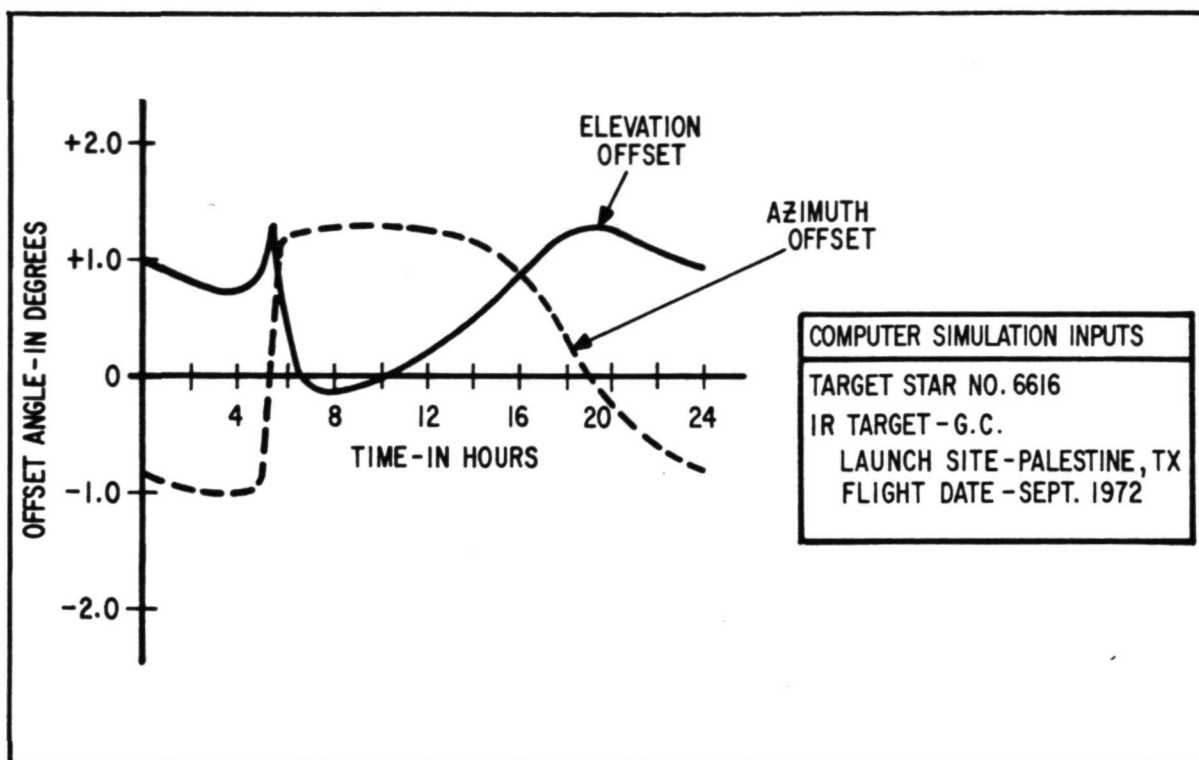


Figure 3 Offset Angles Required to Point at Galactic Center

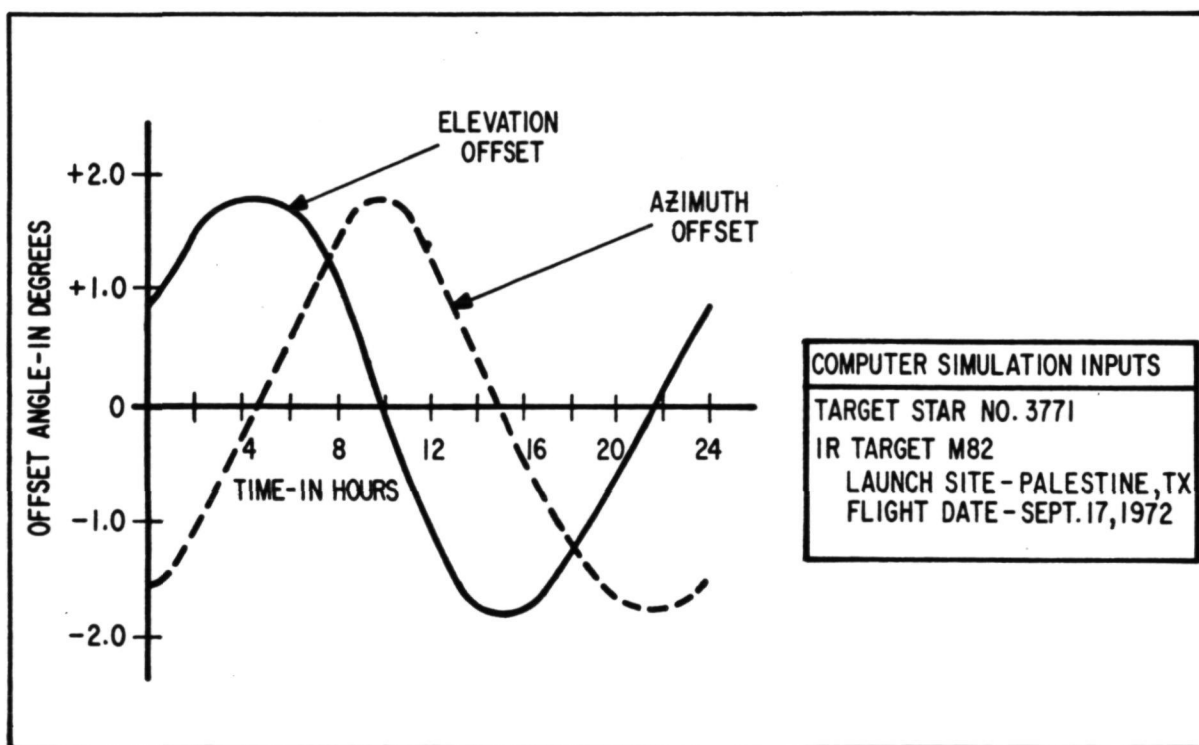


Figure 4 Offset Angles Required to Point at M82

observation time is essentially the same as our own visual observation. If we choose any guide star as a reference and then observe another star with respect to the guide star, the second star will appear to rotate around the guide star once every 24 hours. It is this apparent rotation of the IR source with respect to the target star over a given time interval that is of concern for the BIRAP offset pointing concept. This motion required that the offset angle we command into the star tracker must be continuously updated in order to keep the instrument pointed at the IR source. The rate of change of the two offset angles can be shown to be a function of earth rate, the latitude at which they are observed and the declination angle of the reference target. Figures 3 and 4 depict the change in offset angle required to keep the IR Telescope pointed toward the Galaxitic Center (G.C.) and M82 using star No. 6616 and 3771 respectively as target stars. The computer program from which this data was obtained assumes the payload remains at the latitude and longitude of the Palestine, Texas launch site for the entire 24 hour period. For the launch day shown, the BIRAP restriction to night time pointing would have limited observation of the G.C. from sunset to approximately midnight, the approximate time when the G.C. falls below the earth's horizon. M82 could have been tracked any time during the night. Figures 3 and 4 indicate the offset angle requirement for the entire 24 hour period, ignoring the fact that it is daytime or that the targets might be occulted by the earth or the balloon.

The BIRAP Command System contains the interface necessary to allow automatic offset update using a ground based computer.

During the flight the BIRAP system has four modes of operations, stow, acquisition, fine and offset track. Each mode is initiated by command from the ground.

In the electrical stow mode both of the axes are electrically caged to their respective potentiometers. Both the azimuth and elevation axes will be mechanically locked for ascent. Release is by squib activated pin pullers. The elevation axis will be relatched for parachute recovery. The acquisition, fine and offset modes have been described previously and are discussed in much greater detail in the BAPS papers referenced previously.

SYSTEMS DETAILS

Several subtle but important changes were made to the BAPS mechanical design to adapt the basic gimbal, roll cage and landing platform concept to the BIRAP requirements. The physical appearance of the two systems are quite similar to the casual observer. As shown in Figure 2 the system consists of two major sections, a landing platform and a pointed platform section. The pointed platform section is very similar to BAPS. It consists of the suspension tube, drive case and roll cage. The

drive case, depicted in Figure 5 is nearly identical to BAPS. It contains the bearings drive motors and position potentiometers for both the azimuth and elevation gimbals. It also houses the azimuth slip rings and the secant potentiometers used to keep the azimuth servo loop gain constant. The entire drive case is mounted to the suspension tube by the two azimuth gimbal bearings.

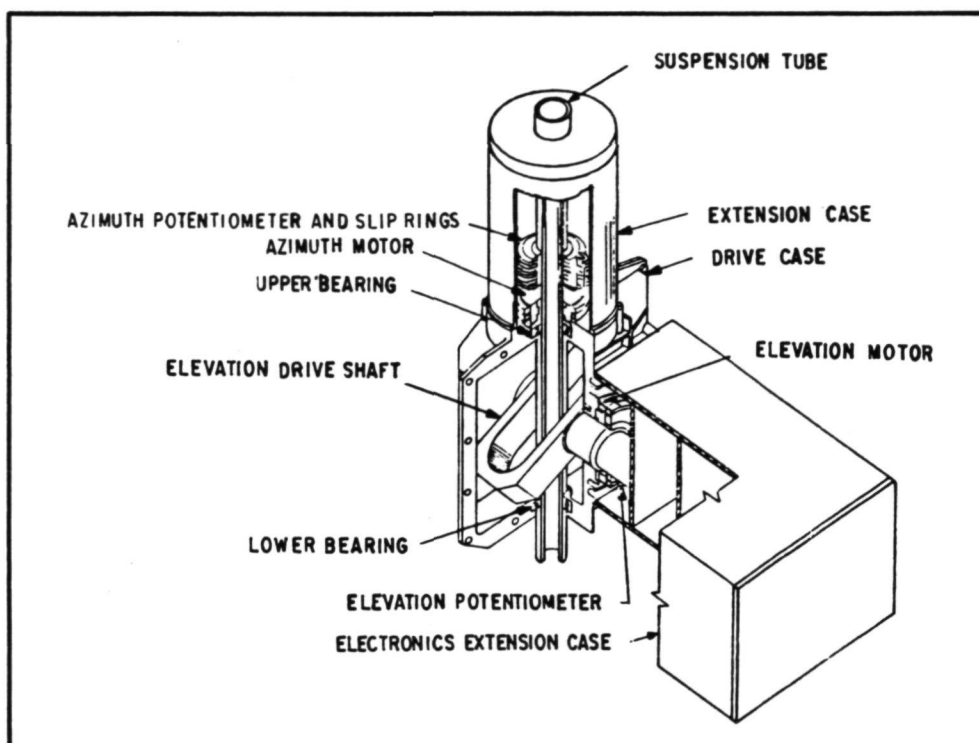


Figure 5 Pointing Control Drive Assembly Details

The elevation shaft is also contained in the drive case. It uses the BAPS yoke configuration shown in Figure 5 to allow the suspension tube to pass through the geometric center of the elevation shaft to the landing platform. The rest of the elevation shaft has been redesigned for BIRAP to accommodate the heavier instrument weight and to improve the bearing loading due to the moments encountered during landing. In BAPS, only the instrument was fastened to the elevation shaft. This caused a large bending moment at the bearing interfaces because of the cantilever effect. Calculations of the bending moments and bearing loading indicate the bending moments are improved considerably if an equivalent weight is added to the shaft on the side opposite the instrument. Even though the total weight on the elevation bearings doubles the increase in friction is negligible.

so the servo performance is very nearly the same. The additional weight was provided by adding a flange to the other end of the elevation shaft and attaching the electronics assembly to it. This approach retained the balance required to keep the suspension tube vertical, improved the bending moment problem and reduces the problem of making electrical connections across the rotating joint between the instrument and the electronics box.

The roll cage, as its name implies, is added to provide protection for the instrument gimbals and electronics if the payload should roll over during landing. The roll cage configuration is similar to the one used for BAPS but it has been reduced in size for easier transport and has been modified to accommodate the wider FOV of the instrument and the greater elevation angle freedom required by the BIRAP system.

The BIRAP landing platform configuration is also similar to BAPS, but it has been scaled down, again for convenience of handling and shipping. The platform is designed to withstand a descent load factor of 15 g's and a ground-traversing load of 10 g's caused by high ground winds and high lateral drift. The crash pads are fabricated from vertical impregnated paper honeycomb panels and columns. They have been tested and exposed to actual flight descent velocities of up to 6 meters/sec (20 fps) and deceleration of 15 g's and with drift velocities up to 10 meters/sec (33 fps).

The star tracker is mounted directly to the IR Telescope house to minimize the alignment changes with temperature, etc. Special mounting feet were developed to thermally isolate the star tracker from the cold environment of the liquid nitrogen cooled IR Telescope. A special insulated and heated housing is also provided for the star tracker.

To avoid excessive heating in the gimbal drive motors, the payload must be very well balanced, particularly about the elevation drive shaft. The IR instrument requires the use of a liquid nitrogen dewar which unfortunately cannot be mounted on the center of rotation of the elevation shaft. The instrument balance assembly has been added to the system to automatically compensate for the loss in cryogenic liquid. Since the electronics box rotates with the IR instrument it was more practical to add the balance unit to the end of the electronics box because the thermal interface problem is avoided and connections to the sensing electronics is much easier.

The control electronics for the system are essentially the same as used in BAPS except for the addition of the instrument balance circuitry, the pendulation measuring gear, and the offset signal summing required for BIRAP. The sensing for the balance system is accomplished by sampling the integrator output in the elevation servo loop. When this output exceeds a steady state preset value, the motor in the balance unit is activated to drive the weight until the integrator output is reduced below the threshold point. The polarity of the integrator output deter-

mines the direction of the motor drive.

Two digital-to-analog converters provide the offset signals to the control system. These converters are loaded with data via the command system. The outputs from the converters are introduced directly into the servo control loop to produce the offset.

The mechanization of the magnetometer loop and the potentiometer loop for acquisition and the servo analysis for all the modes of operation are discussed quite well by Guthals et al (1973) and Gibson et al (1972) therefore they will not be repeated here. It will suffice to say that with the exception of the offset inputs, the changes required for BIRAP were minimal. A system functional diagram of BIRAP is shown in Figure 6. Additional packaging design was done for BIRAP to put the electronics on printed circuit boards instead of the terminal layout method used for the electronics on BAPS. This change simplified the fabrication and increased the reliability of the system.

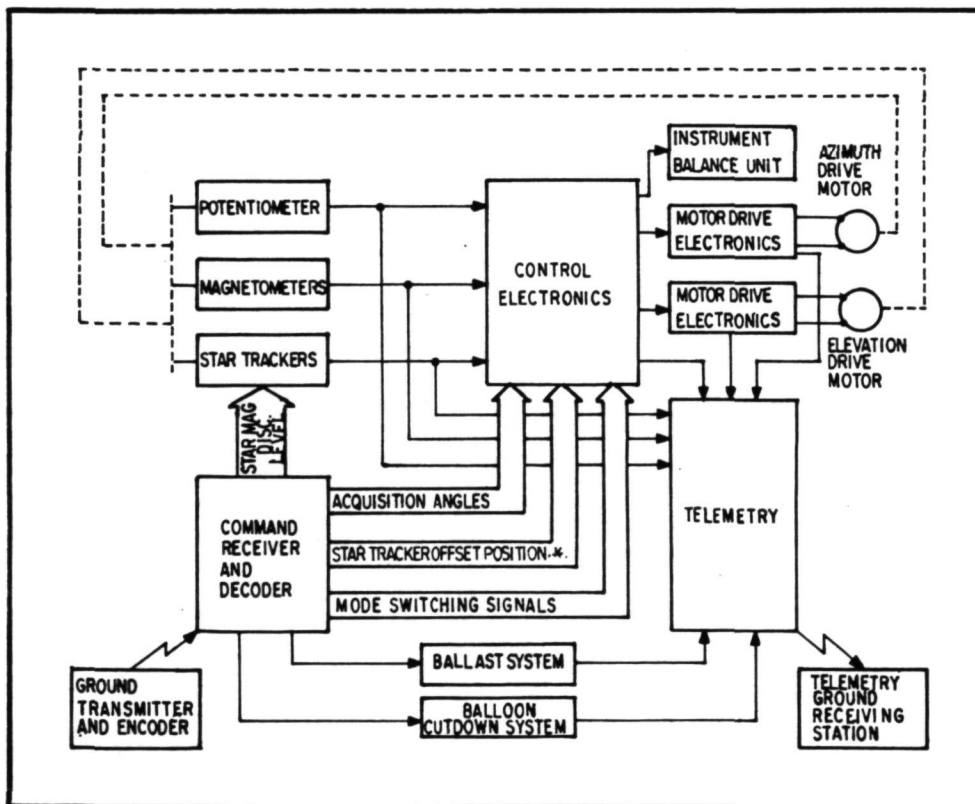


Figure 6 BIRAP System Functional Diagram

An integrating gyro package has been added to BIRAP to measure the pendulous motion which causes movement of the IR instrument that is not corrected by the control system. The intent is to monitor this signal and add that variable into the data reduction. The signal will also be monitored during flight so that if the pendulous motion becomes too large for good data retrieval during a particular measurement, that data can be ignored or a new measurement can be made. The system has a minimum resolution of one arc minute peak pendular swing at a frequency of 5 Hz or less.

The command system used on BIRAP is nearly identical to that used on BAPS. It is a digital coding system with the capability of 16 discrettes (output command pulses) and one 16-bit serial digital word that can be processed by the BIRAP electronics and by the experiment. Included in the command system is a control panel, a ground based encoder, and the command receiver and decoder which mounts in the payload. The ground equipment interfaces with a DR11-A interface unit (customer supplied). The interface unit permits the flight system to accept data directly from a PDP-11 digital computer. The ground equipment allows the offset angle to be updated automatically using the computer. Two sixteen-bit words, four bits for address, twelve for actual data are contained in each two axis command. Each command can be sent at a rate of 30 commands per minute. This command rate is based on a 25 bps clock rate from a 50 Hz line. For a 60 Hz line the rate is 30 bps with a command rate of 37 commands per minute. Manual control is used for mode changes and multiple target acquisition. Backup manual offset command control may also be used.

The two primary sensors used by the control system are the two axis magnetometer and the star tracker. The two axis magnetometer is used to sense the magnetic field direction in the azimuth plane. The electronics uses the output of the two magnetometers and a command input signal to produce an output position angle reference for the azimuth axis. The magnetometer sensor assembly is mounted on the roll cage to isolate it from elements that tend to distort the earth's magnetic field.

The star tracker shown in Figure 7 provides the input signals to the control electronics during the fine and offset pointing modes of operation. It has a total field of view of 8° by 8° square during star acquisition and approximately 10° diameter circular during fine pointing and offset modes. It can acquire and track stars with magnitudes from +2 to +6. The combination assures that there will be at least one target star available regardless of what part of the celestial sphere the star tracker is pointed to. There are some areas of the sky where more than one target star will be visible within the 8° FOV of the star tracker. To be assured that the right star is acquired four different star magnitude discrimination levels (+6, +5, +4, +3) can be set into the star tracker through the command system. The tracker will track only stars that are brighter than or equal to the command level.

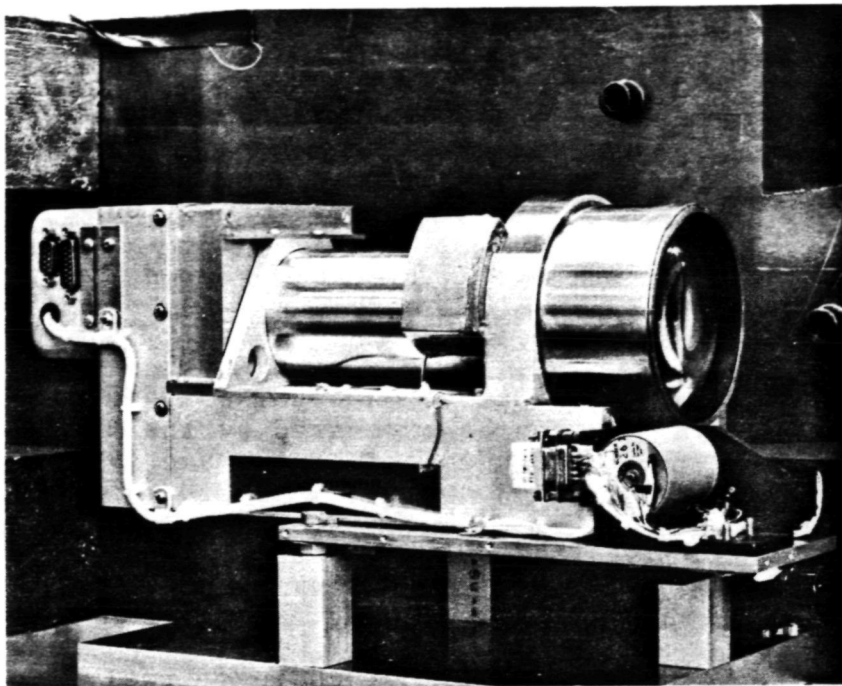


Figure 7 BIRAP Star Tracker

The "initiate search" control command capability of the BIRAP tracker makes it possible to verify that the proper guide star has been acquired if more than one guide star falls within the FOV. The tracker will acquire and track the first star it finds over the threshold set. When the "initiate search" command is given, the tracker will continue through the remaining search pattern and lock onto the next star. By comparing the output angle differences between the two stars, one can verify that the tracker is directed toward the correct star. By varying the magnitude discrimination level, a complete star map can be made to determine the number of stars of the various magnitudes are in the FOV.

The star tracker output stability for the entire range of environments is better than ± 1 arc min. The drift is predictable and repeatable within ± 20 arc sec over its entire field of view for variations in operating temperature, star magnitude, star color temperature and magnetic field variations.

The tracker also contains a bright target detector which automatically closes a shutter to protect the star tracker if a target of -10 magnitude or brighter approaches within 18 ± 2 deg from the tracker null axis.

Another shutter mechanism attached to the front of the star

tracker allows acquisition and tracking of bright stars and planets. The shutter reduces the lens aperture to reduce the total incident light to the lens.

The power for both the BIRAP and the instrument is provided by a battery pack consisting of twenty-six YS-150 silver cadmium cells connected in series. This pack has a nominal output voltage of 28 volts and an output capacity of 150 AH. The battery pack is contained in the landing platform. The power is carried to the pointed section through the azimuth slip rings. All of the regulators are contained in the electronics package.

The BIRAP system contains an eight channel FM-FM telemetry system. The voltage controlled oscillators (VCO) and a 90 channel commutator are contained in the electronics box. The output of the VCO mixer is fed through the slip rings to the 250.7 mc transmitter housed in the landing platform. The telemetry antenna is mounted to the bottom of the landing platform.

Thermal analysis performed on BIRAP has determined the surface paints and the amount of insulation and/or heating that is required to keep the various sections at acceptable operating temperatures. Passive temperature control was found to be adequate for the electronics section. Heaters with simple thermostat controls are used in the star tracker and the drive assembly. The battery box is controlled by using freezing fluid passive control.

CONCLUSIONS

The BIRAP is now completely assembled and is in system performance testing. We are reasonably confident that the system can meet all of the objectives initially established for the system.

ACKNOWLEDGEMENTS

The BIRAP development program was initiated under contract RIB 63.1232 Dept. VI between Ball Brothers Research Corporation and the Department of Space Research, The University of Groningen, Groningen, The Netherlands.

REFERENCES

- Gibson, W.C., D.L. Guthals, J.W. Jensen, and J.A. Eccher, 1972. Pointing and Guidance of the BUSS Telescope, presented in a meeting on Instrumentation in Astronomy, Tuscon, Arizona
- Greeb, M.E., 1965. Design and Development of the Balloon Borne Solar Pointer, BBSP200. Final Report by Ball Brothers Research Corporation, Contract AF19(628)-4314.

Guthals, D.L., W.C. Gibson, 1973. Engineering Aspects of a Balloon-Borne Astral Pointing System (BAPS). Proc., Seventh AFCRL Scientific Balloon Symposium, AFCRL-TR-73-0071.

Toolin, R.B., 1973. Observations of Gondola Motions for High Altitude Flight Systems. Proc., Seventh AFCRL Scientific Balloon Symposium, AFCRL-TR-73-0071.

18781 87W

DISCUSSION SUMMARY — PAPER 4.7

Questions were asked about the cost of the system and the size of the telescope it could hold. The cost was estimated at between \$100,000 and \$150,000. The maximum instrument diameter which can be used with the system is 80 cm and the maximum length is 150 cm. One group is using it for a 60 cm telescope.

PAPER 4.8

A GENERAL PURPOSE STABILISED BALLOON PLATFORM

John How

Stabilised Balloon Platform Project
Marconi Space and Defence Systems Ltd.

ABSTRACT

A requirement exists in the U.K for a general purpose stabilised balloon platform. To meet this requirement MSDS designed and are now developing a three axis stabilised platform capable of being operated in three modes of increasing accuracy. The system relies on angular motion sensing for primary feedback with linear accelerometers, magnetometers and a star sensor for positional information. When under primary control the system will acquire and stabilise on any accessible part of the celestial sphere, a video verification systems is included to provide pointing confirmation. Under improved accuracy control the star sensor is used to lock onto a target star.

1. INTRODUCTION

The Science Research Council awarded MSDS Ltd a Design Study contract to propose a suitable system to meet a requirement in the United Kingdom for a general purpose Stabilised Balloon Platform onto which varied astrophysics experiments could be mounted with the minimum of integration complexity. This short paper is based on the Design Study which has led to a development contract being awarded which started in January and should lead to a flight of a prototype platform in September 1975.

The basic requirement is for a platform capable of being orientated to degree accuracy in a coarse mode with the facility for pointing at a visible source to arc minute accuracy and then, later, utilising experiment derived pointing error signals, to arc second accuracy. A facility to offset the experiment from the visible source in the arc minute mode by up to 5 degrees is included, with an optional extension to point towards the sun if required. To verify the pointing direction of the platform it is proposed to include a video verification system to provide a slow scan image of the star field towards which the platform is being orientated.

2. SYSTEM REQUIREMENTS

General

The control system will orientate the three axes of a balloon payload with respect to a specified accessible part of the celestial sphere. It will be controllable by telecommand and will be capable of observing and verifying an indefinite sequence of targets.

The system will ultimately be capable of being flown in three modes:

(a) Degree Guidance Mode

Using a primary control system to acquire and stabilise on any accessible part of the celestial sphere.

(b) Arcminute Guidance Mode

Using a star sensor or, if necessitated by later experiments, a sun sensor, to improve the system accuracy by locking onto the visible object. The target area may not contain a suitable guide star and it may be necessary to offset the star sensor. The rotation of the field of view due to diurnal rotation will then be removed by telecommand or otherwise.

(c) Arcsecond Guidance Mode

Using an experimenter's error signal in order to give a further improvement in pointing bias.

Applicability

The Stabilisation equipment may be used with a variety of inertial loads other than the nominal 250Kg mass at a radius of gyration of 0.7m.

Provision will be made for adjustment of the control loop gains and any other parameters affected to accommodate experiment masses from zero to the maximum of 500Kg without degradation of accuracy.

Performance - Definitions

If a record is made of the pointing error over a typical observation period of 1 hour and a least-squares fit is made to this record by adjusting the parameters a and b of the time function $a + b.t$, then the bias error is defined as the term, a , the drift error as the coefficient, b , and the noise error as the rms deviation remaining after the least squares fit has been made. The term lateral refers to the elevation axis and the orthogonal axis of star-sensor boresight line movement. The term twist refers to motion of the platform about the boresight line of the star sensor (in the degree guidance mode, about the nominal experiment boresight line).

Performance - Degree Guidance Mode

In this mode the following limits will not be exceeded:

Lateral Bias	1°
Lateral Drift	6 arcminutes/hr
Lateral Noise	1 arcminute rms
Twist Bias	1°
Twist Drift	unspecified
Twist Noise	1 arcminute rms

Performance - Arcminute Guidance Mode

In this mode the following limits will not be exceeded:

Lateral Bias	2 arcminutes
Lateral Drift	1 arcminute/hr
Lateral Noise	10 arcseconds rms
Twist Bias	24 arcminutes
Twist Drift	12 arcminutes/hr
Twist Noise	2 arcminutes rms

Performance - Proposed Arcsecond Guidance Mode

Although forming no part of the present contractual requirement, the system developed under the present contract is expected to be capable of later extension to achieve the following performance limits when fed from a suitable error sensor forming part of the experimenter's optical system:

Lateral Bias 1 arcsecond

Lateral Noise 2 arcseconds rms

Angular Range Requirements

In azimuth the package will have unrestricted angular range. In elevation the package will be capable of directing the boresight axis of the experiment (in the plane of the platform and perpendicular to the elevation axis) from 0° to 95° from the local vertical, however, operation with a star sensor is not required for angles under 20° to the local vertical.

If the roll axis is defined with respect to a nominal (Mean) elevation of the boresight axis of $32\frac{1}{2}^{\circ}$, as the projection of the boresight line into the plane normal to the local vertical, and bearing in mind that the roll axis so defined will depart from the horizontal for elevation angles other than the nominal, then the angular freedom required about this roll axis is a minimum of $\pm 15^{\circ}$.

Video Verification

A video verification system is required to confirm the pointing attitude of the platform. The system will have a field of view and sensitivity sufficient for a mean probability that 10 stars of sufficient magnitude can be viewed in order that the pointing direction can be confirmed by a star pattern recognition technique.

3. CONFIGURATION

In designing the Balloon Platform every attempt has been made to make it general purpose so that a variety of experiments (of different weights and sizes) could be flown with the minimum of complexity and time required for the integration operations. Unlike a number of stabilisation systems where the experiment is orientated within the gondola the present design allows for the whole platform/gondola to be rotated on a three axes gimbal cluster suspended below the balloon. This approach has the very distinct advantage of producing a very flexible system but does produce some control problems which will be discussed in a later section.

The complete system can be considered as two sub-systems namely the mechanics, consisting of the platform, the gimbal cluster including the actuators and the sensors comprising linear accelerometers, magnetometers, and star sensor.

To facilitate easy repair the platform will be a hybrid made up of straight aluminium I-section extrusion and a panel of honeycombe sandwich (aeroweb) material. Equipment mounted on the platform would be rather vulnerable should the platform roll on landing, so a protective cage of fibre glass tubes will be fitted. This will also arrest the suspension column so that it does not collapse onto equipment after the parachute has been released. An advantage of using fibre glass tubes is that they can be repaired in the field with an epoxy glued bandage so avoiding the use of welding.

The gimbal cluster assembly is the heart of the stabilised platform providing both rotational and translational movements. The assembly provides 360 degrees freedom in azimuth, plus 70 to minus 5 degrees in elevation and plus or minus 15 degrees in roll. The gimbals are orientated to the required angles by 9 inch diameter "on shaft" slab D. C. motors. Experiments will normally be mounted directly onto the platform and associated equipment such as the tele-package, batteries etc. arranged to maintain balance. In order to reduce the gimbal motor size a cross slide translational mechanism is incorporated into the gimbal assembly to ensure that the centre of mass of the entire controlled payload remains below the balloon suspension point, so largely eliminating out of balance torques. The translational mechanism will consist of a linear slide formed by a three point support, the axis being defined by 2 recirculating ball bush units working on a hollow tubular shaft and rotation about the bushings being prevented by a third location consisting of a pad of rollers working either side of a parallel platform.

The slides are duplicated with one on top of the other to provide 2 orthogonal axes. The rotational gimbal assembly and hence the platform suspension point will be driven along the slides by means of cranks thus removing the necessity for limit stops. In order to reduce the effort required to drive the weight of the platform along the slides when inclined, a 35 degree wedge will be included between the plane of the slides and the platform so that for the platform elevation range of minus 5 to plus 75 degrees the cross slides are inclined by plus or minus 40 degrees to the horizontal.

Suspension of the platform gimbal assembly to the balloon suspension train is by means of a column. The primary functions of the column are to enable the gimbal rotary drives to react upon the suspension train to produce pitch and roll torques and also to position the azimuth sensing magnetometers away from the platform borne equipment in order to reduce magnetic disturbances to an acceptable level. To control float altitude it is necessary for a balloon package to carry a considerable mass of ballast which can be released on command. This ballast presents a problem because if mounted on the controlled platform it would change the centre of mass considerably when released. To overcome this it is proposed to provide accommodation for a ballast container within the column assembly above the gimbals and to arrange for the ballast to be safely ejected below the platform via the hollow centre tube.

Primary stabilisation feedback for the rotational gimbal motors is provided by an angular motion sensing package mounted close to the gimbal assembly on the platform. When under degree mode control positional information is obtained from magnetometers for azimuth and linear accelerometers for elevation and roll. A two axis fluxgate magnetometer is used with the elements lying in a nominally horizontal plane (a third axis may be included to provide for electronic orthogonalisation of the elements). The outputs from the magnetometer are resolved by multiplying DACs whose gain is controlled by the sine and the cosine of the required azimuth attitude (fed by telecommand) and summed to provide a single error signal having a stable null at the required azimuth position. Positional information for control about the other two axis is obtained from a three axis linear accelerometer package sensing the three components of the earth's gravitational field resolved into the axes of the platform. The outputs from the accelerometers will be resolved by multiplying DACs in the proportions necessary for a particular platform attitude in a similar way to the magnetometers. To avoid alignment problems between the accelerometer package measuring actual position and the experiment which is required to be pointed in a particular direction it is proposed to mount the package on or within the experiment.

When under minute mode control, high accuracy position signals are derived from a star sensor aligned to and mounted on or within the experiment. The sensor provides 2 error signals, one about the elevation axis and the other about the orthogonal axis of the boresight line movement. The elevation error can be used to control the elevation gimbals direct but the orthogonal error controls both the azimuth and roll gimbals in proportions depending on the elevation angle. The star sensor has an AGC system with a range of 60 dB making it possible to view stars between minus 1 and plus 5 magnitudes (visible). The equivalent noise angle when viewing a +5Mv star is 5 arc seconds rms in an 8Hz bandwidth. Should an experiment require to view the sun, then, when under minute control, the star sensor is to be replaced by a twin axis sun sensor.

In addition to the units within the main sub-systems a facility for providing offset guidance is included. The star (or sun) sensor will be mounted on a two axis gimbal assembly capable of being rotated through plus or minus 5 degrees in each axis with a resolution of 1 arc minute. Control of each gimbal will be by means of precision lead screw driven by a stepper motor. Final position will be determined by counting the number of stepper motor drive pulses from a datum null as defined by a variable reluctance pick-off.

To assist in the ground control of the balloon platform whilst in flight and to verify to an experimenter the area of sky that his experiment is viewing it is proposed to include a video verification system. The system will consist of a standard ruggedized closed circuit television camera and a suitably modified control unit to provide a very slow scan rate so that the video signal can be relayed from the balloon by means of a low bandwidth telemetry link. The camera will have a field of view of approximately 120 square degrees and will be capable of discriminating stars down to magnitude (visible) plus 5. The line angular resolution and the resolution along a line will be less than 3 arc minutes. A complete frame will be scanned in less than 20 seconds and the positions of 10 stars monitored. In order to scan a complete frame and yet monitor only 10 stars the system video gain will be adjustable by telecommand so that the limiting magnitude can be varied from plus 1.5 to plus 5 (visible) in 7 increments.

4. CONTROL LOOP CONFIGURATIONS

The stabilised balloon platform utilises gimbals which complicate the control loops because of cross coupling and interaction. The system at present envisaged has sensors mounted on both the platform and the suspension, their errors being routed to the gimbal control motors in proportions depending on the elevation angle. The elevation control loop is the only one to have a unique set of sensors feeding its controlling motor at all times. To avoid ambiguity it is necessary to define two sets of axes, one set for the gimbals and the other for the platform. The gimbal axes are defined as azimuth, elevation and roll whilst the platform axes are defined as twist, elevation and yaw.

Considering the elevation control loop for the degree mode, primary stabilisation is by means of a rate loop consisting of a multiple integrator and a notch filter producing integral control of 4th order. Positional information derived from summed resolved accelerometer signals is suitably shaped to give a high order roll over and summed into the rate loop as a velocity demand. In view of the large platform weights envisaged and the corresponding loading of the gimbal bearings leading to high bearing friction it is proposed that the motors be pulse driven. Instead of a gradual build

up of motor torque until it overcomes stiction the motor will be pulsed all the time so that in theory the bearing is never stationary. A pulse width modulator is proposed producing pulses (both positive and negative) at a constant frequency with varying width depending on the analogue error input from the error processing circuits. The use of a pulsed motor drive has the additional advantage that a simple power amplifier can be used, required to operate in only two states, on or off. Dissipation within the amplifier is kept to a minimum and parasitic instability problems are avoided.

In order to keep the gimbal control motors down to a reasonable size and yet be able to cope with reasonable margins of centre of mass uncertainty the cross slide system has been incorporated into the gimbal assembly to maintain the centre of mass below the platform suspension point.

It is proposed that a cross slide mechanism should be brought into operation when the torque required from a gimbal motor exceeds 30 per cent of its stall torque. There seems little possibility of the platform receiving a sudden rate input which would demand a restoring torque greater than that available from the gimbal motors but large position errors will exist when a new platform attitude is demanded and these will have to be limited so that not more than approximately 60 per cent of the motor torque is demanded. In practise the slewing rate of the platform will be governed by the speed at which the cross slide system can follow the centre of mass offset giving rise to the large demanded motor torques.

The roll control loop is similar to the elevation the only difference being that the rate error is derived from a pair of gyros mounted on the platform, the proportion from each depending on the elevation angle. At present it is proposed to mount a bank of sine/cosine potentiometers on the elevation gimbal shaft but since only gain parameters are involved a more elegant solution is being sought to reduce the number of interconnections.

The azimuth loop is very different from the other loops since the torques involved are lower. Rate signals are again derived from a pair of sensors after suitable resolution by the elevation angle. The position signals are derived from the magnetometers.

Minute mode guidance is achieved by transferring the positional control to the star sensor wherever possible. In the case of the elevation control loop this can be done all the time but the proportion of star errors feeding into the other loops is again dependant upon the elevation angle.

In the ultimate mode of arc second guidance the star sensor error signals will be replaced by signals derived from within the experiment or at least utilising the same primary optics in order that bias errors due to alignment inaccuracies can be reduced to a minimum.

5. CONCLUDING REMARKS

It is hoped that this brief paper gives some idea of the type of platform that Marconi are now developing and of the performance that is anticipated. Once developed and in service it will provide many experimenters of different disciplines with a general purpose platform onto which they can mount their experiments with the minimum of interface problems leaving them free to concentrate on instrument development and hence to further their scientific research.

Whilst a complex problem to model a representative balloon platform including effects caused by the suspension train early simulation results have shown the system noise to be less than 2 arc seconds peak to peak. These results were obtained based on a model including simulated ball races with the usual high stiction values. The possibility of incorporating "flex pivots" with their linear friction/displacement characteristic is being investigated which may lead to a further improvement.

ACKNOWLEDGEMENTS

The author wishes to thank the Technical Director, Marconi Space and Defence Systems Limited, and the Science Research Council for permission to present this paper.

DISCUSSION SUMMARY — PAPER 4.8

A question was asked about how a flex pivot works. It was described as a suspension arrangement having a linear restoring torque for angular displacements and a linear restoring force for lateral displacements. One cylinder is suspended inside another with these pivots. (Ordinarily the lateral displacements are very small.)

In answer to inquiries about the cost, the initial development cost was estimated at \$450,000 and the production platform cost tentatively at \$50,000.

The mass is estimated to be 300 kilograms without the telescope and without NCAR telemetry.

The two experiments from British Universities proposed for initial flights on the platform are an infrared telescope and an ultraviolet instrument. Work on the platform was started January 1, 1974.

NCAR TELEMETRY AND COMMAND SYSTEM

W. Jack Snider

NCAR-National Scientific Balloon Facility

ABSTRACT

Increasingly complex balloon-borne scientific experiments have established a need for sophisticated telemetry and command systems. The National Scientific Balloon Facility (NSBF) has met this need by providing a Pulse Code Modulation (PCM) Data Encoder, a computerized ground station, and a PCM Command System. A description of these systems is presented in this paper.

PCM TELEMETRY SYSTEM

The ability to accurately recover and reproduce data from a balloon borne experiment is the most important function of the electronic support systems provided by NSBF to the scientific user. As experiments have become more complex, the requirements for support in this area have become more demanding. Greater flexibility in number of inputs, sampling format, bit rate, parity and real-time monitoring capability is a necessity for a system which must meet the requirements of a broad range of experiments. The new Pulse-Code Modulation (PCM) data handling system, which is now fully operational, has answered the demands for this capability in a way that is very well received by the scientific community.

The heart of this system is a PCM data encoder, Spacetac 2100 Series. This unit features modular construction, plug-in format and synchronization word storage and programmable system functions; all of which allow the user to select the system configuration to meet his exact needs without requiring a redesign.

The encoder consists of a control unit and expander modules. The control unit contains the electronics necessary to process, assemble, encode and output the multiplexed analog and digital information from the expander modules.

Input select codes are generated in the control unit from information stored in an electrically programmable read only memory (EPROM) in which the telemetry formats are stored. This device is programmed in accordance with the experimenter's requirements to give him a variety of sampling rates for his input data channels. One EPROM set has storage capacity for up to eight formats. The number of formats per EPROM will vary depending on the complexity of the format and the amount of EPROM storage required. The appropriate format for a particular application is selected from the EPROM by hard-wiring or applying logic levels to pins on the programming connector.

Each analog expander unit (multiplexer) is capable of multiplexing sixteen single ended inputs or eight differential inputs or any combination of single ended and differential inputs. These expander units are interconnected to the control unit subassemblies with printed circuit bus cards which are automatically adapted to any system configuration. A maximum of eight analog multiplexers, providing 128 inputs may be utilized at one time. Each analog channel will accept signals between -5 and + 10 volts without degrading the analog to digital conversion accuracy or resolution.

In addition to the analog inputs, up to eight digital multiplexers with capability for four ten-bit inputs each may be included in the system build-up. These units are interfaced into the control unit in the same manner as described above for the analog expanders. High input impedance (100K ohms) and a wide

input signal range (-50 to +50 volts) allows the use of discrete bits for ON/OFF status monitoring of analog signals as well as for digital data. When used in this manner, each digital multiplexer is capable of multiplexing forty discrete event sources into the data stream. These forty inputs are selected as four groups of ten bits each. Associated with the selection of each ten-bit byte is a synchronization signal which rises at least twenty micro-seconds before and falls at least one microsecond after the actual sampling of the ten-bit channel. This signal allows additional data source control.

For frame synchronization a twenty-bit word is stored in a second EPROM set and selected according to the program in the format storage. This word may be expanded up to a maximum of forty bits if required. Subframe synchronization is accomplished by either inverting the frame sync word at the subframe rate or by use of a frame counter.

Programmable functions in addition to format selection include bit rate (1280 bps to 81920 bps with internal oscillator or up to 256K bps with external oscillator), word length (6 to 10 bits), output code (any IRIG code), and parity (odd, even, 1/0 detect, or none). Plug-in pre-mod filters meeting all IRIG specifications are available with frequencies compatible with the standard bit rates. The encoder output drives a subcarrier oscillator which is part of the FM/FM telemetry system. The outputs of all subcarrier oscillators are mixed and used to modulate an L-Band telemetry transmitter for relay to ground receiving stations.

A subcarrier discriminator is used in the receiving station to strip the PCM signal from the frequency multiplex. The data is then processed and recorded using EMR 2700 Series decommutation equipment and a Digital Equipment Corporation PDP-11/20 computer system. The decommutation equipment includes a signal conditioner, frame and subframe synchronizers, binary and decimal displays, and digital to analog converters (DAC's).

After locking onto the incoming signal and establishing synchronization, the frame and subframe synchronizers output parallel data and timing pulses to the PDP-11 computer and to the displays and DAC's for real time monitoring.

The computer system consists of a PDP-11/20 processor featuring 16-bit parallel logic, 24K memory, an extended arithmetic element for hardware multiply and divide, a 64K fixed head disk, a 1.2 million word floating head disk cartridge system, a high speed paper tape reader-punch, and two 7-track, industry compatible magnetic tape units. The telemetry data is processed by the computer for logging on magnetic tape and for real-time display of critical flight parameters on the teletype.

A down-range receiving station is available for use when the flight trajectory extends beyond the range of coverage from Palestine. This station consists of essentially the same equipment outlined above with the exception of the computer. A manual version of the PCM decommutation equipment is available for real-time monitoring and conditioning of the signal for analog recording. The analog tapes are played through the computerized station after the flight to generate the digital tapes. This procedure gives the experimenter a complete set of industry compatible tapes covering his data for the entire flight. These tapes can easily be read into a larger computer for data reduction.

PCM COMMAND SYSTEM

The second most important function of NSBF electronic support is to provide remote control of the experimenter's payload. With the ability to modify his

equipment during a flight, the experimenter can monitor his data in real time and then update the system as necessary. In addition to the scientific requirements, command capability is also necessary for such balloon control functions as the release of ballast or helium and termination of the flight.

To meet these requirements, the NSBF has acquired a Pulse Code Modulation (PCM) command system. The system, developed by United Technology Laboratories, consists of an encoder and a decoder, both of which utilize "Data Communicator" (R) Modules manufactured by Larse Corporation. The module in the encoder, known as the "SEN" (R) unit accepts sixteen bits of data input and provides time-division multiplexing, encoding and frequency-shift-keying for modulation of the command transmitter. In the decoder, the "REDE" (R) unit decodes the data and presents it in its original state as sixteen bits of output.

The SEN unit performs several functions which greatly increase the reliability of this system. These include a special coding of the sixteen data bits and a double transmission of each encoded word. The code consists of a thirty-four bit word to represent sixteen data bits. The word is made up of eight four-bit elements and two synchronization bits. Each element contains two data bits preceded by a low clock bit and followed by a high clock bit. The output signal is frequency-shift keyed (FSK) for modulation of the transmitter. Each bit is represented by a tone of 1440 Hz for a zero state or 1800 Hz for a one state.

The REDE unit in the decoder performs security checks on the data before it is strobed to the output circuitry. Upon receipt of a command transmission, the REDE unit first performs code element checks to ensure that any errors introduced by the communication link are not interpreted as data. The first 34-bit word is then stored until the second transmission has been received and validated. The two words are then compared for bit-by-bit correlation. Upon completion of this check, the last six bits of the data word are released to the output terminals. These bits, designated as address bits, are then patched back into the REDE unit for decoding. If the address is correct, the remaining ten bits are released and a data strobe pulse is generated, indicating that all data is valid for that decoder.

The command encoder provides the selector switches, control logic and timing circuitry necessary to operate the SEN module and to key the command transmitter. There are three modes of operation which are selected using front panel selector switches. In the COMMAND mode, one of forty-eight open-collector drivers in the decoder unit is activated for control of relays or application of logic levels to digital circuitry. The DATA mode allows the transmission of a sixteen-bit data word as one command. The state of the sixteen bits is established by setting toggle switches on the front panel. The REMOTE mode of operation provides for computer control of command transmission. When this mode is selected, all front panel switches are deactivated and the computer is given control of command, data and address selection.

In any of the three modes of operation, the encoder circuitry interprets the switch settings and presents sixteen bits to the SEN unit for encoding and transmission. Bits ten through fifteen are used for address selection in all modes. A total of sixty-four different addresses are possible. In the command mode, bits zero through seven represent the command number and bits eight and nine indicate the type of transmission. For a sixteen-bit data word transmission, the encoder must make two double-scan transmissions. In the first transmission, bits zero through seven of the command word contain data bits zero thru seven. In the second transmission, these bits contain bits eight through fifteen of the data word. Bits eight and nine of the command word are used to identify

the two bytes of the data word. Timing pulses from the SEN unit are used to control the sequence of data word transmissions.

The encoder automatically keys the command transmitter for the required length of time to complete each command.

The command decoder accepts the FSK output from the command receiver, performs decoding and security checks, and presents the sixteen-bit command word to the output circuitry. A data ready pulse from the REDE unit initiates a timed sequence of decoding and command activation.

The output logic interprets bits eight and nine of the command word to determine the mode of operation. If these bits indicate a discrete command, bits zero through five are decoded and used to activate the appropriate open-collector driver. Associated with each command is a twenty-four volt dc output which is turned on by the control circuitry for fifty milliseconds. This voltage is used in conjunction with the driver to activate the command function. A current limit of eighty milliamperes prevents damage to the driver circuitry.

When the data mode of operation is detected, bits zero through seven of the first transmission are loaded into a temporary storage register. When the second transmission is completed, bits eight through fifteen of the data word are loaded into the output register and a data strobe pulse is generated to initiate a parallel dump of the full sixteen bits to the user's circuitry. When used for flight termination, the decoder is assigned an address number which is in the upper thirty-two possible addresses. This is done to prevent accidental termination of a flight. The most significant bit of the address code is protected in the encoder using a switch in series with the address selector switches. In order to transmit a command to a termination decoder, this additional switch must be placed in the "terminate armed" position. A warning light on the encoder gives an indication when either the address selector or the terminate armed switch is set for termination.

DISCUSSION SUMMARY — PAPER 5.1

Several questions regarding technical details of the system were asked. These and the answers given by the speaker are summarized below:

- Q. Does the PCM encoder that you fly go into your FM-FM system?
- A. Yes. We still have the FM-FM in addition to the PCM.
- Q. Do you put those in the Omega and other subcarriers?
- A. Omega occupies Channel 13 band in the FM multiplex. The Rossmont signal is generally put into one of the analog channels of the PCM and in some cases the subcarrier as well.
- Q. Have you ever had problems with the PDP-11 that caused flights to fail and, if so, is it possible that a back-up PDP-11 will be bought?
- A. There do not appear to have been failures during flights which caused loss of data.
- Q. What is the power consumption on the encoder full blown?
- A. Roughly 120 mils at 28 volts.

PAPER 5.2

AIROSCOPE TELEMETRY SYSTEM

Kenneth J. Pitts
Ames Research Center

ABSTRACT

The AIROscope (Ames Infrared Observatory telescope) telemetry system is described from signal conditioning on the gondola to display and storage at the ground station. All analog and digital data from the systems and experiments on the gondola go to a PCM encoder which formats the data into 10-bit words. Therefore, 0.1-percent resolution is inherently available for experimental data. The Bi ϕ -L coded bit stream directly modulates the carrier of the FM transmitter.

To insure reliable transmission over a 650-km range an 11-watt FM transmitter operating at 1483.5 MHz is used on the gondola. Modulation is narrow band FM with a maximum deviation of ± 500 kHz. The maximum modulation frequency is determined by the data bit rate which could be as high as 500 kbps. Presently, a rate of 20.48 kbps is used.

The ground station receiving system includes a steerable antenna (19-dB gain), preamplifier (21-dB gain) and receiver. The output from the receiver is a Bi ϕ -L bit stream like that on the gondola. This signal goes into the PCM decommutator unit which "locks" on and provides data displays (decimal digits, analog meters, or bit lamps) through several data word selector units. Also, selectable data words are routed to strip chart recorders for permanent data storage. All data are recorded on a tape recorder. The recorded signal then can be played back through the PCM decommutator unit at a later time for detailed data analysis by the experimenter.

GENERAL

This paper describes the telemetry system used on AIROscope. Topics covered will be signal conditioning, the RF down-link, data encoding and decoding, formatting, ground station data recovery and display, and tape recording/playback.

GONDOLA DATA GATHERING AND PROCESSING

All data, both scientific and engineering, are routed to a pulse code modulation (PCM) encoder unit to put them in a form that can be transmitted to the ground station. These data include:

- (a) Science/experimental data
- (b) TV star field data (see DeBoo, 1974)
- (c) Battery power

- 33721 25H
- (d) Subsystem power status
 - (e) Telescope optical alignment and direction
 - (f) Limit switch positions
 - (g) Subsystem temperatures
 - (h) Optics control, i.e., focus and collimation
 - (i) Command verification (see Barrows, 1974)

Some of the data are generated by CMOS (Complementary Metal Oxide Semiconductor) logic which produces bi-level (0V, 5V) digital signals. Other data come in analog form (0 to 10V) which also can be encoded. With a 10-bit encoding scheme, a resolution of about 10 mV can be obtained. A half scale level, or 5V, is telemetered to give a convenient check on overall system operation.

The encoder can accommodate up to 290 channels, has a through-put rate of up to 500 kbps, and uses a format-controlled programmable read-only memory. Analog to digital conversion is performed where required. At present, approximately 150 analog and 100 digital channels are processed at 20.48 kbps. Figure 1 illustrates the gondola data handling system.

In order to be decoded when the signal reaches the ground station, the data must be transmitted in a standard format. This formatting is also done by the encoder. The present encoder format has 10 bits per word, 32 words per main frame. In addition, fifteen of the main frame words are divided into two-word subframes (fast), nine of the words are allotted to eight-word subframes (medium) and three main frame words are used for sixteen-word subframes (slow). Using the 20,480 bps rate, the following rates are obtained:

Word rate	- 2048 wps
Main frame rate	- 64 fps
Fast subframe rate	- 32 sfps
Medium subframe rate	- 8 sfps
Slow subframe rate	- 4 sfps

Two channels at the main frame rate are available for scientific data. TV data are commutated at the fast subframe rate. All other data are handled by the other subframes. The first two words in each main frame are used for frame synchronization. Also, one word is used for a subframe I.D. code and is incremented at the frame rate for immediate subframe identification.

The output of the PCM encoder is a non-return to zero level (NRZ-L) serial bit stream at 20,480 bps. This data stream goes to a code converter which converts this signal to bi-phase level (Bi ϕ -L) code. This signal then directly modulates the RF carrier of the transmitter. Bi ϕ -L is used because synchronization is easier when the data may contain a long string of 1's or 0's.

RF TRANSMISSION

The L-band transmitter on the gondola provides a 1.4835 GHz carrier which is narrow-band frequency modulated by the incoming data. Several of the more pertinent transmitter parameters are listed:

Typical power out	- 11 watts
Typical input power	- 28 VDC at 1.3A

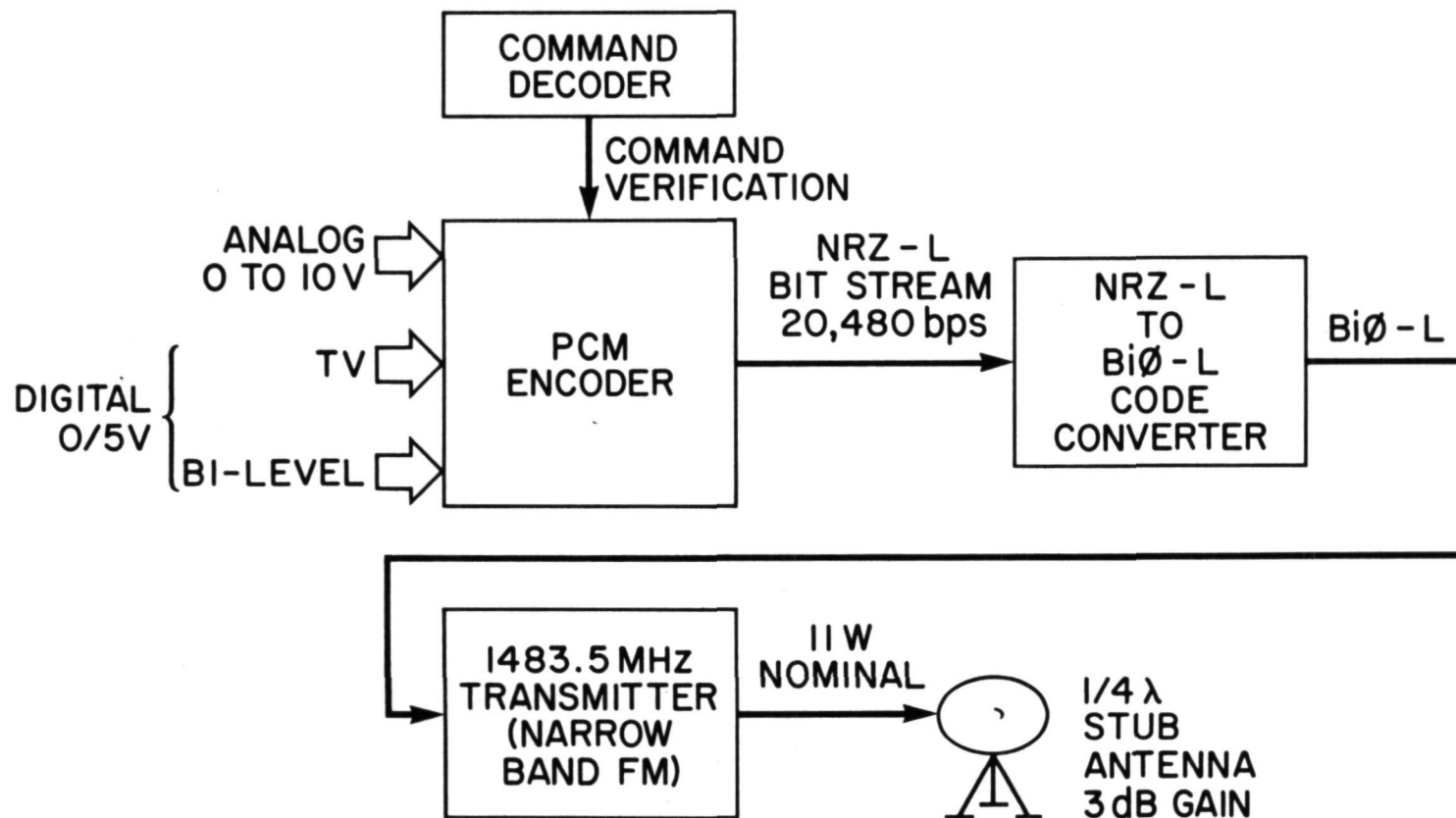


Figure 1. Gondola data gathering and encoding block diagram.

Carrier frequency stability	- ± 0.01 percent
Operating frequency	- 1.4835 GHz
Modulation characteristics	
Type	- Narrow band FM
Deviation sensitivity	- 500 kHz/VRMS
Modulation bandwidth	- to 500 kHz 0 dB, -0.4 dB
Spurious emissions	- Down 70 dB or better

Transmitter power is applied to a 1/4 wave stub antenna which provides approximately 3 dB gain and a broad polar pattern for reliable down range reception.

The RF link just described has the capability of accepting 500 kbps and therefore can easily accommodate the 20,480 bps data rate for AIROscope. This rate is determined primarily by the digitized TV data (see DeBoo, 1974). Most other data vary at much slower rates.

GROUND STATION

The signal is received by a 19-dB parabolic antenna, amplified in an L-band preamplifier and presented to the FM receiver. See Figure 2.

The receiving antenna can be positioned so as to maximize the incoming signal. Some important receiver specifications are listed:

Type	- Double-conversion, crystal-controlled FM
Frequency stability	- ± 0.003 percent
Sensitivity	- 97 dBm at 10 dB quieting
Spurious signal rejection	- 60 dB or better
Noise figure	- 10 dB maximum
Demodulated bandwidth	- 10 Hz to 150 kHz, ± 1.5 dB
Operating frequency	- 1.4835 GHz

The receiver has the capability of adjustable output level and carrier detection. In addition, this receiver contains a spectrum analyzer so that the data spectrum and possible adjacent channel interference can be examined over a 6 MHz bandwidth centered at the first IF of 50 MHz. This bandwidth may be reduced to 100 kHz for increased spectral resolution. Selectable IF bandwidths and video (demodulated) bandwidths are available to optimize signal reception under adverse conditions. The combination of the receiving and transmitting systems is such that at a 650 km maximum range, a signal-to-noise ratio of 4 to 7 dB is expected.

The demodulated output of the receiver is of course contaminated by noise. This output is coupled to the bit synchronizer of the PCM decommutating unit. The bit synchronizer locks on the incoming signal and provides a "clean" serial bit stream and regenerated clock to the code converters. One converter provides NRZ-L to the format synchronizer. The other provides Miller code or DM for tape recording, which was selected because it eliminates the necessity to record DC which can occur when NRZ-L is used.

The format synchronizer operates in one of four modes: Search, Verify, Lock, or Check. Only when the synchronizer is in the Lock mode will valid NRZ-L data be routed to the rest of the ground station. For a flow chart description, refer to Figure 3. When in the Lock mode, the format synchronizer applies frame and word I.D., parallel data, and a strobe to a word select and

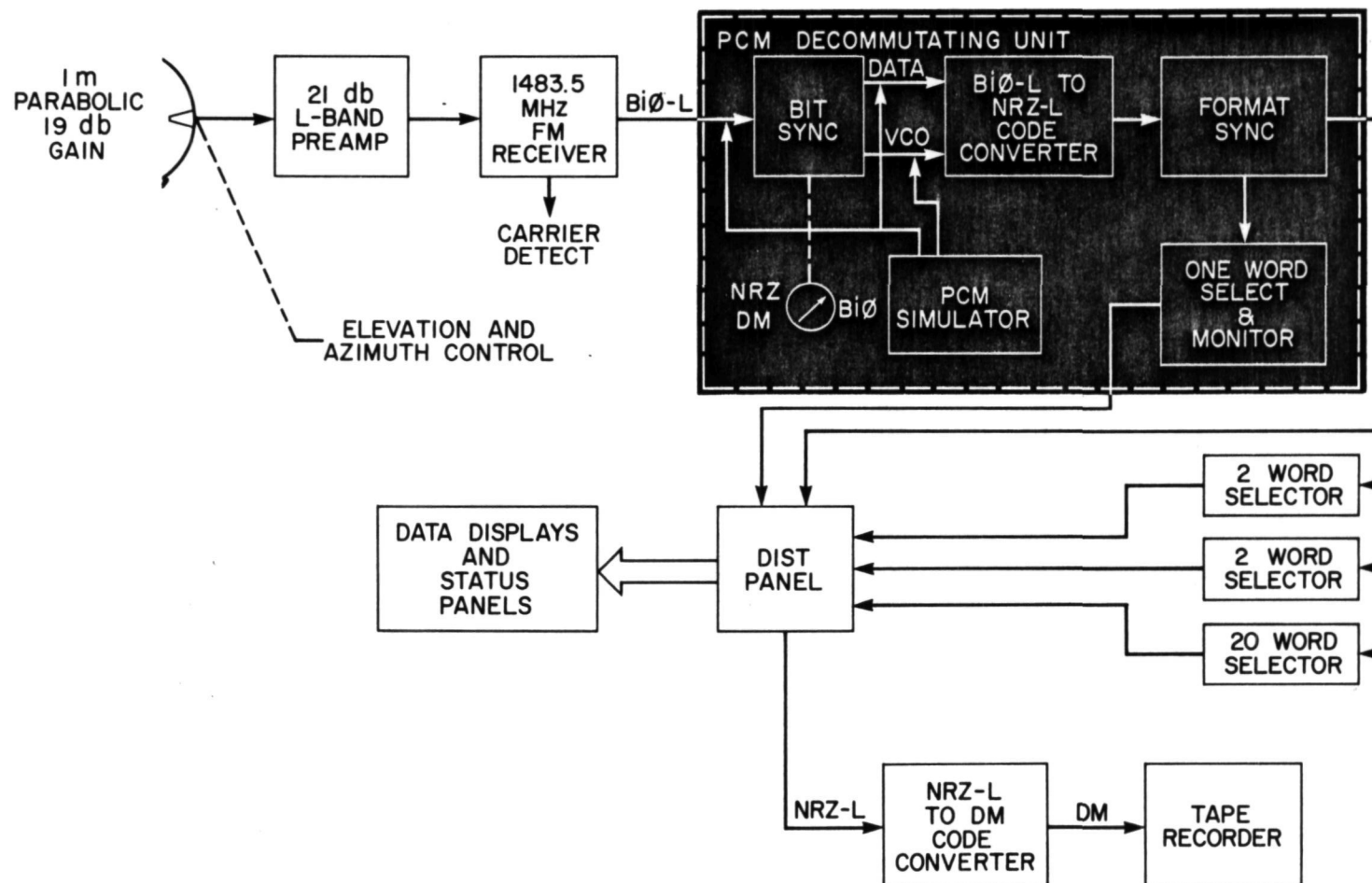


Figure 2. Ground station block diagram.

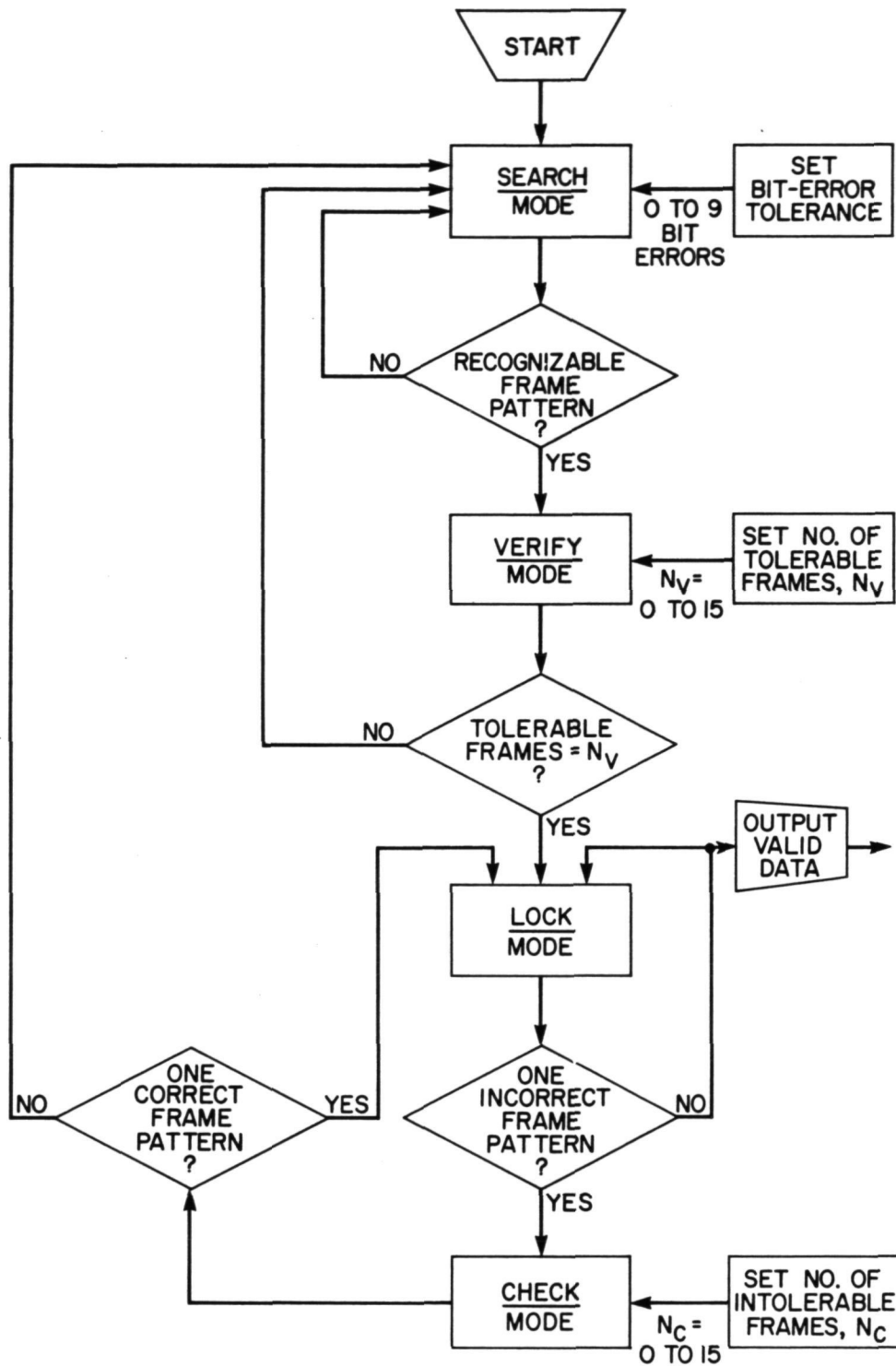


Figure 3. Frame synchronization strategy.

monitor unit. This unit will display the 10 bits of a selected data word on a binary lamp display and a meter. Also, three other word selectors are driven. Each of two of these will select, by thumb-wheel switches, two words and display them on a four decimal, 7-segment readout as well as on lamps and a meter. The third word selector will provide 20 words and is controlled by a punched card program for maximum flexibility. Three of these words are routed to the star field display electronics and the remaining 170 bits are distributed to the status panels and consoles. Therefore, at any one time, a total of 25 10-bit words may be selected by the operator. (See Figure 2.)

The PCM decoding/decommutating unit and associated word selectors utilize Series 7400 TTL and Series 830 DTL Integrated Circuit Logic.

Selected data can be displayed in four areas of the ground station racks, in addition to the word selector displays. These are:

- (a) Bit Status Light Bank — The Bit Status Light Bank provides a quick-look at the health of AIROscope by examining data words on a bit-by-bit basis.
- (b) Engineering Control — The Engineering Control Panel displays various housekeeping data such as optics alignment and subsystem power status.
- (c) Pointing Control — Data displayed on the Pointing Control Panel is associated with the status of telescope pointing for target acquisition. For example, the telemetry will tell the operator whether the telescoping is moving left, right, up, down, or diagonally.
- (d) Filter Spectrometer Control — Status of the IR experiment is displayed on the Filter Spectrometer Control area. Here, the experimenter monitors the state of a filter wheel and IR amplifier gain, as well as other experimental parameters.

In addition, the ground station contains a magnetic tape recorder, strip chart recorders and other devices for recording information and determining the performance of the system. See Figure 2.

When the operator places the input code selector switch on the PCM Decommutating Unit in the "DM" position (see Figure 4) the tape recorder can be used to play back a taped mission through the ground station. In this mode, the Miller Code serial data from the tape is converted back to NRZ-L and all the ground station data displays function as previously described.

CONCLUSION

The AIROscope telemetry system offers a large and expandable capacity, the capability to encode analog and digital data, and a variety of safeguards for reliability of data transmission and command verification. This paper has shown the versatility of the AIROscope system. Its versatility may be utilized to accommodate expanded scientific requirements in future balloon-borne infrared astronomy missions.

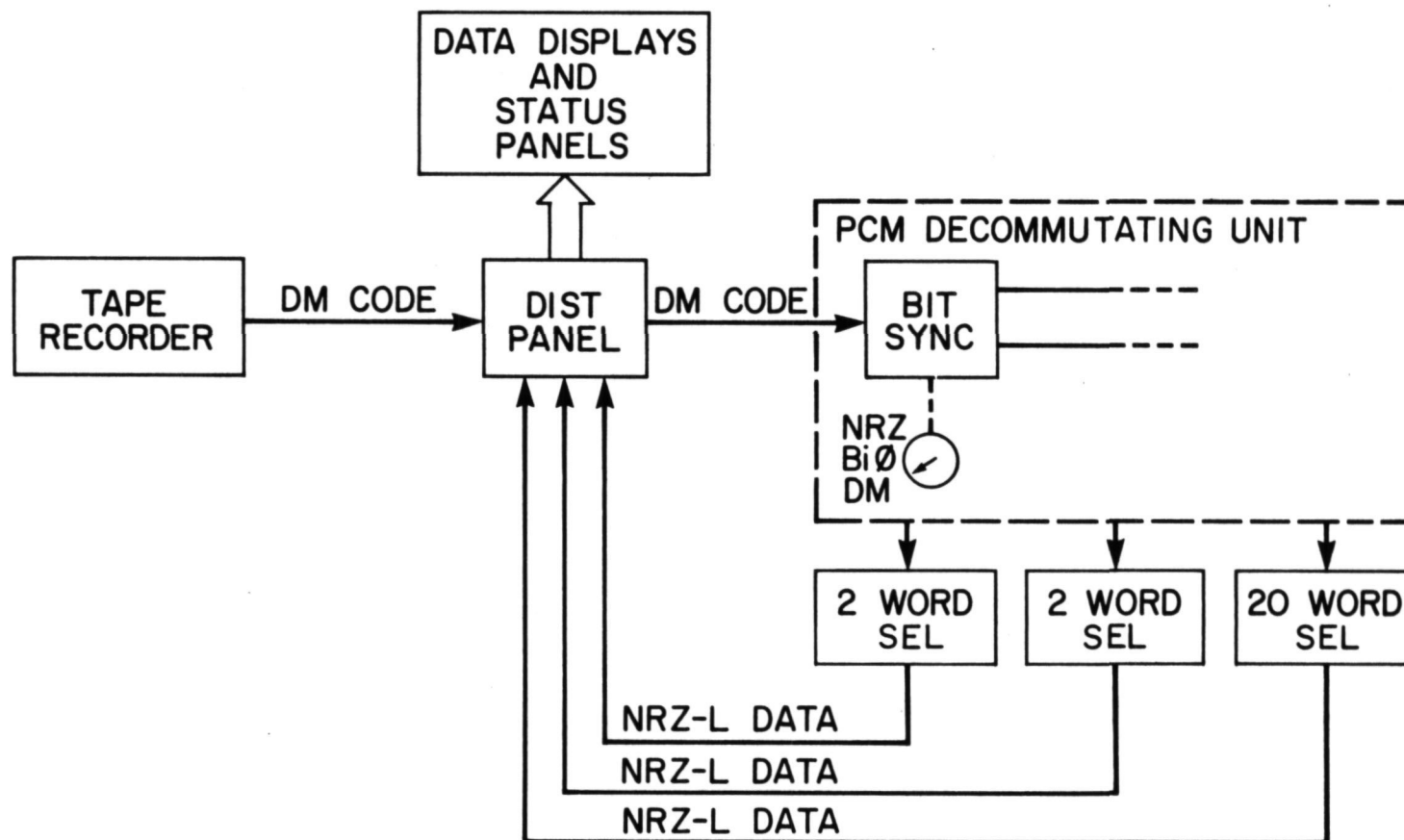


Figure 4. Data playback mode block diagram.

REFERENCES

Barrows, W. AIROscope Command System. These proceedings, 1974.

DeBoo, G., Hedlund, R., and Parra, G. AIROscope Stellar Acquisition System.
These proceedings, 1974.

DISCUSSION SUMMARY — PAPER 5.2

No discussion.

PAPER 5.3

AIROSCOPE COMMAND SYSTEM

W. Barrows
Ames Research Center

ABSTRACT

A PCM telemetry command system is presented having a capacity of 256 unique commands, an end-to-end actuation time of less than 250 milliseconds, and an address plus complementary command code to provide security against the acceptance of anything but intended commands. The system consists of a ground-based ENCODER and a balloon-borne DECODER, both built using low-current drain, high reliability CMOS logic elements. Commands are normally issued by a simple switch closure to +5VDC on the appropriate input line, however as a backup mode, the 8-bit command may be entered manually on 8 toggle switches and executed via a SEND button. In any case, the command is then serialized into a Bi $\bar{0}$ -L PCM bit stream and sent via a P-Band radio link to the DECODER aloft. All 256 outputs from the DECODER are buffered through drivers and thus may be used to drive CMOS, TTL, or DTL logic.

INTRODUCTION

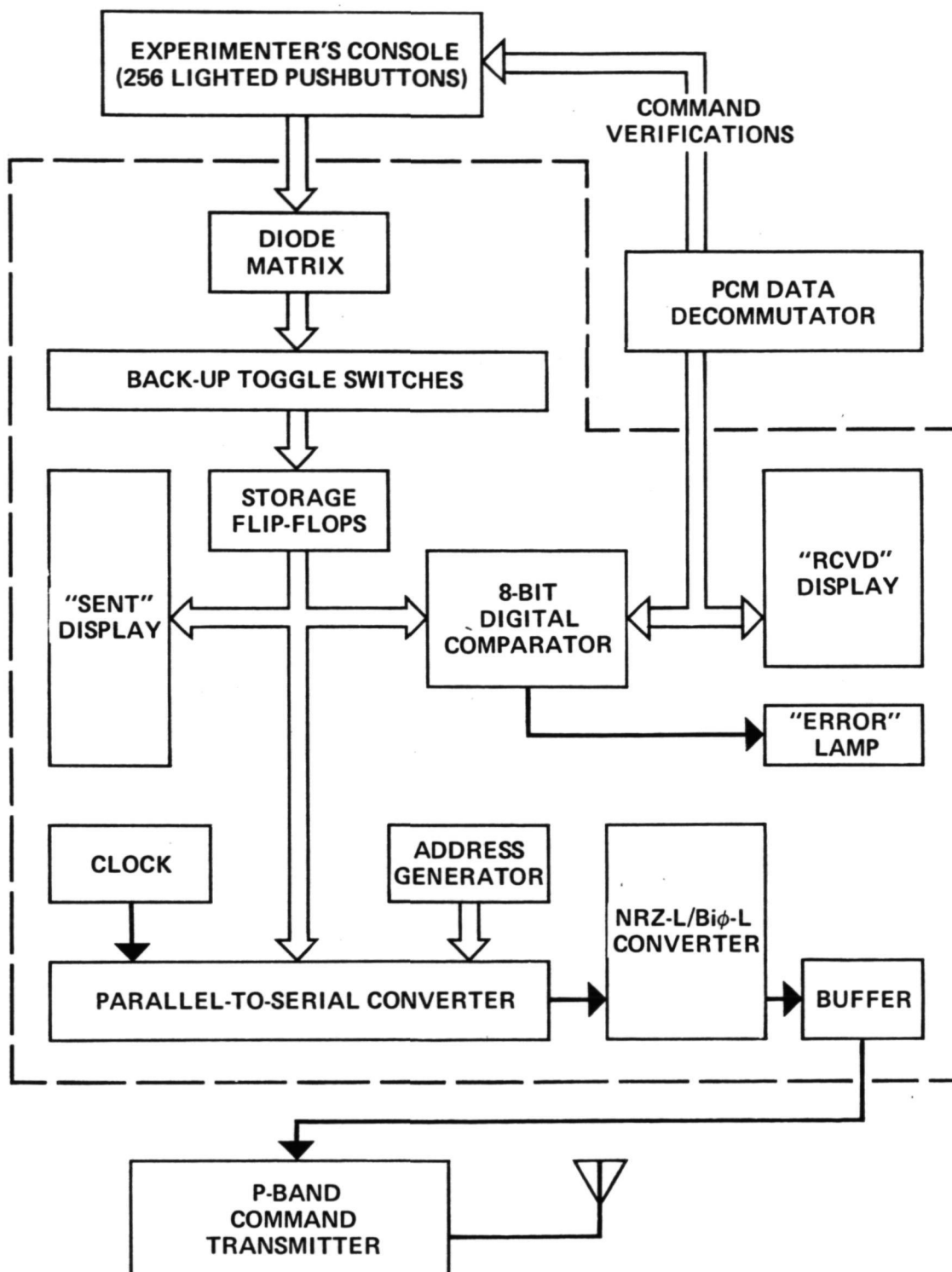
At the inception of the AIROscope redesign effort an attempt was made, primarily through the National Center for Atmospheric Research (NCAR), to determine what command subsystems had been used in the past on balloon systems. It was found that, in general, the systems in use suffered from excessive operational complexity, restricted capability in terms of the total number of discrete commands which could be delivered, and they were not sufficiently generalized to permit the flexibility required by a constantly changing mission science program.

Consequently, it was determined that a Command Encoder-Decoder system would be built in-house using the latest mil-spec temperature range, low current CMOS logic elements. The 256 commands provided by a system based on an 8-bit command word were considered more than adequate for all currently planned AIROscope missions and sufficient to permit a reasonable degree of expansion on foreseeable future missions. Beyond that, two or more such systems operated in parallel could clearly provide nearly unlimited expansion capability, if desired. The parts cost for this system was less than \$2500 and the required delivery schedule for all hardware was met.

ENCODER DESCRIPTION

The various functions performed by the Command Encoder may be understood by referring to the Functional Diagram in Figure 1. In addition, a detailed Schematic Diagram is provided in Figure 2 for the convenience of the reader who would actually like to construct a similar system for his own use.

Referring to the functional diagram, the first function within the dashed outline enclosing the Command Encoder itself is the Diode Matrix.



$\bar{C}_1 C_1 \bar{C}_2 C_2 \bar{C}_3 C_3 \bar{C}_4 C_4 \bar{C}_5 C_5 \bar{C}_6 C_6 \bar{C}_7 C_7 \bar{C}_8 C_8 A_1 A_2 A_3 A_4 A_5 A_6 A_7 A_8$

Figure 1. Command Encoder Functional Diagram

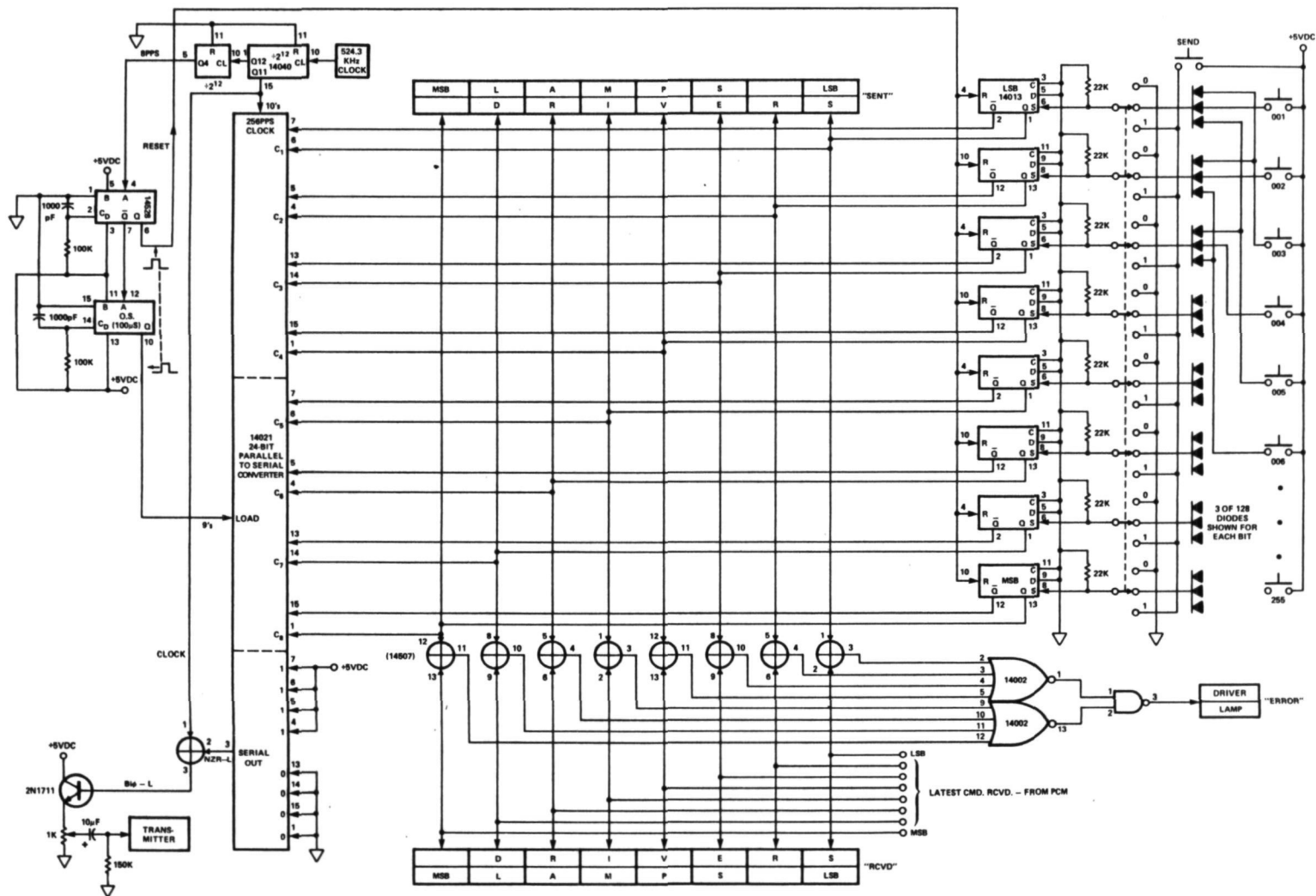


Figure 2. Command Encoder Schematic Diagram

This is an array of 1024 discrete diodes arranged in such a fashion that the actuation of a single (one of a possible 256) normally open switch is encoded into the appropriate "ones" and "zeroes" which make up the 8-bit command. The Backup Toggle Switches permit the operator to bypass the Experimenter's Console and the Diode Matrix and to generate a command directly by switching in the desired 8 command bits and by pressing the SEND button. Regardless of how these 8 bits are generated, they are then entered into the Storage Flip-Flops, the outputs of which are routed to the SENT Display, to the Digital Comparator for comparison with the latest command received by the gondola (RCVD), and to the Parallel-to-Serial Converter. The 8 command bits, along with their complements and an 8-bit recognition address word are simultaneously loaded into the Parallel-to-Serial Converter and clocked out at a rate of 256 bits per second. Every 1/8 second the Clock also updates the Storage Flip-Flops and loads the Parallel-to-Serial Converter. The now serialized NRZ-L bit stream is converted into a BiØ-L PCM code to improve the reliability of transmission and to permit direct tape recording. Finally it goes through a buffer stage where it is made compatible with the input of the Command Transmitter. This up-link UHF transmitter operates in the P-band and develops 10 watts of r.f. power.

Two different levels of command verification are provided by the AIRO-scope system. One results from the comparison of the SENT command with the RCVD command in the Command Encoder itself where any disagreement between the two results in the lighting of the ERROR lamp. A second type of command verification is provided for the AIROscope via the PCM Data Subsystem wherein up to 110 discrete "on-off" digital data channels may be employed to monitor the status of various commandable subsystems on the gondola. These status indications are used to light the appropriate push-buttons on the Experimenter's Console to immediately feed back to the operator the information that the command sent was properly received and that the system to which the command was issued did, in fact, respond.

It is important to note that the Encoder is continually encoding some command, i.e., when no command button is being pressed, the command 000 is sent. This command is processed like any other command on the gondola and its output may be used as a "reset" or a "ready" indication. Even more important is the fact that such an arrangement permits one to check at any time on the continuity of all major links in both the Command Subsystem and the PCM Data Subsystem by simply observing the status of the ERROR lamp.

DECODER DESCRIPTION

The functions performed by the Command Decoder are depicted in Figures 3 and 4. On the gondola the P-Band signal is received by the Command Receiver, buffered to re-create a signal with 0 and 5 volt levels, and re-converted from BiØ-L to NRZ-L plus a clock line. The NRZ-L bit stream is then clocked into the Serial-to-Parallel Converter, the contents of which are constantly being examined by the Valid Command Recognition circuitry. This circuitry verifies that each command bit is immediately preceded by its complement and that these 16 bits are followed by the correct 8-bit recognition address code. If, and only if, all these criteria are met, a "Load" pulse is generated which loads this 8-bit command into a set of 8

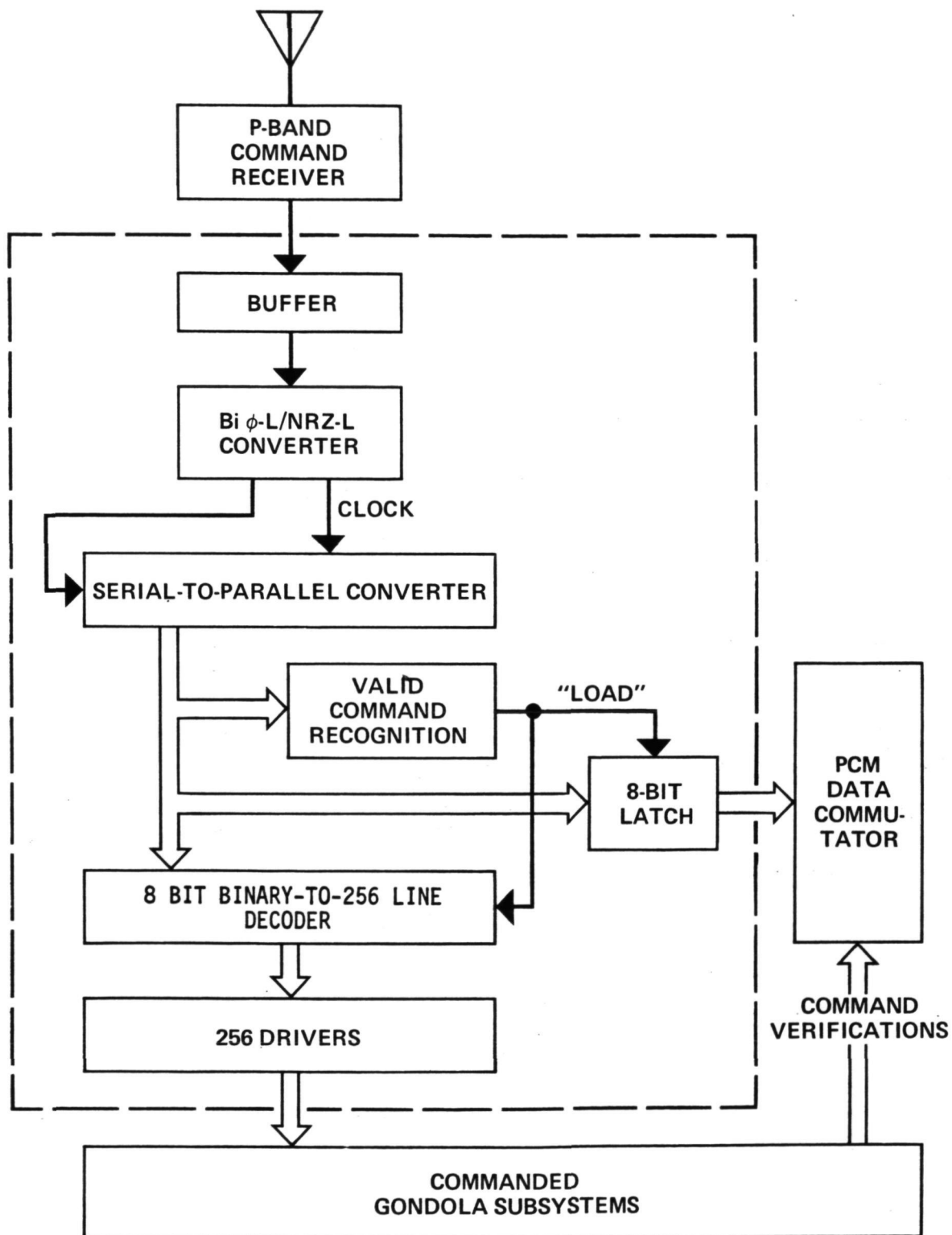


Figure 3. Command Decoder Functional Diagram

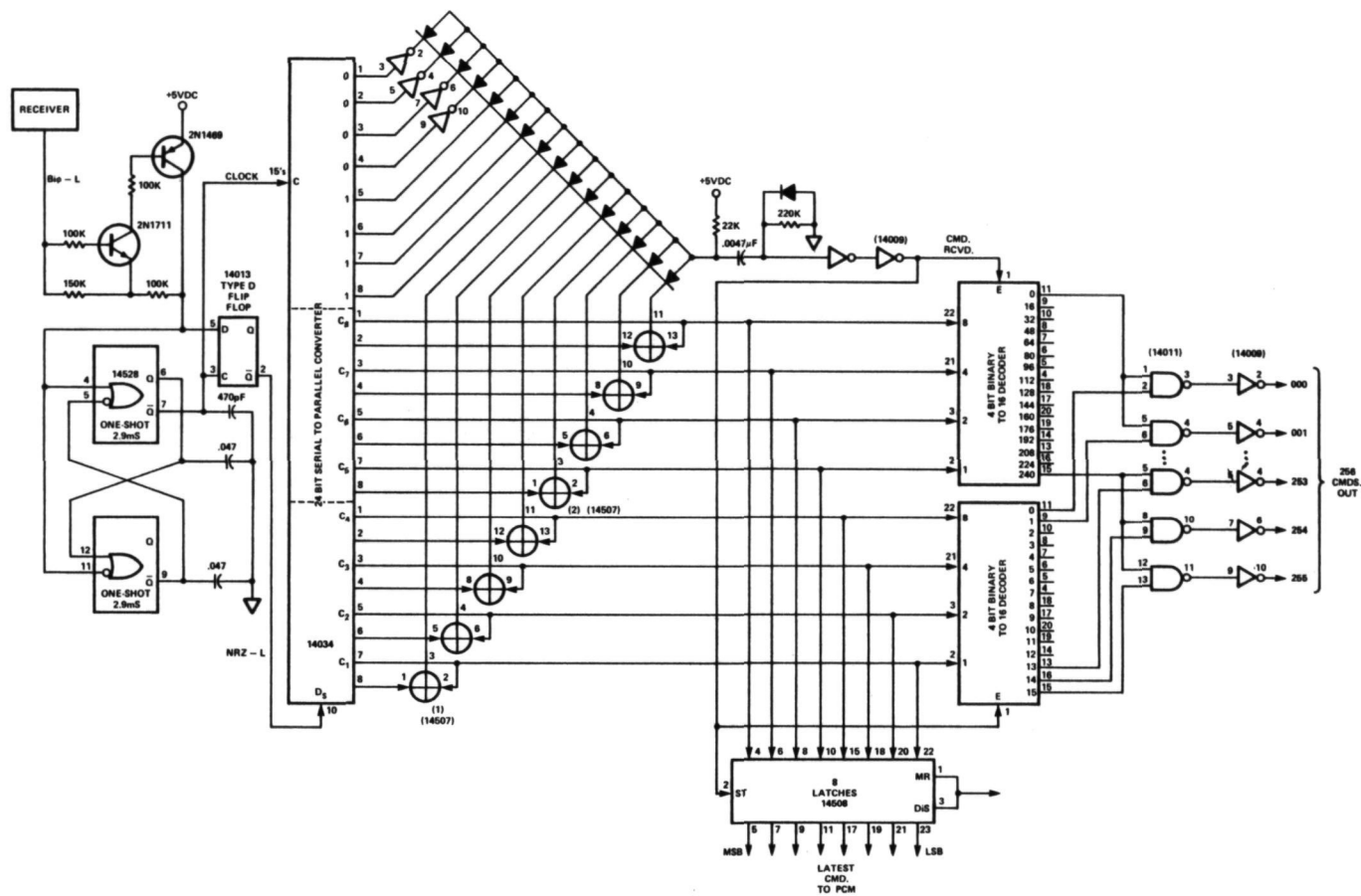


Figure 4. Command Decoder Schematic Diagram

latches which are examined 8 times per second by the PCM Data Commutator for transmission to the ground as the RCVD command. The "Load" pulse also enters the 8-bit command into the 8 Bit Binary-to-256 Line Decoder which routes the command to the proper one of the 256 possible lines as dictated by the 8-bit binary command number. Each output line is buffered through a CMOS driver so that it is capable of interfacing with CMOS, TTL, or DTL 5 volt logic systems.

PERFORMANCE AND OPERATIONAL CONSIDERATIONS

Whenever a command is issued by the operator, the time required for it to be encoded, placed on the serial bit stream, and transmitted to the gondola is between 125 and 250 milliseconds. This is due to the fact that, if the command button is pressed sometime during the clocking out of the Parallel-to-Serial Converter, one must wait up to 125 milliseconds for the desired command to be loaded into the Converter. Then, another 125 milliseconds is required for the clocking out of one complete 'command plus address' sequence. Essentially simultaneously with the generation of this first complete 'command plus address' sequence, the decoder in the gondola is clocking it into its Serial-to-Parallel Converter. Thus, by the time the command is fully serialized on the ground, it has also been entered into the Decoder aloft, verified as a valid command, and directed as a +5 volt logic level to the appropriate gondola subsystem. At most an additional 125 milliseconds is required for either of the two previously mentioned levels of command verification to be telemetered via the PCM Data Subsystem back to the ground station. Thus, the maximum total time required for the issuance and final verification of a typical command is 375 milliseconds.

When the operator presses a command button and holds it in, the appropriate output line on the gondola will rise to a +5 volt level and, in the absence of telemetry drop-outs, will stay at +5 volts until the command button is released (at which time command 000 is decoded). The shortest command which can be given lasts 125 milliseconds. The longest command is indefinite, however, it must be noted that the characteristics of this design dictate that ONLY ONE command may be given at a time. If two different commands were given simultaneously, a third command, most likely unrelated to either, would probably be generated. This caveat turns out not to be too restrictive but it does present some operational constraints which must be reflected in the design of the overall Control and Data system. If it is desired that a gondola subsystem be activated for more than a few seconds, a latch may be built into that subsystem and two commands may be assigned, one to set the latch and another to reset it.

The availability of only 8 command bits at a time also has system design implications. For example, one cannot simply command a motor to position a shaft to one of several thousand possible orientations. What must be done is to have one command which rotates the shaft, another command to stop its rotation, and a 10-bit telemetry word which reports back to the ground station operator the exact orientation of the shaft. This method of achieving precise control over subsystems on the gondola has proved to be totally acceptable for the implementation of all investigations proposed thus far for the AIROscope.

An additional and particularly useful feature of this design is that the Command Encoder and the Command Decoder may be connected directly

together with a single BNC coaxial cable (bypassing the r.f. link) for use during pre-flight ground testing. The Encoder can thus function independently of the rest of the ground station, as a piece of ground support equipment with which any of the 256 commands can be generated and the desired gondola subsystems exercised.

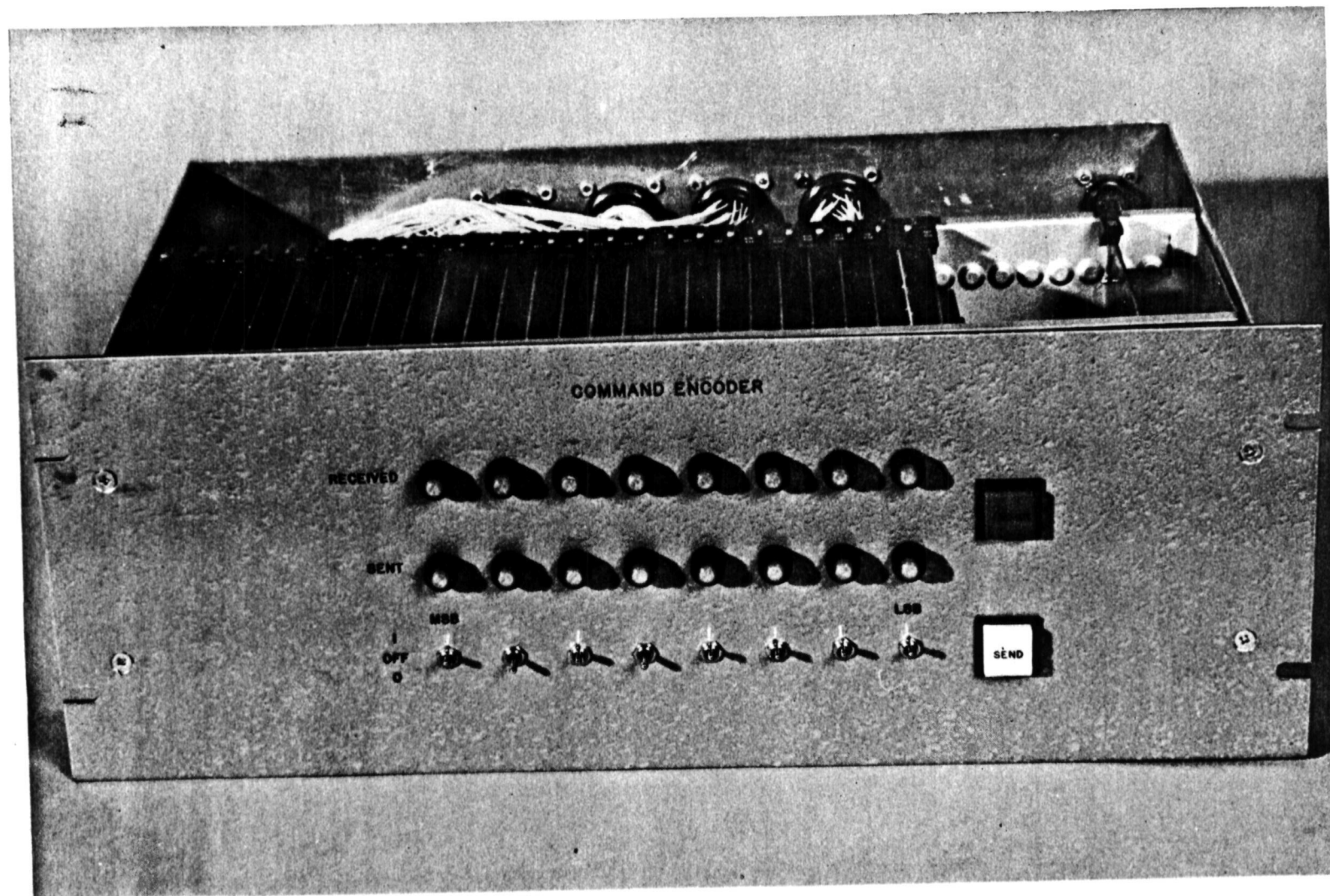


Figure 5. Command Encoder Hardware

DISCUSSION SUMMARY — PAPER 5.3

No discussion.

APPENDIX

LIST OF ATTENDEES

Mr. Gordon C. Augason
Mail Stop N-245-6
Ames Research Center
National Aeronautics & Space Admin.
Moffett Field, CA 94035
PHONE: (415) 965-5502

Dr. Michel Bader
Mail Stop N-200-4
Ames Research Center
National Aeronautics & Space Admin.
Moffett Field, CA 94035
PHONE: (415) 965-5409

Dr. Ronald E. Baker
The University Southampton
SO9-5NH
Southampton
Hampshire, ENGLAND
PHONE:

Mr. William F. Barrows
Mail Stop N-244-13
Ames Research Center
National Aeronautics & Space Admin.
Moffett Field, CA 94035
PHONE: (415) 965-6520

Dr. Frank Bartko
Martin Marietta Aerospace
Denver Division (Mail No. 0471)
P.O. Box 179
Denver, CO 80201
PHONE: (303) 794-5211, Ext. 5130

Mr. Jack D. Beemer
Raven Industries, Inc.
205 E. 6th Street
Sioux Falls, SD 57101
PHONE: (605) 336-2750

Mr. Robert W. Boese
Mail Stop 245-6
Ames Research Center
National Aeronautics & Space Admin.
Moffett Field, CA 94035
PHONE: (415) 965-5501

Dr. Nancy W. Boggess
Code SG
National Aeronautics & Space Admin.
Washington, DC 20546
PHONE: 8-202-755-3649

Mr. Jerome G. Borucki
Mail Stop N-245-6
Ames Research Center
National Aeronautics & Space Admin.
Moffett Field, CA 94035
PHONE: (415) 965-6261

Dr. Murray F. Campbell
Steward Observatory
University of Arizona
Tucson, AZ 85721
PHONE: (602) 884-1291

Dr. Charles Chackerian, Jr.
Mail Stop N-245-6
Ames Research Center
National Aeronautics & Space Admin.
Moffett Field, CA 94035
PHONE: (415) 965-6300

Dr. Dean R. Chapman
Mail Stop N-200-4
Ames Research Center
National Aeronautics & Space Admin.
Moffett Field, CA 94035
PHONE: (415) 965-5065

Mr. Ralph J. Cowie
USAF-CRL-LCC
L.G. Hanscom Field
Bedford, MA 01730
PHONE: (617) 861-3006

Mr. Harry Cygielman
Mail Stop N-244-14
Ames Research Center
National Aeronautics & Space Admin.
Moffett Field, CA 94035
PHONE: (415) 965-6525

Mr. Thomas T. Danaher
Air Force Cambridge Research Lab (USAF)
L.G. Hanscom Field
Bedford, MA 01730
PHONE: (617) 861-3006, 223-2100

Mr. Arthur G. DeBell
Rockwell International (DC23)
3370 Miraloma Ave.
Anaheim, CA 92803
PHONE: (714) 632-6292

Mr. Gordon J. Deboo
Mail Stop N-213-3
Ames Research Center
National Aeronautics & Space Admin.
Moffett Field, CA 94035
PHONE: (415) 965-5473

Mr. Larry E. Edsinger
Mail Stop N-202-8
Ames Research Center
National Aeronautics & Space Admin.
Moffett Field, CA 94035
PHONE: (415) 965-5891

Dr. Edwin F. Erickson
Mail Stop N-245-6
Ames Research Center
National Aeronautics & Space Admin.
Moffett Field, CA 94035
PHONE: (415) 965-5508

Dr. Giovanni G. Fazio
Center for Astrophysics
Harvard College Obs. and Smithsonian
Astrophysics Obs.
60 Garden St.
Cambridge, MA 02138
PHONE: (617) 864-7910, Ext. 226

Dr. Carl L. Frederick
Cornell University
Center for Radiophysics & Space Research
Ithaca, NY 14850
PHONE: 8-607-272-1064

Dr. Michael W. Friedlander
Department of Physics
Washington University
St. Louis, MO 63130
PHONE: (314) 863-0100, Ext. 4036

Dr. Thomas Gehrels
Lunar and Planetary Laboratory
University of Arizona
Tucson, AZ 85721
PHONE: (602) 884-1222

Dr. Lawrence P. Giver
Mail Stop N-245-6
Ames Research Center
National Aeronautics & Space Admin.
Moffett Field, CA 94035
PHONE: (415) 965-5502

Prof. Marcel Golay
Republique et Canton de Genève
Observatoire
CH-1290 Sauverny
Switzerland
PHONE:

Dr. David Goorvitch
Mail Stop N-245-6
Ames Research Center
National Aeronautics & Space Admin.
Moffett Field, CA 94035
PHONE: (415) 965-6493

Mr. Mack O. Gore
National Center for Atmospheric Research
National Scientific Balloon Facility
P.O. Box 1175
Palestine, TX 75801
PHONE: (214) 729-0271

Mr. Willis C. Goss
Jet Propulsion Laboratory
4800 Oak Grove Drive
Pasadena, CA 91103
PHONE: 8-213-354-6730

Mr. Marvin E. Greeb
Ball Brothers Research Corp.
Boulder Industrial Park
Boulder, CO 80300
PHONE: (303) 441-4215

Mr. Robert C. Gunnell
Data Control Systems Inc.
7150 Fenwick Lane, Suite 221
Westminister, CA 92683
PHONE: (714) 894-4471

Mr. Thomas H. Hamon
Mail Stop N-213-6
Ames Research Center
National Aeronautics and Space Admin.
Moffett Field, CA 94035
PHONE: (415) 965-5465

Mr. Q. Marion Hansen
Mail Stop N-244-7
Ames Research Center
National Aeronautics & Space Admin.
Moffett Field, CA 94035
PHONE: (415) 965-6540

Mr. Thomas H. Harmount
Mail Stop N-244-13
Ames Research Center
National Aeronautics and Space Admin.
Moffett Field, CA 94035
PHONE: (415) 965-6543

Dr. Nathan L. Hazen
Harvard College Obs.
60 Garden Street
Cambridge, MA 02138
PHONE: (617) 495-4947

Mr. Roger C. Hedlund
Mail Stop N-213-3
Ames Research Center
National Aeronautics and Space Admin.
Moffett Field, CA 94035
PHONE: (415) 965-5473

Dr. William F. Hoffmann
Steward Observatory
University of Arizona
Tucson, AZ 85721
PHONE: (602) 884-1291

Mr. John How
Marconi Space & Defense Systems Ltd.
Chobham Road
Camberley, Surrey
United Kingdom
PHONE:

Dr. Alvin Howell
Dept. of Electrical Engineering
Tufts University
Medford, MA 02155
PHONE: 8-617-628-5000

Dr. Daniel A. Huguenin
Observatoire de Genève
CH - 1290 Sauverny
Geneva, Switzerland
PHONE: (022) 55.26.11 Geneva

Dr. W. Neil Johnson
Code 7120.11
U.S. Naval Research Lab
Washington, DC 20375
PHONE: (202) 767-3028

Mr. Elliott D. Katzen
Mail Stop N-200-4
Ames Research Center
National Aeronautics and Space Admin.
Moffett Field, CA 94035
PHONE: (415) 965-6345

Mr. John B. Kirkpatrick
Mail Stop N-244-14
Ames Research Center
National Aeronautics & Space Admin.
Moffett Field, CA 94035
PHONE: (415) 965-6525

Maj. Joseph Koehly
AFCRL Det. 3 Commander
Chico, CA 95926
PHONE: 8-916-343-5011

Mr. Rocky Koga
Physics Dept.
University of Calif., Riverside
Riverside, CA 92502
PHONE: (714) 787-5642

Mr. Owen L. Koontz
Mail Stop N-245-6
Ames Research Center
National Aeronautics & Space Admin.
Moffett Field, CA 94035
PHONE: (415) 965-5526

Mr. Robert S. Kubara
National Center for Atmospheric Research
National Scientific Balloon Facility
P.O. Box 1175
Palestine, TX 75801
PHONE: (214) 729-0271

Dr. Walter H. G. Lewin
MIT Center for Space Research - Rm 37-527
77 Massachusetts Avenue
Cambridge, MA 02139
PHONE: (617) 253-4282

Dr. Ernest V. Loewenstein
Optical Physics Lab
AFCRL
L.G. Hanscom Field
Bedford, MA 01730
PHONE:

Mr. Bonne C. Look
Mail Stop N-244-7
Ames Research Center
National Aeronautics & Space Admin.
Moffett Field, CA 94035
PHONE: (415) 965-6542

Dr. Frank J. Low
Lunar & Planetary Laboratory
University of Arizona
Tucson, AZ 85721
PHONE: (602) 884-2727

Dr. Hans Mark
Mail Stop N-200-1
Ames Research Center
National Aeronautics & Space Admin.
Moffett Field, CA 94035
PHONE: (415) 965-5111

Mr. Ramsey K. Melugin
Mail Stop N-244-14
Ames Research Center
National Aeronautics & Space Admin.
Moffett Field, CA 94035
PHONE: (415) 965-6525

Prof. K. Wolfgang Michel
Max-Planck-Institut fur Physik
Und Astrophysik
8046 Garching b.
Munich, GERMANY
PHONE:

Mr. Wayne A. Millard
Physics Department
University of Calif., Riverside
Riverside, CA 92502
PHONE: (714) 787-5642

Dr. Victorio Manno
European Space Research Organization
Direction Centrale
Headquarters
114, Avenue Charles-de-Gaulle
(92) Neuilly-Sur-Seine, FRANCE

Dr. Allan J. Mord
Mail Stop N-245-6
Ames Research Center
National Aeronautics and Space Admin.
Moffett Field, CA 94035
PHONE: (415) 965-5101

Dr. Thomas H. Morgan
TN23 (Astrophysics Section)
Johnson Space Center
National Aeronautics & Space Admin.
Houston, TX 77058
PHONE: (713) 483-6467

Mr. James P. Murphy
Mail Stop N-244-14
Ames Research Center
National Aeronautics and Space Admin.
Moffett Field, CA 94035
PHONE: (415) 965-6530

Dr. Henk Olthof
Dept. of Space Research
University of Groningen
P.O. Box 800
Groningen, The Netherlands
PHONE: 050-116631 Telex: 53572

Dr. Lydick T. Ostwald
Ball Bros. Research Corp.
P.O. Box 1062
Boulder, CO 80302
PHONE: (303) 441-4035

Mr. Ernest J. Ott
Code SG
National Aeronautics & Space Admin.
Washington, DC 20546
PHONE: 8-202-755-3693

Mr. Gilbert T. Parra
Mail Stop N-213-3
Ames Research Center
National Aeronautics & Space Admin.
Moffett Field, CA 94035
PHONE: (415) 965-5473

Mr. Mike S. Pavey
National Center for Atmospheric Research
National Scientific Balloon Facility
P.O. Box 1175
Palestine, TX 75801
PHONE: (214) 729-0271

Dr. Michael R. Pelling
Physics Dept.
University of California, San Diego
P.O. Box 109
LaJolla, CA 92037
PHONE: (714) 453-2000, Ext. 1887 or 2640

Mr. Kenneth J. Pitts
Mail Stop N-245-6
Ames Research Center
National Aeronautics & Space Admin.
Moffett Field, CA 94035
PHONE: (415) 965-5512

Mr. Ilia G. Poppoff
Mail Stop N-245-10
Ames Research Center
National Aeronautics & Space Admin.
Moffett Field, CA 94035
PHONE: (415) 965-5027

Dr. Boris Ragent
Mail Stop N-213-3
Ames Research Center
National Aeronautics & Space Admin.
Moffett Field, CA 94035
PHONE: (415) 965-5476

Dr. David Ramsden
The University Southampton
SO9-5NH
Southampton
Hampshire, ENGLAND
PHONE:

Mr. Ray T. Reynolds
Mail Stop N-245-3
Ames Research Center
National Aeronautics & Space Admin.
Moffett Field, CA 94035
PHONE: (415) 965-5527

Dr. George R. Ricker
MIT Center for Space Research
RM 37-527
77 Massachusetts Ave.
Cambridge, MA 02139
PHONE: (617) 253-7532 or 253-7464

Mr. Aidan E. Roche
Lockheed Palo Alto Research Labs.
3251 Hanover
Palo Alto, CA 94306
PHONE: (415) 493-4411

Mr. Phil M. Salomon
Jet Propulsion Lab
4800 Oak Grove
Pasadena, CA 91103
PHONE: 8-213-354-6214

Mr. Richard W. Schaupp
Mail Stop N-202-8
Ames Research Center
National Aeronautics & Space Admin.
Moffett Field, CA 94035
PHONE: (415) 965-5891

Mr. Stanley G. Scott
Mail Stop N-245-6
Ames Research Center
National Aeronautics & Space Admin.
Moffett Field, CA 94035
PHONE: (415) 965-5512

Mr. Alfred Shipley
National Center for Atmospheric Research
National Scientific Balloon Facility
P.O. Box 1175
Palestine, TX 75801
PHONE: (214) 729-0271

Mrs. Janet P. Simpson
Mail Stop N-245-6
Ames Research Center
National Aeronautics & Space Admin.
Moffett Field, CA 94035
PHONE: (415) 965-5511

Mr. Sheldon M. Smith
Mail Stop N-245-6
Ames Research Center
National Aeronautics & Space Admin.
Moffett Field, CA 94035
PHONE: (415) 965-6330

Mr. William J. Snider
National Center for Atmospheric Research
National Scientific Balloon Facility
P.O. Box 1175
Palestine, TX 75801
PHONE: (214) 729-0271

Mr. Irving J. Spiro
Aerospace Corp.
Box 92957
Los Angeles, CA 90009
PHONE: (213) 648-7408

Dr. Jacob E. Stoecker
Max-Planck-Institut für Physik
Und Astrophysik
8046 Garching b.
Munich, GERMANY
PHONE:

Mr. Charles D. Swift
Mail Stop N-245-6
Ames Research Center
National Aeronautics & Space Admin.
Moffett Field, CA 94035
PHONE: (415) 965-5508

Mr. Paul J. Titterton
GTE-Sylvania Inc.
P.O. Box 188
Mt. View, CA 94040
PHONE: (415) 966-2826

Dr. William A. Towlson
Dept. of Physics and Astronomy
University College London
Gower Street
London WC1E 6BT, ENGLAND
PHONE: 01 387-7050 Telex 28722

Dr. John S. Vogel
Dept. of Physics
Case Western Reserve University
10900 Euclid Ave.
Cleveland, OH 44106
PHONE: (216) 368-2997

Dr. Curtis W. Wells
Lockheed Electronics (Mail Code C23B)
16811 El Camino Real
Houston, TX 77058
PHONE: (713) 483-6467

Mr. James A. Winker
Raven Industries, Inc.
Post Office Box 1007
Sioux Falls, SD 57101
PHONE: (605) 336-2750

Dr. Fred C. Witteborn
Mail Stop N-245-6
Ames Research Center
National Aeronautics & Space Admin.
Moffett Field, CA 94035
PHONE: (415) 965-5528

Mr. Lou S. Young
Mail Stop N-244-13
Ames Research Center
National Aeronautics & Space Admin.
Moffett Field, CA 94035
PHONE: (415) 965-6520

Mr. Harry R. Zabower
Mail Stop N-244-13
Ames Research Center
National Aeronautics & Space Admin.
Moffett Field, CA 94035
PHONE: (415) 965-6520

Dr. Rodolphe J. Zander
Institute of Astrophysics
University of Liège
5, Av. de Cointe
B-4200 Cointe-Ougrée
BELGIUM
PHONE: Belgium 04/52.99.80